MILLENNIAL-SCALE CHANGES IN SEA SURFACE TEMPERATURES AND INTERMEDIATE WATER CIRCULATION IN THE NORTHWEST PACIFIC DURING THE PAST 20,000 YEARS

Dissertation

zur Erlangung des Doktorgrades der Naturwissenschaften

am Fachbereich Geowissenschaften

der Universität Bremen

vorgelegt von

Lars Max

Bremerhaven, Mai 2012

Gutachter:

Prof. Dr. Ralf Tiedemann

Prof. Dr. Dirk Nürnberg

Meinen Großeltern

Abstract

During the late Pleistocene to Holocene transition global climate changed dramatically. In particular, during the end of the late Pleistocene, the large-scale shift from the last glacial state to the recent interglacial state took place (between 18,000–11,000 years ago) and was accompanied by millennial-scale climate fluctuations that are well known from the North Atlantic realm. On the other hand, detailed paleoceanographic reconstructions of the subarctic North Pacific climate history are scarce and patchy, thus an incomplete picture of short-term climate fluctuations of the late Pleistocene to Holocene remains so far. The principal aim of this thesis was the reconstruction of the poorly studied (millennial-scale) climate variability of the subarctic northwest Pacific, which has become more into focus of climate research, as it is believed that past climate dynamics in this region are a key to gain more understanding in the mechanisms that drove late Pleistocene climate dynamics. For this purpose, a variety of different geochemical proxies were used for detailed paleoceanographic investigations in order to give detailed insights into past dynamics of sea surface temperatures, sea-ice variability and intermediate water ventilation characteristics of the northwest Pacific realm during the past 20,000 years. From high-resolution SST records it has been shown that the deglacial SST changes in the far northwest Pacific realm matched the climate variability in other parts of the North Pacific and beyond that, were remarkably similar to the timing and nature of the North Atlantic/Greenland temperature variability. From this, a close linkage to deglacial variations in the Atlantic Meridional Overtuning Circulation was inferred, which invoked rapid atmospheric teleconnections to allow a quasi-synchronous (on centennial time-scales) SST development between the North Atlantic and the North Pacific. Reconstructions of past sea-ice variability points to strong changes in sea-ice extent and a close coupling to SST fluctuations in the subarctic North Pacific, thereby further underpins the sensitivity of the atmosphere/cryosphere in the subarctic northwest Pacific realm to rapid climate fluctuations during the last deglacial period. By combination of different SST-proxies (Mg/Ca ratio from planktonic foraminifers/alkenone-paleothermometry) it has also been shown that the structure of the upper-ocean was subject to tremendous changes during millennial-sale climate variability of the last deglaciation. It also points to a more recent development of the density-driven upper-ocean stratification in the subarctic northwest Pacific during the Preboreal. Furthermore, investigations of past ventilation changes revealed that the North Pacific Ocean was marked by enhanced intermediate water formation during cold stages of Heinrich 1 and the Younger Dryas and are related to tremendous changes in upper-ocean hydrography occurred during the deglaciation. Altogether these results are in accordance with the proposed impact of rapid atmospheric teleconnections between the North Atlantic and North Pacific during meltwater-driven reductions of the Atlantic Meridional Overtuning Cell, which induced fast (on centennial time-scales) dynamics in climate and oceanography in the western North Pacific during the last deglaciation. Hence, the sensitivity of the subarctic North Pacific Ocean to millennial-scale climate fluctuations of the past has to be taken much more in consideration to gain an accurate understanding of past and future climate dynamics.

Kurzfassung

Während des Übergangs vom späten Pleistozän zum Holozän unterlag das globale Klima dramatischen Veränderungen. Insbesondere das Ende des späten Pleistozäns ist gekennzeichnet durch den großen Klimaumschwung aus dem letzten Glazial in das heutige Interglazial (zwischen 18.000 – 11.000 Jahre vor heute) und wurde begleitet von kurzweiligen Klimaschwankungen. Diese Schwankungen sind im nordatlantischen Raum gut erfasst, jedoch sind detaillierte paläozeanographische Rekonstruktionen (auf tausendjährigen Zeitskalen) über den subarktischen Nordpazifik nur sehr begrenzt vorhanden und liefern ein unpräzises Abbild der Klimadynamik über den Zeitraum des späten Pleistozäns bis Holozäns. Das primäre Ziel dieser Doktorarbeit war die Rekonstruktion der Klimavariabilität des subarktischen Nordwestpazifiks auf tausendjährigen Zeitskalen, welche zwar mehr in den Fokus der Klimaforschung gerückt dennoch nur unzureichend erfasst ist. Gerade die vergangene Klimaentwicklung in dieser Region gilt als Schlüssel zum Verständnis relevanter Anfachungsmechanismen für die Klimadynamik des späten Pleistozäns. Zu diesem Zweck wurde eine Vielzahl an unterschiedlichen, geochemischen Proxies angewendet, um ein umfassenderes Bild über die Klimadynamik des subarktischen Nordwestpazifiks während des Zeitraumes der letzten 20.000 Jahre zu bekommen. Im Fokus standen hierbei Veränderungen der Meeresoberflächentemperatur, Änderungen der Meereisverbreitung und Unterschiede in der Ventilation im nordwestlichen Pazifik. Anhand von hochauflösenden Temperaturrekonstruktionen konnte gezeigt werden, dass das Einsetzen und die Ausprägung deglazialer Temperaturveränderungen im Nordwestpazifik der generellen Temperaturentwicklung aus anderen Regionen des Nordpazifiks, sowie dem grönländisch- nordatlantischen Temperaturmuster gleichen. Hieraus ergibt sich die Schlussfolgerung, dass die Temperaturveränderungen zwischen Nordatlantik und Nordpazifik mit deglazialen Schwankungen der Zirkulationsschleife im Nordatlantik und den damit einhergehenden atmosphärisch gekoppelten Fernwirkungen zusammenhängen. Dies erlaubte eine synchrone Temperaturentwicklung zwischen Nordatlantik und Nordpazifik auf Zeitskalen von einigen hundert Jahren. Die Sensitivität des subarktischen Nordpazifiks gegenüber rapiden Klimaschwankungen während des letzten Deglazials zeigt sich darüber hinaus auch in Änderungen der Meereisverbreitung, welche stark an die Temperaturveränderungen gekoppelt ist. Ferner ließen sich auch Änderungen in der Struktur der Wasseroberfläche mit der deglazialen Klimadynamik in Verbindung bringen, welche durch eine Kombination verschiedener Temperaturproxies (Mg/Ca-Verhältnisse planktischer Foraminiferen/Alkenontemperaturen) erfasst wurden. Demnach bildete sich die heutige, dichteabhängige Statifizierung im subarktischen Nordwestpazifik erst im frühen Präboreal aus. Die grundlegenden Veränderungen der Oberflächenhydrographie der letzten 20,000 Jahre gingen außerdem mit Ventilationsänderungen einher, die vor allem während des Heinrich 1 Schmelzwasserereignisses aber auch der Jüngeren Dryas zu verstärkter Bildung von Zwischenwasser im Nordpazifik geführt haben. Insgesamt weisen die Untersuchungen aus dem Nordwestpazifik deutlich auf die postulierten atmosphärischen Fernwirkungen zwischen Nordatlantik und Nordpazifik

hin. Diese standen widerum im engen Zusammenhang mit Schmelzwassereignissen und den damit einhergehenden Veränderungen der thermohalinen Zirkulationsschleife und führten demnach zu rapiden Veränderung (auf Zeitskalen einiger hunderter Jahre) der Zirkulation und Ozeanographie im Nordpazifik. Diese Arbeit liefert klare Hinweise über die Sensibilität des subarktischen Pazifiks gegenüber schnellen Klimaschwankungen der Vergangenheit, welche in Zukunft mehr Berücksichtigung finden sollten, um ein präziseres Verständnis vergangener und zukünftiger Klimaveränderungen zu erreichen.

Acknowledgements

First of all, I would like to thank my supervisor Prof. Dr. Ralf Tiedemann, who gave me the opportunity to do this study and spent plenty of time to help me tackling all kinds of troubles during the past three years. Thank you very much for all the fruitful discussions, the great support and sagacious advice. I would also like to appreciate my second advisor Prof. Dr. Dirk Nürnberg for the support and freedom to develop my own interests during my PhD. Despite their busy schedules, both always kept an open eye on my study and helped me to improve all the different kinds of abstracts, manuscripts and presentations through constructive comments and reviews over the years.

I owe particular thanks to Jan-Rainer Riethdorf, who sailed with me through the Bering Sea and shared with me the different stages of highs and lows as PhD student during the past years. Thank you very much for the efforts you put on the work and all the constructive discussions. At the end of this journey you have become more a friend than a colleague. I want to thank Lester Lembke-Jene for several hours of inspiring discussions and its contribution to improve this work. I also would like to acknowledge my Russian colleagues of the research project KALMAR. большо́е спаси́бо for all the nice KALMAR meetings and the great cooperation from your side.

My thanks also go to the "AWI allstars" (Ralf, Birgit and Julia) for two wonderful cruises and the time we shared together on the research vessel SONNE. I would like to express my special thank to Birgit Glückselig, who always gave me warm words and coffee to survive my daily grind at the AWI. Furthermore, I'd like to say a big thank you to Kirsten Fahl and Walter Luttmer for the patience in introducing me into the biomarker world. I wish to thank Adelina Manurung and Lukas Belz for all the months of good HiWi work and valuable efforts in the geochemical lab. I also would like to appreciate the help of Prof. Dr. Andreas Mackensen and Lisa Schönfeld and thank for the measurements (sometimes on short-notice) in the stable isotopes lab. I thank Rita Fröhlking, Susanne Wiebe, Michael Seebeck and Dietmar Penshorn for the help with technical issues as well as the laboratory staff in general. I wish to thank Aysel Sorensen for proof reading of the manuscripts and her encouragement to help in various bureaucratic hurdles (e.g. how to submit a Dienstreiseantrag ?). My office mates are thanked for their patience when listening to my scientific stories.

I would like particularly to thank my grandparents. Honour to whom honour is due. Thank you for all the opportunities in my life. Together, we succeeded! I am particular grateful to my beloved Corinna. Thank you for all your patience, all your love and all you are for me, not only during the last three years. Let's go to Sardegna! I further want to thank all my friends for sharing wonderful times in Bremen and around. Thank you all for bearing with me during the hard-times. Finally, sincere thanks are given to my flat mates. There is no place like home! Thank you very much for all the great time in the DobbenWG.

Table of Contents

Lars Max, Jan-Rainer Riethdorf, Ralf Tiedemann, Maria Smirnova, Lester Lembke-Jene,
Kirsten Fahl, Dirk Nürnberg, Alexander Matul and Gesine Mollenhauer,

Paleoceanography (in review)

Jan-Rainer Riethdorf, Lars Max, Dirk Nürnberg, Lester Lembke-Jene and Ralf Tiedemann

Paleoceanography (to be submitted)

Lars Max, Lester Lembke-Jene, Jan-Rainer Riethdorf, Ralf Tiedemann and Dirk Nürnberg

Nature Geoscience (to be submitted)

Chapter 1: Introduction

1.1 Preamble

Since the discovery of several millennial-scale climate fluctuations recorded in Greenland ice cores [*Dansgaard et al.*, 1993; *Grootes et al.*, 1993], North Atlantic [e.g. *Bond et al.*, 1993] and North Pacific sediment records [*Kotilainen and Shackleton*, 1995; *Behl and Kennett*, 1996; *Lund and Mix*, 1998; *Mix et al.*, 1999; *Kiefer et al.*, 2001] during the late Pleistocene, relative timing and global transmission of these short-term climate instabilities are still a matter of ongoing research. As the subarctic North Atlantic was characterized by rapid warm/cold oscillations, which are related to a variable strength of the Atlantic meridional overturning circulation (AMOC), the far field effects on distant regions as the subarctic North Pacific are not well constrained. In particular, the high latitudes of the North Pacific Ocean are considered to be a major component of the climate system due to the large quantities of atmospheric carbon dioxide (CO_2) stored in the deeper ocean interior (Figure 1.1). Late Pleistocene changes in the state of the subarctic North Pacific oceanography and thus its ability to store or release huge quantities of dissolved inorganic carbon are believed to be a crucial factor to explain changes in the global carbon cycle and past climate dynamics [e.g. *Haug et al.*, 1999; *Galbraith et al.*, 2007]. However, the paleoceanography of the subarctic North Pacific Ocean is less well studied compared to the North Atlantic Ocean.
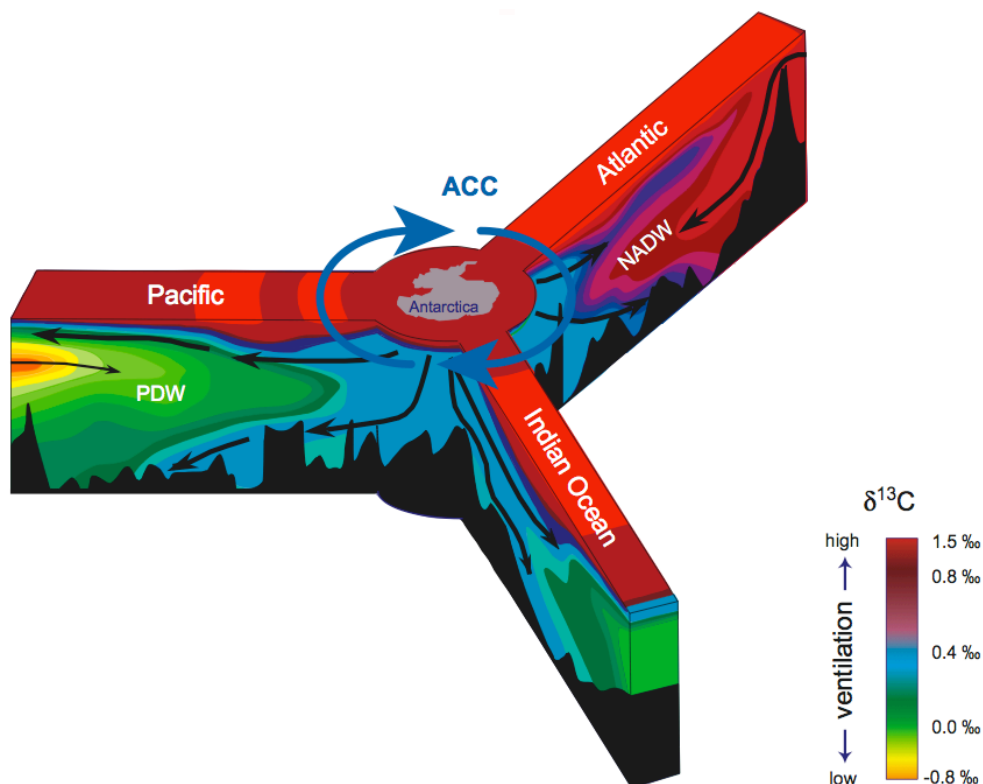
Figure 1.1: General distribution of $\delta^{13}C$ in the world oceans indicative of deep water ventilation. High $\delta^{13}C$ values characterize young, well-oxygenated water masses in the North Atlantic and the Southern Ocean. Low $\delta^{13}C$ values mark old and CO_2-rich water masses in the deep North Pacific [modified after *Charles and Fairbanks*, 1992].

In particular, during the end of late Pleistocene the large-scale shift from the last glacial state to the recent interglacial state took place (between 18,000–11,000 years ago) and were accompanied by millennial-scale climate fluctuations repeatedly, known to have had great impact on the North Atlantic paleoceanography. On the other hand, detailed paleoceanographic reconstructions are scarce and patchy in the North Pacific, leading to an incomplete picture of the late Pleistocene to Holocene climate development so far. However, some studies based on planktonic foraminiferal isotopes from northeast Pacific sediments point to millennial-scale changes in sea surface temperatures (SST) of the North Pacific during the last glacial-interglacial transition. These fluctuations correlate well with rapid climate fluctuations that are known from Greenland ice cores and North Atlantic marine sediments [e.g. *Behl and Kennett*, 1996; *Kienast and McKay*, 2001; *Hendy and Kennett*, 2002], thus implying an in-phase behaviour of these two ocean basins. In contrast, other studies located in the open subarctic North Pacific also suggest millennial-scale fluctuations in SST, but apparently out-of phase to the Greenland/North Atlantic climate pattern [*Kiefer and Kienast*, 2005; *Sarnthein et al.*, 2006; *Gebhardt et al.*, 2008]. As available records of the past surface-water hydrography show a quite inconsistent picture it is still not clear how the subarctic North Pacific Ocean was affected during rapid climate fluctuations of the late Pleistocene. The same holds true for the past O_2 and CO_2 contents of intermediate and deep waters in the North Pacific. Studies based on benthic foraminiferal stable isotopes and marine radiocarbon ages generally point to better-ventilated water masses, which existed at intermediate depths (above 2,000 m) during the Last Glacial Maximum (LGM) with relatively small changes at greater depths [*Keigwin*, 1987; *Duplessy et al.*, 1988; *Mix et al.*, 1991; *Keigwin*, 1998; *Matsumoto et al.*, 2002]. The notion of unchanged or more sluggish renewal of old deep water is in direct conflict with the evidence for better ventilated Pacific glacial deep water masses as deep as ~2700 m, inferred from Cd/Ca ratios of benthic foraminifera [*Ohkouchi et al.*, 1994]. Hence, detailed information on paleoceanographic changes are equivocal in the North Pacific from available marine records but of paramount importance to further constrain its impact on global climate, in particular during rapid climate fluctuations of the late Pleistocene.

This thesis focuses on the reconstruction of SST and intermediate water ventilation of the subarctic northwest Pacific (NW-Pacific) and its marginal seas (Bering Sea and Sea of Okhotsk) during the most recent period of the late Pleistocene to Holocene (the last 20,000 years), which has remained poorly understood yet. In particular, during the last deglacial period the transition from the LGM to the Holocene took place and was punctuated by several millennial-scale climate fluctuations, for example the Heinrich Event 1, the Bølling warm phase or the Younger Dryas cold spell. However, the global extent of these short-lasting climate fluctuations is still a matter of considerable debate. In this thesis, I studied the manifestation of these shorter climate events and its impact on the subarctic NW-Pacific paleoceanography, a necessary precondition to further decipher the role of the North Pacific Ocean in the global climate system during rapid climate fluctuations of the past.

1.2 The subarctic NW-Pacific and its marginal seas

1.2.1 Modern oceanographic conditions

The modern surface circulation of the subarctic NW-Pacific and its marginal seas can be described as a large-scale cyclonic pattern of surface currents, which transport heat and nutrients between the different ocean regions (Figure 1.2) [*Stabeno et al.*, 1999]. Superimposed on several small cyclonic circulation cells, the most prominent feature in the subarctic NW-Pacific is the large-scale, counter-clockwise circulation regime of the western subarctic gyre (WSAG). The southern boundary of the WSAG consists of the Kuroshio - North Pacific Current system, which transports relatively warm water masses along the subarctic front (SAF) into the northeast Pacific. The northern rim of the WSAG is formed by the Alaskan Stream, which brings warm water masses along the Aleutian Islands into the NW-Pacific, thereby entering the Bering Sea in the north through several passes between the Aleutian Islands [*Stabeno et al.*, 1999]. The inflow of Alaskan Stream waters drives a large-scale counter-clockwise surface circulation in the Bering Sea, formed by the Aleutian North Slope Current (ANSC) and Bering Slope Current (BSC). To some extent surface waters leave the Bering Sea via the Bering Strait into the Arctic Ocean but the main circulation path is through the Kamchatka Strait back into the North Pacific as East Kamchatka Current (EKC). Along with the EKC, nutrient-rich waters from the Bering Sea are delivered back into the NW-Pacific, thereby forming the Oyashio Current (OC), which represents the western branch of the WSAG. On its path to the south, a part of the EKC enters the Sea of Okhotsk through the Kurile Island Arc, thereby driving the water mass signature of the Okhotsk gyre.
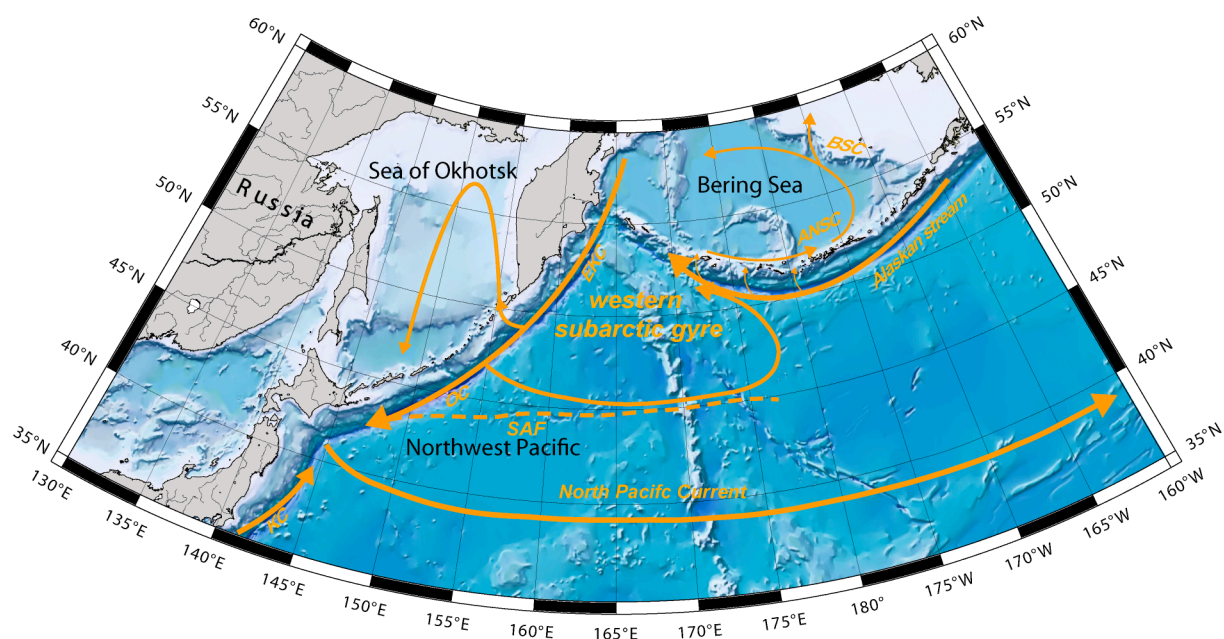

Figure 1.2: Bathymetric chart of the subarctic NW-Pacific and its marginal seas with general surface circulation indicated by orange arrows (BSC = Bering Slope Current; ANSC = Aleutian North Slope Current; EKC = East Kamchatka Current; OC = Oyashio Current; KC = Kuroshio Current; SAF = subarctic front) [modified after *Stabeno et al.*, 1999].

The subarctic NW-Pacific regions are characterized by a large, seasonal variability in SST and sea-ice distribution. During winter, the contrast between the Siberian High and Aleutian Low-Pressure System (ALPS) brings cold air masses from the Arctic to the subarctic NW-Pacific and promotes surface cooling, mixing of the uppermost water column and sea-ice formation in the Bering Sea and Sea of Okhotsk [e.g. *Niebauer*, 1998]. During summer, increased insolation and weakening of the ALPS lead to warm SST, ice-free conditions and strong upper-ocean stratification [*Ohtani et al.*, 1972]. At present, the subarctic North Pacific and its marginal seas are marked by a permanent, steep vertical salinity gradient (halocline) between extremely low-salinity surface waters on top (Figure 1.3a) and high-salinity subsurface water masses below. The halocline promotes strong stratification of the subarctic North Pacific today. As the excessive evasion of nutrient-rich subsurface water masses into the photic zone is strongly hampered by the halocline, available nutrients are almost completely consumed by biological activity, which leads to the highest carbon export efficiency in the world oceans and a net sink of atmospheric CO_2 [*Honda et al.*, 2002].

Another prominent feature of the subarctic North Pacific is the presence of intermediate water masses with higher oxygen content and lower salinity (Figure 1.3b). This North Pacific Intermediate Water (NPIW) is the only new formed water mass in the North Pacific today and defined by a salinity minimum (at isopycnal $\sigma_\theta = 26.8$; according to *Van Scoy et al.*, [1991]). The water mass signature of NPIW is strongly coupled to physical processes in the Sea of Okhotsk, where Okhotsk Sea Intermediate Water (OSIW) is formed in coastal polynyas during initial wintertime sea-ice production [*Talley*, 1993; *Shcherbina et al.*, 2003]. The Sea of Okhotsk is the only oceanic region in the North Pacific, where fresh surface water masses are subducted into the deeper ocean interior. NPIW is formed is in the NW-Pacific east of Japan, where the fresh and cold intermediate water from the Sea of Okhotsk merges with warmer, more saline and less dense waters delivered from the Kuroshio Current from the south. NPIW is formed as blend of these water masses. It spreads throughout the North Pacific between 300 - 800 m water depths (Figure 1.3b). The deep North Pacific is only slowly replenished due to the absence of deep water formation in the North Pacific [*Warren et al.*, 1983]. In contrast to NPIW, the deep North Pacific waters are ventilated by water masses originated in the Southern Ocean (see also Figure 1.1). In the Antarctic, Circumpolar Current the Circumpolar Deep Water (CDW) is formed, which enters the southwest Pacific area east of the New Zealand Plateau and Chatman Rise by forming a Deep Western Boundary Current [*Tomczak and Godfrey*, 1994; *Talley*, 2008]. This water masses are moving slowly from the South Pacific to the North Pacific, whereas the oxygen content decreases by ongoing respiration and its nutrient content increases gradually by continuous biological export production from above. It reaches the North Pacific as Pacific Deep Water (PDW) and hosts the oldest, most nutrient- and CO_2-enriched waters in the world oceans (Figure 1.3c). The corrosive water masses of the PDW fill the depth interval between 2,000– 4,000 m in the North Pacific and leads to a shallow position of the Carbonate Compensation Depth (< 2500 m).
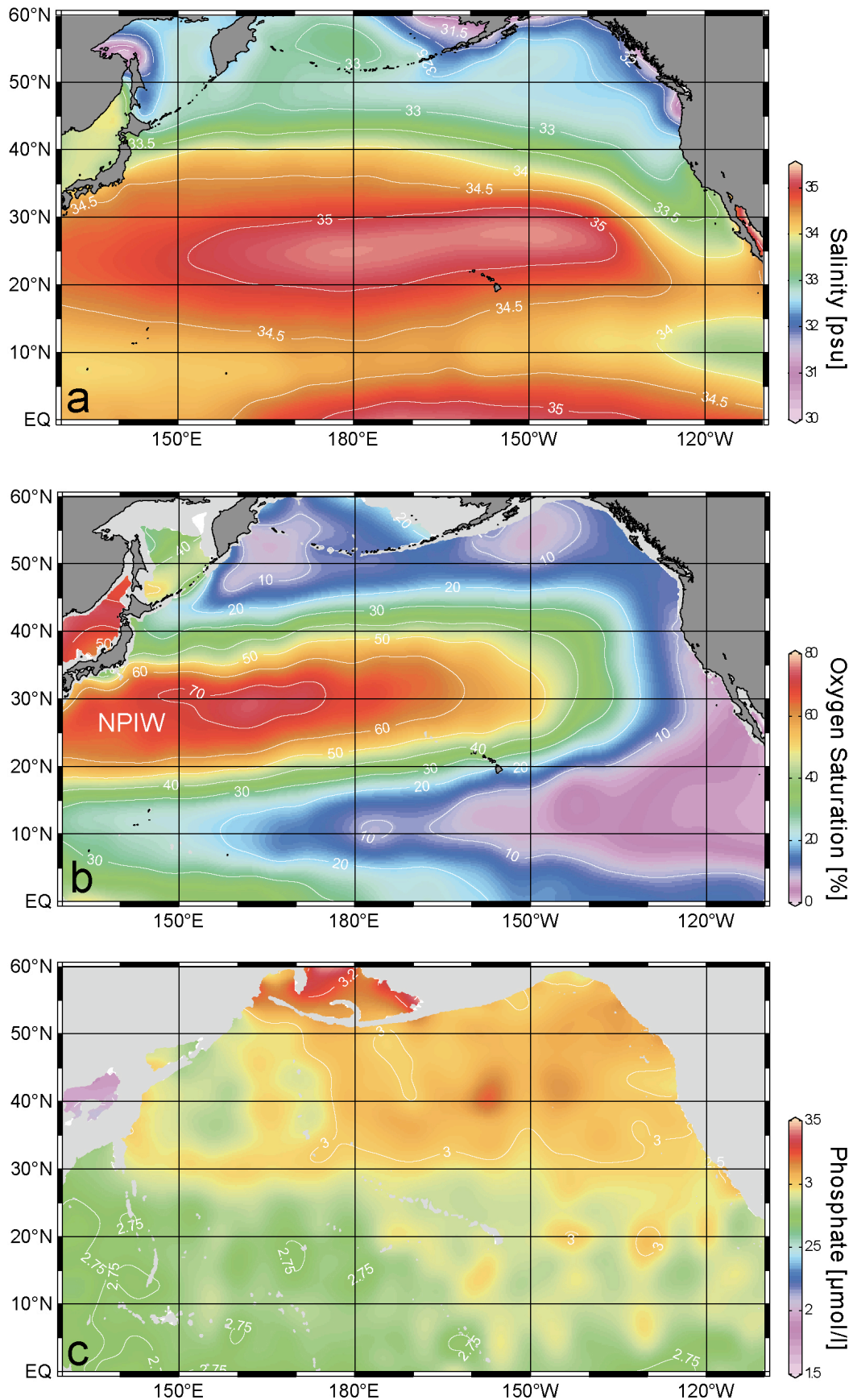
Figure 1.3: Modern oceanographic setting of the North Pacific with (a) salinity (psu) at the sea surface and (b) oxygen saturation (%) at 500 m water depth, NPIW = North Pacific Intermediate Water, and (c) phosphate concentrations at 2,000 m water depth. This figure was created with Ocean Data View [*Schlitzer*, 2011] using the World Ocean Atlas (2009) database [*Locarnini et al.*, 2010].

1.2.2 Previous paleoceanographic studies

Deglacial changes in SST could have led to tremendous changes in upper-ocean stratification, the amount of sea-ice cover, vertical mixing and ventilation of the deeper ocean of the subarctic NW-Pacific. Whether and how the NW-Pacific SST was affected by rapid climate oscillations during the last deglaciation is a key question in paleoceanography. Establishing the relative timing of millennial-scale climate events in the North Pacific and North Atlantic are crucial to understand the mechanisms responsible for their generation and transmission. Both, an in-phase behaviour invokes rapid atmospheric teleconnections [e.g. *Mikolajewicz et al.*, 1997] as well an out-of-phase behaviour [e.g. *Saenko et al.*, 2004] due to slow reorganizations of the AMOC has been proposed to dominate the transmission of these climate events.

However, the deglacial evolution of SST and climate in the subarctic NW-Pacific is poorly known on centennial to millennial time-scales and limited to a few sediment records from the open NW-Pacific and its marginal seas. Available information on past SST variability in the open NW-Pacific comes from two pelagic sediment records, sediment core MD01-2416 and ODP Hole 883D, recovered from the northern Emperor Seamounts. Based on planktonic Mg/Ca ratios and from census counts of planktonic foraminifera using the SIMMAX transfer function as proxies of past SST, these records suggest millennial-scale fluctuations in SST during the last deglacial period [*Kiefer et al.*, 2001; *Kiefer and Kienast*, 2005; *Sarnthein et al.*, 2006]. In particular, sediment core MD01-2416 shows strong SST fluctuations during the last deglaciation, which indicates a pronounced temperature maximum during stadial Heinrich Event 1 (H1) and a subsequent cooling during interstadial Bølling/Allerød, apparently out-of-phase with the Greenland/North Atlantic temperature pattern (Figure 1.4). In contrast, an alkenone-based SST record derived from sediment core PC6 at the continental margin of Japan, suggests coldest temperatures during H1, followed by continuous warming towards the Holocene and no millennial-scale oscillations during the deglaciation [*Minoshima et al.*, 2007] (Figure 1.4).

Other SST reconstructions are restricted to the marginal seas, the Sea of Okhotsk [*Ternois et al.*, 2000; *Seki et al.*, 2004a; *Harada et al.*, 2006b; *Harada et al.*, 2008; *Seki et al.*, 2009] and the Bering Sea [*Caissie et al.*, 2010] and also provide a quite inconsistent picture. Some alkenone-based SST records from the Sea of Okhotsk show deglacial SST fluctuations, which are similar to the Greenland/North Atlantic temperature pattern [*Harada et al.*, 2008; *Seki et al.*, 2009; *Harada et al.*, 2012] whereas some SST records show no direct relationship to SST fluctuations in the North Atlantic [e.g. *Seki et al.*, 2004a]. However, based on alkenone-derived SST reconstructions from high-resolution record MD01-2412 in the southern Sea of Okhotsk, *Harada et al.* [2008] suggested a close linkage and synchronicity of deglacial climate fluctuations within a few centuries between the Pacific and the Atlantic sides of the Northern Hemisphere (Figure 1.4), which was also inferred from alkenone-based SST reconstructions in the northeast Pacific [*Kienast and McKay*, 2001; *Barron et al.*, 2003].
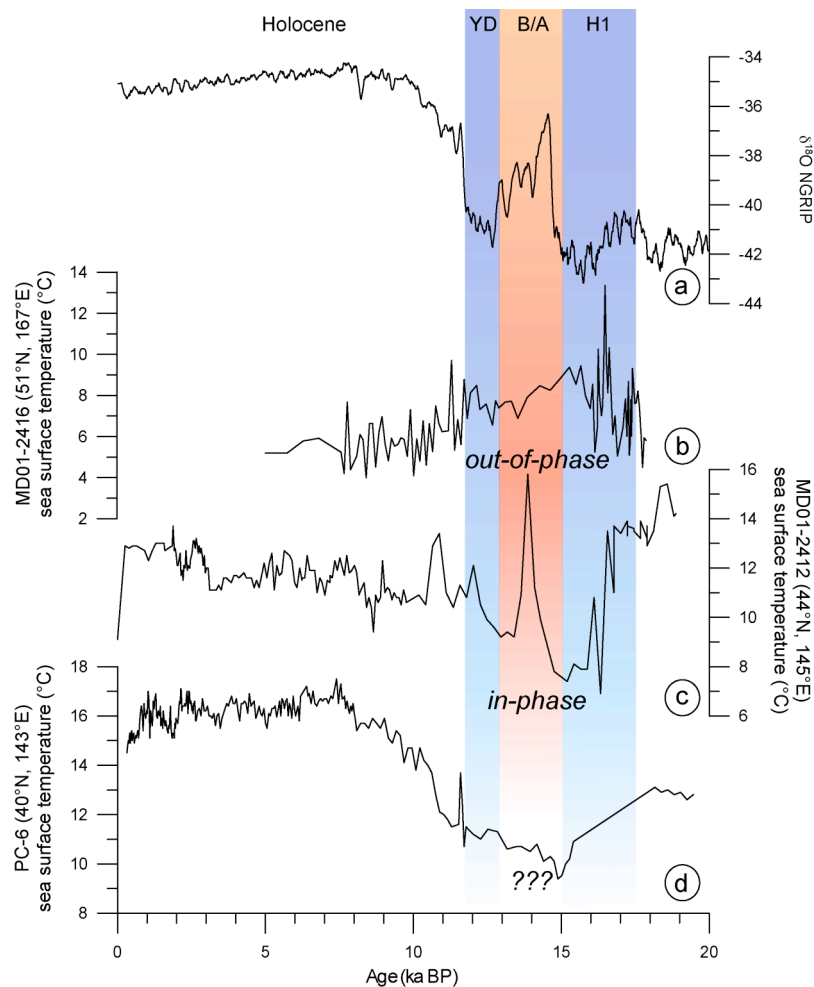
Figure 1.4: Deglacial to Holocene SST reconstructions from the NW-Pacific realm compared to (a) NGRIP ice-core record [NGRIP members, 2004; GICC05 timescale, Rasmussen et al., 2006]. (b) Mg/Ca-based SST reconstructions from sediment record MD01-2416 [*Sarnthein et al.*, 2006]. (c) SST reconstructions from Sea of Okhotsk record MD01-2412, based on alkenone-paleothermometry [*Harada et al.*, 2008]. (d) SST reconstructions from sediment record PC6 off Japan, based on alkenone paleothermometry [*Minoshima et al.*, 2007]. Blue shaded bars indicate stadial Heinrich Event 1 (H1) and the Younger Dryas (YD), red shaded bar marks the interstadial Bølling/Allerød (B/A), respectively.

Nevertheless, from available paleoceanographic records the deglacial pattern of SST variability in the subarctic North Pacific realm as well as the timing of SST changes between the North Atlantic and North Pacific are inconclusive and not well understood so far. A first attempt to investigate the spatial and temporal SST variability between the North Pacific and North Atlantic realm during the Holocene was done by *Kim et al.* [2004]. For this purpose, available alkenone-based SST reconstructions from the North Atlantic and North Pacific were combined with the data analysis of a coupled atmosphere-ocean general circulation model (AOGCM) to infer the dominant climate mode between both ocean basins. According to their results, the North Pacific experienced a long-term warming trend whereas in the North Atlantic a long-term-cooling trend is observed during the past 7,000 years. This led to the hypothesis of a Holocene temperature seesaw between the North Atlantic and the North Pacific and has been explained by a shift of the atmospheric circulation field in the Northern Hemisphere to be responsible for the inverse long-term SST development between both ocean basins [*Kim et al.*, 2004].

However, the proposed long-term warming trend in the North Pacific was inferred from a few records in the North Pacific Ocean. In particular, only one alkenone-based SST record from the subarctic NW-Pacific realm was considered and thus the climate variability in this region is probably underestimated. Hence, the hypothesis of a long-term North Atlantic - North Pacific temperature seesaw during the Holocene stands on shaky grounds and its evaluation requires much more high-resolution records from the subarctic North Pacific realm.

Another important aspect in paleoceanography is the intermediate and deep water ventilation history of the North Pacific, which is believed to have played a substantial role in global climate change during the late Pleistocene to Holocene due to its significant capacity to store or release heat and various dissolved species of gases and salts. The intermediate and/or deep water ventilation is strongly coupled to changes in the sea surface conditions (as SST or salinity) and ocean circulation. Studies on intermediate and deep water circulation changes are usually based on the carbon isotopic composition of epibenthic foraminifera (δ^{13}C) and radiocarbon age differences between benthic and planktonic foraminifera as proxies for ventilation changes of water masses. Several studies addressed general ventilation changes between the LGM and the Holocene in the subarctic North Pacific [*Keigwin*, 1987; *Duplessy et al.*, 1988; *Keigwin et al.*, 1992; *Stott et al.*, 2000]. Accordingly, the glacial water column of the North Pacific Ocean was better-ventilated above 2.000 m during the LGM compared to the Holocene. This is expressed as positive excursion in δ^{13}C values recorded in the upper North Pacific, whereas below 2.000 m the proxy-records points to stagnation in ventilation. These results seem to be robust for large parts of the subarctic North Pacific and were also recorded in δ^{13}C transects from the NW-Pacific and the Sea of Okhotsk [*Keigwin*, 1998]. However, the notion of less well ventilated deep water during the LGM are in conflict with North Pacific records based on the Cd/Ca-ratio of benthic foraminifera, which indicate a better ventilation of glacial deep water masses as deep as 2.700 m [*Ohkouchi et al.*, 1994]. Aside from that controversy, *Matsumoto et al.* [2002] compiled the available δ^{13}C data from the Pacific Ocean in a zonally averaged profile, which indicate a shadow zone of minimum ventilation in the North Pacific. This ventilation minimum was located between 1.000 - 2.000 m water depths in the Holocene but deepened by 1.000 m during the LGM (Figure 1.5). The deepening of better-ventilated water masses suggests a scenario in which intensified glacial NPIW production allowed waters to sink to about 1.000 m deeper than today. On the other hand, some authors claimed a southern source (a modification of Glacial North Atlantic Intermediate Water from the Southern Ocean) of better-ventilated water-masses or a combination of different sources. A combination of different sources is not mutually exclusive and cannot be ruled out due to the scarcity of ventilation records in the mid-depth subarctic North Pacific.

In particular, the marginal seas of the NW-Pacific are potential candidates as source region for better ventilated intermediate water masses but adequate ventilation records from these regions are not
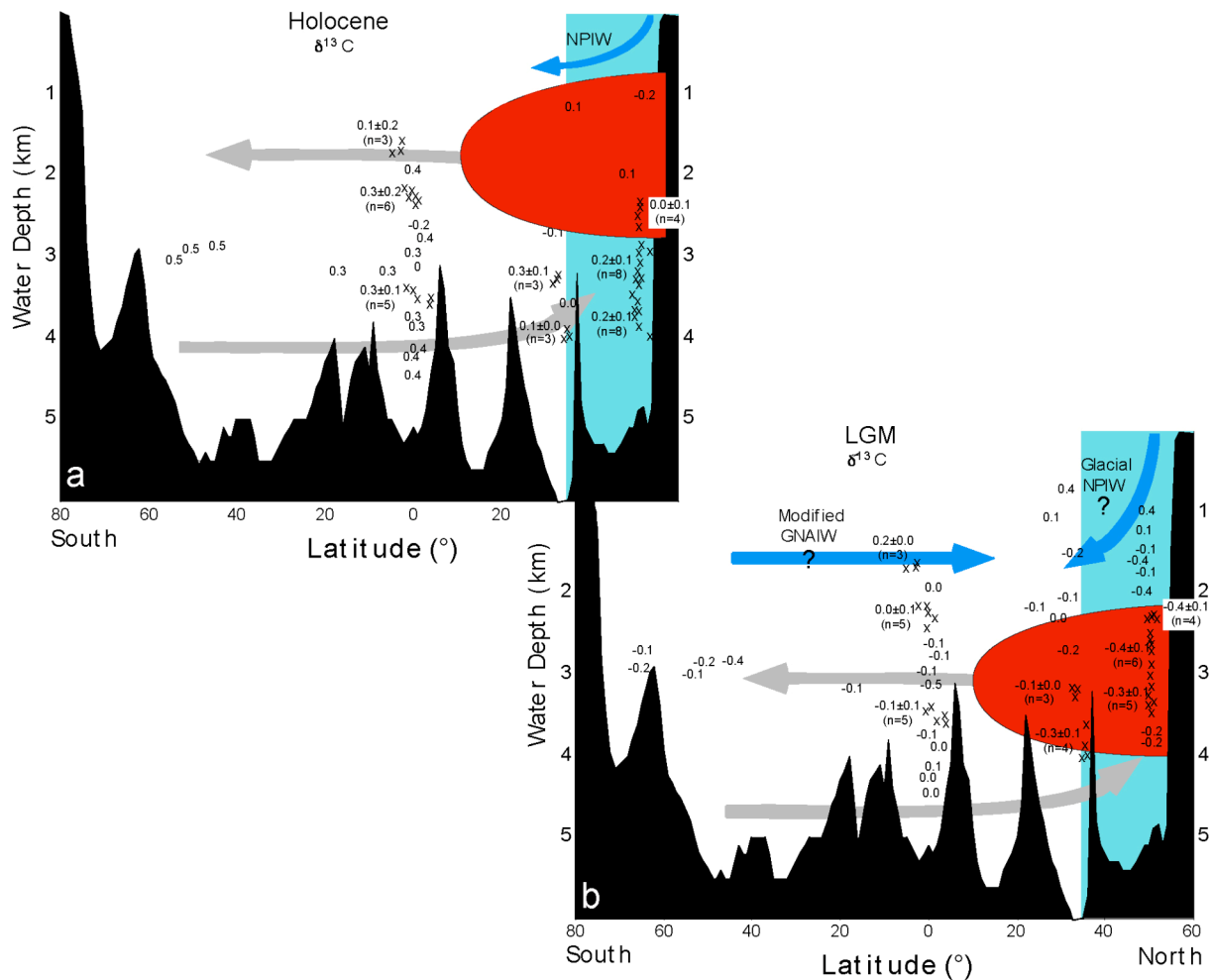
Figure 1.5: Changes in meridional distribution of benthic foraminiferal δ^{13}C in the western Pacific Ocean for the LGM and Holocene. (a) lowest δ^{13}C values are indicated by red shading and found in the deep North Pacific centered around 2,000 m water depth during the Holocene and (b) around 3,000 m during the LGM. Arrows indicate suggested circulation. Blue arrows mark higher δ^{13}C values in the upper 2,000 m in the North Pacific, which reflect a local source of newly ventilated glacial NPIW (GNPIW), influx of modified Glacial North Atlantic Intermediate Water (GNAIW) or a combination of both. The subarctic North Pacific region is highlighted in light blue [modified after *Matsumoto et al.*, 2002].

available so far. Furthermore, information on millennial-scale ventilation changes during the last deglacial period, derived from high-resolution sediment records, is even more limited. Available paleoceanographic reconstructions on ventilation changes from the marginal seas are based on low-resolution microfossil- and trace metal studies [*Tanaka and Takahashi*, 2005; *Horikawa et al.*, 2010] and point to shifts in the ventilation regimes between the Sea of Okhotk and Bering Sea during the last deglacial period. A recent study compiled the available information on the intermediate to deep water history in the subarctic North Pacific in combination with a general circulation model (GCM) [*Okazaki et al.*, 2010]. The authors emphasize the role of millennial-scale climate variability during the last glacial termination to have had a tremendous impact on ventilation changes in the NW-Pacific. In their model runs, a freshwater pulse was applied in the North Atlantic Ocean to mimic meltwater discharges occurred during H1 (~17,500 – 15,000 years ago) in the subarctic North Atlantic. The simulated freshwater perturbation in the North Atlantic weakens the AMOC and leads to a rapid onset

of a Pacific Meridional Overturning Circulation (PMOC) in the North Pacific. In this scenario the PMOC is maintained by the poleward advection of salinity from the subtropical regions and a southward displacement of the Intertropical Convergence Zone due to atmospheric reorganizations, acting on years to decades. As a result, an increased poleward heat transport lead to a warming and onset of deep water formation in the subarctic NW-Pacific during H1 as direct response to suppressed oceanic heat transport (AMOC shutdown) and cooling in the subarctic North Atlantic (Figure 1.6a) [*Okazaki et al.*, 2010]. This Atlantic - Pacific seesaw was originally proposed by *Saenko et al.* [2004] and describes a ventilation asymmetry between the North Atlantic and North Pacific Ocean. However, as both models show a similar effect of an AMOC shutdown on North Pacific SST and circulation patterns (Figure 1.6a and b), the timing and transmission of these climate anomalies are substantially different from each other. The model runs of *Okazaki et al.* [2010] invoke rapid atmospheric teleconnections (atmospheric forcing) to induce the ventilation seesaw on decadal time-scales. In contrast, the proposed ventilation seesaw of Saenko et al. [2004] invokes mainly salinity-driven large-scale oceanic reorganizations (oceanic forcing) due to readjustments of the global conveyor circulation. Thus, in this scenario the spin-up of a PMOC takes thousands of years to act on the North Pacific circulation. Despite this inconsistency in the proposed scenarios, whether an AMOC shutdown triggered a PMOC and warming in the North Pacific during H1 is still a controversial issue. Several model studies also claimed on rapid, atmospherically coupled signal transmissions from the North Atlantic to the North Pacific as main driver for SST and circulation changes [e.g. *Mikolajewicz et al.*, 1997; *Vellinga and Wood*, 2002; *Okumura et al.*, 2009]. Conversely, these model simulations indicate rapid atmospheric reorganizations in the subarctic North Pacific via an atmospheric bridge, which led to an intensification of atmospheric low-pressure systems (Aleutian Low) and strong cooling in the North Pacific during substantial weakening of the AMOC. A more recent study focused on the climate variability in North Pacific during H1 by using two different coupled climate models [*Chikamoto et al.*, 2012]. Surprisingly, this model experiments also suggest cooler SST in the far NW-Pacific similar to the North Atlantic during H1 in cases of a strong and a weak PMOC (Figure 1.6c). According to that, intermediate to deep water formation in the NW-Pacific not necessarily requires an increased poleward heat transport from the tropics to the extratropics and is probably a consequence of complex ocean-atmosphere feedback mechanisms in the NW-Pacific.

In summary, the overwhelming bulk of model simulations propose that short-term, millennial scale oscillations during the last deglaciation had an enormous effect on the subartic North Pacific Ocean climate variability. In any case, fundamental understanding of causes and consequences of these short-term climate oscillations cannot be constrained by the limited amount of existing paleoclimate records in the North Pacific. A tremendous quantity of high-resolution archives are necessary, in particular from the subarctic NW-Pacific realm, to decipher how ocean-atmosphere feedback mechanisms act on climate, whereas the high latitude ocean regions on Earth in general are believed to play a key role.
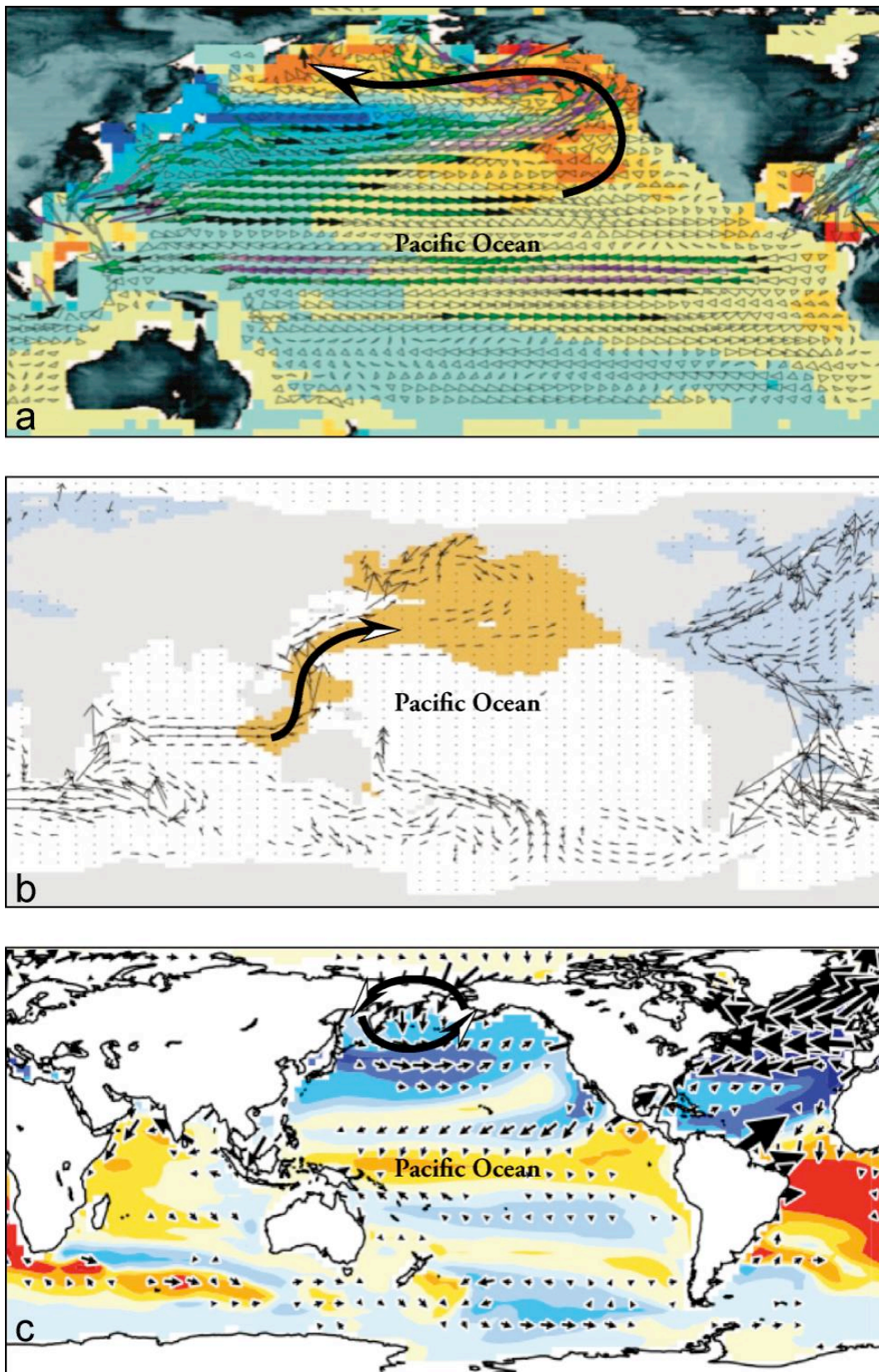
Figure 1.6: Results from different model simulations of the Pacific Ocean during freshwater hosing (AMOC shutdown) in the North Atlantic. (a) Simulated upper-ocean SST and wind anomalies during H1 [modified after *Okazaki et al.*, *2010*]. (b) State of upper-ocean salinity and circulation anomalies ~2.000 years after freshwater forcing in the North Atlantic [modified after *Saenko et al.*, *2004*]. (c) Annual SST and surface wind stress in the Pacific Ocean during H1 simulated with an coupled atmosphere-ocean general circulation model (MIROC) [modified after *Chikamoto et al.*, *2012*]. Black arrows in (a) and (b) indicate main circulation path of the PMOC, black arrows in (c) indicate atmospheric circulation anomalies.

1.3 Rationale and objectives of this study

To understand the causes and consequences of rapid climate variability during the last 20,000 years of climate history are one of the main aspects in global climate research. Since several decades, the paleoclimate community tries to decipher the several modes of ocean-atmosphere interactions and feedbacks on past climate to draw conclusions on future climate development. The sensitivity of the high latitude oceans in the climate system, in particular during millennial-scale climate fluctuations in the past, is widely acknowledged but detailed climate reconstructions are principally realized in the North Atlantic Ocean. In contrast, our knowledge of millennial-scale fluctuations and its impact on the high latitudes of the North Pacific Ocean in the past still lacks on detailed climate-archives and the paleoceanograhy of the subarctic NW-Pacific realm is essentially not understood. At the same time, the few paleoceanographic records from the subarctic NW-Pacific indicate that this region was subject to dynamics in climate and oceanography during rapid climate fluctuations at the end of the late Pleistocene. Moreover, several studies with climate models emphasize the impotance of abrupt climate fluctuations and its impact on changes in the far NW-Pacific. With respect to the various underlying mechanisms different climate models draw on to explain millennial-climate fluctuations in these ocean regions, it is of fundamental importance to focus on detailed paleoceanographic reconstructions from climate archives, sufficient in temporal resolution, to infer urgently needed climatic boundary conditions from the past and to make realistic estimations about future climate change.

In the following chapter of this thesis the material and methods used in this study were briefly described. Chapters 3 to 5 consist of three manuscripts, providing detailed paleoceanographic reconstructions from high-resolution sediment records to infer changes in the SST development, sea-ice variability, changes in upper-ocean stratification and intermediate water ventilation of the subarctic NW-Pacific and its marginal seas during the past 20, 000 years. The conclusions and implications of this study as well as future perspectives are given in Chapter 6.

The major objectives of the three manuscripts constitute this thesis were:

(Chapter 3) detailed reconstructions of SST and sea-ice variability of the subarctic NW-Pacific and its marginal seas during the past 15,000 years from a suite of sediment records to tackle following questions:

➢ How is the deglacial SST development in the subarctic NW-Pacific coupled to short-term climate oscillations of the North Atlantic?

➢ Is the long-term SST development of the NW-Pacific and North Atlantic marked by opposing SST trends (temperature seesaw) during the past 7,000 years?

➢ Is there any change in sea-ice extent during millennial-scale fluctuations of the past 15 kyr?

(Chapter 4) (sub)SST and salinity reconstructions of the subarctic NW-Pacific and its marginal seas for the last 20,000 years based on Mg/Ca analysis of planktonic foraminifers to give answers on following questions:

- ➢ Is there any temporal change in Mg/Ca-derived sub(SST) variability compared to the SST signal based on alkenone-paleothermometry?
- ➢ Do alkenones and Mg/Ca-based SST reconstructions reproduce the same SST-signal and if not, how can this be explained?
- ➢ Are there any changes in upper-ocean stratification during the deglaciation and Holocene, which can be inferred by combination of different SST-proxies?

(Chapter 5) high-resolution carbon isotope records in combination with marine radiocarbon ages to provide a first comprehensive view on past ventilation changes in the Bering Sea and Sea of Okhotsk during the past 20,000 years based on following questions:

- ➢ What is/are the source region/s of better-ventilated intermediate water masses in the subarctic North Pacific during the last deglaciation?
- ➢ What happened to the intermediate to deep water ventilation in the North Pacific Ocean when the meridional overturning circulation in the North Atlantic ceased?
- ➢ Was deep water formed in the subarctic NW-Pacific during rapid climate oscillations of the last glacial termination?

Chapter 2: Material and methods

2.1 Research project "KALMAR"

This study was involved in the German-Russian multidisciplinary research project "KALMAR - Kurile-Kamchatka and Aleutean Marginal Sea-Island Arc Systems: Geodynamic and Climate Interaction in Space and Time". Research project KALMAR was mainly a marine research project, but also included terrestrial climate archives to provide a more comprehensive view on land/ocean climate interactions in the Kurile-Kamchatka-Aleutean arc system. It was based on a scientific approach, where investigators from different disciplines were involved and focused on the effects of the geodynamic and oceanographic processes in this area, on matter distribution and cycles, water mass formation and circulation, climate and natural hazards, carried out in five subprojects:

> ➢ SP 1 Neotectonics
> ➢ SP 2 Geodynamics
> ➢ SP 3 Volcanolgy
> ➢ SP 4 Paleoceanolgy
> ➢ SP 5 Limnology

The research of this study was conducted within the framework of SP 4, which aimed at investigating the Pleistocene to Holocene climate development and oceanography in the subarctic NW-Pacific and its marginal seas on centennial to millennial time-scales. Main objective of KALMAR subproject 4 was the development of climate time-scales from high-resolution sediment archives of the eastern continental slope of Kamtchatka and in the western Bering Sea. Based on a multi-proxy approach, changes in SST and salinity, the distribution of sea-ice, the stratification of the ocean, changes in intermediate water formation and biological productivity were addressed within SP 4.

The main part of the material used for this study was collected during KALMAR cruise SO201 Leg 2 with the research vessel SONNE in fall 2009. During cruise SO201 Leg 2, several high-resolution sediment cores were recovered from various oceanic settings in the NW-Pacific and western Bering Sea (Figure 2.1). Sediment records were collected at the eastern continental slope of Kamchatka and on Meiji Drift in the open NW-Pacific (working Area B). Two sediment records were recovered from northwestern slope of Kamchatka in the western Bering Sea (working area D). A bunch of long sediment records were retrieved in the Komandorsky Basin and Shirshov Ridge in the western Bering Sea. At Shrishov Ridge, several sediment cores, spanning a north to south oriented depth transect, were obtained. Core LV29-114-3 from the Sea of Okhotsk was collected during KOMEX cruise LV29 in 2002 and was also implemented in this study. This record was recovered proximal to the northern Kurile Islands near Krusenstern Strait (Figure 2.1)
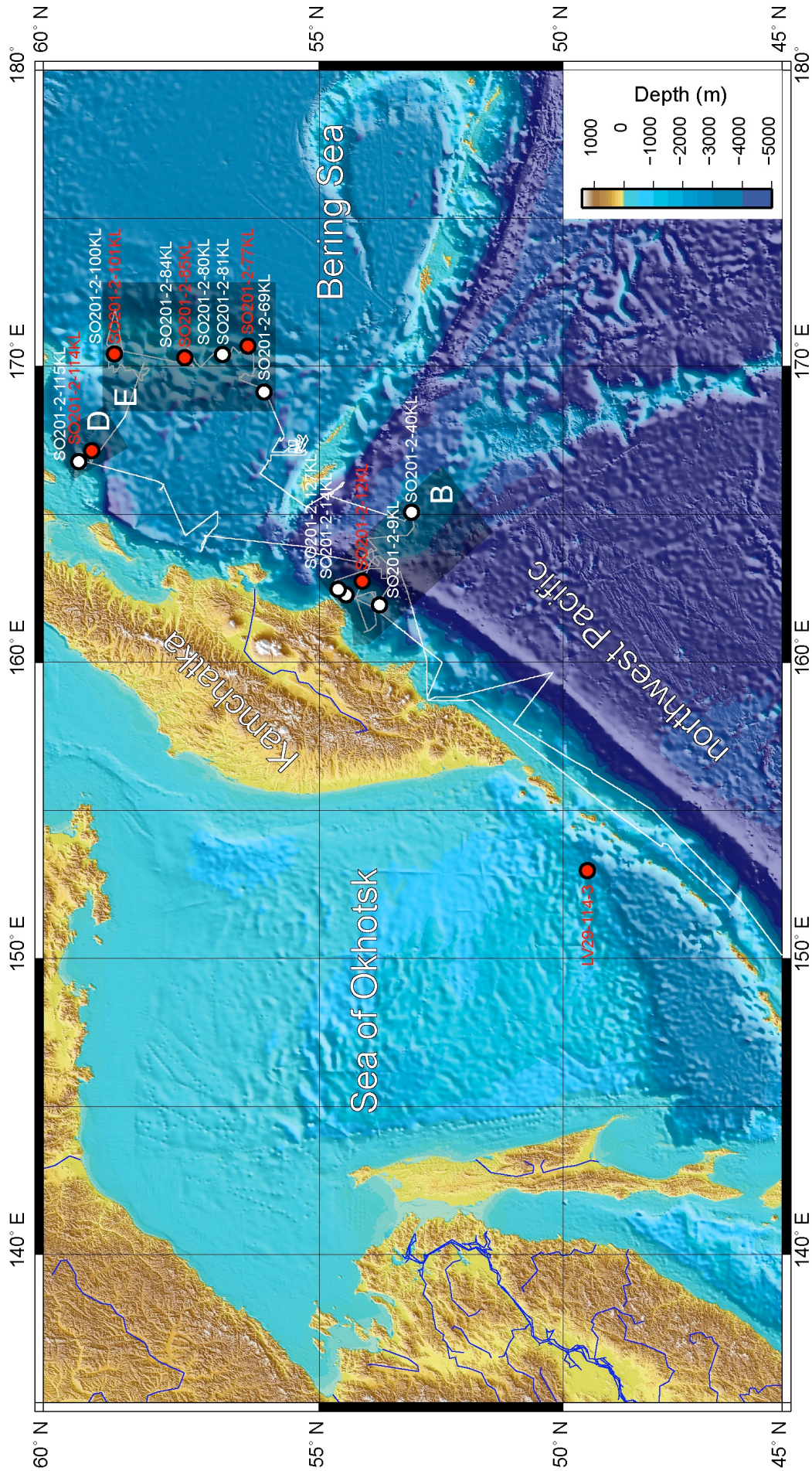
Figure 2.1: Bathymetric chart of the NW-Pacific with the western Bering Sea in the north and the Sea of Okhotsk in the west, together with coring sites (filled circles). Red circles mark sediment records used for this study. Shading highlights different working areas in the NW-Pacific (A) and western Bering Sea (D and E), respectively. White line indicates the cruise track of KALMAR cruise SO 201-2 in 2009. Core LV29-114-3 from the Sea of Okhotsk was recovered during KOMEX cruise LV29 in 2002.

2.2 Sample material

The sediment material of SO201 Leg 2 cruise relevant for this study was recovered with a piston-corer and multicorer device. Directly after recovery of the sediment records, liners of the piston-cores were orientated and cutted into 1 m sections on deck. Multicorer sediments were sampled immediately as whole slices in cm steps after recovery and stored. Magnetic susceptibility measurements were applied on every section of the piston cores by using a Multi-Sensor Core Logger (GEOTEK). The shipboard core logging is briefly described in the SO201 Leg 2 cruise report [*Dullo et al.*, 2009]. After logging, sections were splitted into working and archive halves, respectively. The archive halves were used for visual core description and color reflectance measurements of the sediment records. The working halves were continuously sampled as whole slices every cm and stored in plastic bags (Whirl-Paks) at ~4 °C until further treatment. For core LV29-114-3 recovery, pretreatment and lithological description of the sample material is explained in the cruise report of LV29 cruise KOMEX II [*Biebow et al.*, 2003]. An overview of all used sediment records and the performed proxy studies are summarized in Table 2.1 below and are explained in the methods chapter (Chapter 2.3).

Table 2.1: Core locations in the subarctic NW-Pacific, Sea of Okhotsk and western Bering Sea with performed proxy studies.

Sediment core	Latitude (°N)	Longitude (°E)	water depth (mbsl)	total length (cm)	Study area	performed proxy studies*
LV29-114-3	49°22.54'	152°53.23'	1765	964	Sea of Okhotsk	U^K_{37}, IP_{25}, $CaCO_3$+TOC, CL,[14]C
SO201-2-12KL	53°59.47'	162°22.51'	2145	905	NW-Pacific	U^K_{37}, IP_{25}, CL,[14]C
SO201-2-77KL	56°19.83'	170°41.98'	2135	1178	Bering Sea	U^K_{37}, IP_{25}, $CaCO_3$+TOC, SI, CL,[14]C
SO201-2-85KL	57°30.30'	170°24.77'	968	1813	Bering Sea	U^K_{37}, IP_{25}, $CaCO_3$+TOC, SI, CL,[14]C
SO201-2-101KL	58°52.52'	170°41.45'	630	1832	Bering Sea	U^K_{37}, IP_{25}, CL,[14]C
SO201-2-114KL	59°13.87'	166°59.32'	1376	789	Bering Sea	U^K_{37}, IP_{25}, $CaCO_3$+TOC, CL,[14]C

* U^K_{37} - alkenone paleothermometry; IP_{25} - sea-ice diatoms biomarker; SI - stable isotope measurements; $CaCO_3$ + TOC - wt.% $CaCO_3$ and TOC; CL - Core logging; [14]C - AMS ^{14}C datings

Within the framework of this thesis, sample material from six sediment records was used for detailed paleoceanographic reconstructions in the NW-Pacific, western Bering Sea and Sea of Okhotsk. Sediment core SO201-2-12KL was recovered at the Kronotsky continental margin (working area B; see also Figure 2.1) and is mainly composed of diatomaceous sediments replaced by sandy to silty sequences and high portions of terrestrial organic matter. The major part of sediment records used in this study were collected on Shirshov Ridge in the western Bering Sea from various water depths (working area E; see also Figure 2.1). Shirshov Ridge sediments are generally characterized by high terrigenous (siliciclastic) material contents, which alternate with sequences of diatomaceous ooze deposition. In the far northern Bering Sea continental margin sediment core SO201-2-114KL was recovered and also implemented in this study (working area E; see also Figure 2.1). In particular, this record features several types of glacial silty to sandy sequences followed by deglacial diatom rich parts, which contain fine-grained laminated sediment sequences (working area D; see also Figure 2.1).

2.3 Methods

The sediment samples arrived at the Alfred Wegener Institute for Polar and Marine Research in December 2009. All sediment material was freeze-dried prerequisite for further analysis and splitted into sub-samples according to the various performed proxy studies. In the following, all methods realized in this study are briefly described and contribution of the results to the scientifc manuscripts (Chapter 3 to 5) outlined.

2.3.1 SST reconstructions

The SST reconstructions are based on alkenone-paleothermometry ($U^{k'}_{37}$). Alkenones are highly resistant, long-chained mono-ketones that are produced by members of the *Gephyrocapsacae* family, primarily by the cosmopolitan coccolithophore (single-celled phytoplankton) *Emiliania huxleyi* [e.g., *Volkman et al.*, 1980]. *Brassel et al.* [1986] discovered that these algae change the degree of unsaturation of the C_{37} alkenones (relationship $C_{37:3}$: $C_{37:2}$) according to the temperature of the ambient water they live in. These organic compounds are intensively studied for the well-defined relationship between relative composition of the C_{37} di- and triuntaturated homologs and sea surface temperature and led to the development of the widely established alkenone unsaturation index ($U^{k'}_{37}$) used in various oceanic regions [e.g. *Sikes et al.*, 1997; *Bard et al.*, 2000; *Kienast and McKay*, 2001; *Caissie et al.*, 2010]. $U^{k'}_{37}$ is calculated as the relative abundance of the di- and tri-unsatured alkenones as proxy for paleo-SST as follows:

$$U^{k}_{37}{}' = \frac{C_{37:2}}{C_{37:2} + C_{37:3}} \qquad [\textit{Prahl and Wakeham}, 1987]$$

To calculate the paleo-SST ($U^{k'}_{37}$), several analytical steps are necessary to isolate the alkenones from the sample material. For this purpose, discrete samples (5 – 10 g) were selected from freeze-dried bulk sediment, homogenized and extracted with an accelerated solvent extractor (ASE-200, Dionex) at 100 °C and 1000 psi for 15 minutes by using dichlormethane (DCM) as a solvent. Remaining extracts were separated by silica gel column chromatography into three sub-fractions with the following mixture of solvents: fraction 1, 5 ml Hexane; fraction 2, a mixture of 5 ml DCM\Hexane (1:1); fraction 3, 5 ml DCM. Alkenones are eluted in the third fraction and measured, using a HP 6890 gas chromatograph, equipped with a cold injection system, a DB-1MS fused silica capillary column (60 x 0.32 mm inner diameter, film thickness of 0.25 µm) and a flame ionization detector. Individual alkenone ($C_{37:3}$, $C_{37:2}$) identification was based on the retention time and the comparison with an external standard, which were also used for controlling the instrument stability. The replicability of alkenone measurements with the used equipment was most times better than ±0.3 °C.

The alkenone unsaturation index ($U^{k'}_{37}$) as proxy for SST was calculated following the relationship between $U^{k'}_{37}$ and temperature as proposed by *Müller et al.* [1998], which is based on a global core-top calibration (60 °N – 60 °S):

$$U^{k'}_{37} = 0.033\,T\ (°C) + 0.044$$

The standard error of this calibration is reported to be ±0.050 $U^{k'}_{37}$-units or ±1.5 °C. However, it should be mentioned that the temperature calibration after *Müller et al.* [1998] calculates annual sea surface temperatures. On the other hand it is also known that in the subarctic N-Pacific, alkenone blooms are limited to specific seasons and represent more likely the late summer/early fall SST [e.g. *Seki et al.*, 2004a]. For critical evaluation of the used temperature function to calculate paleo-SST, temperatures were calculated from surface samples and compared to the modern SST distribution in the western Bering Sea (Figure 2.2). The calculated SST from surface samples falls into the modern late summer/early fall SST range (August to September) of the surface water (~25 m) with respect to the given error range of the calibration. This is in accordance with sediment trap studies from the NW-Pacific, which showed that the modern alkenone signal reflects the late summer/autumn SST with a maximum of *Emiliania huxleyi* blooms occurs around 10 - 30 m water depth [*Harada et al.*, 2006a].

The results of the alkenone-based SST reconstructions were used to investigate the SST variability in the NW-Pacific and marginal seas of the past 15 kyr (Chapter 3) and for comparison with Mg/Ca-based SST reconstructions to infer deglacial changes in upper-ocean stratification in the NW-Pacific realm (Chapter 4).
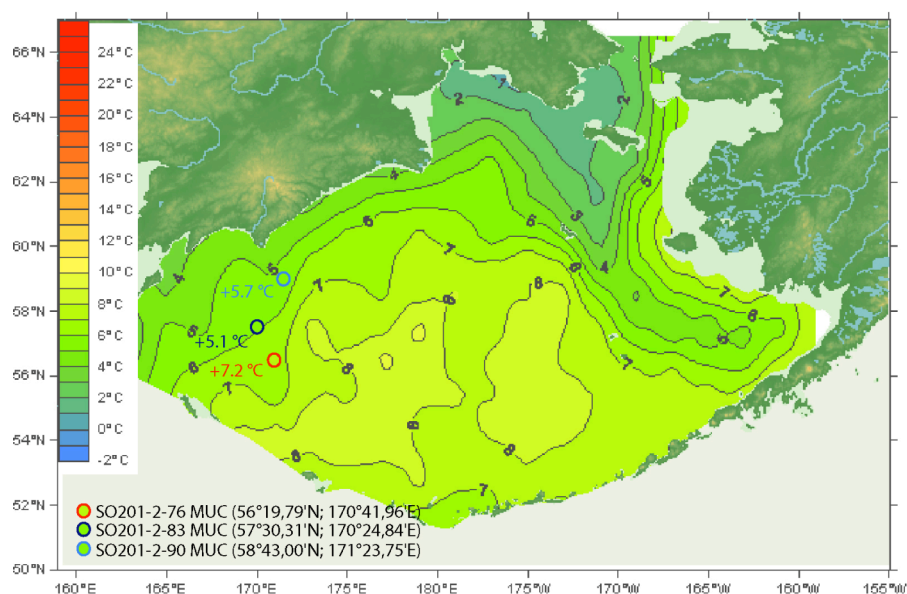

Figure 2.2: Modern late summer temperatures in the Bering Sea at 25 m water depth shown for August [data source: NOAA] and estimated SST calculated from Multicorer surface samples with the temperature calibration of *Müller et al.*, [1998]. The position of the surface samples is indicated by circles, SST is given in °C.

2.3.2 IP$_{25}$ measurements

Recently, a newly developed organic biomarker (IP$_{25}$) was introduced to reflect past sea-ice variability based on the monounsaturated C$_{25}$ isoprenoid molecule produced by diatoms, which are living in the sea-ice [*Belt et al.*, 2007]. Since then, IP$_{25}$ was preferentially used to reconstruct sea-ice variability in the Arctic Ocean and its applicability confirmed to record past variations in sea-ice [e.g. *Müller et al.*, 2009]. However, the absence of IP$_{25}$ in marine sediments might reflect either the absence of sea-ice or, in turn, point to a permanent ice cover (no algal growth) and thus limits this proxy to regions without perennial sea-ice cover. More recently, a study conducted in the eastern Bering Sea showed that IP$_{25}$ could also be used in the Bering Sea to reconstruct past variations in sea-ice [*Meheust et al.*, 2012].

To estimate past sea-ice variability, qualitative assessment of IP$_{25}$ was performed on discrete samples. For this purpose the polar fraction (fraction 1; recovered from silica gel column chromatography during the preparation steps for alkenone analysis) of these samples were measured with an Agilent 6850 GC (30 m HP-5MS column, 0.25 mm i.d., 0.25 µm film thickness) coupled to an Agilent 5975 C VL mass selective detector. The GC oven was heated from 60 °C to 150 °C at 15 °C min-1, and then at 10 °C min-1 to 320 °C (held 15 min.). Operating conditions for the mass spectrometer were 70 eV and 230 °C (ion source). Helium was used as carrier gas. The identification of IP$_{25}$ is based on comparison of its retention time and mass spectra with published data [*Belt et al.*, 2007].

The results of the qualitative sea-ice reconstructions were used to investigate the sea-ice extent in the NW-Pacific and its marginal seas during the last glacial termination (Chapter 3).

2.3.3 CaCO$_3$- and TC measurements

Total organic carbon (TOC) and CaCO$_3$ contents are useful to estimate changes in marine productivity. For the analysis, bulk sediment samples (40 – 50 mg) were homogenized and total organic carbon (TOC) contents determined (relative precision of ±3 %) with a Carbon-Sulphur Analyzer (CS-125, Leco). Prior to the analysis CaCO$_3$ was removed by adding 1M solutions of hydrochloric acid (500 µl) and leaving the sample on a hot plate (150 °C for 1 hour). Total carbon (TC) contents were measured on bulk sediments and carbonate contents calculated according to following equation:

$$CaCO_3 = (TC - TOC) \times 8.333$$

where 8.333 is the stoichiometric calculation factor for CaCO$_3$.

The results of these measurements contributed to a manuscript, which focused on the reconstruction of past millennial-scale changes in marine productivity and terrigenous matter supply in the NW-Pacific during the last glacial-interglacial cycle (Appendix 1).

2.3.4 Stable isotope analysis

A major tool in paleoceanography is the analysis of stable oxygen and carbon isotopes ($\delta^{18}O$, $\delta^{13}C$) from calcite tests of benthic foraminifera. Benthic $\delta^{18}O$ data are often used for stratigraphic purposes as it provides information of changes in past ice volume (global ice effect) and can be used to correlate sediment records globally to a common oxygen isotope time-scale [*Lisiecki and Raymo*, 2005]. More important for this study is the $\delta^{13}C$ record of epibenthic foraminifera, a well-established paleoceanographic tool to reconstruct changes in past deep water circulation. In principle, high $\delta^{13}C$ values reflect low nutrient and CO_2 concentrations and well-ventilated (rich in O_2) water masses [*Kroopnick*, 1985]. This signature is typical for young intermediate and deep water masses proximal to its source region. As the water masses leave its origin, it becomes successively depleted in $\delta^{13}C$ due to the ongoing oxidation of ^{12}O-rich organic matter (aging effect). Numerous studies have shown that the $\delta^{13}C$ signal of epibenthic foraminifera (mostly *Cibicidoides wuellerstorfi*) reliably reflects the carbon isotope composition (dissolved inorganic carbon) of the ambient seawater [e.g. *Zahn et al.*, 1986; *Curry et al.*, 1988; *Duplessy et al.*, 1988; *Curry and Oppo*, 2005] and thus is a widely acknowledged tool to reconstruct deep water circulation changes. However, the $\delta^{13}C$ signal can also be affected by strong changes in marine productivity and export production, hence some caution is needed in interpreting changes in the carbon isotope composition of epibenthic foraminifers as proxy for past circulation changes [*Mackensen et al.*, 1993].

For stable isotope analysis bulk sediment samples were washed over a 63 μm screen, dried and separated in several sub-fractions. The benthic species *Uvigerina peregrina* (*U. peregrina*) and *Cibicidoides lobatulus* (*C. lobatulus*) were picked from 250 – 355 μm fractions. Stable isotopes on endobenthic foraminifera *U. peregrina* was preferentially analysed for stratigraphic purposes. Two to five specimens of each sample were measured on a Finnigan MAT 251 isotope ratio mass spectrometer coupled to an automatic carbonate preparation device (Kiel II). The external reproducibility of these measurements is reported to be better than ±0.04 ‰ for $\delta^{13}C$ and ±0.06 ‰ for $\delta^{18}O$. Additional measurements were done on epibenthic foraminifera *C. lobatulus* to estimate the past $\delta^{13}C_{DIC}$ of ambient seawater As no *Cibicidoides wuellerstorfi* was found in the sediment samples, measured downcore variations in $\delta^{13}C$ are limited to the $\delta^{13}C$ signal of *C. lobatulus*. However, *C. lobatulus* has been observed to preferentially live attached to hard substrate on, or slightly above the sediment surface [*Lutze and Thiel*, 1989; *Schweizer et al.*, 2009] and faithfully records the $\delta^{13}C_{\sum CO_2}$ of overlying bottom waters. For this purpose one to three species were picked every sample and measured with a Thermo Finnigan MAT 253 isotope ratio mass spectrometer coupled to an automated KIEL CARBO preparation device. Overall analytical reproducibility of the measurements is ±0.06 ‰ for $\delta^{13}C$ and ±0.08 ‰ for $\delta^{18}O$. Calibration was achieved via National Bureau of Standards NBS19 and NBS 20 material as well as through an internal laboratory standard of Solnhofen limestone. All values are reported as against the Vienna Pee Dee Belemnite Standard (expressed as ‰ vs. V-PDB).

In addition, water samples were measured to study the modern distribution of $\delta^{13}C_{DIC}$ in the water column. The water column samples were collected during the R/V Sonne S0201-2 via a water sampling rosette device [*Dullo et al.*, 2009]. Immediately after sub-sampling of Niskin bottles, water samples were poisoned with a saturated solution of mercury, sealed with wax and stored at 4 °C temperature until further treatment. On shore, 1 ml of water was injected through a septum into a vial with ca. 3 ml concentrated phosphoric acid flushed with pure Helium. After storage at room temperature for complete reaction the resultant CO_2 was transferred via a Finnigan Gas Bench II to a Finnigan MAT 252 gas mass spectrometer for determination of stable carbon isotopes. Results are given in δ-notation versus V-PDB. The precision of $\delta^{13}C$ measurements based on an internal laboratory standard has been reported to be better than ± 0.1 ‰.

The modern distribution of $\delta^{13}C_{DIC}$ shows large differences between the Sea of Okhotsk, the Bering Sea and the NW-Pacific (Figure 2.3). In the Bering Sea and NW-Pacific, the measured $\delta^{13}C_{DIC}$ of the water columns indicate a steep gradient, which is located around 100 m water depth and marks the mixed layer depth (MLD) of surface water with underlying water masses in winter. Beyond the MLD, $\delta^{13}C_{DIC}$ values decline to -0.6 to -0.7 ‰ and indicate the absence of fresh intermediate-water masses today. In turn, the $\delta^{13}C_{DIC}$ profile from the Sea of Okhotsk shows the presence of better-ventilated OSIW, expressed as a gently decline in $\delta^{13}C_{DIC}$ values within the water column between 200 – 800 m (Figure 2.3).
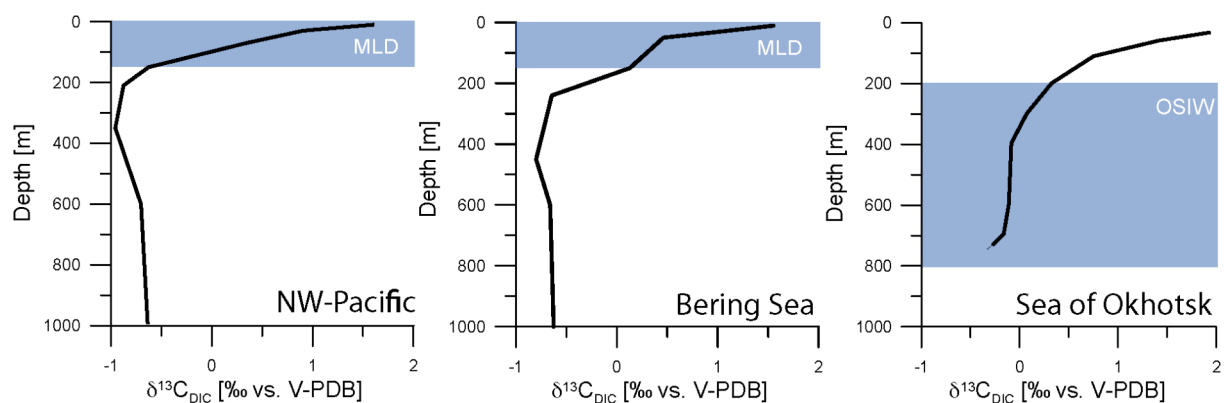
Figure 2.3: Modern distribution of $\delta^{13}C_{DIC}$ in the NW-Pacfic realm. on the left side: $\delta^{13}C_{DIC}$ profile of the water column inferred from Station SO201-2-2 (53° 55' N, 161° 49' E) in the NW-Pacific. in the middle: $\delta^{13}C_{DIC}$ profile of the water column inferred from Station SO201-2-67 (56° 04' N, 169° 14' E) in the western Bering Sea. on the right side: $\delta^{13}C_{DIC}$ profile of the water column inferred from Station LV29-84-3 (52° 42' N, 144° 13' E) in the Sea of Okhotsk [*Biebow et al.*, 2003]. Blue shaded areas mark the position of the MLD and OSIW, respectively.

The results of the $\delta^{13}C$ measurements on C. lobatulus contributed to the manuscript of past changes in intermediate water formation in the North Pacific during the last glacial termination, presented in Chapter 5. Results of stable isotope measurements on U. peregrina are integrated into the manuscript focuses on reconstruction of past millennial-scale changes in marine productivity and terrigenous matter supply in the NW-Pacific during the last glacial-interglacial cycle (Appendix 1).

2.3.5 Radiocarbon measurements

Radiocarbon measurements are mandatory to achieve a tight age control for high-resolution time series studies and were achieved from dozens of accelerated mass spectrometry ^{14}C age (AMS ^{14}C age) measurements on calcareous tests of planktonic foraminifera. Sample material for AMS ^{14}C age measurements comes from monospecific samples of the planktonic foraminifera *Neogloboquadrina pachyderma* sinistral. For this purpose 1000 – 1500 specimen were picked from the 125 – 250 μm fraction of the sieved sediment samples. In addition (and whenever possible), benthic foraminifera (mostly *U. peregrina*) were picked from larger fractions of the same samples to infer paleo-ventilation ages by means of the measured raw ^{14}C age difference between planktonic and benthic foraminifera. The radiocarbon dating has been performed by the National Ocean Science Accelerator Mass Spectrometry Facility (NOSAMS) at Woods Hole Oceanographic Institute (WHOI) and Leibniz-Laboratory for Radiometric Dating and Isotope Research at Kiel University. Radiocarbon ages have been reported according to the convention outlined by *Stuiver and Polach* [1977] and *Stuiver* [1980]. All radiocarbon ages from planktonic foraminifera were converted into calibrated 1-sigma calendar age ranges using the calibration tool Calib Rev 6.0 [*Stuiver and Reimer*, 1993] with the Intcal09 atmospheric calibration curve [*Reimer et al.*, 2009] and considering a constant reservoir age throughout the time period covered by the sediment records (discussed in section 2.3.7 Stratigraphy).

2.3.6 X-ray fluorescence measurements

The X-ray fluorescence (XRF) core scanner is a common tool to analyze the relative chemical composition of sediments directly at the surface of a split sediment core. XRF measurements have several advantages compared to conventional chemical analysis as it is non-destructive and relatively easy to achieve due to no time-consuming sample preparation. The XRF core scanning technique is based on the ejection of electrons from the inner shells of atoms, initiated by incoming X-ray radiation. The generated energy difference of the atomic shells, forced by the incoming X-ray radiation, leads to the emission of electromagnetic radiation, which is detected. Each element displays defined wavelengths of emitted radiation. The amplitudes of the peaks of different wavelengths (chemical elements) in the XRF spectrum are proportional to the concentration of the elements in the sediment [*Richter et al.*, 2006]. Sedimentary information from XRF measurements provide nearly continuous information of the chemical inventory of sediments due to the high sampling rate of the XRF core scanner and are an excellent tool to assess high-resolution time-series studies, stratigraphic correlations, and detailed sedimentary and climatic reconstructions on different time-scales.

Relative sedimentary elemental composition was measured using an Avaatech X-ray fluorescence (XRF) core scanner. The archive halves of the split sediment cores were covered with a 4 μm thin SPEXCerti Prep Ultralene® foil to prevent contamination of the measurement unit and desiccation of the sediment during the XRF measurements. Each core segment was triple-scanned for element

analysis at 1 mA and tube voltages of 10 kV (Al, Si, S, K, Ca, Ti, Fe), 30 kV (Cu, Zn, Br, Rb, Zr, Sr, Mo) and 50 kV (Ag, Cd, Sn, Te, Ba), using a sampling resolution of 1 cm and 30 s count time. Results are typically given as counts per second (cps).

The X-ray fluorescence measurements conducted during this study were used to assess a high-resolution chronostratigraphy (discussed in section 2.3.7 Stratigraphy) and also contributed to the manuscript on the reconstruction of past millennial-scale changes in marine productivity and terrigenous matter supply in the NW-Pacific during the last glacial-interglacial cycle (Appendix 1).

2.3.7 Stratigraphy

The deglacial stratigraphy is based on a set of radiocarbon measurements (AMS ^{14}C ages) and is further constrained with XRF core scanner data and shipboard logging data (color b*) for detailed inter-core correlation (Figure 2.4). The Ca intensity records (XRF) have been used to correlate prominent and similar structures between the different sediment records. Carbonate maxima (maxima in foraminifera abundance), which are indicated by maxima in Ca intensities (XRF), were preferentially dated to circumstance the problem of bioturbation effects. The Ca intensity pattern of all sediment records is marked by two intervals with high Ca intensities. These pronounced carbonate maxima are well known in the NW-Pacific realm and mark the B/A and the interval of the early Holocene [*Keigwin et al.*, 1992; *Keigwin*, 1998; *Gorbarenko et al.*, 2002; *Gorbarenko et al.*, 2005; *Caissie et al.*, 2010]. The observed carbonate maxima range from ca. 13,410 (core SO201-2-114KL) to 11,950 ^{14}C years (core SO201-2-85KL) and from ca. 10,800 (core SO201-2-12KL) to 9,570 ^{14}C years (SO201-2-77KL). The structure of these carbonate maxima is best resolved in NW-Pacific sediment record SO201-2-12KL, which provides sedimentation rates of up to 80 cm/kyr during these intervals. However, high-resolution record SO201-2-12KL indicates that the maxima consist of a sequence of carbonate spikes, which are not completely resolved in the other sediment cores. In particular, sediment records from Shirshov Ridge (Bering Sea) show lower average sedimentation rates of 10 – 15 cm/kyr and thus bioturbation effects could lead to stratigraphic uncertainties in these records. Hence, an average age of the carbonate spikes of the early Holocene carbonate maximum between cores SO201-2-77KL and SO201-2-85KL were calculated by the corresponding ^{14}C ages. By doing so the average ages of the carbonate spikes were defined (spike 1 = 9,760 ^{14}C years; spike 2 = 10,383 ^{14}C years). In general, the sequence of raw ^{14}C ages and their assignment to prominent carbonate structures is consistent between the sediment records (within a range of a few hundred years) and can be traced from the Bering Sea to the NW-Pacific and even into the Sea of Okhotsk (Figure 2.4). Thus, the registered temporal pattern of the carbonate maxima seems not to be significantly biased by water depth-dependent differences in carbonate dissolution at the investigated records, which range from 630 to 2200 m water depth. However, the ^{14}C ages of the carbonate maxima in the sediment records from the western Bering Sea records are about 200 years younger than in the
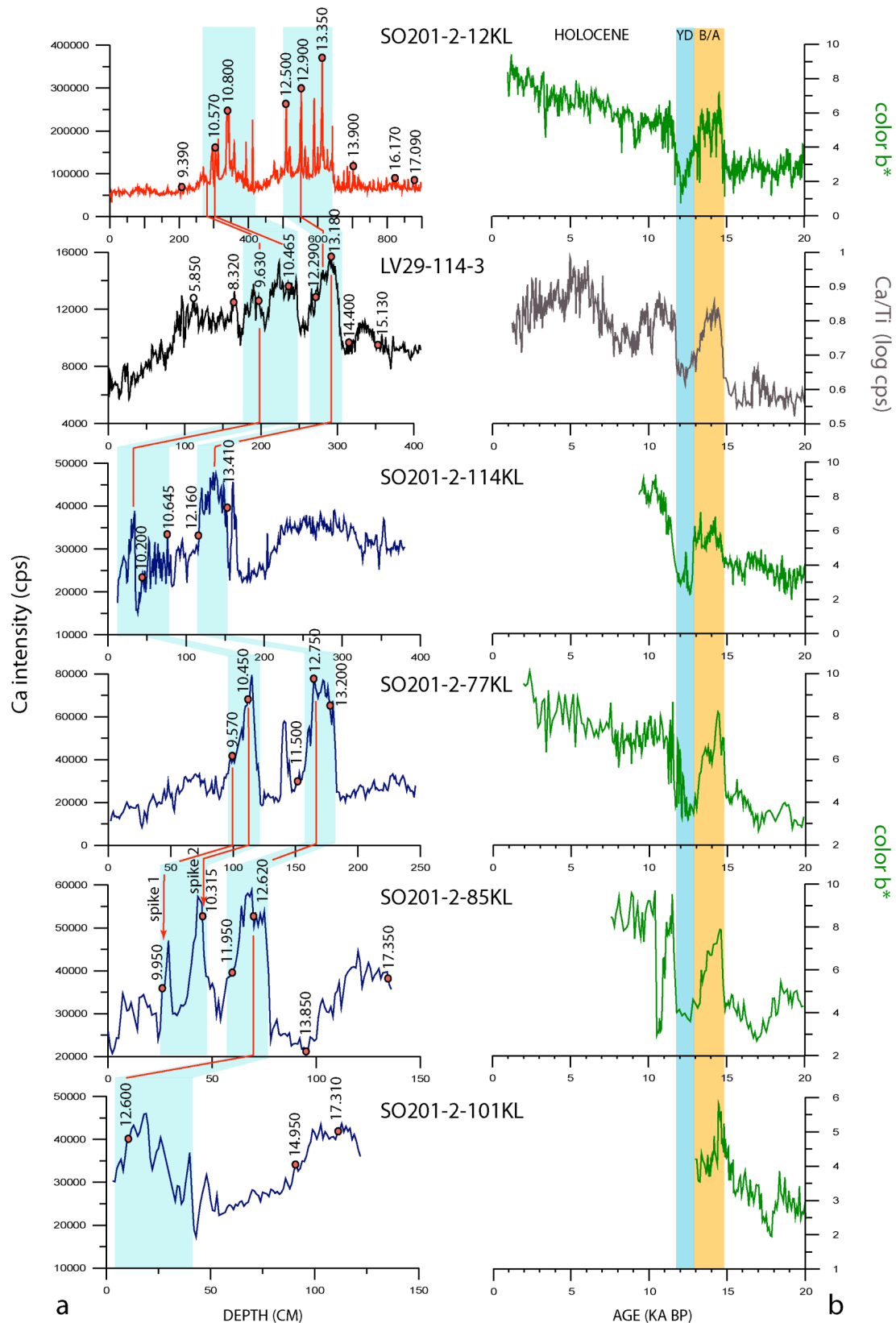
Figure 2.4: Deglacial stratigraphy of the sediment records used in this study. (a) XRF Ca intensity records from the NW-Pacific (in red), Sea of Okhotsk (in black) and Bering Sea records (in blue). Red spots and numbers indicate raw ^{14}C ages, red lines indicate stratigraphic cross correlation tie points. The raw ^{14}C age of 5,850 years in core LV29-114-3 was derived by correlation with neighbour core V34-98 [*Gorbarenko et al.*, 2002]. Blue shaded areas mark prominent carbonate maxima. (b) Shipboard core logging data (color b*, in green) used for detailed inter-core correlation of the sediment records from SO201-2 cruise. Core LV29-114-3 was correlated via Ca/Ti ratio derived from XRF data (in black). Blue and orange shaded areas in (b) mark the B/A and YD, respectively.

NW-Pacific and the Sea of Okhotsk. Since the Bering Sea records cover the full range of water depth (630 to 2200m) the temporal offset is likely caused by regionally different ^{14}C surface ocean reservoir effects.

The mid to late Holocene time interval is marked by very low carbonate contents in the NW-Pacific realm (Figure 2.4). Accordingly, the low abundance or complete absence of foraminifers impedes the planktonic ^{14}C-dating of the sediment records during this interval. However, the age control for core LV29-114-3 from the Sea of Okhotsk is improved in the middle Holocene via correlation to the well-dated neighbour core V34-98 [*Gorbarenko et al.*, 2002] in the Sea of Okhotsk (not shown) and thus provided one additional ^{14}C age to core LV29-114-3 (5,850 years) (Figure 2.4). In general, the Holocene stratigraphy of the sediment records is poorly conceived compared to the deglacial stratigraphy due to the lack of enough foraminiferal material preserved in the sediments.

To convert radiocarbon ages in calendar years a correction for the surface ocean reservoir age is necessary to balance for the ^{14}C reservoir effect of disequilibrium between the atmosphere and the upper-ocean and the input of old deep waters into the mixed layer. In the North Pacific, the surface ocean reservoir age has been reported to range from 600 to 1,000 years [*Southon et al.*, 1990; *Kuzmin et al.*, 2001; *McNeely et al.*, 2006; *Yoneda et al., 2007*]. Recent studies show some evidence that the reservoir age strongly varied over the course of the last 20 kyr. *Sarnthein et al.* [2006] and *Gebhardt et al.* [2008] suggest variable ^{14}C reservoir ages for the last 20 kyr derived from ^{14}C-plateau tuning. However, a more recent study claims that the surface ocean reservoir age was close to 730 years and varied by less than ±200 years during the last deglaciation in the NE-Pacific [*Lund et al.*, 2011]. Unfortunately, it is not possible to assess the variability of paleo-reservoir ages as the ^{14}C datings achieved here are not dense enough to identify the age-calibrated ^{14}C-plateaus. Hence, a constant reservoir age over time was applied with 700 years for the western Bering Sea cores and 900 years for the NW-Pacific and the Sea of Okhotsk records. Nevertheless, the comparison between both approaches (constant and variable reservoir age correction) makes sense at this point and is given in Figure 2.5. If variable reservoir ages were assumed for the deglacial portion of the sediment records according to the ^{14}C-plateaus [*Sarnthein et al.*, 2007], it would only slightly affect the stratigraphy compared to constant reservoir ages. As exemplarily shown for an SST record in the western Bering Sea, the first SST maximum in the B/A (according to the age model with constant reservoir ages) would be around 14.3 ka BP. Compared to the age model with variable reservoir ages, the first SST maximum would occur at 14.5 ka BP within ^{14}C-plateau 1 (P1), which ranges from 14.25 – 14.85 ka BP (Figure 2.5). However, after converting the ^{14}C ages into calendar years, the application of regionally different reservoir ages (constant over time) provides the best chronostratigraphic match between the high-resolution core-logging records (Figure 2.4 b). This also assumes that the pattern of XRF Ca/Ti ratios in the Sea of Okhotsk and in all the other records occurred synchronously. Color b*
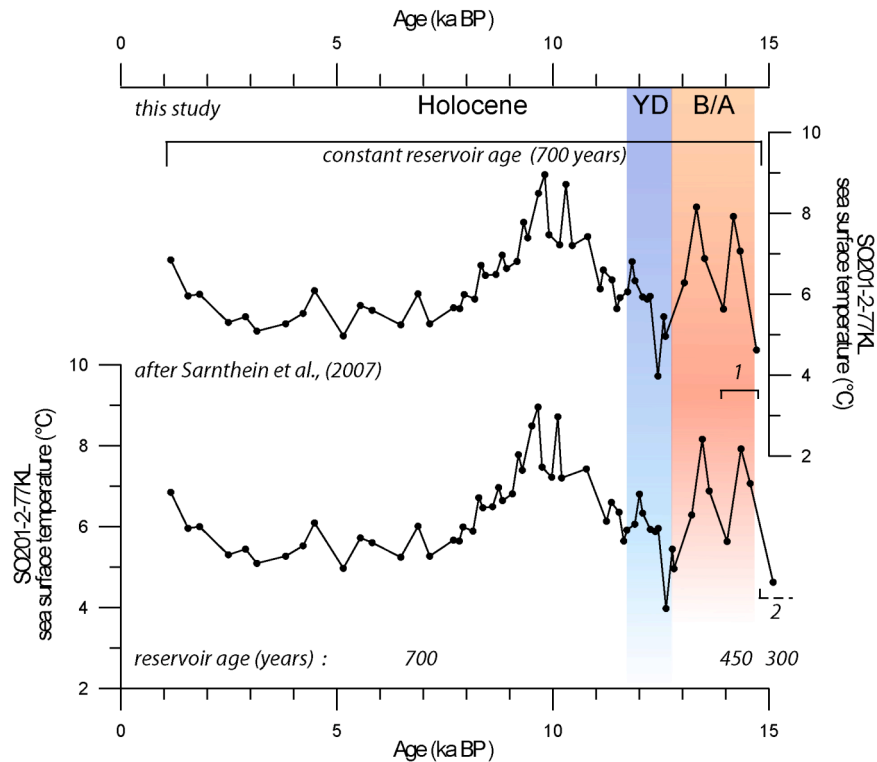
Figure 2.5: Comparison of different age constraints applied on sediment core SO201-2-77KL from the western Bering Sea. (lower curve): SST record from sediment core SO201-2-77KL with variable reservoir age correction according to the ^{14}C-plateaus [*Sarnthein et al.*, 2007]. Black lines indicate the position and boundaries of the ^{14}C-plateaus (P1 and P2). Reservoir age corrections are shown at the bottom. (upper curve) SST record from sediment core SO201-2-77KL with constant reservoir age correction over time (used in this study).

is reported to be a good proxy for variations in biogenic opal and total organic matter content of anoxic sediments [*Debret et al.*, 2006] and generally correlates with those of measured biogenic opal in the sediment records (not shown). The Sea of Okhotsk is marked by strong changes in $CaCO_3$ content rather than an increase of diatom production during the deglaciation [*Seki et al.*, 2009]. Hence, the high-resolution core logging data (XRF Ca/Ti and color b*) was used to improve the age constraints by moving the age control points within the 1-sigma calendar age range between all records. This provides a remarkable fit between the various records as indicated by the tight inter-core correlation of all sediment records. It allows the comparison to other sediment archives in the subarctic North Pacific and far beyond on millennial time-scales (within an uncertainty of a few hundred years) prerequisite for all paleoceanographic reconstructions outlined in the following chapters.

Chapter 3: Sea surface temperature variability and sea-ice extent in the subarctic northwest Pacific during the past 15,000 years

Lars Max[1], Jan-Rainer Riethdorf[2], Ralf Tiedemann[1], Maria Smirnova[3], Lester Lembke-Jene[1], Kirsten Fahl[1], Dirk Nürnberg[2], Alexander Matul[3] and Gesine Mollenhauer[1]

[1]Alfred Wegener Institute for Polar and Marine Research, Am Handelshafen 12, D-27570 Bremerhaven, Germany; E-Mail: Lars.Max@awi.de

[2]GEOMAR | Helmholtz-Zentrum für Ozeanforschung Kiel, Wischhofstr. 1-3, D-24148 Kiel, Germany

[3]P.P. Shirshov Institute of Oceanology, Nakhimovsky prospect 36, 117997 Moscow, Russia

Abstract

Past changes in North Pacific sea surface temperatures and sea-ice conditions are proposed to play a crucial role in deglacial climate development and ocean circulation but are less well known than from the North Atlantic. Here we present new alkenone-based sea surface temperature records from the subarctic northwest Pacific and its marginal seas (Bering Sea and Sea of Okhotsk) for the time interval of the last 15 kyr, indicating millennial-scale sea surface temperature fluctuations similar to short-term deglacial climate oscillations known from Greenland ice-core records. Past changes in sea-ice distribution are derived from relative percentage of specific diatom groups and qualitative assessment of the IP$_{25}$ biomarker related to sea-ice diatoms. The deglacial variability in sea-ice extent matches the sea surface temperature fluctuations. These fluctuations suggest a linkage to deglacial variations in Atlantic meridional overturning circulation and a close atmospheric coupling between the North Pacific and North Atlantic. During the Holocene the subarctic North Pacific is marked by a complex sea surface temperature pattern, which does not support the hypothesis of a Holocene seesaw trend in temperature development between the North Atlantic and the North Pacific.

3.1 Introduction

Knowledge of the deglacial SST development and variability in sea-ice extent in the subarctic Pacific provide important climate boundary conditions to understand oceanic/atmospheric teleconnections between the Atlantic and the Pacific and evaluating most recent hypotheses related to deep water formation in the North Pacific (N-Pacific). The pattern of sea surface temperature (SST) variability in the subarctic N-Pacific realm as well as the timing of SST changes during the last glacial termination and the Holocene have remained elusive. In general, the spatial and temporal development of SSTs in the N-Pacific on centennial-millennial time-scales is not well conceived for several reasons: (1) SST

reconstructions from the N-Pacific are sparse (Figure 3.1); (2) The available SST reconstructions are based on a variety of different temperature proxies, which may lead to inconsistent temperature signals as the recording of each proxy can be afflicted with a seasonal bias and/or is related to a different water depth; (3) The availability of carbonate-bearing sediment records with high sedimentation rates is restricted to shallow water depths due to the shallow position of the calcite compensation depth in the N-Pacific (< 3000 m); (4) The absence of carbonate for major parts in N-Pacific sediments excludes the application of carbonate-based proxies and ^{14}C-datings on planktonic foraminifers, thus limiting detailed climate reconstructions; (5) Changes in paleo-^{14}C reservoir ages are not well defined and may lead to imprecise age models in the N-Pacific [*Sarnthein et al.*, 2004].

As a consequence, model simulations and proxy-based interpretations led to partly contradictory results concerning the deglacial and Holocene SST variability in the N-Pacific and its underlying mechanisms during the past 15 kyr. Studies with general circulation models (GCMs) suggest both an in-phase behavior of deglacial SST pattern (~15 - 10 ka BP) between the North Atlantic (N-Atlantic) and the N-Pacific [*Mikolajewicz et al.*, 1997; *Vellinga and Wood*, 2002; *Okumura et al.*, 2009; *Chikamoto et al.*, 2012] as well as an out-of-phase response [*Saenko et al.*, 2004; *Schmittner et al.*, 2007; *Okazaki et al.*, 2010]. The in-phase behavior has been related to rapid atmospheric teleconnections, acting on years to decades. The out-of-phase response has been attributed to oceanic readjustments of the Atlantic meridional overturning circulation (AMOC). More specifically, the simulated reduction of the AMOC as a consequence of enhanced sea surface freshening in the N-Atlantic (like during Heinrich 1 and the Younger Dryas) resulted in a strengthening of the Pacific meridional overturning circulation (PMOC) and an associated warming in the N-Pacific. The warming resulted from an enhanced poleward heat transport from the subtropics to the N-Pacific. Accordingly, the proposed seesaw between AMOC reduction and PMOC intensification suggests a N-Pacific warming during Heinrich 1 (H1) and the Younger Dryas (YD). In turn, the reestablishment of the AMOC (shutdown of PMOC) leads to a surface cooling in the N-Pacific during the Bølling/Allerød (B/A) and the early Holocene. Consequently, the interplay between the two meridional overturning cells is expected to provide millennial-scale out-of-phase fluctuations in SST between the N-Atlantic and the N-Pacific [e.g. *Saenko et al.*, 2004].

The few available deglacial SST proxy records from the N-Pacific and its adjacent seas also provide a quite inconsistent picture. They support both an in-phase and out-of-phase relationship with regard to the N-Atlantic SST development or show a pattern of continuously cold SSTs from the last glacial to the onset of the Holocene (no warming event during the B/A). For example, a remarkable similarity between the Greenland/N-Atlantic temperature pattern and changes in subarctic N-Pacific SST, based on alkenone paleothermometry, radiolarian assemblages and dinocyst studies, was found in sediment records from the subarctic northeast Pacific (NE-Pacific) [*Kienast and McKay*, 2001; *Pisias et al.*, 2001; *Seki et al.*, 2002; *Barron et al.*, 2003], the Bering Sea [*Caissie et al.*, 2010] and the Sea of
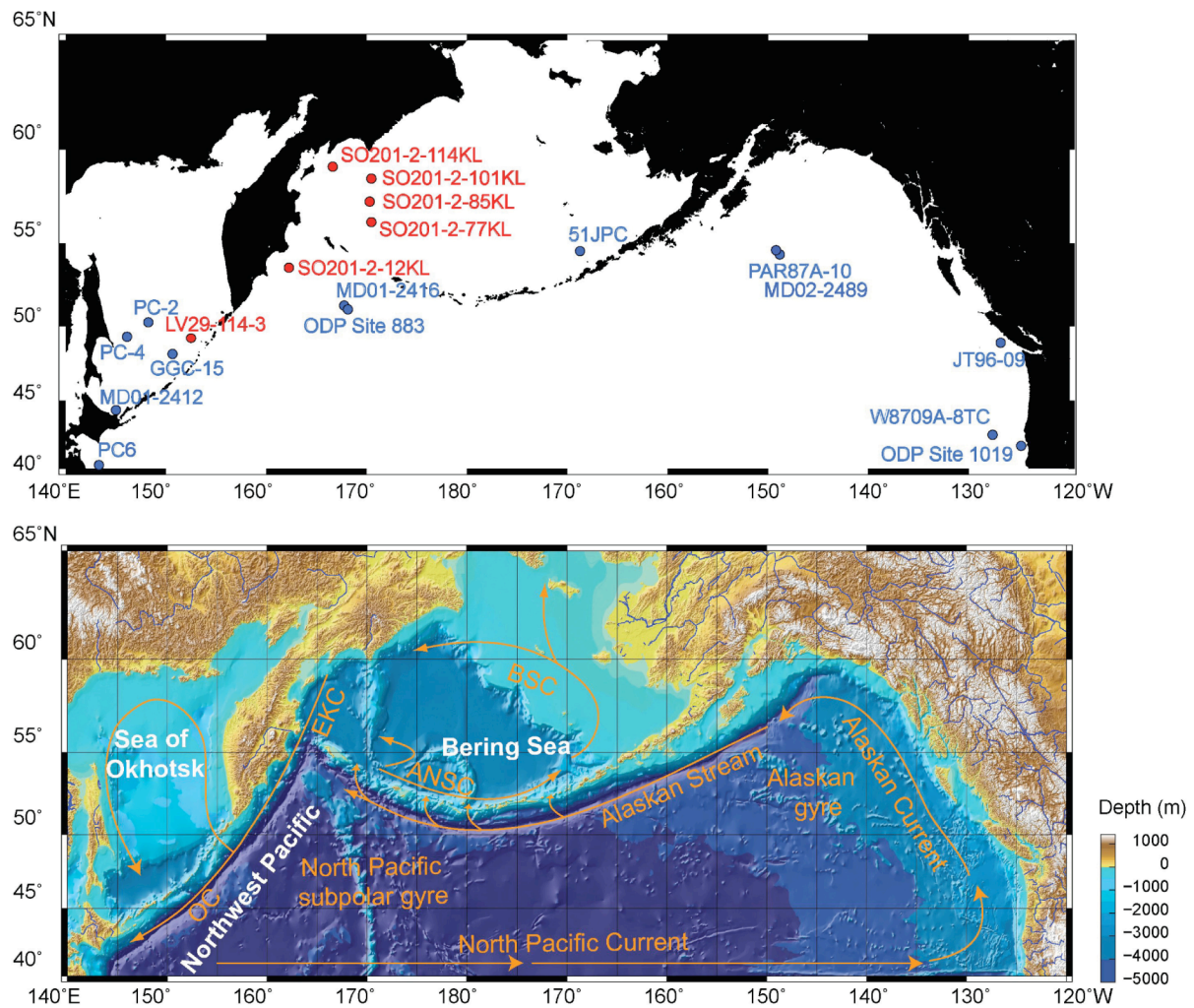
Figure 3.1 (upper hand): Core sites in the subarctic Pacific from this study (in red), together with published sediment records (in blue) in the Sea of Okhotsk (PC-2 and PC-4, *Seki et al.*, 2004a; GGC-15, *Ternois et al.*, 2000; MD01-2412, *Harada et al.*, 2006b) the Bering Sea (51JPC, *Caissie et al.*, 2010) and the N-Pacific (PC6, *Minoshima et al.*, *2007*; ODP Site 883, *Kiefer et al.*, *2001*; MD01-2416, *Sarnthein et al.*, *2004*; PAR87A-10, *Pisias et al.*, 2001; MD02-2489, *Gebhardt et al.*, 2008; JT96-09, *Kienast and McKay*, 2001; W8709A-8TC, *Pisias et al.*, 2001; ODP Site 1019, *Barron et al.*, 2003). (lower hand): Bathymetric chart of the subarctic Pacific with the general surface circulation pattern indicated by orange arrows (modified after *Stabeno et al.*, 1999). OC = Oyashio Current; EKC = East Kamchatka Current; ANSC = Aleutian North Slope Current; BSC = Bering Slope Current.

Okhotsk [*Ternois et al.*, 2000]. These records rather argue for an in-phase relationship of temperature fluctuations between the N-Pacific and N-Atlantic. On the other hand N-Pacific SST records from pelagic core MD01-2416 and MD02-2489, derived from planktonic Mg/Ca ratios and from census counts of planktonic foraminifera using the SIMMAX transfer function, indicate a different SST development. These records suggest temperature maxima during H1 and the YD and thus millennial-scale fluctuations out-of-phase with the Greenland/N-Atlantic temperature pattern [*Sarnthein et al.*, 2004; *Kiefer and Kienast*, 2005; *Sarnthein et al.*, 2006; *Gebhardt et al.*, 2008]. The timing of temperature changes is possibly best constrained in sediment record MD01-2416 from the pelagic NW-Pacific. Unfortunately, this record allowed no direct comparison between Mg/Ca- and alkenone-derived SSTs. Other records provide inconsistent patterns of deglacial SST variability. For example, records from the Sea of Okhotsk and the Pacific continental margin of Japan show no SST maximum

during the B/A and the deglacial temperature rise does not appear before the end of the YD [*Seki et al.*, 2004a; *Minoshima et al.*, 2007].

For the Holocene, *Kim et al.* [2004] summarized alkenone-based SST reconstructions from the N-Pacific and the N-Atlantic and used a coupled atmosphere-ocean general circulation model to assess the inter-oceanic teleconnected climate variability. Their investigations led to the hypothesis of a long-term temperature seesaw between the N-Atlantic and the N-Pacific. Their model-supported proxy-interpretation suggests a warming trend in the N-Pacific and a cooling trend in the N-Atlantic for the time period of the last 7 kyr. The inverse SST trends between the N-Atlantic and the N-Pacific have been attributed to an atmospheric interaction of the positive Pacific North American (PNA) and the negative North Atlantic Oscillation (NAO) phase. However, the derived warming trend in the N-Pacific relies on one proxy record from the NW-Pacific only [*Ternois et al.*, 2000], which is marked by low alkenone concentrations (close to the detection limit) within the time interval spanning the last 8 kyr BP.

Apart from the differences in Holocene and deglacial Pacific SST patterns, an exact chronostratigraphic correlation between Greenland ice-core records and ^{14}C-dated deglacial marine climate records is limited to assumptions about the ^{14}C reservoir age of the surface water, the habitat in which planktonic foraminifera incorporate the ^{14}C signal into their carbonate shells. Knowledge of the ^{14}C reservoir age is a necessary precondition for converting radiocarbon ages into calendar years in order to balance for the ^{14}C disequilibrium between the upper ocean and the atmosphere. Since the variability of past reservoir ages is largely unknown, most studies assume a constant reservoir effect over time, thereby taking an uncertainty of several hundred years into account. Such uncertainties may increase to more than thousand years within time intervals associated with prominent atmospheric ^{14}C-plateaus (i.e. intervals of very low ^{14}C change with calendar age). Such plateaus especially mark the period of the last deglaciation. Accordingly, the lead and lag of different proxies indicative of rapid climate change in the subarctic Pacific are difficult to constrain in comparison to the Greenland climate signal.

Here we present the first alkenone-derived high-resolution SST estimates from the subarctic NW-Pacific continental margin and the western Bering Sea as well as a new record from the southeastern Sea of Okhotsk. Our study provides a stratigraphic framework for the NW-Pacific realm, which is based on detailed core-to-core correlations and 37 AMS ^{14}C datings. This framework is best developed between 20 to ~6 ka BP and can be used via X-ray fluorescence (XRF) core scanner data (e.g. Ca intensities) to transfer ages to other available and future sediment records. The relatively high sedimentation rates enable us to investigate past SST changes on multi-centennial to millennial time-scales in comparison to rapid climate oscillations known from other parts of the N-Pacific and the N-

Atlantic for the last 15 kyr. Additionally, relative percentages of specific diatom groups in combination with qualitative measurements of the C_{25} monounsaturated hydrocarbon (IP_{25}) are used to assess past changes in the sea-ice extent [*Belt et al.*, 2007; *Müller et al.*, 2009] with regard to short-term warm/cold fluctuations. Our data suggest that the subarctic NW-Pacific region is characterized by a deglacial pattern of SST fluctuations, which shows a strong similarity to the Greenland/N-Atlantic SST pattern. The sea-ice distribution is closely coupled to the pattern of SST development. The SST records from the NW-Pacific realm presented here close a spatial gap in the N-Pacific and provide new insights into the spatio-temporal pattern of millennial-scale SST variability during the deglacial period from ~15 - 10 ka BP and the Holocene. Our results shed new light onto the discussion of whether the deglacial temperature development in the NW-Pacific supports an in-phase or an out-of-phase behavior with respect to the N-Atlantic SST development and the related seesaw between AMOC and PMOC. With respect to the Holocene the SST reconstructions are also used to reconsider the hypothesis of a seesaw mechanism that led to a contrasting long-term temperature trend between the N-Atlantic and the N-Pacific (temperature seesaw) during the past 7 kyr.

3.2 Regional setting

The subarctic Pacific regions are characterized by a large, seasonal variability in SST and sea-ice distribution, tightly coupled to atmospheric pressure cells, which in turn are influenced by large-scale interannual-decadal variability associated with the Pacific - North American Oscillation (PNA) and the Pacific Decadal Oscillation (PDO) [*Niebauer*, 1988; *Mantua et al.*, 1997; *Niebauer*, 1998; *Overland et al.*, 2002]. During winter, the contrast between the Siberian High and Aleutian Low-Pressure System (ALPS) brings cold air masses from the Arctic to the subarctic Pacific, which results in strong sea surface cooling and mixing of nutrient-rich subsurface waters and favors the expansion of sea-ice in the Bering Sea and Sea of Okhotsk. During summer, both increased insolation and weakening of the ALPS lead to warm SSTs, ice-free conditions and strong upper ocean stratification [*Ohtani et al.*, 1972]. This leads to strong, seasonal temperature differences between winter (0 – 2 °C) and summer (8 – 10 °C) SSTs in the subarctic NW-Pacific and its marginal seas. Maxima in biogenic productivity occur during spring (dominated by diatoms) and late summer (dominated by coccolithophorids).

The structure of the upper water column is characterized by the presence of a strong halocline, which is a permanent feature of the subarctic Pacific. It forms a barrier for the heat and gas exchange between the deep ocean and the atmosphere as well as for the supply of nutrients into the photic zone. This leads to the highest carbon export efficiency in the world oceans and a net sink of atmospheric CO_2 today [*Honda et al.*, 2002].

The surface circulation of the subarctic NW-Pacific follows a large-scale cyclonic pattern of surface currents, which regulate the exchange of heat and nutrients between different ocean regions. The

superior large-scale circulation pattern in the subpolar N–Pacific consists of the Kuroshio - North Pacific Current system in the south and two counterclockwise circulating systems: the Alaskan gyre in the east and the western North Pacific subpolar gyre (Figure 3.1). The North Pacific Current (the Kuroshio extension) transports relatively warm water masses eastward into the Alaskan gyre. The Alaskan Stream forms the northern boundary current and transports water masses from the Alaskan gyre along the Aleutian Islands into the western subpolar gyre, thereby entering the Bering Sea through several passages between the Aleutian Islands. This inflow drives a large-scale counterclockwise surface circulation in the Bering Sea. The surface waters leave the Bering Sea via the Bering Strait into the Arctic Ocean but mainly through the Kamchatka Strait back into the N–Pacific via the East Kamchatka Current (EKC). The EKC delivers nutrient-rich waters from the Bering Sea into the NW-Pacific [*Stabeno et al.*, 1999] and represents the western branch of the North Pacific subpolar gyre. On its path to the south, a part of the EKC enters the Sea of Okhotsk through the Kurile Island Arc, thereby influencing the water mass signature of the Okhotsk gyre. During winter, the intrusion of the relatively warm EKC promotes ice-free conditions around the southern tip of Kamchatka [*Seki et al.*, 2004b] (Figure 3.1).

3.3 Material and Methods

We investigated six piston cores from the western Bering Sea, the continental slope of east Kamchatka and the southeastern Sea of Okhotsk (Figure 3.1). Sediment records were obtained during cruises LV29 KOMEX Leg 2 with RV Akademik Lavrentyev in 2002 and RV Sonne during SO201 KALMAR Leg 2 in 2009. Core site selection was done by intensive sediment echo-sounding studies onboard to detect high-resolution sediment deposits, which are located well above the shallow calcite compensation depth (CCD). Our sediment records provide sufficient amounts of carbonate-bearing material for detailed paleoceanographic reconstructions (Table 3.1) except the younger part of the Holocene. During the last 6 kyr, when the productivity of calcareous plankton was generally low in the NW-Pacific, the productivity of diatoms was high. High amounts of silicious diatom tests further diluted the quantity of planktonic carbonate shells within the sediments [*Gorbarenko et al.*, 2002].

Table 3.1: Core locations in the subarctic NW-Pacific, Sea of Okhotsk and western Bering Sea as well as the performed proxy studies.

Sediment core	Latitude (°N)	Longitude (°E)	Depth (mbsl)	Study area	performed proxy* studies
LV29-114-3	49°22.54'	152°53.23'	1765	Sea of Okhotsk	$U^{K'}_{37}$, IP_{25}, $CaCO_3$, CL, [14]C
SO201-2-12KL	53°59.47'	162°22.51'	2145	NW-Pacific	$U^{K'}_{37}$, IP_{25}, Opal, DS, CL, [14]C
SO201-2-77KL	56°19.83'	170°41.98'	2135	western Bering Sea	$U^{K'}_{37}$, IP_{25}, CL, [14]C
SO201-2-85KL	57°30.30'	170°24.77'	968	western Bering Sea	$U^{K'}_{37}$, IP_{25}, CL, [14]C
SO201-2-101KL	58°52.52'	170°41.45'	630	western Bering Sea	$U^{K'}_{37}$, IP_{25}, CL, [14]C
SO201-2-114KL	59°13.87'	166°59.32'	1376	western Bering Sea	$U^{K'}_{37}$, IP_{25}, CL, [14]C

* $U^{K'}_{37}$ - alkenone paleothermometry; IP_{25} - sea-ice diatoms biomarker; Opal - wt.% biogenic opal; $CaCO_3$ - wt.% $CaCO_3$; CL - Core logging; [14]C - AMS ^{14}C datings; DS - Diatom studies

3.3.1 Stratigraphic approach

3.3.1.1 AMS-14C-dating

AMS ^{14}C-ages were measured on monospecific samples of the planktonic foraminifera *Neogloboquadrina pachyderma* sinistral (*N. pachyderma* sin.) from 125 – 250 µm fraction. The radiocarbon dating has been performed by the National Ocean Science Accelerator Mass Spectrometry Facility (NOSAMS) at Woods Hole Oceanographic Institute (WHOI) and Leibniz-Laboratory for Radiometric Dating and Isotope Research at Kiel University. Radiocarbon ages have been reported according to the convention outlined by *Stuiver and Polach* [1977] and *Stuiver* [1980]. All radiocarbon ages were converted into calibrated 1-sigma calendar age ranges using the calibration tool Calib Rev 6.0 [*Stuiver and Reimer*, 1993] with the Intcal09 atmospheric calibration curve [*Reimer et al.*, 2009] and considering a constant reservoir age throughout the time period covered by the sediment records (Table 3.2).

3.3.1.2 Biogenic Opal and CaCO$_3$

Biogenic opal and CaCO$_3$ were measured at GEOMAR, Kiel. Biogenic opal concentrations were determined from bulk sediment, using the automated leaching method according to *Müller and Schneider* [1993] by molybdate-blue spectrophotometry. Results are given with respect to the mineral correction of *DeMaster* [1981].

Total carbon contents (TC) were determined with a CARLO ERBA Model NA 1500 CNS analyzer. TC was measured on bulk sediments, total organic carbon was derived from decalcified samples. The inorganic carbon (CaCO$_3$) content was calculated as the difference between TC and TOC as follows:

$$CaCO_3 = (TC - TOC) \times 8.333 \quad (Eq.1)$$

3.3.1.3 Core logging data

Relative sedimentary elemental composition was measured using the Avaatech X-ray fluorescence (XRF) core scanner at the Alfred Wegener Institute for Polar and Marine Research, Bremerhaven.

Each core segment was triple-scanned for element analysis at 1 mA and tube voltages of 10 kV (Al, Si, S, K, Ca, Ti, Fe), 30 kV (Cu, Zn, Br, Rb, Zr, Sr, Mo) and 50 kV (Ag, Cd, Sn, Te, Ba), using a sampling resolution of 1 cm and 30 s count time.

Color and light reflectance properties of the sediment cores have been measured with a Minolta CM 508d hand-held spectrophotometer directly after core splitting onboard [*Dullo et al.*, 2009]. Measurements were conducted at 1 cm interval. Reflectance data was converted into L*, a* and b* color space with the software Spectramagic.

Table 3.2: AMS ^{14}C ages of the sediment records with calibrated calendar age ± 1σ (years) and applied reservoir age correction used in this study.

Laboratory Number	Sediment Core	Core Depth (cm)	Radiocarbon Age (years)	Calendar Age ±1σ (years)	Reservoir Age (years)
transferred age	LV29-114-3	108	5850±60[1]	5607-5730	900
OS-88042		162	8320±40	8236-8310	900
KIA30864		197	9630±50	9764-10067	900
KIA30863		232	10465±50	10808-11080	900
KIA30867		272	12290±55	13164-13308	900
KIA30865		292	13180±60	13960-14457	900
KIA30868		317	14400±80	16538-16827	900
KIA30866		352	15130±80	17117-17497	900
OS-85655	SO201-2-12KL	210	9390±40	9484-9527	900
KIA44680		295	10570±50	11080-11191	900
OS-87895		340	10800±65	11231-11368	900
OS-92047		508	12500±50	13340-13498	900
OS-87891		550	12900±50	13782-13918	900
OS-87902		610	13350±65	14219-14752	900
OS-92150		695	13900±55	15227-15872	900
KIA44682		820	16160±80	18491-18666	900
KIA44683		875	17090±90	19254-19457	900
OS-85671	SO201-2-77KL	105	9570±45[2]	10051-10152	700
OS-85658		115	10450±40[3]	11174-11222	700
OS-90700		155	11500±50	12608-12727	700
OS-85657		167-170	12750±50	13823-13967	700
OS-85664		180	13200±45	14501-14945	700
OS-85665	SO201-2-85KL	26	9950±40[2]	10378-10507	700
KIA42231		45	10315±65[3]	10791-10966	700
OS-85669		60	11950±45	13104-13217	700
KIA42232		70	12620±90	13665-13887	700
OS-87896		95	13850±55	15822-15803	700
OS-87890		135	17350±65	19575-19895	700
KIA42233		155	20720±160	23706-24194	700
OS-87887	SO201-2-101KL	10	12600±55	13686-13838	700
OS-88041		90	14950±60	17165-17506	700
KIA42229		110	17310±120	19541-19919	700
transferred age		140	20720±160[4]	23706-24194	700
KIA42230		190	22510±190	25876-26351	700
KIA42506		260	29270±440	32121-33539	700
KIA42235	SO201-2-114KL	39	10200±70	10660-10805	700
KIA42236		76-78	10645±50	11249-11404	700
KIA42237		114	12160±80	13249-13403	700
KIA42238		153	13410±100	14727-15237	700

[1] - [14]C age transferred from sediment core V34-98 [*Gorbarenko et al.*, 2002]

[2] - [14]C ages used to define the carbonate spike 1

[3] - [14]C ages used to define the carbonate spike 2

[4] - [14]C age transferred from sediment core SO201-2-85KL

3.3.2 Alkenone analysis and sea surface temperatures ($U^{k'}_{37}$)

Discrete samples (5 – 10 g) were taken from bulk sediment, freeze-dried and stored frozen until further analysis. Samples were extracted with an accelerated solvent extractor (ASE-200, Dionex) at

100 °C and 1000 psi for 15 minutes by using dichlormethane (DCM) as a solvent. Remaining extracts were separated by silica gel column chromatography into three sub-fractions with the following mixture of solvents: fraction 1, 5 ml Hexane; fraction 2, a mixture of 5 ml DCM\Hexane (1:1); fraction 3, 5 ml DCM. Alkenones were eluted in the third fraction and prepared in 100 µl Hexane. The third fraction was measured at the Alfred Wegener Institute for Polar and Marine Research (AWI), Bremerhaven, using a HP 6890 gas chromatograph, equipped with a cold injection system, a DB-1MS fused silica capillary column (60 x 0.32 mm inner diameter, film thickness of 0.25 µm) and a flame ionization detector. Individual alkenone (C37:3, C37:2) identification was based on the retention time and the comparison with an external standard, which were also used for controlling the instrument stability. The alkenone unsaturation index ($U^{k'}_{37}$) as proxy for SST [*Brassell et al.*, 1986; *Prahl and Wakeham*, 1987] was calculated following the relationship between $U^{k'}_{37}$ and temperature as proposed by *Müller et al.* [1998], which is based on a global core-top calibration (60 °N – 60 °S):

$$U^{k'}_{37} = 0.033\,T\ (°C) + 0.044 \quad (Eq.2)$$

The standard error of this calibration is reported as +/- 0.050 $U^{k'}_{37}$-units or +/- 1.5 °C. However, it has to be mentioned that for the lower end of the used temperature calibration a larger error is reported, but still keeps its significance in conjunction to other results from this study. It is also known that in the subpolar N-Pacific, alkenone producers are limited to specific seasons and represent more likely the late summer/early fall SST [*Harada et al.*, 2003; *Harada et al.*, 2006a; *Seki et al.*, 2007]. Nevertheless, for a direct comparison to other studies, we decided to use the calibration after *Müller et al.* [1998] mentioned above, which is widely used in the N-Pacific and other regions rather than the polar temperature function of the Southern Ocean as proposed by *Sikes et al.* [1997].

3.3.3 Qualitative assessment of sea-ice distribution (IP_{25}) and microfossil studies (diatoms)

Recently it has been recognized that when detected in marine sediments, the C_{25} isoprenoid lipid (IP_{25}) biosynthesized by Arctic sea-ice diatoms acts as a proxy for previous spring sea-ice occurrence and subsequent melt [*Belt et al.*, 2007]. We performed qualitative IP_{25} analysis on selected samples, based on significant changes in our proxy records and reflecting different climate intervals according to our age model. For this purpose the polar fraction (fraction 1, see above) of selected samples were measured with an Agilent 6850 GC (30 m HP-5MS column, 0.25 mm i.d., 0.25 µm film thickness) coupled to an Agilent 5975 C VL mass selective detector. The GC oven was heated from 60 °C to 150 °C at 15 °C min^{-1}, and then at 10 °C min^{-1} to 320 °C (held 15 min.). Operating conditions for the mass spectrometer were 70 eV and 230 °C (ion source). Helium was used as carrier gas. Identification of IP_{25} is based on comparison of its retention time and mass spectra with published data [*Belt et al.*, 2007]. The measurements were carried out using SIM (selected ion monitoring) mode (for further details see *Müller et al.*, 2011; *Fahl and Stein*, in review). The Kovats index is 2085.

Diatom analysis was carried out on discrete samples (approximately every 10 cm) for NW-Pacific core SO201-2-12KL. Observations using a compound light-microscope were made at 1000X magnification; at least 300-500 valves were counted per sample. The number of diatom valves per gram of sediments was estimated. Results are given as relative percentage of diatom species *Fragilariopsis oceanica* (Cleve) Hasle (*F. oceanica*) as sea-ice indicator, and *Neodenticula seminae* (Simonsen & Kanaya) Akiba & Yanagisawa (*N. seminae*) related to open-water conditions.

3.4. Results

3.4.1 Age model

The color and XRF records have been used to correlate prominent and similar structures between sediment records. This approach also enabled a transfer of conventional ^{14}C ages from one core to another (Figure 3.2; Table 3.2). We preferentially dated carbonate maxima (maxima in planktonic foraminifer abundance), which are indicated by maxima in Ca intensities (XRF), to avoid age artefacts due to bioturbation effects. Figure 3.2 shows the Ca intensity records and a detailed core-to-core correlation of our studied core sites. The pattern is marked by two intervals with high Ca intensities. These pronounced carbonate maxima are well known in the NW-Pacific realm and mark the B/A and the interval of the early Holocene [*Keigwin et al.*, 1992; *Keigwin*, 1998; *Gorbarenko et al.*, 2002; *Gorbarenko et al.*, 2005; *Caissie et al.*, 2010]. The prominent carbonate maxima range from ca. 13,410 (SO201-2-114KL) to 11,950 ^{14}C years (SO201-2-85KL) and from ca. 10,800 (SO201-2-12KL) to 9,570 ^{14}C years (SO201-2-77KL). The structure of these carbonate maxima is best resolved in NW-Pacific sediment record SO201-2-12KL, which provides sedimentation rates of up to 80 cm/kyr for these intervals. However, this record suggests that the maxima consist of a sequence of carbonate spikes, which are not fully resolved in the other cores. At Shirshov Ridge, the interplay of lower sedimentation rates and bioturbation effects may have led to stratigraphic uncertainties in the early Holocene. In Shirshov cores SO201-2-77KL and SO201-2-85KL, the match between carbonate spikes 1 and 2 (Figure 3.2) and their corresponding ^{14}C ages provide an uncertainty of up to a few hundred years. In this case, we calculated and used an average ^{14}C age for each carbonate spike (spike 1 = 9,760 ^{14}C years; spike 2 = 10,383 ^{14}C years). At high-resolution core SO201-2-114KL from the northwestern continental margin of the Bering Sea, laminated sediment deposits characterize the intervals of both carbonate maxima (Figure 3.2).

The mid to late Holocene time interval is marked by low carbonate contents in the NW-Pacific realm. Accordingly, the low abundance or complete absence of foraminifers prevented planktonic ^{14}C-dating of our records. However, for core LV29-114-3 from the Sea of Okhotsk, we improved the age control via correlation to the well-dated neighbor core V34-98 [*Gorbarenko et al.*, 2002] and assigned one additional ^{14}C age to core LV29-114-3 (5,850 years) as given in Figure 3.3.
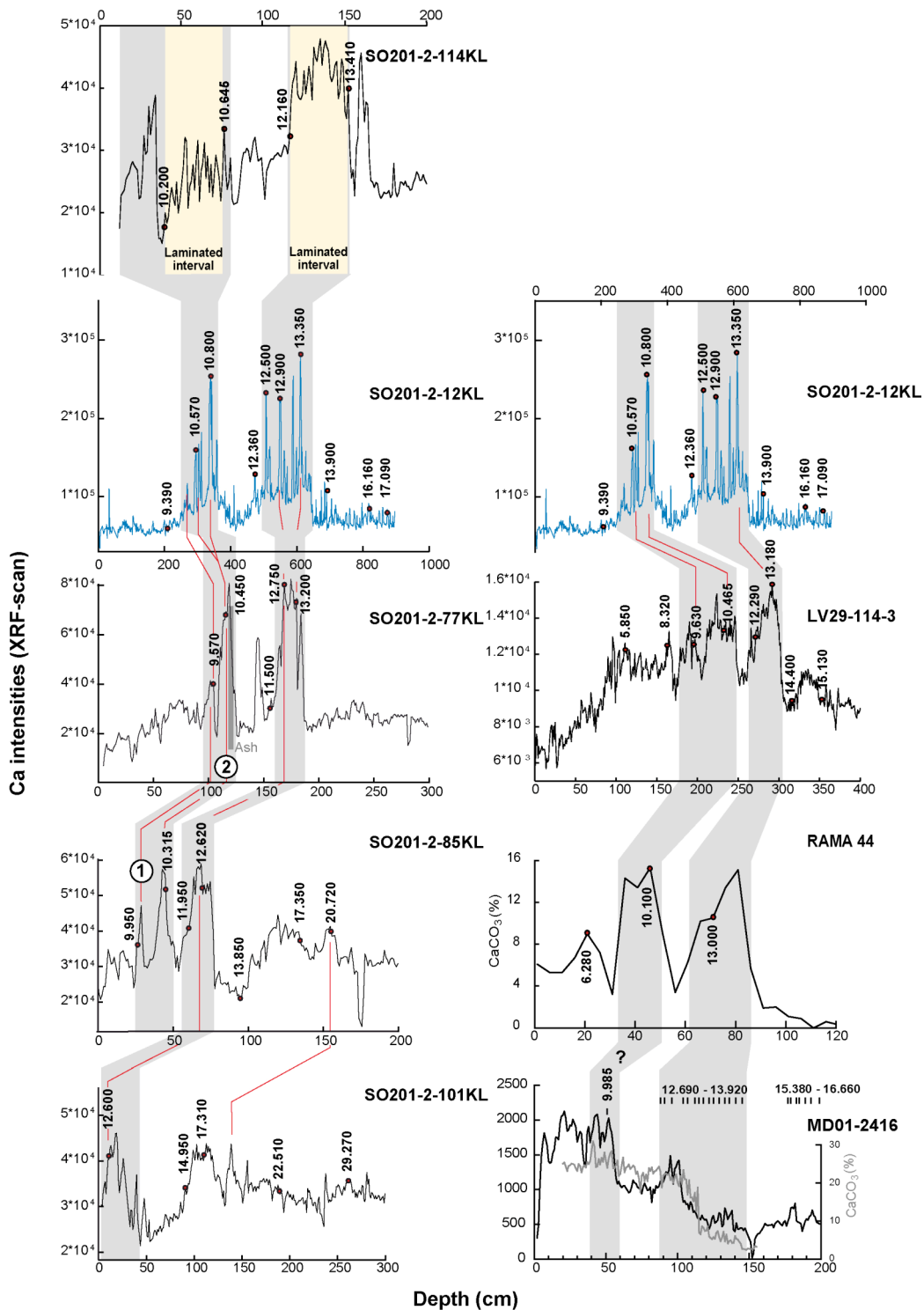
Figure 3.2 (left panel): Stratigraphic framework of sediment records from the western Bering Sea and correlation with high-resolution record SO201-2-12KL record (blue curve) from the subarctic NW-Pacific. The stratigraphy is based on Ca intensity studies, derived from core logging data (XRF), together with raw AMS ^{14}C datings (red spots with vertical numbers). Gray shaded areas mark prominent carbonate maxima. Defined carbonate spikes (spike 1 = 9,760 ^{14}C years; spike 2 = 10,383 ^{14}C years) are numbered and red lines indicate correlation points between the sediment records. (right panel): Comparison of Ca intensity data from high-resolution record SO201-2-12KL from the NW-Pacific (in blue) and LV29-114-3 from the Sea of Okhotsk to already published records from the open NW-Pacific (RAMA 44, *Keigwin*, 1998 and MD01-2416, *Gebhardt et al.*, 2008) Ca intensity and CaCO$_3$ (%) data. Red spots (vertical numbers) mark raw AMS ^{14}C datings and gray shaded areas indicate carbonate maxima in the sediment records. Sediment record MD01-2416 provides best age control based on ^{14}C-plateau tuning. However, no correlation was done to the records of this study due to discrepancies between the carbonate records of MD01-2416 and our sediment records.
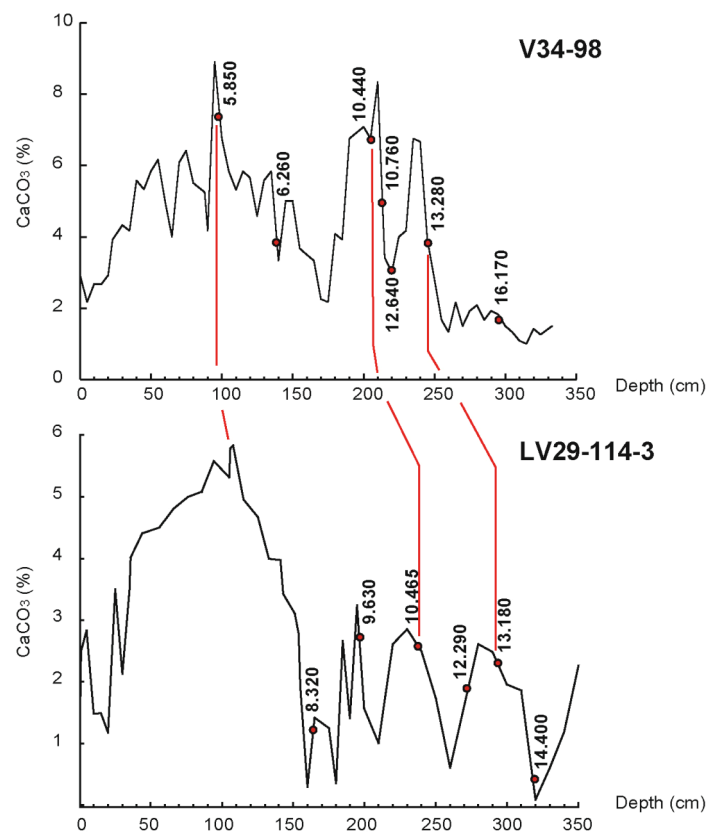
Figure 3.3: Correlation of sediment record LV29-114-3 with core V34-98 [*Gorbarenko et al.*, 2002] based on CaCO$_3$ (%) data. Numbers with red spots indicate raw ^{14}C ages and red lines give correlation points. However, only the raw ^{14}C age of 5,850 years was transferred to sediment record LV29-114-3 to improve stratigraphic control in the upper part of this sediment core.

In addition, we also correlated the Ca intensity pattern of NW-Pacific core SO201-2-12KL and Sea of Okhotsk core LV29-114-3 to the pattern of NW-Pacific cores RAMA 44PC [*Keigwin et al.*, 1992] and MD01-2416 [*Sarnthein et al.*, 2004; *Gebhardt et al.*, 2008]. This correlation provides a good match with the RAMA 44PC carbonate record. Sediment record MD01-2416 has an excellent age model, including 15 planktonic ^{14}C-datings, which covers the interval of the first pronounced carbonate maximum between H1 and the B/A. However, the carbonate maximum is less clearly developed in comparison to all other records presented here (Figure 3.2). A clear correlation is only possible by considering the ^{14}C ages. Furthermore, the Ca and CaCO$_3$ structure at 9,985 ^{14}C years in core MD01-2416, which possibly marks the first Ca-spike of the second carbonate maximum in the early Holocene, appears to be several hundred years too young in comparison to the age assignments of our Ca-records from the NW-Pacific, the Bering Sea and the Sea of Okhotsk (Figure 3.2). Hence, we transferred no ^{14}C ages from core MD01-2416 to our records.

In general, the sequence of ^{14}C data and their assignment to prominent carbonate structures is consistent between cores (within a range of a few hundred years) and can be traced from the Bering Sea to the NW-Pacific (except for core MD01-2416) and even into the Sea of Okhotsk. Hence, the

registered temporal pattern of the carbonate maxima seems not to be significantly biased by water depth-dependent differences in carbonate dissolution at our investigated records, which range from 630 to 2200 m water depth. However, the ^{14}C ages of the carbonate maxima at our sediment records from the western Bering Sea (630 to 2200 m water depth) are about 200 years younger than in the NW-Pacific (2170 m water depth) and the Sea of Okhotsk (1765 m water depth). Since the Shirshov Ridge records cover the full range of water depth (630 to 2200m), we ascribe the temporal offset to regionally different ^{14}C surface ocean reservoir effects rather than to changes in carbonate dissolution.

The conversion of radiocarbon ages in calendar years requires a correction for the surface ocean reservoir age to balance for the ^{14}C effect of disequilibrium between the atmosphere and the upper ocean and the input of deep waters into the mixed layer. In the N-Pacific, the surface ocean reservoir age has been reported to range from 600 to 1,000 years [*Southon et al.*, 1990; *Kuzmin et al.*, 2001; *McNeely et al.*, 2006; *Yoneda et al.*, 2007]. There is increasing evidence that the reservoir age also varied over the course of the last 20 kyr, which has been attributed to global thermohaline reorganizations as well as to changes in the upper ocean stratification. For the N-Pacific, *Sarnthein et al.* [2006] and *Gebhardt et al.* [2008] suggest variable ^{14}C reservoir ages for the last 20 kyr, which have been derived by ^{14}C-plateau tuning. For the ^{14}C-plateaus at 12.3 kyr, 12.8 - 13.4 kyr and 14.9 - 15.3 kyr (raw ^{14}C ages), reservoir ages of 450, 300 and 1350 years have been suggested [*Sarnthein et al.*, 2007], respectively. In contrast, a more recent study claims that the surface ocean reservoir age was close to 730 years and varied by less than ±200 years during the last deglaciation in the NE-Pacific [*Lund et al.*, 2011]. Since our ^{14}C datings are not dense enough to identify the age-calibrated ^{14}C- plateaus, we were not able to assess the variability of paleo-reservoir ages. Instead, we used constant reservoir ages over time with 700 years for the western Bering Sea cores and 900 years for the NW-Pacific and the Sea of Okhotsk records, which are within the range of NW-Pacific modern surface ocean reservoir ages. After converting the ^{14}C ages into calendar years, the difference in regional reservoir ages provides the best chronostratigraphic match between our high-resolution core-logging records (color b* and XRF-Ca/Ti ratios). This assumes that the pattern of XRF-Ca/Ti ratios and color b* occurred synchronously in the NW-Pacific realm. Trends in the color b* generally correlate with those of biogenic opal (Figure 3.4). Color b* is reported to provide a good proxy for variations in biogenic opal and total organic matter content of anoxic sediments [*Debret et al.*, 2006]. The Sea of Okhotsk is marked by an increase in CaCO$_3$ content rather than an increase of diatom production during the deglaciation [*Seki et al.*, 2009]. Thus, we used the pattern of Ca/Ti ratios in the Sea of Okhotsk record, which reflects changes in carbonate contents versus terrigenous siliciclastic input. Our age-depth control points within each record have been moved within the 1-sigma calendar age ranges to improve the fit between records. This also results in a good correlation to the Greenland temperature record (NGRIP) [*Rasmussen et al.*, 2006] shown in Figure 3.4.
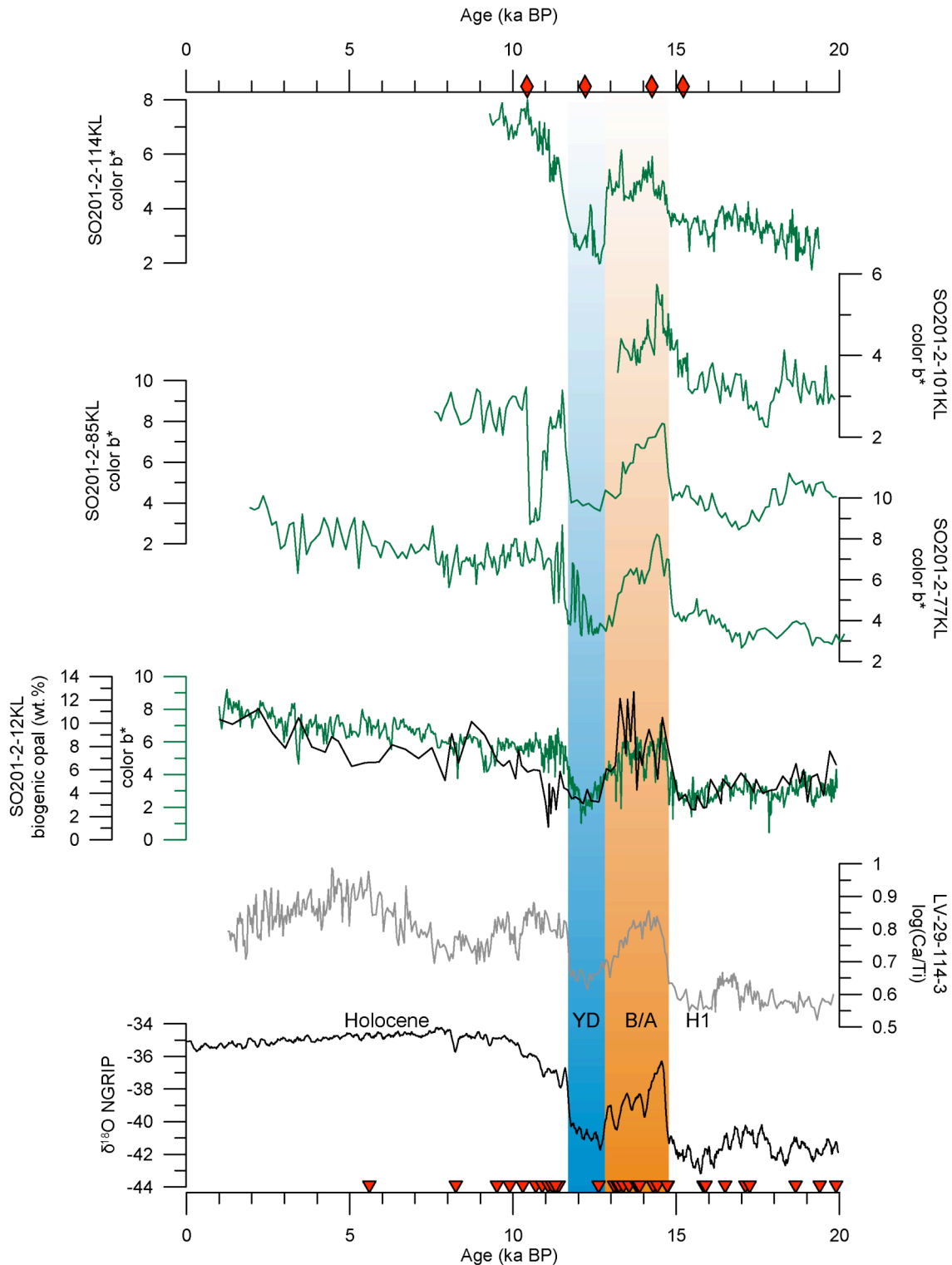
Figure 3.4: Spectrophotometric measurements (color b*, green curves) from sediment records of the western Bering Sea, together with SO201-2-12KL from the NW-Pacific and logCa/Ti ratio (XRF element intensities) of LV29-114-3 from the Sea of Okhotsk (in gray) against the NGRIP isotope record (in black) for the last 20 kyr BP. Additionally, biogenic opal (%) (thin black line) is given for SO201-2-12KL. Red triangles at the bottom mark ^{14}C age control points used in this study. Note the excellent correlation of all studied sediment records with the Greenland isotope record during the last 15 kyr BP. Prominent climate stages as the B/A (shaded in orange), the YD (shaded in blue) as well as the onset of the early Holocene are mimicked in the color b* proxy records. Red diamonds on top (representative of all sediment records) mark time slices used for the qualitative assessment of the IP_{25} sea-ice proxy. IP_{25} measurements were conducted on individual sediment records from samples according to the selected time slice.

3.4.2 SST reconstructions

Calculated alkenone SSTs spanning the time period of the last 15 kyr BP are given in Figure 3.5. As expected, the SST records reflect successively increasing temperatures from north to south. At the southernmost site (core LV29-114-3), the SSTs are about 3 °C warmer than at the northernmost site (core SO201-2-114KL). A general feature of all records is the consistent pattern of temperature variability during the last glacial termination from 15 ka BP to 10 ka BP. This temperature pattern is very similar to that reconstructed from Greenland ice-core records, which mark the temperature rise from H1 into the B/A, the subsequent cold spell of the YD and the following warming into the early Holocene (Figure 3.5). The early warming step into the B/A does not capture the full amplitude of the SST increase, since all of our records are characterized by alkenone contents below the detection limit prior to 15 ka BP. Hence, the amplitudes of the early temperature increase represent minimum ranges between 3 and 5 °C at our studied sites, with lowest SSTs of 2 - 5.5 °C at 15 ka BP and highest values ranging between 6 and 8 °C during the B/A. The following temperature decrease into the YD is marked by amplitudes of 1.5 - 5 °C with lowest amplitudes in Sea of Okhotsk core LV29-114-3. At each site, the following temperature increase of up to 5 °C consistently culminates in an early Holocene SST maximum between 11 and 9 ka. All records display a maximum with SSTs of 9 – 10 °C except for the northernmost core SO201-2-114KL from the Bering Sea, where the SST maximum remains approx. 3 °C cooler. The temperature development during the Holocene is only preserved in Bering Sea core SO201-2-77KL, northwest Pacific core SO201-2-12KL and Sea of Okhotsk core LV29-114-3. These records point to a smooth and gradual SST decrease over the past 9 kyr. However, in Sea of Okhotsk core LV29-114-3, this temperature trend is interrupted by a cold spell between 9 - 7 ka BP. This pronounced SST minimum displays temperatures as cold as those found during the YD. Nevertheless, the SST trend in this record also suggests a gradual cooling in SST (2 °C), which is best developed since 6 ka BP. Another subtle difference is observed for the time interval of the last 3.5 kyr. While the Bering Sea record suggests a slight warming, the records from the NW-Pacific and the Sea of Okhotsk indicate a further decline in SST.

3.4.3 Sea-ice distribution

To assess past variations in sea-ice extent, we compared relative percentages of diatom species *F. oceanica* (indicative of sea-ice presence) and *N. seminae* (indicative of open water conditions) from sediment record SO201-2-12KL with qualitative measurements of the IP_{25} proxy (indicative of sea-ice presence), derived from specific time slices in all sediment records. The percentages of the diatom species (*F. oceanica* and *N. seminae*) provide a temporal pattern of millennial-scale variability in sea-ice presence, which is consistent with the SST development during the last 15 kyr (Figure 3.6). Moderate amounts of *F. oceanica* mark the last glacial. Extremely low contents are typical for the B/A. Highest percentages characterize the YD and the subsequent warming phase at the end of termination 1. The SST maximum between approx. 10.5 - 9 ka BP is marked by the absence of *F.*
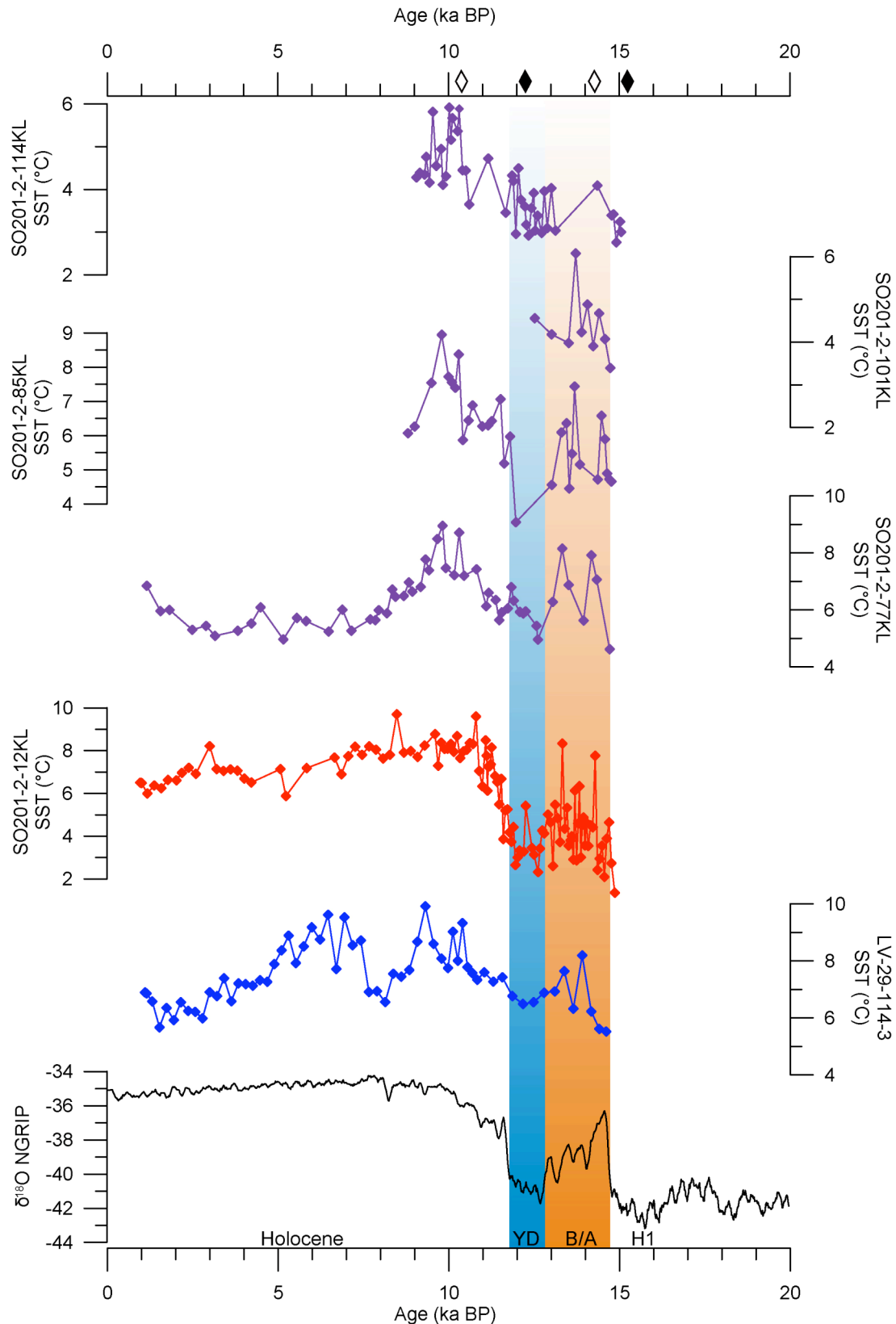
Figure 3.5: Results of the SST reconstructions from the western Bering Sea (in purple), the NW-Pacific (in red) and Sea of Okhotsk (blue curve) compared with the Greenland ice-core record for the last 15 kyr BP. Orange shaded area marks the B/A and blue shaded bar indicate the YD cold spell in the records. Diamonds on top mark time slices used for the qualitative assessment of the IP$_{25}$ sea-ice proxy (representative of all sediment records). Black diamonds on top mark time slices (H1 and YD), where the IP$_{25}$ biomarker was found at all core sites and thus the presence of sea-ice inferred. In turn, white diamonds indicate time slices (B/A and early Holocene) where IP$_{25}$ biomarker was absent at all core sites and no sea-ice cover inferred.

oceanica. The last 9 kyr are marked by a slight increase in *F. oceanica*. *N. seminae* provides an opposite pattern, which is best developed between 15 - 10.5 ka BP, suggesting open water conditions with reduced sea-ice presence during the B/A and the Holocene SST maximum between 10.5 - 9 ka BP. Moderate contents of both *F. oceanica* and *N. seminae* are observed during the past 9 kyr and may indicate temporal variations in sea-ice cover, allowing for both open water conditions as well as sea-ice presence.

As mentioned above, we further applied the IP_{25} proxy indicative of past variations in sea-ice extent. In all records (LV29-114-3, SO201-2-12KL, SO201-2-77KL, SO201-2-85KL, SO201-2-101KL, SO201-2-114KL) we measured IP_{25} at selected time slices (15.1 ka BP, 14.3 ka BP, 12.2 ka BP and 10.5 ka BP), which are representative for distinct climate extremes (H1, B/A, YD, early Holocene SST maximum) recognized in our SST records (Figure 3.5). As shown for NW-Pacific core SO201-2-12KL, by direct comparison between *F. oceanica* content and the occurrence of the IP_{25} biomarker, a consistent pattern of sea-ice variability is documented and supports the applicability of the IP_{25} biomarker as sea-ice proxy in the subarctic NW-Pacific (Figure 3.6). The IP_{25} time slice reconstructions suggest that sea-ice was present during phases of H1 and the YD at each core location in the study area. Conversely, no IP_{25} was found in all sediment samples from the B/A and the early Holocene SST maximum. Accordingly, ice-free conditions mark the positions of all cores during these intervals.
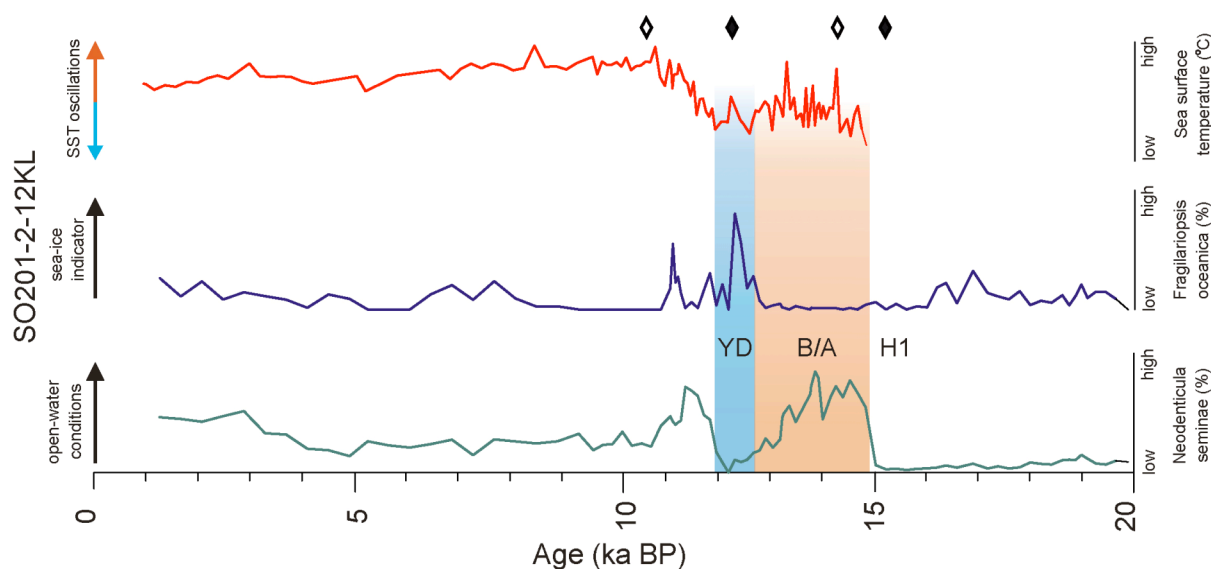

Figure 3.6: Results of the SST reconstructions from sediment record SO201-2-12KL (NW-Pacific) in red together with relative percentage of diatom *Fragilariopsis oceanica* (in blue) and *Neodenticula seminae* (in green). Orange shaded area marks the B/A and blue shaded bar indicate the YD cold spell in the sediment records. Diamonds on top mark time slices used for the qualitative assessment of the IP_{25} sea-ice proxy (representative of all sediment records). Black diamonds on top mark time slices (H1 and YD), where the IP_{25} biomarker was found at all core sites and therefore the presence of sea-ice inferred. In turn, white diamonds indicate time slices (B/A and early Holocene) where no IP_{25} biomarker was found at all core sites and thus no sea-ice cover inferred.

3.5 Discussion

3.5.1 Deglacial SST development in the subarctic NW-Pacific

The deglacial SST development in the subarctic NW-Pacific realm is reminiscent of the temporal pattern associated with millennial-scale climate variations as revealed by temperature records from Greenland and the N-Atlantic [e.g. *Bard et al.*, 2000]. The alkenone temperature records obtained from the subarctic NW-Pacific, the Sea of Okhotsk and the Bering Sea suggest a two-step type of deglacial warming, with a first warming at the onset of the B/A (14.7 - 12.9 ka BP), subsequently interrupted by a cooling associated with the YD cold phase (12.8 - 11.8 ka BP) and continued by a second and more pronounced warming step into the early Holocene. Hence, this SST development matches the millennial-scale temperature fluctuations recognized in Greenland ice-core records and N-Atlantic SST records. It has also been reported in previous studies, which established alkenone-derived SST records from other parts of the N-Pacific realm as the NE-Pacific [*Kienast and McKay*, 2001; *Barron et al.*, 2003], the eastern Bering Sea [*Caissie et al.*, 2010], the Sea of Okhotsk [*Ternois et al.*, 2000; *Harada et al.*, 2006b; *Seki et al.*, 2009; *Harada et al.*, 2012] and off Japan [*Harada et al.*, 2012]. These records show remarkable similarities to both the temporal structure and timing of SST changes presented here (Figure 3.7). On the basis of our age models, the deglacial pattern of SST variability in the NW-Pacific realm seems to be rather in-phase than out-of-phase with the temperature changes in the N-Atlantic. This would suggest a quasi-synchronicity between the N-Atlantic and N-Pacific SST development during the last glacial termination and argues for a strong atmospheric coupling between the N-Pacific and the N-Atlantic.

The majority of model results also favors this interpretation and provides insights into the mechanisms linking the development of SST between the N-Atlantic and the N-Pacific. Numerous studies with coupled General Circulation Models (GCMs) examined whether and how the millennial-scale climate oscillations in the N-Atlantic would impact the N-Pacific SST development via atmospheric and oceanic teleconnections during the last glacial termination. All models propose a close linkage to deglacial variations in AMOC. The temperature changes in the N-Atlantic region are closely coupled to a change in the strength of the AMOC, which is strongly modulated by freshwater forcing due to the instability of the Northern Hemisphere ice-sheets and melting icebergs [*Rahmstorf*, 1995; *McManus et al.*, 2004; *Yin and Stouffer*, 2007]. The freshwater input into the N-Atlantic led to a reduced thermohaline overturning, which also resulted in a reduced northward advection of saline and warm subtropical surface waters into the N-Atlantic [*Manabe and Stouffer*, 1988]. *Manabe and Stouffer* [1988] was among the first who demonstrated that the climatic impact of an AMOC shutdown is of global significance. Subsequent freshwater perturbation experiments also suggest, beyond the Atlantic basin, a robust response over the N-Pacific [e.g., *Mikolajewicz et al.*, 1997; *Vellinga and Wood*, 2002; *Okumura et al.*, 2009; *Timmermann et al.*, 2010]. When the AMOC is substantially weakened (e.g. during H1 and the YD), N-Pacific summer and winter SSTs are suggested to have

cooled by up to 3 – 6 °C. Most studies attribute the cooling to enhanced thermal advection of cold air masses from the N-Atlantic via westerly winds [*Manabe and Stouffer*, 1988]. As a result, the deepening of the Aleutian Low, the intensification in ocean-to-atmosphere heat flux and southward Ekman transport in combination with the southward shift of the oceanic frontal system would further cool the N-Pacific. More recently, model experiments also provide hints for another atmospheric bridge between the N-Pacific and the subtropical Pacific/Atlantic that may have the potential to
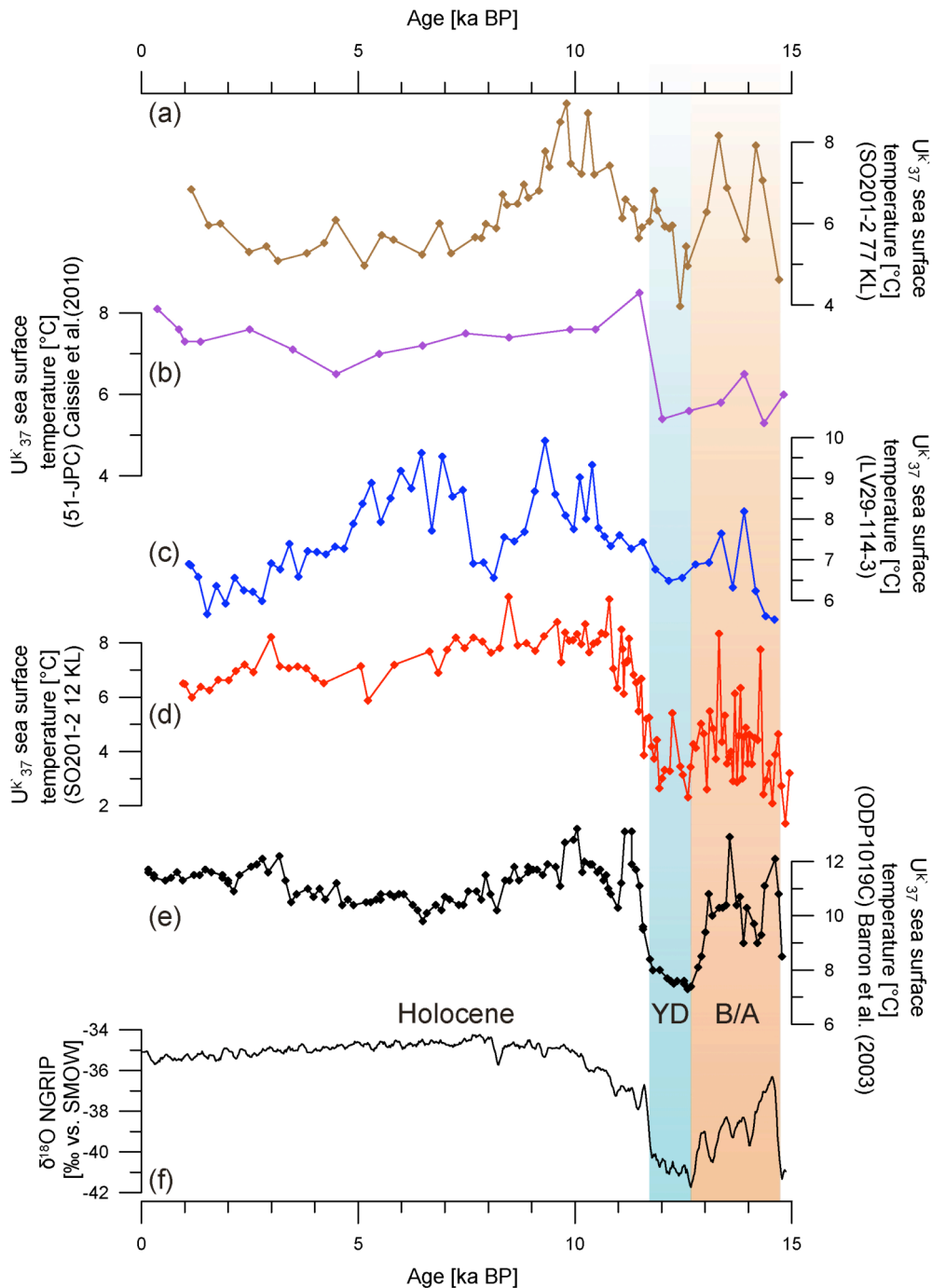

Figure 3.7: Alkenone-based SST reconstructions for the subarctic N-Pacific, including detailed comparison of (a) western Bering Sea (b) eastern Bering Sea (c) Sea of Okhotsk (d) NW-Pacific and (e) NE-Pacific SST records compared with (f) NGRIP isotope record for the past 15 kyr. Orange shaded area marks the B/A and blue shaded bar indicate the YD cold spell in the records.

influence the strength of the anomalies in both the Atlantic and Pacific are found to be important for the barotropic response of the Aleutian Low [*Okumura et al.*, 2009]. These mechanisms represent AMOC-induced fast-acting atmospheric teleconnections on decadal time-scales and suggest a similar temperature development between the N-Atlantic and the N-Pacific.

In contrast, *Kiefer and Kienast* [2005] and *Gebhardt et al.* [2008] found an inversed millennial-scale pattern of SST oscillations with SST maxima at H1 and the YD in the NW-Pacific (core MD01-2416 and ODP883) as indicated by Mg/Ca-derived and planktonic foraminiferal SIMMAX-based SSTs. This temporal pattern of NW-Pacific SST development is in harmony with model results from *Huang et al.* [2000] and *Okazaki et al.* [2010]. According to *Huang et al.* [2000], a slowdown of the Meridional Overturning Circulation in the N-Atlantic (like during H1 and YD) may result in N-Pacific warming due to a reduction of upwelling of cold and nutrient-rich Pacific Deep Water in the N-Pacific subpolar gyre. However, the model experiments of *Huang et al.* [2000] do not consider the environmental background conditions associated with expanded Northern Hemisphere ice-sheets during H1 and YD. The study of *Okazaki et al.* [2010] also suggests a warming in the N-Pacific during times of AMOC slowdown but due to the establishment of the PMOC. Enhanced meridional overturning would result in strengthened northeastward upper-ocean heat transport via the North Pacific Current, thereby warming the N-Pacific, in particular in the Pacific Northeast. Recently, *Chikamoto et al.* [2012] simulated an AMOC shutdown using glacial boundary conditions (also considering a closed Bering) and examined the impact on N-Pacific climate history by using two different models. Their results indicate that the spatial temperature pattern in the N-Pacific is strongly coupled to the strength of the PMOC. This model experiments suggest cooler SSTs in the NW-Pacific for both cases, a strong and a weak PMOC. However, in case of a strong PMOC the NE-Pacific experienced surface warming due to an enhanced poleward transport of heat and salt from the subtropics to the extratropics via the Kuroshio - North Pacific Current system. Hence, the PMOC associated impact on SSTs seems to be too weak to compensate for the SST cooling in the NW-Pacific during times of expanded Northern Hemisphere ice-sheets. These results favor AMOC-induced atmospheric teleconnections as the main driver for the SST development in the subarctic N-Pacific and are in accordance with our SST reconstructions from the NW-Pacific.

However, the inconsistent deglacial pattern in the subarctic N-Pacific between alkenone-derived SSTs (this study) and Mg/Ca-derived and planktonic foraminiferal SIMMAX-based SSTs [*Kiefer and Kienast*, 2005; *Gebhardt et al.*, 2008] raise the question of whether the differences can be explained by stratigraphic uncertainties, by the use of different SST proxies and/or regional oceanographic deviations. The stratigraphic differences are mainly based on the application of different paleo-reservoir ^{14}C ages (chapter 4). Compared to our age model, their radiocarbon-based age constraints rely on variable reservoir ages [*Sarnthein et al.*, 2006; *Sarnthein et al.*, 2007]. If we apply this variable

reservoir correction to our age model (not shown), it would slightly and comparably affect the stratigraphic position of the B/A temperature maximum in all our records. The temperature increase at the transition from the glacial into the B/A would lag, relative to our age model, by 100 - 200 years. The end of this temperature maximum would lead that of our age model by up to 350 years. As a result, the temperature maximum remains within the interval of the B/A and will not result in an anti-phased SST pattern between the N-Pacific and the N-Atlantic in our records. The different appearance of the temperature maxima between our and other records (core MD01-2416, ODP-Site 883) cannot easily be ascribed to age model discrepancies. Assuming that the original planktonic ^{14}C ages (uncorrected) within the NW-Pacific region are marked by similar reservoir ages over time, the SST maxima and minima would occur at different time intervals anyway. For example, the most pronounced temperature maximum at core MD01-2416 occurs between 14,430 – 13,820 ^{14}C years (original) and has been assigned to the beginning of a ^{14}C-plateau that ranges between 16,700 – 15,300 calendar years BP. The most pronounced temperature maximum in our SST records occurs between 13,350 – 12,500 ^{14}C years (original). These ages would correspond to another ^{14}C-plateau, which marks the beginning of the B/A from 14,900 – 14,200 calendar years BP [*Gebhardt et al.*, 2008]. However, core MD01-2416 provides no SST maximum at this stratigraphic position.

Hence, we speculate that the different SST proxies are afflicted with diverse temperature signals due to seasonal bias and formation of the proxy signal at different water depths. The modern alkenone signal has been shown to reflect the late summer/autumn SST (0 – 30 m) in the NW-Pacifc [*Harada et al.*, 2003; *Harada et al.*, 2006a; *Seki et al.*, 2007]. The Mg/Ca-based temperatures are derived from the planktonic foraminifer *N. pachyderma sin*, which is believed to calcify within the upper 200 m of the water column close to the thermocline [e.g. *Bauch et al.*, 2002]. From this it seems reasonable to assume that the proxy-related differences in the temperature signals rather reflect variations in upper ocean stratification than local differences in oceanography.

3.5.2 Holocene SST pattern of the N-Pacific and its marginal seas

Alkenone-derived SST reconstructions from the NW-Pacific region are characterized by a pronounced temperature maximum during the early Holocene between 11 and 9 ka BP (Figure 3.5 and 3.8). This temperature maximum coincides with the maximum in Northern Hemisphere summer insolation (June – August) [*Laskar et al.*, 2004]. In addition, recent model experiments suggest the reopening of the Bering Strait as another forcing mechanism that has the potential to influence the SST development in the Bering Sea and the NW-Pacific [*Hu et al.*, 2010; *Okumura et al.*, 2009]. The reopening of the Bering Strait due to deglacial sea-level rise has been dated to ca. 11 ka BP [*Elias et al.*, 1996; *Elias et al.*, 1997]. According to the model results, a reopening of the Bering Strait would increase the freshwater flux from the N-Pacific to the N-Atlantic. This would result in a weakening of the AMOC and a cooling in t he N-Atlantic. The N-Pacific would become slightly warmer due to an increased
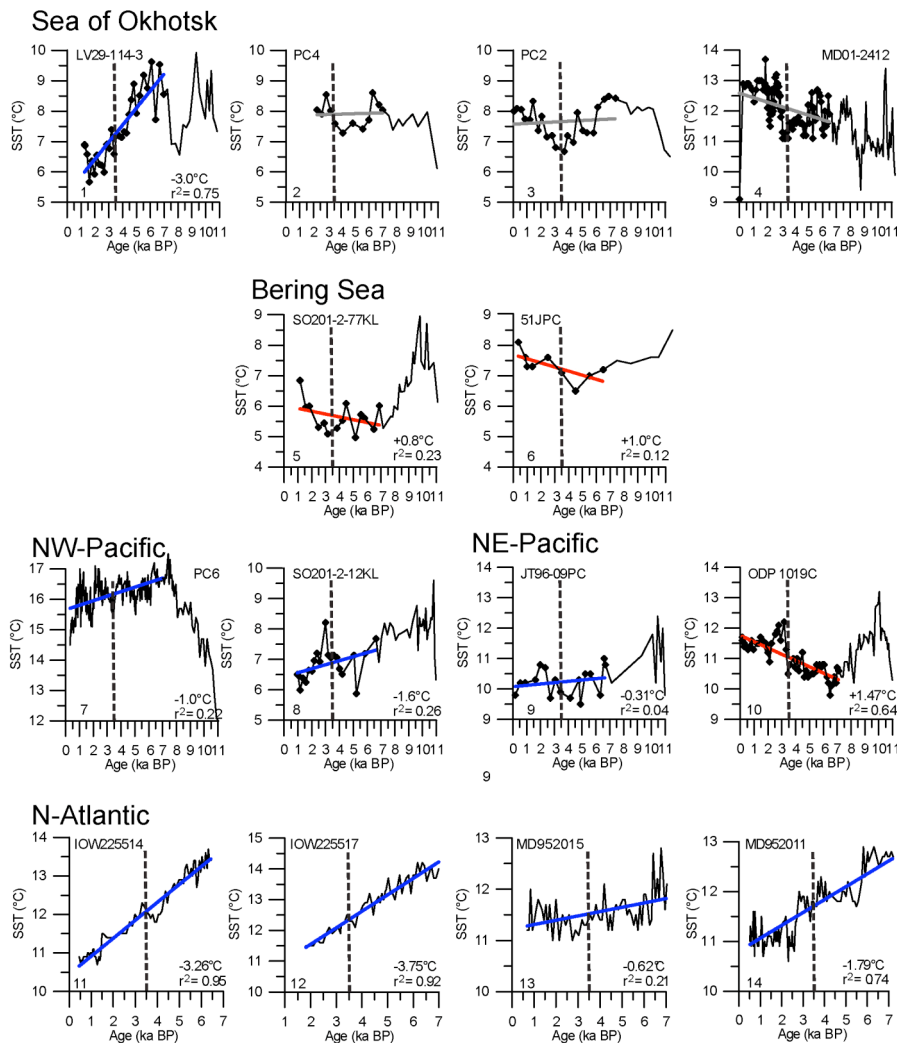
Figure 3.8: Holocene compilation of alkenone-based SST reconstructions for the Sea of Okhotsk (1-4) Bering Sea (5-6) subarctic NW-Pacific (7-8), subarctic NE-Pacific (9-10) compared with subarctic N-Atlantic alkenone-derived SSTs (11-12, *Emeis and Dawson*, 2003; 13-14, *Marchal et al.*, 2002; 14, *Calvo et al.*, 2002) from the middle to late Holocene. The stippled vertical lines indicate the middle to late Holocene boundary in every record. Linear regression trends are given for all records (blue, red and gray thick lines) for the last 7 kyr BP. Correlation coefficients r^2 are shown in the lower right corners, respectively.

meridional heat transport from the tropics to the extratropics. In addition to the insolation forcing, the gateway-related oceanic forcing may have contributed to extra warming in the NW-Pacific region during the early Holocene. The gateway-induced forcing may have been active for a restricted time interval, which may represent the phase of progressive marine inundation of the Bering Strait during rapid early Holocene sea level rise (11 - 8 ka BP) [*Fleming et al.*, 1998]. Whether the SST maximum in the Bering Sea (11 - 9 ka BP) is related to the opening of the Bering Strait gateway remains elusive since the maximum also coincides with the maximum in Northern Hemisphere summer insolation.

Our SST records in combination with existing SST records from the N-Pacific are further used to reassess the hypothesis of the long-term inverse temperature development between the N-Atlantic and N-Pacific from the middle to late Holocene [*Kim et al.*, 2004]. According to *Kim et al.* [2004], SST trends resemble a basin-scale, long-term N-Pacific warming while the N-Atlantic cools (IOW225514

and IOW225517, *Emeis and Dawson*, 2003; MD952015 and MD952011, *Calvo et al.*, 2002, *Marchal et al.*, 2002) during the last 7 kyr. However, the interpretation of *Kim et al.* [2004] is based solely on one record from the subarctic NW-Pacific (GGC-15, *Ternois et al.*, 2000), located in the Sea of Okhotsk. Our more comprehensive compilation of alkenone-based SST records from the N-Pacific and its marginal seas reveal no basin-scale, long-term warming trend over the past 7 kyr in the N-Pacific. The compilation of SST records from the N-Pacific realm hints to complex regional differences in temperature development during the middle to late Holocene (Figure 3.8).

In the Sea of Okhotsk, the middle to late Holocene SST development is characterized by different trends with relatively large temperature fluctuations (Figure 3.8). Core LV29-114-3 from the southeastern Sea of Okhotsk shows a clear cooling trend (-2.5 °C) during the last 7 kyr. In contrast, at neighbor core GGC-15, which was the only NW-Pacific record included in the study of *Kim et al.* [2004], shows increased temperatures during this interval [*Ternois et al.*, 2000]. However, this SST record is possibly biased by low alkenone contents in the middle to late Holocene interval [*Ternois et al.*, 2000]. Three SST records from the central Sea of Okhotsk (XP98-PC 2 and -PC4, *Seki et al.*, 2004a) and the southwestern Sea of Okhotsk (MD01-2412, *Harada et al.*, 2006b) are marked by a pronounced temperature minimum between 6 - 3 ka BP. Only core MD01-2412 shows a clear SST trend, which points to a warming during the late Holocene (Figure 3.8). Altogether, we partly ascribe the differences in SST development to a variable inflow of surface water masses from the N-Pacific and the Japan Sea. Core LV29-114-3 is located at the main entrance of Pacific water masses delivered by the EKC (via Krusenstern Strait), which transports relatively cold water-masses to the Sea of Okhotsk. The Holocene cooling trend at core LV29-114-3 thus might be related to temperature changes in the source region of the EKC. On the other hand core MD01-2412 is influenced by the inflow of warm water masses from the Japan Sea via the Soya Strait. The warming trend may indicate a strengthened influence of the Japan Sea.

In the Bering Sea, the middle to late Holocene SST development is derived from two sediment records only, one from the eastern (HLY0202-51JPC, *Caissie et al.*, 2010) and one from the western part (SO201-2-77KL, this study). Both temperature records reveal a consistent pattern of SST development with a net warming indicated by the linear regression trend (Figure 3.8). This trend seems to be related to a SST rise around the mid- to late Holocene transition (ca. 3.5 ka BP).

The subarctic NW-Pacific SST records reveal a cooling trend from the middle to late Holocene (PC6, *Minoshima et al.*, 2007; SO201-2-12KL, this study; Figure 3.8). Available temperature records from the subarctic NE-Pacific margin show no consistent picture of SST development during the last 7 kyr BP (JT96-09PC, *Kienast and McKay*, 2001; ODP 1019C, *Barron et al.*, 2003; Figure 3.8). As the SST record from core JT96-09PC indicates weak cooling over the last 7 kyr, SSTs at ODP site 1019 are marked by a clear warming trend.

In summary, the compilation of alkenone-derived SST records from the N-Pacific and its marginal seas show no consistent SST trends and thus do not corroborate the basin-scale, long-term warming from the middle to late Holocene in the N-Pacific [*Kim et al.*, 2004]. Regionally consistent pattern in SST development are distinguished for the Bering Sea and the subarctic NW-Pacific, however with opposing trends during the last 7 kyr. The Bering Sea is marked by a warming trend and the subarctic NW-Pacific is characterized by a cooling trend from the middle to late Holocene. The SST development within the Sea of Okhotsk is rather diverse. If the Holocene SST development in the NW-Pacific has been directly affected by variations in local insolation (external forcing), one would expect a consistent response. A direct response to the long-term weakening in Northern Hemisphere summer insolation (June-July) would call for a decrease in SSTs from the middle to late Holocene. Accordingly, the cooling trend in the NW-Pacific could be partly attributed to the decrease in summer insolation. On the other hand the opposing SST development in the Bering Sea as well as the diverse SST pattern in the Sea of Okhotsk also call for a strong imprint of other processes (internal forcing), involving atmosphere – ocean interactions. AMOC-induced changes, which apparently played a key role for the SST development in the NW-Pacific during the last deglacial period, seems to be of minor importance since the thermohaline circulation has been reported to be relatively stable during the middle to late Holocene [e.g. *McManus et al.*, 2004]. Regardless of the underlying forcing mechanism, changes in upper-ocean circulation have to be considered for understanding the complex Holocene SST variability in the NW-Pacific.

3.5.3 Changes in sea-ice extent

The variability in sea-ice distribution during the last glacial termination is closely coupled to the general SST development in the subarctic Pacific realm, although the alkenone-derived SSTs most likely reflect summer-autumn temperature variations and are not associated with the seasonal maximum in sea-ice extent. The qualitative assessment of sea-ice extent (IP_{25}) in the subarctic NW-Pacific suggests a highly dynamic sea-ice cover (Figure 3.9), which at least oscillated over several hundred miles during the last deglaciation. The advancement of sea-ice reached all core sites in the study area during phases of H1 and the YD cold stages and is accompanied by coldest temperatures, derived from our SST records in the NW-Pacific (Figure 3.5). Due to the limited spatial coverage of sediment cores, the maximum expansion in seasonal sea-ice cover may have been much larger during these intervals. Conversely, the absence of the IP_{25} suggests ice-free conditions at all our core locations during phases of the B/A and the early Holocene warm intervals, which is also in accordance with warmest intervals, derived from our SST records (Figure 3.5). During the early Holocene the maximum in sea-ice extent was even more limited compared to today [*Zhang et al.*, 2010] (Figure 3.9). This is suggested by the absence of IP_{25} at the northernmost core site SO201-2-114KL, which today is influenced by sea-ice advances during winter. These findings are underpinned by pronounced millennial-scale shifts in diatom assemblages at core SO201-2-12KL, indicative for changes in
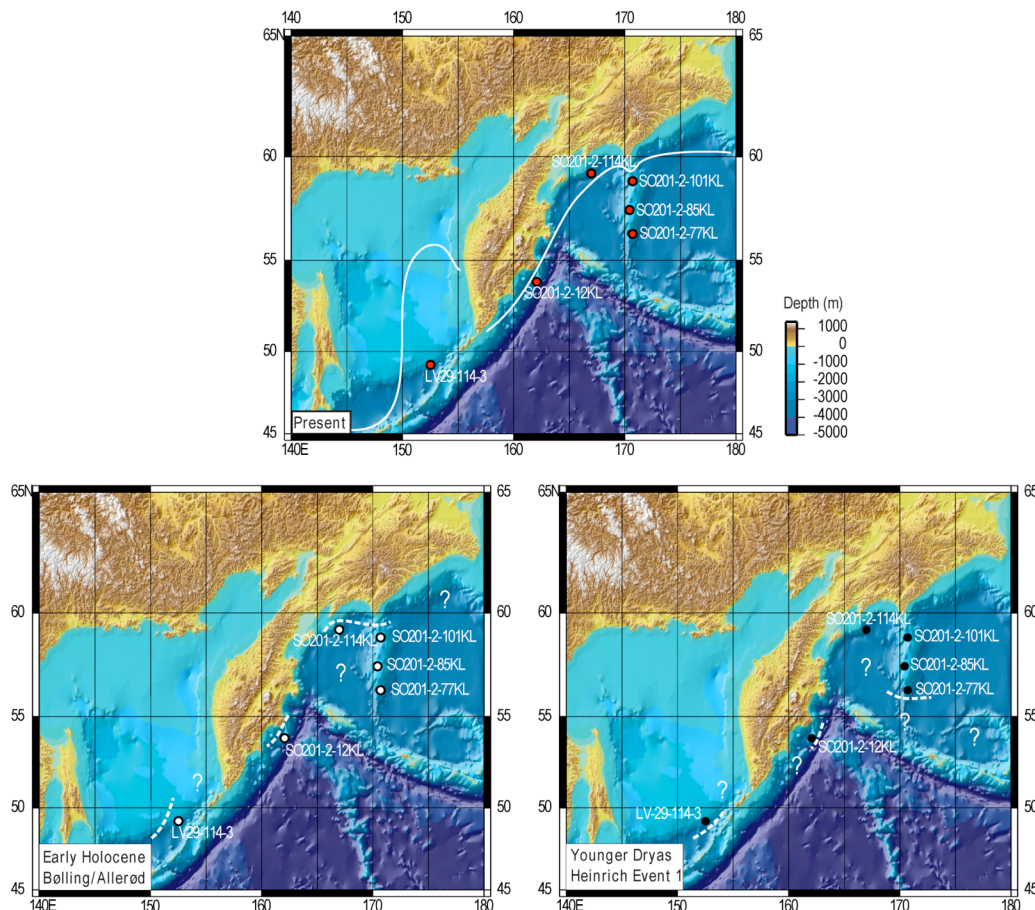
Figure 3.9: Sea-ice extent (dashed lines) derived from occurrence/absence of IP$_{25}$ sea-ice diatoms biomarker measured on a set of six sediment records during time slices of the Bølling/Allerød and Early Holocene (lower left panel), the Younger Dryas and Heinrich Event 1 (lower right panel) compared with the modern sea-ice distribution (redrawn after *Zhang et al.*, 2010) in the subarctic NW-Pacific today (upper panel). Question marks indicate regions where no information of the past sea-ice coverage is available. White circles indicate that no IP$_{25}$ was found and black circles mark samples where IP$_{25}$ was detected in the sediment records according to the time slice. Note the strong expansion of sea-ice in the subarctic NW-Pacific during times of H1 and YD, where IP$_{25}$ was detected in every sediment record and thus the maximum sea-ice boundary was shifted several hundred miles to the South (especially in the western Bering Sea) compared to today. During phases of the B/A and early Holocene IP$_{25}$ was absent in all sediment records and thus no sea-ice presence inferred at the core sites.

seasonal sea-ice cover during the past 15 kyr (Figure 3.6). High percentages of *F. oceanica* are indicative of the presence of sea-ice during the YD. High percentages of *N. seminae* reflect open water conditions during the B/A and the early Holocene. Combining the information of both proxies (IP$_{25}$ and diatom assemblages) also enables to identify different stages of sea-ice conditions, e.g. permanent sea-ice coverage versus seasonal or no sea-ice presence. With respect to the position of core SO201-2-12KL high amounts of *F. oceanica* during the YD and relatively low amounts during the last glacial provide not necessarily a discrepancy. Since *N. seminae* is marked by extremely low values during both intervals, we infer that the glacial position of the sea-ice margin was in comparison to the YD further offshore of core SO201-2-12KL. At the core site, perennial sea ice cover prevailed during the glacial and the retreat of the summer sea-ice boundary may have reached the core location only occasionally. This interpretation is also supported by low total diatom abundance during the last glacial, as resulted from enhanced sea ice coverage, which further limits phytoplankton growth. After

~15 ka BP (beginning of the B/A) total diatom abundance is by an order of magnitude higher (not shown). Our results are also in harmony with previous sea-ice reconstructions based on diatom assemblages and paleo-productivity studies [*Sancetta*, 1983; *Sancetta and Robinson*, 1983; *Sancetta*, 1992; *Cook et al.*, 2005; *Katsuki and Takahashi*, 2005; *Okazaki et al.*, 2005; *Sakamoto et al.*, 2006; *Katsuki et al.*, 2009; *Caissie et al.*, 2010]. The conclusive variability between SST and the IP_{25}-proxy highlights the potential of this relative new sea-ice proxy for more detailed spatial time slice reconstructions in the N-Pacific realm to assess the climate dynamics and feedback mechanisms during millennial-scale climate fluctuations of the last deglaciation.

3.6 Conclusions

(1)   Alkenone-temperatures derived from high-resolution sediment records in the subarctic NW-Pacific, the Sea of Okhotsk and the western Bering Sea show a deglacial temperature pattern similar to the NE-Pacific and even to the N-Atlantic and Greenland temperature variability. From this we suggest a close linkage to deglacial variations in AMOC associated with rapid atmospheric teleconnections, which resulted in a quasi-synchronous SST development between the N-Atlantic and the N-Pacific during the last glacial termination. Although the SST pattern between the N-Atlantic and N-Pacific show striking temporal similarities, uncertainties in age control related to a lack of knowledge in ^{14}C reservoir ages of N-Pacific surface waters may bias the timing of SST changes by up to several hundred years.

(2)   During the middle to late Holocene, the subarctic N-Pacific reveals a complex SST pattern, suggesting strong regional overprints. The compilation of alkenone-derived SST records from the NW-Pacific, the Bering Sea and the Sea of Okhotsk does not support the hypothesis of a long-term Holocene temperature seesaw between the N-Atlantic and N-Pacific associated with a basin-scale warming trend in the N-Pacific during the last 7 kyr. Only the Bering Sea records reveal a tendency towards warmer temperatures compared to a slight cooling in the NW-Pacific. The records from the Sea of Okhotsk exhibit both cooling and warming trends as well as large fluctuations during the middle to late Holocene.

(3)   Past sea-ice expansion were reconstructed from a set of six sediment records by qualitative assessment of the IP_{25} biomarker for cold (H1 and YD) and warm (B/A and early Holocene) stages and compared to diatom studies during the last glacial termination in the NW-Pacific. Our results suggest a strong variability of sea-ice extent and a close coupling to SST fluctuations in the N-Pacific. The sea-ice advanced at least by several hundred miles during phases of H1 and YD. During the phases of B/A and the early Holocene the maximum in sea-ice cover seems to have been even more reduced compared to today.

Acknowledgements

Chapter 4: Deglacial development of (sub) sea surface temperature and salinity in the subarctic NW-Pacific: Implications for upper-ocean stratification

Jan-Rainer Riethdorf[1], Lars Max[2], Dirk Nürnberg[1], Lester Lembke-Jene[2], Ralf Tiedemann[2]

[1]GEOMAR | Helmholtz-Zentrum für Ozeanforschung Kiel, Wischhofstr. 1-3, D-24148 Kiel, Germany; E-Mail: jriethdorf@geomar.de

[2]Alfred Wegener Institute for Polar and Marine Research, Am Handelshafen 12, D-27570 Bremerhaven, Germany

Abstract

It is speculated that in the subarctic North Pacific salinity-driven stratification weakened during the last deglaciation, which might have contributed to the deglacial rise in CO_2. Here, we present high-resolution sub sea surface temperature (subSST$_{Mg/Ca}$) and sub sea surface salinity-approximating ($\delta^{18}O_{ivc-sw}$) records across the last 20,000 years from the subarctic North Pacific and its marginal seas, derived from combined stable oxygen isotopes and Mg/Ca-ratios of the planktonic foraminiferal species *Neogloboquadrina pachyderma* (sin.). Our results indicate regionally different changes of subsurface conditions. In general, during the Heinrich Event 1 and the Younger Dryas cold phases our sites were subject to reduced thermal stratification and increased advection of low-salinity water from the Alaskan Stream and East Kamchatka Current. The warm phases of the Bølling-Allerød instead, was characterized by strengthened thermal stratification and high-salinity surface water due to less dilution. From direct comparison with alkenone-based SST$_{Uk'37}$ estimates, we suggest that deglacial thermocline changes were closely related to changes in seasonality and upper-ocean stratification. The modern halocline seems to have been developed only since the Preboreal.

4.1 Introduction

4.1.1 State of knowledge

No deep water is formed in the modern subarctic N-Pacific. Here, a relatively steep salinity-gradient (halocline) prevents surface water from becoming dense enough to sink thereby isolating it from the underlying nutrient-rich deep water [*Haug et al.*, 1999]. The upper-ocean stratification most likely developed 2.7 million years ago [*Haug et al.*, 1999; *Sigman et al.*, 2004] and is maintained by several processes [*Warren*, 1983; *Emile-Geay et al.*, 2003; *Kiefer*, 2010]: (i) a restricted meridional exchange between subpolar and subtropical waters, (ii) atmospheric low-latitude moisture transport from the

Atlantic to the Pacific, and (iii) northward moisture flux by the Asian monsoon. As a consequence of salinity-driven stratification, the exchange of gas, heat, and nutrients between deep and surface water is limited in the N-Pacific. In contrast, the modern Southern Ocean releases carbon dioxide to the atmosphere, which is stored in deep waters. This led to the assumption that high-latitude ocean stratification drives changes in atmospheric CO_2-concentrations during recent glacial cycles [*Haug et al.*, 1999; *Sigman and Boyle*, 2000; *Sigman and Haug*, 2003; *Sigman et al.*, 2004; *Jaccard et al.*, 2005; *Sigman et al.*, 2010]. However, growing paleoceanographic evidence [e.g. *Okazaki et al.*, 2010] suggests that during the last deglaciation deep water was formed in the N-Pacific and that the halocline has not been a permanent feature. Hence, the N-Pacific might have played a more active role in the deglacial rise of atmospheric CO_2 than previously thought.

High-resolution records depicting the deglacial paleoceanographic evolution in the subarctic N-Pacific are sparse for various reasons: first, a shallow lysocline and corrosive bottom waters limit $CaCO_3$ preservation and restrict most carbonate-bearing records to shallow depths. Second, low $CaCO_3$ contents in cores from intermediate and deep levels result in stratigraphic uncertainties and limiting the use of carbonate-based proxies. Third, regional reservoir ages of surface waters are only little known and potentially subject to strong variations [e.g. *Sarnthein et al.*, 2004].

Nevertheless, available reconstructions of (sub) sea surface temperature (SST) and salinity (SSS) indicate strong oceanographic changes and climate oscillations in the subarctic N-Pacific during the last deglaciation (20-10 ka BP) similar to those recorded in Greenland ice [*Grootes et al.*, 1993; *NGRIP members*, 2004], namely the cold periods of the Heinrich Event 1 (H1) and the Younger Dryas (YD), and the warm phases of the Bølling-Allerød (B/A) and the Preboreal (PB). Recent studies found indirect evidence for enhanced deep water ventilation in the NW-Pacific during H1 and the YD [*Ahagon et al.*, 2003; *Ohkushi et al.*, 2004; *Sagawa and Ikehara*, 2008; *Okazaki et al.*, 2010], while at the same time the Atlantic Meridional Overturning Circulation (AMOC) collapsed or declined [*McManus et al.*, 2004]. In contrast, poor ventilation of NW-Pacific water masses occurred during the B/A, when AMOC accelerated.

In agreement with this observation, general circulation models (GCM) predict that the strengthening of the Pacific Meridional Overturning Circulation (PMOC) results from a rise in SSS in the N-Pacific due to a weakened AMOC [e.g. *Menviel et al.*, 2012]. These studies controversially argue either for an atmosphere-controlled in-phase [*Mikolajewicz et al.*, 1997; *Krebs and Timmermann*, 2007; *Okumura et al.*, 2009], or for an ocean-controlled anti-phase [*Schmittner et al.*, 2003, 2007; *Saenko et al.*, 2004; *Okazaki et al.*, 2010] relationship between the thermal evolution of the N-Atlantic and the N-Pacific.

Geochemical support for increased SSS during H1 and thus, for a potential disappearance of the halocline comes from Mg/Ca-based reconstructions derived from planktonic foraminifera in NW-Pacific sediment cores MD01-2416 [*Sarnthein et al.*, 2006; *Gebhardt et al.*, 2008], and GH02-1030 [*Sagawa and Ikehara*, 2008]. Results from core MD01-2416 suggest that during H1 maxima in SSS were accompanied by maxima in SST, hence supporting an anti-phase relationship with the N-Atlantic [*Sarnthein et al.*, 2006; *Gebhardt et al.*, 2008].

This, however, is in direct conflict with alkenone-based SST reconstructions, which indicate restricted marine productivity during H1 and a maximum in SST during the B/A in the NE-Pacific [*Kienast and McKay*, 2001; *Barron et al.*, 2003], the Bering Sea [*Caissie et al.*, 2010; *Max et al.*, in review], and the Okhotsk Sea [*Ternois et al.*, 2000; *Harada et al.*, 2006b; *Seki et al.*, 2009]. Mg/Ca-based results from core GH02-1030 also show a rise in SST during the B/A [*Sagawa and Ikehara*, 2008], which may point to a regionally different development of the thermocline.

Consequently, additional reconstructions of SST and SSS, which allow for a direct comparison between alkenone- and Mg/Ca-based results, are essential to elucidate changes in upper-ocean stratification and SST development in the subarctic N-Pacific. Especially for the Okhotsk and Bering seas, which are key areas for the formation of North Pacific Intermediate Water (NPIW), salinity reconstructions are absent.

Here, we report combined stable oxygen isotope and Mg/Ca-based reconstructions of sub sea surface temperatures (subSST$_{Mg/Ca}$) and $\delta^{18}O_{ivc-sw}$ (approximating sub sea surface salinity, subSSS) for the last 20 kyr from sediment cores recovered in the southern Okhotsk Sea, the NW-Pacific off Kamchatka, and the western Bering Sea. Our results, which are compared to alkenone-based SST estimates (SST$_{Uk'37}$) derived from the same samples [*Max et al.*, in review], suggest strong deglacial variations in the thermal structure of the upper-water column. Moreover, we present supportive evidence that modern salinity-driven stratification in the N-Pacific is a relatively recent feature as suggested by *Sarnthein et al.* [2004].

4.1.2 Regional setting

The subarctic N-Pacific is characterized by a large-scale cyclonic surface circulation pattern (Figure 4.1). At ~40 °N the N-Pacific Current, an extension of the subtropical Kuroshio Current, flows eastward and brings relatively warm water (~10 °C) into the Alaskan gyre in the NE-Pacific. Here, the Alaskan Current that is fed by freshwater discharge from the North American continent [*Kowalik et al.*, 1994; *Weingartner et al.*, 2005] transports surface water to the north. Subsequently, the Alaskan Stream flows westward along the Aleutian Island Arc thereby causing surface water to flow into the Bering Sea through several passes. Within the Bering Sea a cyclonic surface circulation develops with

the East Kamchatka Current (EKC) and the Bering Slope Current (BSC) acting as western and eastern boundary currents, respectively. Cold and nutrient-rich surface waters leave the Bering Sea through the Bering Strait into the Arctic Ocean, but main outflow occurs back into the NW-Pacific via Kamchatka Strait [e.g. *Stabeno et al.*, 1999]. The northern straits of the Kurile Islands provide inflow of Pacific water from the EKC into the Okhotsk Sea [e.g. *Gorbarenko et al.*, 2002]. In the Okhotsk Sea, brine rejection due to sea-ice formation leads to the production of Okhotsk Sea Mode Water (OSMW), a major component of NPIW. OSMW flows out through the southern Kurile Straits thereby mixing with Pacific water and forming Oyashio Current water [*Yasuda*, 1997; *You*, 2003]. The Oyashio Current transports this relatively cold (~4 °C), low-salinity (~33 psu) water along the Kurile Islands to the east of Japan, where it meets with warmer and saltier water (~34-35 psu) from the Kuroshio. Both, the EKC and the Oyashio, act as western boundary currents and represent the western edge of the N-Pacific subpolar gyre.
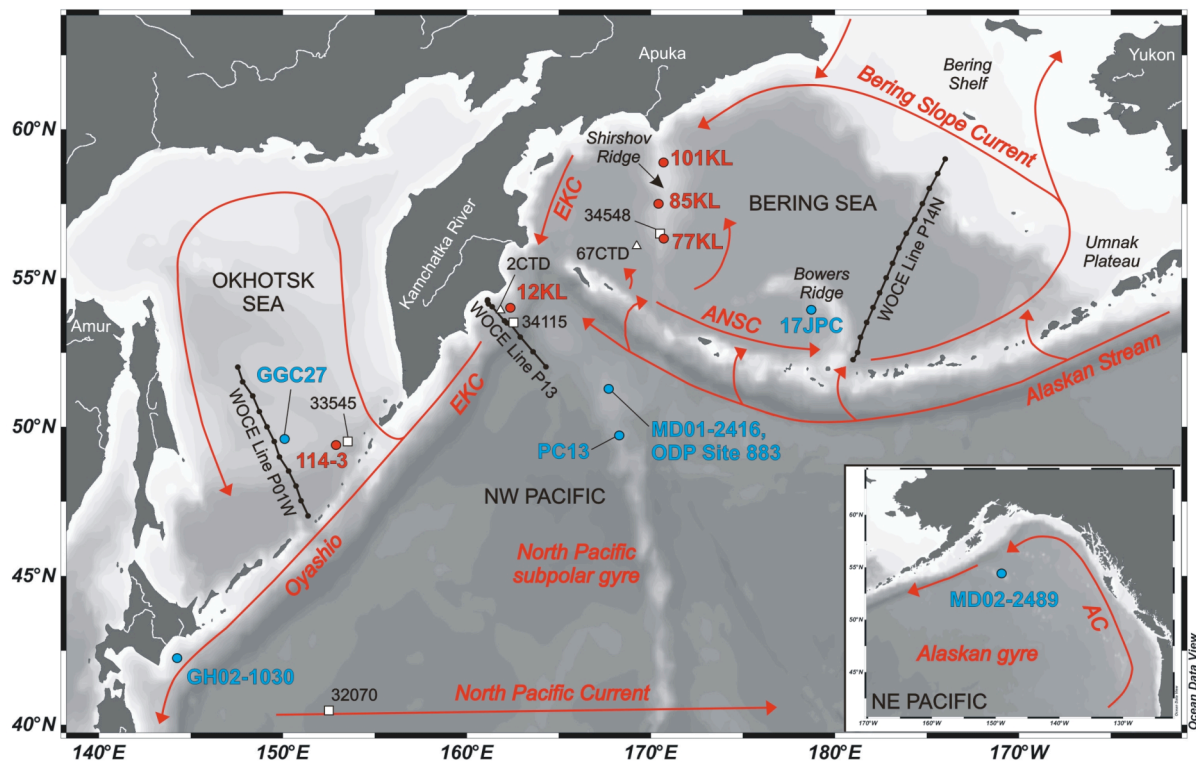

Figure 4.1: Bathymetric map of the subarctic NW-Pacific, Okhotsk Sea, Bering Sea, and NE-Pacific (inlet). Red dots indicate sediment cores studied here, blue dots denote published reference records: MD01-2416 and ODP Site 883 [*Sarnthein et al.*, 2004, 2006; *Gebhardt et al.*, 2008], and PC13 [*Brunelle et al.*, 2010] from the NW-Pacific, MD02-2489 from the NE-Pacific [*Gebhardt et al.*, 2008], GH02-1030 off Japan [*Sagawa and Ikehara*, 2008], GGC27 from the Okhotsk Sea [*Brunelle et al.*, 2010], and HLY-02-02-17JPC from Bowers Ridge [*Brunelle et al.*, 2007, 2010]. CTD-stations from R/V Sonne expedition SO201-2 (white triangles; *Dullo et al.*, 2009), stations from the World Ocean Atlas 2009 (white squares; *Locarnini et al.*, 2010), and stations from the World Ocean Circulation Experiment (WOCE; black dots) referred to in the text, are included. The general surface circulation pattern [after *Tomczak and Godfrey*, 1994; *Stabeno et al.*, 1999] is indicated by red arrows. AC = Alaskan Current, EKC = East Kamchatka Current, ANSC = Aleutian North Slope Current. This map was generated with „Ocean Data View" [*Schlitzer*, 2011].

4.1.3 Modern hydrography and carbonate dissolution

Characteristic oceanographic features of the subarctic NW-Pacific are a strong seasonal variability of SST and SSS (Figure 4.2) as well as upper-ocean stratification. Both are linked to the seasonal interplay between the atmospheric pressure systems of the Siberian High and the Aleutian Low, which
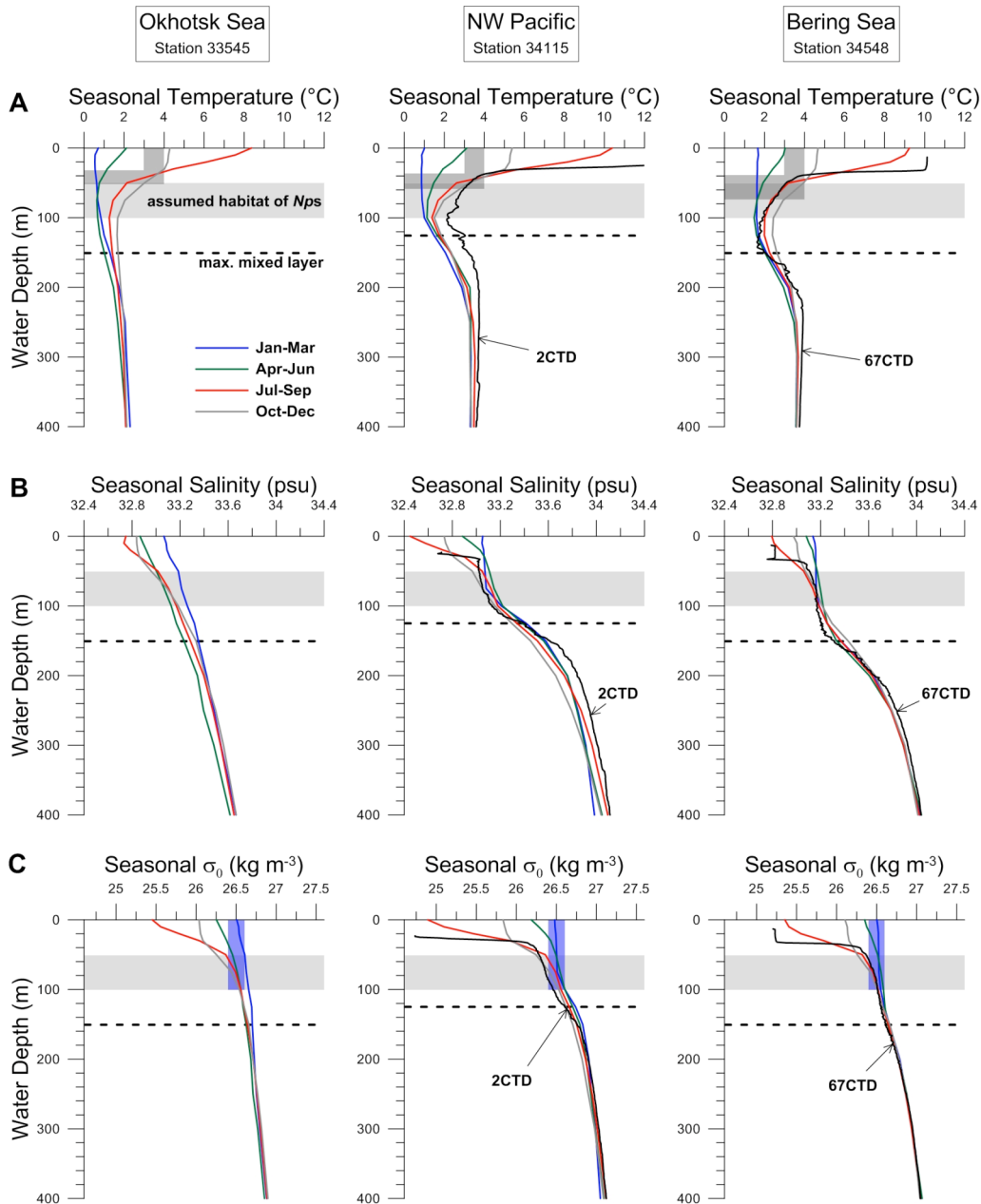

Figure 4.2: Modern seasonal profiles of in situ temperature (A), salinity (B), and potential density (σ_0; C) for the southern Okhotsk Sea, the subarctic NW-Pacific, and the western Bering Sea. Stations lying in the vicinity of our core locations were chosen from the World Ocean Atlas 2009 (WOA; stations 33545, 34115, 34548; *Locarnini et al.*, 2010) and are shown together with CTD-measurements conducted during R/V Sonne expedition SO201-2 in September 2009 (stations SO201-2-2CTD, -67CTD; *Dullo et al.*, 2009). The habitat of the planktonic foraminifer *N. pachyderma* (sin.) is assumed to lie in 50-100 m water depth (light gray-shaded bars) and to be associated with an isopycnal layer of ~26.4-26.6 kg m^{-3} (blue-shaded bars in C). Depths of the maximum mixed layer (dashed line) are inferred from *Miura et al.* [2002] and fit with WOA- and CTD-data. Note that the Mg/Ca-based average Holocene temperatures of 3-4 °C (dark gray-shaded bars) only correspond to water temperatures recorded during modern summer (July-September; red line) and fall (October-December; gray line) in the assumed habitat.

in the Okhotsk and the Bering seas leads to intense winter mixing and sea-ice formation [e.g. *Niebauer et al.*, 1999]. Stratification during summer arises from increased insolation and melting sea-ice, while a temperature minimum layer (dichothermal layer) remains at ca. 100 m water depth. Waters from this layer are supposed to be formed during winter mixing in the Bering and Okhotsk seas and to be subsequently exported to the NW-Pacific [*Ohtani et al.*, 1972; *Miura et al.*, 2002]. As a consequence of this variability, the modern seasonal thermo- and pycnoclines mainly lie within the upper ~30-70 m water depth at our study sites.

The subarctic N-Pacific is characterized by a shallow-lying lysocline. Data obtained from the World Ocean Circulation Experiment (WOCE), used to estimate the calcite saturation state for seawater ($\Delta[CO_3^{2-}]$), reveal that the calcite saturation horizon (CSH) in the subarctic NW-Pacific lies between 150-300 m water depth (Figure 4.3). Critical values of ~18-26 µmol kg^{-1} for $\Delta[CO_3^{2-}]$ below, where selective removal of Mg^{2+} ions from calcitic foraminiferal tests during calcite dissolution is assumed to start [*Regenberg et al.*, 2006], are already reached at shallower depths (~120-200 m). As all sediment cores investigated in this study were recovered below the modern CSH, foraminiferal tests must have been affected by calcite dissolution.
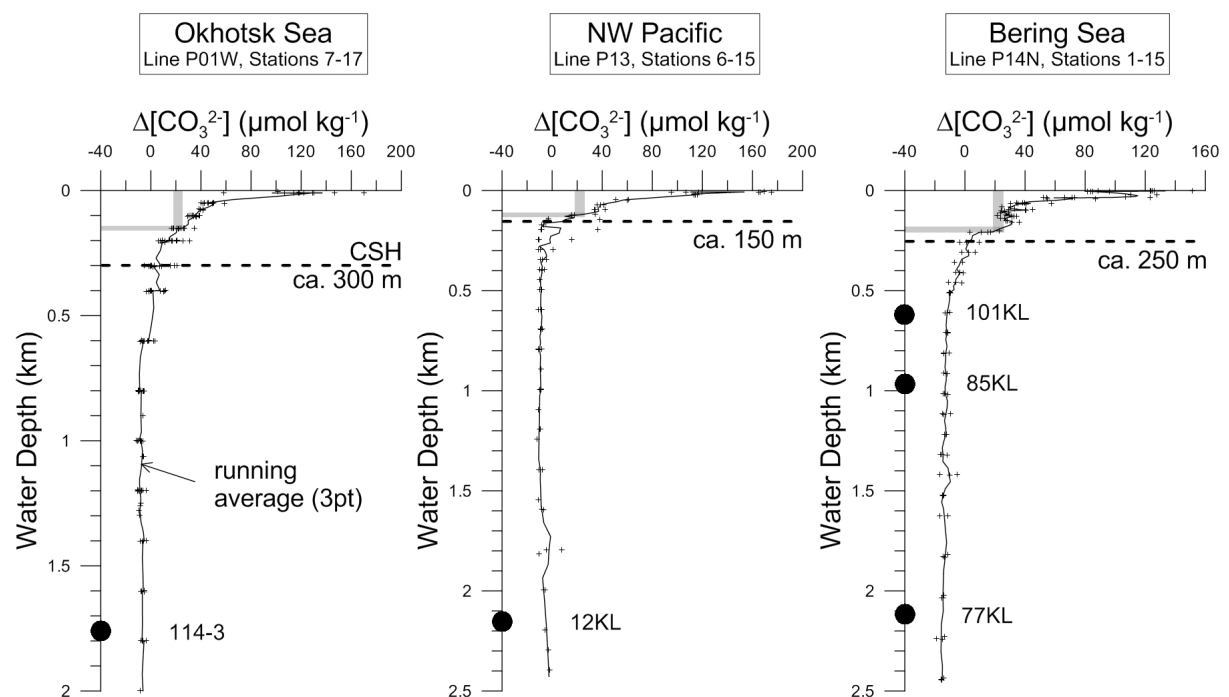
Figure 4.3: Profiles of $\Delta[CO_3^{2-}]$, defined as the difference between the in situ carbonate ion concentration ($[CO_3^{2-}]_{insitu}$) (calculated using the CO2SYS macro for MS Excel; *Pierrot et al.*, 2006) and $[CO_3^{2-}]$ at saturation (calculated after *Jansen et al.*, 2002) for the Okhotsk Sea, subarctic NW-Pacific, and Bering Sea. Total alkalinity and total CO_2 data were obtained from WOCE lines P01W (stations 7-17), P13 (stations 6-15), and P14N (stations 1-15) (available at http://cchdo.ucsd.edu/). Dashed horizontal lines mark the depth of the calcite saturation horizon (CSH), where $\Delta[CO_3^{2-}] = 0$, which represents the approximate top of the lysocline. Gray bars mark the critical $\Delta[CO_3^{2-}]$ threshold of ~18-26 µmol kg^{-1}, at which Mg^{2+} removal from foraminiferal tests is assumed to start [*Regenberg et al.*, 2006]. Black dots mark water depths of core locations, lying clearly below the critical $\Delta[CO_3^{2-}]$ threshold.

4.2 Material and methods

4.2.1 Sedimentology

This study is based on piston cores SO201-2-12KL, -77KL, -85KL, and -101KL recovered during RV Sonne cruise SO201 KALMAR Leg 2 in 2009 in the subarctic NW-Pacific and western Bering Sea [*Dullo et al.*, 2009]. Cores 77KL, 85KL, and 101KL lie on a 280 km-long North-South transect on Shirshov Ridge in the western Bering Sea in shallow to deep intermediate water depths (630-2135 m; Table 4.1). Core 12KL was recovered from the continental slope off eastern Kamchatka close to Kronotsky Peninsula (2145 m) and is lying in the path of the EKC. The sedimentology of cores 77KL, 85KL, and 101KL is characterized by monotonous sequences of siliciclastic material of mainly clay and silt size. Relatively thin layers of diatomaceous ooze/silt are intercalated. Sediments of core 12KL are characterized by monotonous siliciclastic sandy/clayey silt series that are overlain by a diatomaceous sequence. All cores commonly contain calcitic shell fragments, dropstones, and plant remains. Turbiditic sand layers and volcanic ashes are frequently found.

Table: 4.1.Site information.

Core	Latitude (°N)	Longitude (°E)	Depth (mbsl)	Recovery (m)
LV29-114-3	49°22.54'N	152°53.23'E	1765	9.64
SO201-2-12KL	53°59.47'N	162°22.51'E	2145	9.05
SO201-2-77KL	56°19.83'N	170°41.98'E	2135	11.78
SO201-2-85KL	57°30.30'N	170°24.77'E	968	18.13
SO201-2-101KL	58°52.52'N	170°41.45'E	630	18.32

Additional samples were obtained from core LV29-114-3 (Table 4.1) retrieved from the southern Okhotsk Sea in 2002 during LV29 KOMEX Leg 2 cruise with RV Akademik Lavrentyev [*Biebow et al.*, 2003]. Core 114-3 in the eastern Kurile Basin is influenced by the EKC entering the Okhotsk Sea. The sedimentary succession shows a 175 cm thick layer of diatomaceous sediment that is followed by terrigenous sediments with high magnetic susceptibility values. All cores contain only low contents of $CaCO_3$ (< 5 wt.%). However, all cores show increased contents during the B/A, reaching maximum values of up to 30 wt.% in cores 12KL and 77KL.

4.2.2 Age model

The stratigraphic framework of all cores is presented in *Max et al.* [in review] in high detail. For the last 20,000 years, the age models are based on a combined chronostratigraphic approach including color and X-ray fluorescence (XRF) core logging data for intercore correlations, as well as AMS-^{14}C dating of the planktonic foraminiferal species *Neogloboquadrina pachyderma* (sin.) (Figure 4.4). Planktonic AMS-^{14}C-ages were converted to calendar ages using the IntCal09 calibration [*Reimer et al.*, 2009] assuming spatially different reservoir age corrections for the Bering and Okhotsk seas. For the last deglaciation the investigated sediment records provide sedimentation rates between 5 and 30
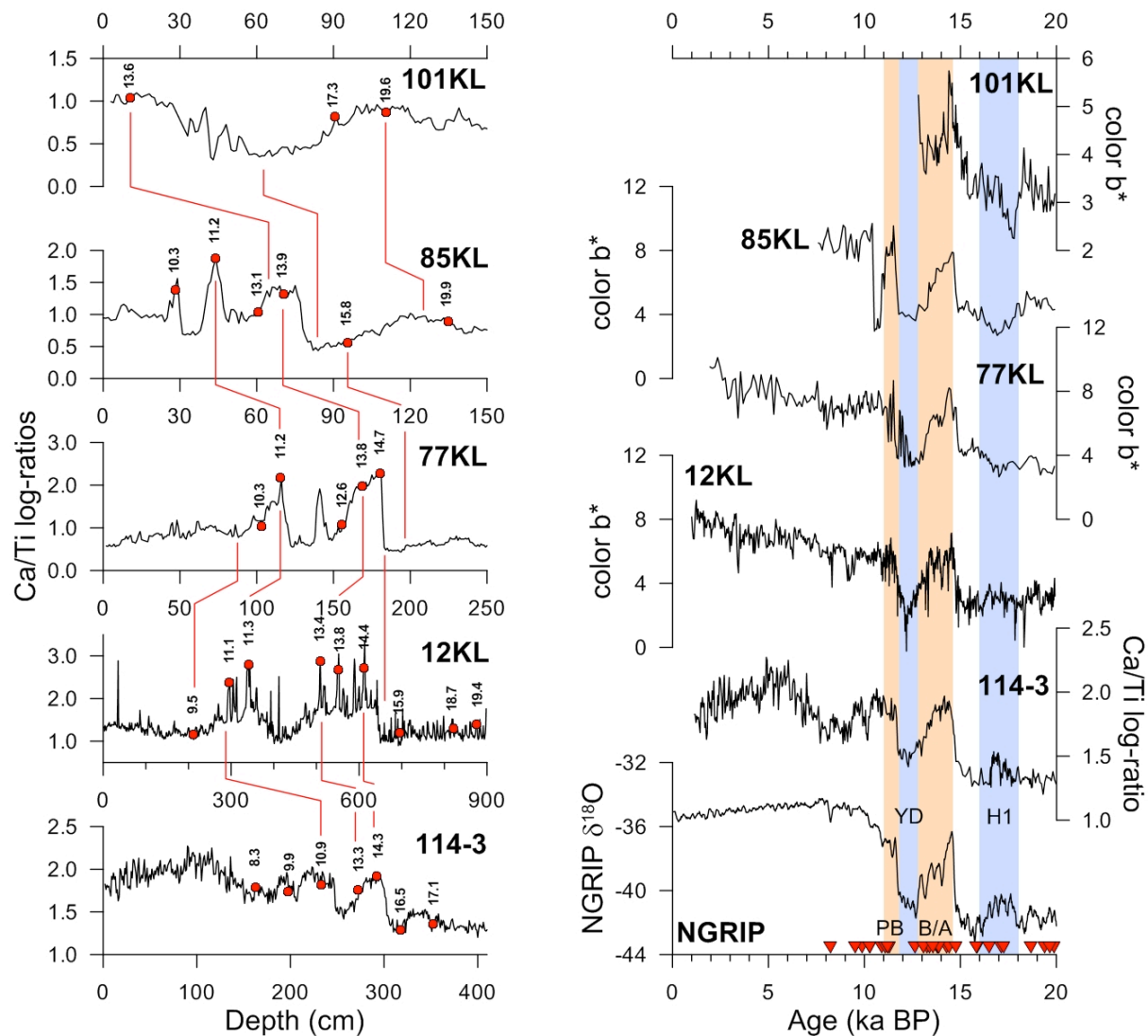
Figure 4.4: Stratigraphy for cores used in this study. Left hand: XRF Ca/Ti log-ratios (shown vs. depth) are used for intercore correlations. Filled red circles mark AMS-^{14}C datings (vertical numbers indicate calendar ages). Right hand: Records of color b* and XRF Ca/Ti log-ratios provide a pattern of variability similar to that registered in the NGRIP ice core from Greenland [NGRIP members, 2004; GICC05 timescale, *Rasmussen et al.*, 2006]. Red triangels indicate age control points.

cm kyr^{-1}, for core 12KL even up to 125 cm kyr^{-1}, hence allowing for a centennial to millennial-scale time resolution in our reconstructions.

4.2.3 Stable isotope and Mg/Ca analyses

Combined stable isotope and Mg/Ca analyses were performed on ~100-150 specimens (~500 µg) of the polar to subpolar shallow-dwelling planktonic foraminifer *Neogloboquadrina pachyderma* (sin.) (now referred to as *Nps*), which were selected from the 125-250 µm size fraction. We focused on the most abundant "square-shaped" (four-chambered) specimen of *Nps* from a relatively narrow size fraction to avoid potential bias due to shell size [*Elderfield et al.*, 2002] and such linked to different morphotypes [*Healy-Williams*, 1992]. Abundance of foraminifera was sufficient in all investigated

sediment cores, except for core 12KL, which did not contain enough foraminiferal tests from 0-125 cm core depth (< 1 wt.% $CaCO_3$).

Foraminiferal tests were gently crushed between two glass plates to open chambers and mixed with a brush for homogenization. Material was divided into two sub-samples with two thirds used for Mg/Ca and one third for stable isotope analyses, and then transferred into acid-cleaned vials. Prior to stable isotope measurements, sub-samples were rinsed three times with ultra-pure water and twice with ethanol including ultrasonic treatment steps of 20 seconds in order to remove clays. Dried samples were measured on a Thermo Finnigan MAT253 mass spectrometer coupled with a Thermo Scientific Kiel IV Carbonate device at GEOMAR, Kiel. Results were calibrated to the VPDB scale and referenced to the NBS19 standard. Analytical long-term precision (2σ, n > 1000 samples) of the used in-house Bremen carbonate standard (Solnhofen limestone) was 0.06 ‰ for $\delta^{13}C$ and 0.10 ‰ for $\delta^{18}O$.

Cleaning of planktonic foraminifera for Mg/Ca analyses followed the protocol of *Barker et al.* [2003] and included a reductive cleaning step using hydrazine (N_2H_4) as reducing agent to remove metal oxides. The oxidation step using hydrogen peroxide (H_2O_2) to remove the remaining organic matter was applied after a sample transfer to new acid-leached vials. Final leaching was performed using 0.001 M nitric acid (HNO_3). Samples were dissolved immediately before analysis with ultra-pure 0.075 M HNO_3 including 25 min of ultrasonic treatment and subsequent centrifugation. About 500 μl of supernatant was then transferred into polypropylene tubes and diluted with 1.8 ml of 0.075 M HNO_3 containing 10 ppm of yttrium as an internal standard.

Samples were measured on an axial viewing ICP-OES (VARIAN 720-ES coupled with SPS3 Sample Preparation System). We used spectral lines 279.553 nm for Mg and 370.602 nm for Ca. Post-processing included automatic correction for analytical drift and normalization to the ECRM 752-1 standard, which is used as internal consistency standard applying a reported Mg/Ca ratio of 3.761 mmol mol^{-1} [*Greaves et al.*, 2008]. For Mg/Ca measurement the analytical long-term precision of the ECRM752-1 standard, which was measured after each batch of 10 samples including 1 blank, was 0.1 mmol mol^{-1} (2σ). Due to very low carbonate contents of the sediments and hence, general low abundance of foraminifera, full sample treatment was only repeated for 11 samples that were considered as outliers. These replicate analyses provided discrepancies between 0.1-0.7 mmol mol^{-1} for Mg/Ca that may indicate a contamination of the samples. Benthic and planktonic $\delta^{18}O$, as well as foraminiferal element ratios (Mg/Ca, Mn/Ca, Fe/Ca, Al/Ca) are shown in the supplementary information (Figure. S4.1).

To detect possible contamination by detrital material and secondary diagenetic coatings, which might affect foraminiferal Mg/Ca ratios [e.g. *Boyle*, 1983; *Rosenthal et al.*, 2000; *Barker et al.*, 2003;], ratios

of foraminiferal Mn/Ca, Fe/Ca, and Al/Ca were monitored simultaneously with Mg/Ca. Our cores featured relatively high average Fe/Ca, Mn/Ca, and Al/Ca ratios ranging between 0.21-1.84 mmol mol^{-1}, 0.02-0.06 mmol mol^{-1}, and 0.08-0.20 mmol mol^{-1}, respectively. In particular Fe/Ca ratios were higher than the 0.1 mmol mol^{-1} suggested by *Barker et al.* [2003] for uncontaminated foraminiferal tests. Each core was individually tested for linear relationships between Mg/Ca and the other ratios (see Figure S4.2 in the supplementary information). In case of linear correlation coefficients (R^2) higher than 0.6, we considered our Mg/Ca analyses possibly affected by contamination and defined core-specific thresholds for Fe/Ca, Mn/Ca, and Al/Ca. No samples from the last 20 ka BP were excluded according to this approach and hence are supposedly not contaminated. Two samples were rejected due to very high Mg/Ca ratios (2.2 and 2.4 mmol mol^{-1}) as indicated in the supplementary information (S4.2).

To improve sampling resolution for core LV29-114-3, Mg/Ca-results based on former measurements of 30 specimens for stable isotopes and 50 specimens for Mg/Ca selected from the 150-250 μm size fraction were included in our dataset. These samples were also cleaned according to the protocol of *Barker et al.* [2003] but without a reductive cleaning step and analyzed using a radially viewing ICP-OES (Ciros CCD SOP, Spectro A.I.) at the Institute of Geosciences, University of Kiel, on spectral lines 183 nm for Ca and 270 nm for Mg. Samples cleaned with the reductive step show either similar or relatively increased Mg/Ca ratios, albeit without any systematically differences with respect to non-reductively cleaned samples. We consider the results of both datasets as consistent as the mean offset between both datasets is not constant and lies within the error range of the measurements (ca. 0.1 mmol mol^{-1}), in agreement with studies comparing both cleaning methods [e.g. *Rosenthal et al.*, 2004; *Groeneveld et al.*, 2008].

4.2.4 Mg/Ca paleothermometry and temperature signal of Nps

As there is no locally established Mg/Ca-temperature calibration for *Nps* in the subarctic N-Pacific, we used the linear equation of *Kozdon et al.* [2009] to calculate sub sea surface temperatures from Mg/Ca ratios of *Nps* (subSST$_{Mg/Ca}$):

$$Mg/Ca \ (mmol \ mol^{-1}) = 0.13*T \ (°C) + 0.35 \qquad (Eq.1)$$

Considering the slope in Eq.1, the long-term analytical precision of our Mg/Ca measurements translates into an error of ±0.8 °C. This temperature calibration is based on Holocene core-top samples from high-latitude Nordic Seas used in a cross-calibration approach between Mg/Ca and independent $\delta^{44/40}$Ca measurements. In contrast, most other temperature calibrations for *Nps* are of exponential character and assume constant calcification depths.

We used this specific relationship because we consider the depth habitat of *Nps* most likely to be related to the seasonal thermo- and pycnocline, similar to the Nordic Seas and the Arctic Ocean. Studies conducted in these areas show that shell calcification of *Nps* mostly occurs at or close to the depth of the main thermocline between 50 and 200 m [*Kohfeld et al.*, 1996; *Bauch et al.*, 1997; *Simstich et al.*, 2003]. Based on these studies *Sarnthein et al.* [2004, 2006] assume a depth range of 30-100 m in the NW-Pacific. *Bauch et al.* [2002] for the Okhotsk Sea calculated $\delta^{18}O$-based average calcification depths lying within the upper 50-200 m, which is in accord with maximum abundances of *Nps*. From their results, *Bauch et al.* [2002] speculates that *Nps* lives at the bottom of the thermocline. Comparison with temperatures inferred from $\delta^{18}O$ and hydrographic data indicate variable calcification depths of *Nps* that are associated with an isopycnal layer [*Kozdon et al.*, 2009]. *Kuroyanagi and Kawahata* [2004] from tow samples from the western N-Pacific and Japan Sea report a depth habitat of Nps lying below the pycnocline (> 20 m w.d.) supporting this indication.

WOA data show that the average depth of the pycnocline lies at ~30 m w.d., and that the thermocline extends to ca. 70 m with a temperature minimum of 1-2 °C in ~100 m at our study sites during boreal summer (July-September) (Figure 4.2). At all sites an isopycnal layer with a potential density (σ_0) of 26.4-26.6 kg m^{-3} is present within almost the same depth interval (50-100 m). If *Nps* occupies a habitat that lies below the pycnocline and is related to an isopycnal layer covering depths down to the bottom of the thermocline, then the depth habitat of *Nps* must lie between 50-100 m at our sites. The assumption that *Nps* records a summer signal is supported by our reconstructed average Holocene (< 8 ka BP) subSST$_{Mg/Ca}$-estimates, which range between 3-4 °C and therefore only correspond to summer and fall (October-December) temperatures in the suggested depth habitat. In contrast, modern boreal winter (January-March) and spring (April-June) temperatures lie below 3 °C (Figure 4.2), which also lie below our reconstructed temperatures. Accordingly, we assume *Nps* Mg/Ca data to reflect temperatures recorded during late summer and early fall in 50-100 m water depth.

We do not follow the assumption of *Sarnthein et al.* [2006] and *Gebhardt et al.* [2008] in part based on sediment trap studies from the open subarctic N-Pacific [*Takahashi et al.*, 2002] that *Nps* rather records both, late spring and late summer/early fall temperatures. In the southern Bering Sea, *Takahashi et al.* [2002] observed two maxima of biological CaCO$_3$ fluxes during spring/summer and fall that are caused by enhanced foraminifera abundances. However, in contrast to our core locations, their sediment trap studies were conducted at locations that are not dominantly influenced by seasonal sea-ice inhibiting marine productivity during spring. Furthermore, the southern Bering Sea primary CaCO$_3$ maximum occurred during October to November [*Takahashi et al.*, 2002]. Similar observations are reported from sediment traps along the Subarctic Front in the NW-Pacific [*Mohiuddin et al.*, 2005], which is in accord with our interpretation of the (main) temperature signal.

Application of the multispecies calibration of *Elderfield and Ganssen* [2000] and the relationship of *Nürnberg et al.* [1996] specific for *G. sacculifer* and *Nps* to our Mg/Ca data would produce a larger temperature variability and would result in subSST$_{Mg/Ca}$ that were on average warmer by about +1 °C and +3 °C, respectively. Consequently, mean Holocene temperature estimates would not fit with modern instrumental data within the assumed habitat of *Nps* when using the equation of *Nürnberg et al.* [1996], whereas the difference to the calibration of *Elderfield and Ganssen* [2000] lies within the error range of our method. We thereby consider our subSST$_{Mg/Ca}$ results as reliable and the choice of the temperature calibration as justified.

Mg/Ca-based paleotemperature estimations are constrained by the influence of calcite dissolution of the foraminiferal tests in conjunction with selective removal of Mg^{2+} ions [e.g. *Regenberg et al.*, 2006 and references therein]. However, although all sediment cores investigated in this study were recovered below the modern CSH, we resigned from correcting the initial Mg/Ca values for potential dissolution effects. Nevertheless, we admit that our Mg/Ca ratios are to an unknown degree affected by dissolution and discuss the application of procedures to correct planktonic foraminiferal Mg/Ca for dissolution effects in the supplementary information (S4.3). In Shirshov Ridge cores we identified samples that were eventually altered by early diagenetic processes, which is also discussed in the supplementary information (S4.4). However, respective samples are from core intervals > 20 ka BP and not used in the context of our paleoceanographic interpretations.

4.2.5 Alkenone temperature signal

We compare our subSST$_{Mg/Ca}$ records with the alkenone-based sea surface temperature (SST$_{Uk'37}$) records of *Max et al.* [in review], which were derived from the same samples. SST$_{Uk'37}$ estimates are calculated according to the global (60 °N - 60 °S) core-top calibration of *Müller et al.* [1998], which is widely used for N-Pacific temperature reconstructions:

$$U^{k'}_{37} = 0.033*T\ (°C) + 0.044 \qquad (Eq.2)$$

The standard error of this calibration is given as ±1.5 °C [*Müller et al.*, 1998]. A core-top calibration in the eastern Bering Sea suggests that most alkenones are synthesized during September [*Harada et al.*, 2003]. *Harada et al.* [2006a] showed that *Emiliania huxleyi* is the most abundant alkenone producer in the NW-Pacific, which is present within the upper 50 m w.d. and shows maximum export fluxes between July and November. For the western Okhotsk Sea, definitely influenced by seasonal sea-ice, maximum alkenone export fluxes were reported during September and October [*Seki et al.*, 2007]. Mean insolation calculated after *Laskar* [2004] for July-September at 65 °N is in good agreement with the SST$_{Uk'37}$ records (Figure 4.5) supporting a restriction to late summer/early fall. Other calibrations, e.g. that of *Prahl et al.* [1988] and *Sikes et al.* [1997], in our cores produce
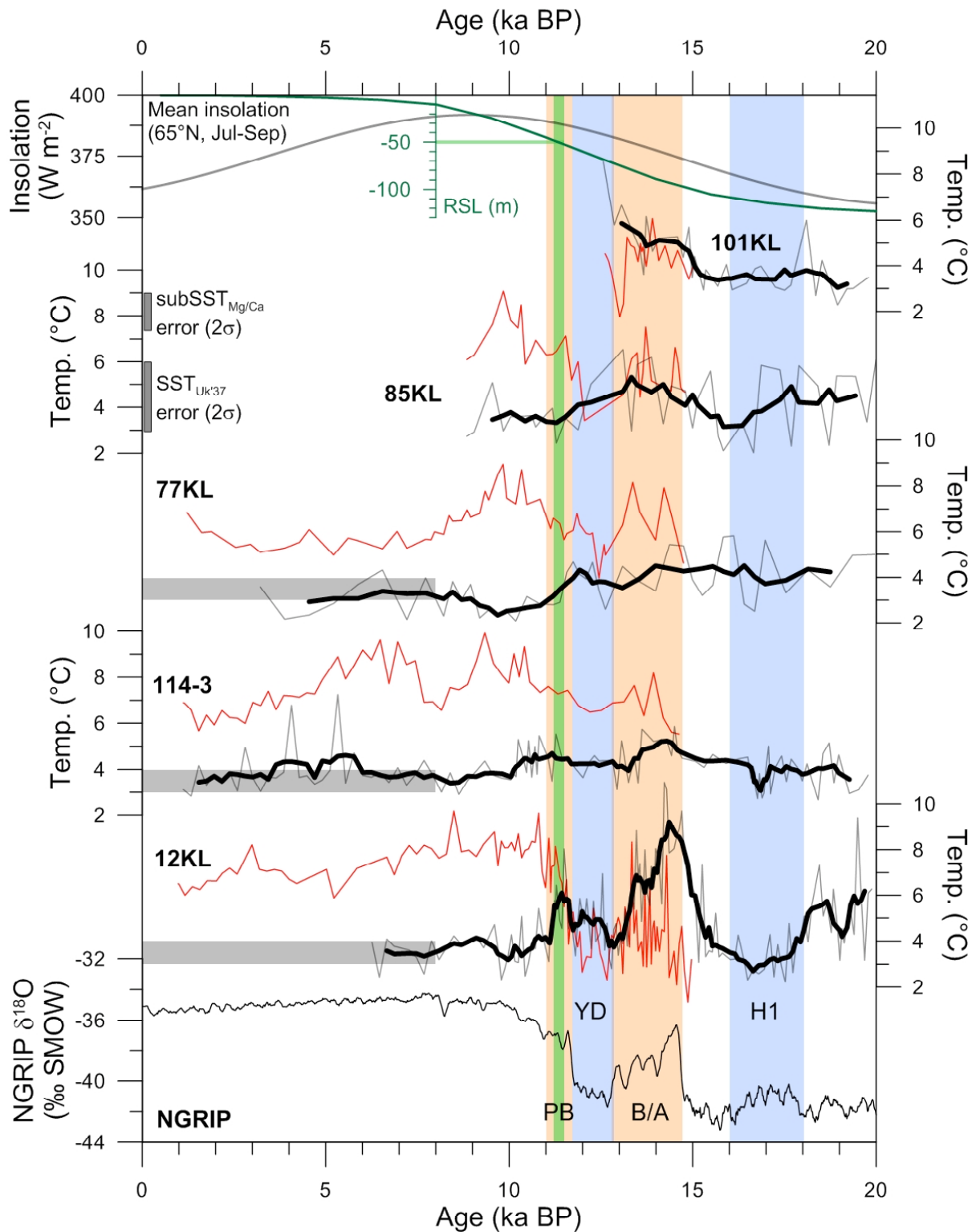
Figure 4.5: Temperature reconstructions over the last 20 kyr from the Bering Sea (SO201-2-101KL, -85KL, -77KL), the subarctic NW-Pacific off Kamchatka (SO201-2-12KL), and the southern Okhotsk Sea (LV29-114-3). The NGRIP ice core oxygen isotope record [*NGRIP members*, *2004*; GICC05 timescale, *Rasmussen et al.*, 2006] is given for reference. Our subSSTMg/Ca records (light gray lines) are shown together with alkenone-based SST$_{Uk'37}$ records (thin red lines) from *Max et al.* [in review] on the same scale. Running 5-point-averages of subSST$_{Mg/Ca}$ (thick black lines) are given to emphasize temporal trends. The calculated error of our temperature estimates is given (see sections 2.4 and 2.5). Average middle to late Holocene (< 8 ka BP) temperature estimates of 3-4 °C are highlighted (gray vertical bars). Relative sea-level (RSL, green line) is derived from [*Waelbroek et al.*, 2002]. Mean insolation calculated for boreal summer (July-September) at 65 °N (gray line) was calculated after *Laskar* [2004]. Pale orange and pale blue shadings represent the B/A and PB, and H1 and YD, respectively.

temperatures that are higher by up to 0.1 °C and 3 °C, respectively. However, our reconstructed mean Holocene alkenone- and Mg/Ca-based temperature estimates fit with the modern instrumental range. Moreover, general temporal trends are not affected when other calibrations are applied.

Differences between alkenone- and Mg/Ca-paleotemperatures can be the result of seasonal bias, as in general coccolithophorids are assumed to record boreal winter temperatures, whereas planktonic foraminifera reflect a boreal summer or mean annual temperature signal [*Leduc et al.*, 2010]. Due to the influence of seasonal sea-ice formation at our sites, we consider a restriction of both, alkenone producers and planktonic foraminifera, to the sea-ice-free late summer/early fall season to be more likely. Nevertheless, we consider seasonal bias possible in case of a disappearing sea-ice influence. Regarding depth habitats, in this study the alkenone signal is thought to represent temperatures from the sea surface, while Mg/Ca-results represent temperatures from the colder subsurface (50-100 m w.d.).

4.2.5 Salinity estimation

Past changes in subSSS are approximated from seawater $\delta^{18}O$ estimates. The oxygen isotope signal recorded in foraminiferal calcite ($\delta^{18}O_{Cc}$) is a combination of the local seawater isotopic composition ($\delta^{18}O_{sw}$; reported in ‰ vs. SMOW) and temperature. Local $\delta^{18}O_{sw}$ is influenced by changes in global ice volume and regional variations of salinity that are mainly controlled by local changes of the evaporation-precipitation budget [e.g. *Schmidt et al.*, 2004]. In this study, $\delta^{18}O_{sw}$ is therefore calculated by applying the relationship of *Shackleton* [1974] that includes our foraminiferal $\delta^{18}O$-values in combination with the corresponding Mg/Ca-based paleotemperature estimates:

$$\delta^{18}O_{sw} = \delta^{18}O_{Cc} + 0.27 - (4.38 - SQRT(4.38^2 - 4*0.1*(16.9 - Temp.)))/(2*0.1) \; (Eq.3)$$

This equation extends the results of an inorganic precipitation study [*O'Neil et al.*, 1969] to the endobenthic foraminifera *Uvigerina peregrina*, assumed to calcify in isotopic equilibrium with seawater. *Mulitza et al.* [2003] found that the T- $\delta^{18}O$-relationships of *N. pachyderma* and epibenthic foraminifera species *Cibicides* are nearly identical, a species that is reported to show a negative $\delta^{18}O$-disequilibrium offset on the order of 0.64 ‰ relative to *U. peregrina* [*Shackleton*, 1974]. However, *N. pachyderma* shows a mean slope of 0.28 ‰ per °C which is in agreement with that of *U. peregrina* within -2 °C to +13 °C [*Mulitza et al.*, 2003]. We therefore decided to use the equation of Shackleton [1974] based on *U. peregrina*. The factor of 0.27 ‰ in Eq.3 is due to the conversion of $\delta^{18}O_{sw}$ from the PDB to the SMOW scale [*Hut*, 1987]. Finally, we correct for the global ice-volume signal following *Waelbroek et al.* [2002] based on a $\delta^{18}O_{sw}$ change of 1.1 ‰ per 130 m relative sea-level change [*Yokoyama et al.*, 2000] to produce ice-volume corrected seawater estimates ($\delta^{18}O_{ivc-sw}$).

The absolute estimation of salinity from $\delta^{18}O_{sw}$ relies on regional calibrations and hence from actual measurements of water samples, as variations in the ratio of evaporation to precipitation can cause different $\delta^{18}O_{sw}$-salinity relationships. Such calibrations exist for the Okhotsk Sea and western subarctic Pacific [*Yamamoto et al.*, 2001], but not for the Bering Sea. However, the uncertainty of the $\delta^{18}O_{sw}$-approach already cumulates to ~0.3 ‰, which would translate into a salinity error of ca. ±0.8 psu applying the calibration of *Yamamoto et al.* [2001]. Since our study sites are characterized by a modern seasonal salinity range of ~32.4-33.6 psu within the upper 150 m (Figure 4.2), we consider this error as too large and do not apply a conversion into salinity estimates. We rather interpret regional hydrological changes from relative changes of our $\delta^{18}O_{ivc-sw}$ results in such that heavier (more positive) $\delta^{18}O_{ivc-sw}$-values are equivalent to a rise in local subSSS, while a drop in subSSS are indicated by lighter (more negative) $\delta^{18}O_{ivc-sw}$-values.

4.2.6 Biogenic opal

Biogenic opal was measured via molybdate-blue spectrophotometry applying the automated leaching method of *Müller and Schneider* [1993]. We used 20 mg of freeze-dried bulk sediment samples mixed with 100 ml of sodium hydroxide (1 M) in a water bath at 85 °C for 45 min. The procedure of *DeMaster* [1981] was used to calculate weight percentages of biogenic opal. Analytical precision (2σ) of replicate measurements was ±2 wt.%.

4.3 Results

4.3.1 Temperature reconstructions

Figure 4.5 shows our temperature reconstructions for the last 20 kyr together with the alkenone-based $SST_{Uk'37}$ records from *Max et al.* [in review]. Reconstructed $subSST_{Mg/Ca}$ show a similar range in all cores of about 2 °C to 6 °C, except for core 12KL, which extends this range to a maximum of ~9 °C. Also, this core records the most pronounced amplitude variations, whereas the temperature variability of the cores from both Pacific marginal seas is low. We found similar $subSST_{Mg/Ca}$ in the Bering and Okhotsk seas during the last deglaciation as reflected by reconstructions from the northernmost site (101KL) and the southernmost site (114-3).

In contrast, alkenones, which prior to 15 ka BP are characterized by concentrations below detection limit, point to increasing $SST_{Uk'37}$ of ~3 °C from the north to the south [*Max et al.*, in review]. Relative temperature changes of both proxy records (Figure 4.5) are consistent amongst each other in all records during the last glacial termination and almost parallel the thermal evolution registered in the NGRIP ice core from Greenland until the onset of the early Holocene. However, in part, $subSST_{Mg/Ca}$ and $SST_{Uk'37}$ records show different trends which result in temperature differences between the surface and subsurface (ΔT).

All cores, except core 101KL, show a minimum in subSST$_{Mg/Ca}$ between 18-16 ka BP and values of ca. ~3-4 °C (supposedly reflecting the H1 cold phase), which corresponds to H1 in the N-Atlantic. This minimum is most pronounced in NW-Pacific core 12KL and only short-lived in core 114-3 from the Okhotsk Sea. Due to the lower time-resolution it is not well resolved in Bering Sea cores 77KL and 85KL. Moreover, in core 85KL the Mg/Ca variability during 20-17 ka BP is larger than expected.

A warming is recorded at the transition from H1 into the following B/A. Within a period of only 1,000 to 2,000 years subSST$_{Mg/Ca}$ increase by 2-4 °C to maxima of ~5-6 °C at sites 114-3, 77KL, 85KL, and 101KL, and to ~9 °C at Site 12KL. SST$_{Uk'37}$ show increases from 2-6 °C at 15 ka BP to 6-8 °C during the B/A [*Max et al.*, in review]. While Bering Sea cores 85KL and 101KL record almost similar subSST$_{Mg/Ca}$ and SST$_{Uk'37}$ until the Preboreal (PB), cores 114-3 and 77KL show ΔT of ~2-3 °C during the B/A. In contrast to the other records, core 12KL shows a two-step subSST$_{Mg/Ca}$ cooling during the B/A and, most notably, negative ΔT values of up to -6 °C. ΔT is minimal at the onset of the B/A and subsequently increasing, until temperatures from both proxies converge at the end of the B/A at a value of ~4 °C.

Cores 114-3, 12KL and 77KL record a cooling of subSST$_{Mg/Ca}$ following the early B/A-maximum. Subsequently, subSST$_{Mg/Ca}$ minima of 3-4 °C are recorded at either the end of the B/A (114-3) or at the beginning of the YD (12KL, 77KL). In contrast, core 85KL shows the temperature maximum at the end of the B/A and decreasing values since. During the YD cores 114-3 and 77KL record almost stable subSST$_{Mg/Ca}$ (~4 °C), while core 12KL is characterized by a slight warming. SST$_{Uk'37}$ show a decrease of 2-5 °C into the YD [*Max et al.*, in review]. ΔT is reduced to about +2° C at sites 114-3 and 77KL, to 0 °C at Site 85KL, and again becomes negative (-2 °C) at Site 12KL.

Core 12KL records a pronounced and short-lived subSST$_{Mg/Ca}$ maximum of ~6 °C during the PB (~11.5 ka BP), whereas Okhotsk Sea core 114-3 is characterized by a stronger variability between 4 °C and 5 °C during ~11.5-10.0 ka BP. Bering Sea cores 77KL and 85KL show decreasing and minimum subSST$_{Mg/Ca}$ of ~3 °C, respectively during the PB. At all sites the PB is either subject to a cooling to subSST$_{Mg/Ca}$ of ~3-4 °C or followed by a respective cooling during the early Holocene. The timing for this is different at the respective sites. At Site 77KL it starts at the onset of the PB, while sites 12KL and 114-3 experience a later cooling at ~11 ka BP and ~10 ka BP, respectively. SST$_{Uk'37}$ increase by up to 5 °C subsequent to the YD and culminate in maximum values of 9-10 °C between 11-9 ka BP [*Max et al.*, in review]. Consequently, in all cores both proxies start to significantly diverge in the PB until ~10 ka BP, with ΔT-maxima of up to 6 °C. The Holocene SST$_{Uk'37}$ maximum occurs simultaneous with the insolation maximum calculated after Laskar [2004] for boreal summer (July-September) at 65 °N (Figure 4.5). Notably, SST$_{Uk'37}$-estimates from core 12KL became higher than subSST$_{Mg/Ca}$ only since the PB.

The later Holocene subSST$_{Mg/Ca}$ development is characterized by almost constant values that are ~1 °C warmer in cores 114-3 and 12KL than in Bering Sea core 77KL. In core 85KL, for which sediments are not preserved after 9 ka BP, subSST$_{Mg/Ca}$ remains at ~3 °C. Holocene subSST$_{Mg/Ca}$ estimates are lower than those of the B/A and YD but compare with those recorded during H1. For the last 9 kyr SST$_{Uk'37}$ records from cores 114-3, 12KL, and 77KL point to a gradual ~2 °C decrease in SST$_{Uk'37}$, which in core 114-3 is interrupted between 9-7 ka BP by a cooling to YD-levels [*Max et al.*, in review]. Hence, the temporal evolution of ΔT during the middle to late Holocene follows the SST$_{Uk'37}$ signal and records a ΔT-minimum between 9-7 ka BP in core 114-3.

4.3.2 Reconstruction of δ^{18}O$_{ivc-sw}$

Reconstructed δ^{18}O$_{ivc-sw}$ values approximating subSSS on average range between -1 ‰ vs. SMOW (fresher) to +1 ‰ vs. SMOW (more saline) during the last 20,000 years and are shown in Figure 4.6. The most prominent variability is recorded in NW-Pacific core 12KL, while our northernmost Bering Sea cores 85KL and 101KL show less amplitude variations in a narrower range of ca. -0.3 to +0.3 ‰. Notably, core 85KL shows a distinct variability around a value of 0 ‰. Okhotsk Sea core 114-3 records almost only negative values between -0.4 ‰ and 0 ‰, showing a variability not significantly higher than the error estimate for δ^{18}O$_{ivc-sw}$. In general, relative changes of δ^{18}O$_{ivc-sw}$ are regionally different, but at each site a general covariation between δ^{18}O$_{ivc-sw}$ and subSST$_{Mg/Ca}$ is observed.

During 20-18 ka BP cores 12KL, 77KL, and 85KL show positive average values (0 to 0.4 ‰), whereas δ^{18}O$_{ivc-sw}$ is negative at sites 114-3 and 101KL (-0.3 ‰ to 0 ‰). The interval 18-16 ka BP (thought to reflect H1) in core 12KL is marked by a δ^{18}O$_{ivc-sw}$ decrease of about -0.6 ‰ until 17 ka BP. Bering Sea cores are characterized by low temporal resolution in combination with high variability of δ^{18}O$_{ivc-sw}$ results during 20-16 ka BP, and hence do not show consistent and significant changes within that interval. Core 77KL at the end of H1 features positive values of about +0.3 ‰. Although in Okhotsk Sea core 114-3 a restricted negative H1-excursion of about -0.2 ‰ occurs at ~16.8 ka BP but δ^{18}O$_{ivc-sw}$ variability during H1 is lower than its error estimate.

During the transition from H1 into the B/A, data from cores 114-3 and 77KL show decreasing δ^{18}O$_{ivc-sw}$. In contrast, δ^{18}O$_{ivc-sw}$ recorded in cores 12KL and 101KL is increasing during that time. Results from core 85KL still vary around an almost constant level, with slightly higher δ^{18}O$_{ivc-sw}$ during the B/A. During the B/A cores 114-3 and 77KL show generally lower values than during H1 of about -0.2 ‰, whereas the other cores have positive values, which are maximal in core 12KL with δ^{18}O$_{ivc-sw}$ of up to +1 ‰. This core is characterized by a 2-step decrease in δ^{18}O$_{ivc-sw}$ until a minimum of -0.2 ‰ is reached at the end of the B/A. Here, a minimum is also recorded in core 114-3. Core 77KL shows decreasing δ^{18}O$_{ivc-sw}$ already since ~16 ka BP until the onset of the YD.
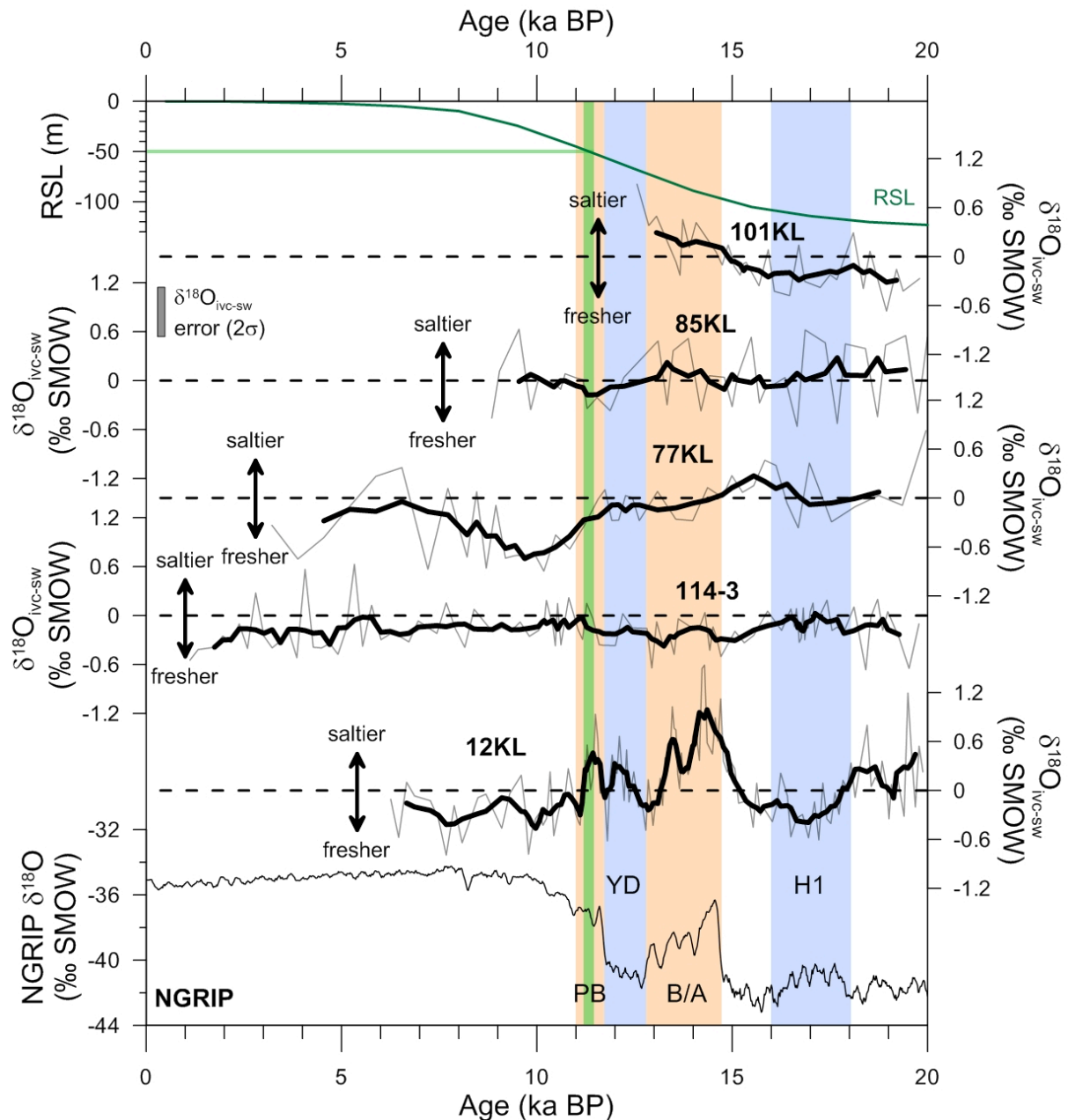
Figure 4.6: Ice-volume corrected $\delta^{18}O$-estimates of seawater ($\delta^{18}O_{ivc-sw}$) from the Bering Sea (SO201-2-101KL, -85KL, -77KL), the subarctic NW-Pacific off Kamchatka (SO201-2-12KL), and the southern Okhotsk Sea (LV29-114-3) during the last 20 kyr, together with the NGRIP $\delta^{18}O$ record [*NGRIP members*, 2004; GICC05 timescale, *Rasmussen et al.*, 2006]. Running 5-point-averages (thick black lines) emphasize temporal trends. Trends towards heavier (lighter) $\delta^{18}O_{ivc-sw}$-signatures are equivalent to increasing (decreasing) local subsurface salinity. Dashed lines indicate $\delta^{18}O_{ivc-sw}$ = 0 ‰ SMOW. Pale orange and pale blue shadings represent the B/A and PB, and the H1 and YD, respectively. During the Holocene, after relative sea-level (RSL; green line, after *Waelbroek et al.*, 2002) has risen above the sill depth of Bering Strait (-50 m), all cores are characterized by negative average $\delta^{18}O_{ivc-sw}$ values.

The YD is characterized by rising $\delta^{18}O_{ivc-sw}$ in core 12KL to +0.3 ‰ at 12.0 ka BP, whereas cores 114-3, 77KL, and 85KL only show insignificant changes around -0.2 ‰. Further, core 12KL shows a short-lived drop to ~0 ‰ at the YD-PB boundary around 11.8 ka BP, before a second pronounced maximum (ca. +0.5 ‰) is reached in the PB near ~11.5 ka BP. This PB maximum is only found in core 12KL, where it is followed by a sharp subsequent decrease until 10 ka BP. In core 114-3 the

$\delta^{18}O_{ivc-sw}$ record, like the subSST$_{Mg/Ca}$ record, is characterized by a stronger variability around ca. -0.1 ‰ between 11.5 and 10.0 ka BP. Only Bering Sea core 77KL shows decreasing $\delta^{18}O_{ivc-sw}$ values since the PB until a minimum of -0.7 ‰ between 9 and 10 ka BP, whereas $\delta^{18}O_{ivc-sw}$ in core 85KL continues to vary around ~0 ‰.

Early to late Holocene $\delta^{18}O_{ivc-sw}$ values are negative at all sites. At Site 12KL these vary between -0.1 ‰ and -0.5 ‰ with a local minimum at ~8 ka BP. Core 114-3 shows small variations between -0.1 ‰ and -0.4 ‰ and gradually fresher values until the late Holocene. Bering Sea core 77KL from 9 ka BP until ~6 ka BP shows increasing $\delta^{18}O_{ivc-sw}$ to about -0.1 ‰ and is characterized by a strong variability. Fresher conditions are subsequently preserved until a minimum of -0.6 ‰ at 4 ka BP.

4.4. Discussion

4.4.1 Deglacial variability of temperature and salinity in the subarctic NW-Pacific
Our Mg/Ca-based reconstructions from the southern Okhotsk Sea, the NW-Pacific off Kamchatka and the western Bering Sea indicate synchronous changes in subSST$_{Mg/Ca}$ and $\delta^{18}O_{ivc-sw}$ during the last glacial termination with most pronounced amplitude variations recorded at Site 12KL. These changes reflect variations between warm/more saline and cold/fresher subsurface waters. Regional differences are found regarding the deglacial subSSS development, with more saline subsurface conditions during the B/A and PB in the NW-Pacific (Site 12KL), while the Bering Sea cores are characterized by opposing trends during the B/A. At the same time, sites 114-3 and 77KL in the southern Okhotsk and Bering seas, respectively, show fresher subSSS. However, all cores indicate fresher subsurface waters during H1, and since the early Holocene. The deglacial SST$_{Uk'37}$ evolution is different from subSST$_{Mg/Ca}$ and characterized by two warmings that occurred during the B/A (14.6-12.8 ka BP) and the PB (11.8-11.0 ka BP), respectively. They are preceded and interrupted by two cold phases associated with H1 (~18-16 ka BP) and the YD (12.8-11.8 ka BP), and followed by a cooling step during the early Holocene and stable temperatures since. The temporal variations of SST$_{Uk'37}$, hence, are quasi-synchronous with the deglacial N-Atlantic climate evolution [*Max et al.*, in review].

Heinrich Event 1
Our cores show a decrease in subSST$_{Mg/Ca}$ while $\delta^{18}O_{ivc-sw}$ indicates fresh subsurface conditions between 18-16 ka BP. This is most evident for Site 12KL. We consider this to be caused by increased advection of cold, low-salinity waters from the Alaskan Current via the Alaskan Stream at times when the Bering Strait was closed. Today, the Alaskan Stream as continuation of the Alaskan Current provides relatively fresh surface waters [*Stabeno et al.*, 1999]. Given that land masses surrounding the subarctic NW-Pacific do not contribute to major fluvial runoff or meltwater discharge from glacial ice-sheets [e.g. *Sarnthein et al.*, 2004], *Gebhardt et al.* [2008] related drops in salinity during H1 to

North American river and meltwater discharge and their subsequent transport via the Alaskan Current and Alaskan Stream to the NW-Pacific.

South of the Aleutian Island Arc, at Ocean Drilling Program (ODP) Site 883D and at the International Marine Global Changes Program (IMAGES) core location MD01-2416 from Detroit Seamount [*Sarnthein et al.*, 2006; *Gebhardt et al.*, 2008; Figure 4.1], SSTs during H1 were clearly higher and characterized by three sharp increases of ~4-6 °C, most likely excluding sea-ice formation. As these SST-pulses are accompanied by locally increased salinity, they were explained by either short-term incursions of warm and salty Kuroshio waters [*Sarnthein et al.*, 2006] or by northward expansions of the N-Pacific gyre filled with Kuroshio waters [*Gebhardt et al.*, 2008]. Alkenone-based reconstructions off central Japan showed that SSTs of Kuroshio waters ranged between 20-24 °C during the last deglaciation [*Sawada and Handa*, 1998] and hence, were considerably warmer than in the far NW-Pacific (Figure 4.5). NE-Pacific core MD02-2489 does not show significantly enhanced SSTs during H1, except for one data point at 17.2 ka BP with a temperature rise of 2 °C [*Gebhardt et al.*, 2008]. Also, *Sagawa and Ikehara* [2008] reported only a minor increase in subSST$_{Mg/Ca\ G.bulloides}$ of ~1 °C at ~15.5 ka BP off Hokkaido (GH02-1030; Figure 4.1), followed by a sharp 2 °C drop. Their salinity reconstruction implied that relatively saline conditions prevailed at least since the LGM, with a maximum at 15.5 ka BP and a subsequent decrease.

Gebhardt et al. [2008] argued for short phases of pronounced seasonal sea-ice formation in the subpolar N-Pacific that induced vertical mixing during H1 due to brine rejection. Evidence for increased vertical mixing and/or intensified overturning during H1 and the YD comes from reduced reservoir ages of surface waters [*Gebhardt et al.*, 2008], and reduced ventilation ages [*Ohkushi et al.*, 2004; *Sarnthein et al.*, 2007; *Sagawa and Ikehara*, 2008; *Okazaki et al.*, 2010], and is supported by climate modelling studies [e.g. *Okazaki et al.*, 2010; *Chikamoto et al.*, 2012; *Menviel et al.*, 2012]. Increased ventilation and the potential disappearance of the halocline [*Menviel et al.*, 2012] in the N-Pacific during H1 and the YD would require an increased salinity, which is consistent with the reconstructions of *Sarnthein et al.* [2006] and *Sagawa and Ikehara* [2008], but not supported by our study.

SST$_{Uk'37}$ is of no help in this respect. Indeed, prior to ~15 ka BP alkenone concentrations were non-determinable in our sediments or insufficient for any reliable paleotemperature calculation. This indicates either limited alkenone-preservation or restricted alkenone-production from haptophycean algae (coccolithophorids). The restriction in alkenone-production, in particular during H1, is most likely attributed to insufficient availability of light and nutrients, which at our sites might have been caused by enhanced sea-ice formation during an elongated winter season.

Bølling-Allerød

Our subSST$_{Mg/Ca}$ results indicate a maximum at the onset (~14.6 ka BP) or during the B/A and a subsequent cooling until the YD, most prominent at Site 12KL, and less pronounced at sites 85 and 101 (Figure 4.5), while more positive $\delta^{18}O_{ivc-sw}$ values remain until ~14.0 ka BP and the subsequent decrease imply more saline conditions at sites 12KL, 85KL, and 101KL (Figure 4.6). This subSST pattern is congruent with Mg/Ca-based results from NE-Pacific core MD02-2489 [*Gebhardt et al.*, 2008] and NW-Pacific core GH02-1030 [*Sagawa and Ikehara*, 2008], and supported by alkenone-based SST reconstructions from the NE-Pacific [*Kienast and McKay*, 2001; *Barron et al.*, 2003], the Bering Sea [*Caissie et al.*, 2010; *Max et al.*, in review], and the Okhotsk Sea [*Ternois et al.*, 2000; *Harada et al.*, 2006b; *Seki et al.*, 2009]. The presence of warmer and more saline subsurface waters at most of our core locations during the B/A is best explained by the reduced contribution of cold and fresh Alaskan Stream and EKC waters in combination with less vertical mixing and hence, stronger stratification of the upper water column. Enhanced stratification during the B/A is supported by increased ventilation ages found in the N-Pacific [*Adkins and Boyle*, 1997; *Ahagon et al.*, 2003; *Ohkushi et al.*, 2004; *Sagawa and Ikehara*, 2008; *Okazaki et al.*, 2010]. Thermal stratification at the northernmost Shirshov Ridge cores 85KL and 101KL might have been less developed than at the other sites by the still extended sea-ice season and the low seasonal contrast at these locations as indicated by ΔT-values of 0-1 °C. It might further be speculated that at times when the Bering Strait was still closed, the net-inflow of Alaskan Stream waters into the Bering Sea was reduced. Hence, the Alaskan Stream might still have influenced Site 77KL but not necessarily have reached sites 85KL and 101KL further to the north.

At the southernmost Shirshov Ridge core location (77KL) and in the southern Okhotsk Sea (114-3), fresher subsurface conditions characterize the B/A, consistent to surface freshening off Japan from 14.6 ka BP to 13.6 ka BP [*Sagawa and Ikehara*, 2008]. Freshening during the B/A has previously been suggested for the southern Okhotsk Sea [*Gorbarenko et al.*, 2004; *Seki et al.*, 2004b], and for Bowers Ridge in the southern Bering Sea [*Gorbarenko et al.*, 2005] from the observation of negative shifts in planktonic $\delta^{18}O$ and increasing abundances of diatom species *Paralia sulcata*. The freshening at these sites may be attributed to invigorated melting of sea-ice close to the ice margin during the warm season, accelerated by the presence of the EKC and hence, potentially favoring a seasonal halocline. In both cores, the B/A subSST$_{Mg/Ca}$ are similar to those of the northernmost sites 85KL and 101 KL, whereas SST$_{Uk'37}$ estimates are higher by 2-3 °C (Figure 4.7c, B). Consequently, at sites 114-3 and 77KL an enhanced seasonal contrast with respect to H1 might have resulted in stronger thermal stratification during summer.

A possible explanation for warmer subSST$_{Mg/Ca}$ than SST$_{Uk'37}$ in core 12KL during the B/A involves the formation of a permanent thermocline and warm SST$_{Uk'37}$ that reduce the sea-ice season. In that case seasonal bias of proxy signal formation arises and the colder SST$_{Uk'37}$ most likely represent early

spring conditions, while the subSST$_{Mg/Ca}$ signal still formed during late summer/early fall. If this notion is correct, the seasonal bias was limited to the subarctic NW-Pacific (Site 12KL) and did not occur in the marginal seas. Unfortunately, alkenone-based temperature reconstructions are not available for core MD01-2416 from Detroit Seamount to verify this assumption. Evidence for a modern subarctic N-Pacific coccolithophorid bloom occurring in spring comes from the sediment trap study of *Takahashi et al.* [2002]. *Seki et al.* [2004a] already suggested for the Okhotsk Sea a seasonal bias to explain alkenone-based temperatures during the LGM that were as high as during the Holocene.
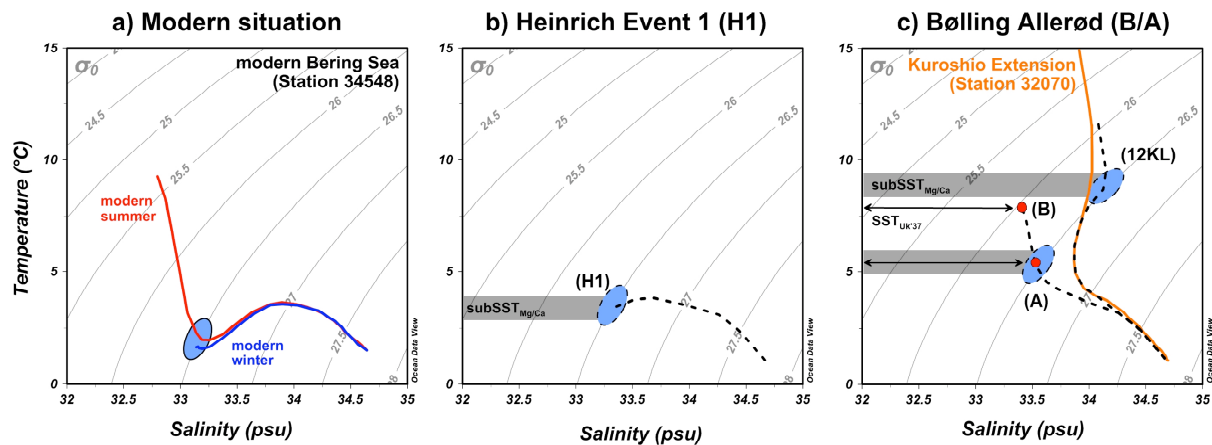

Figure 4.7: TS-diagrams showing temperature, salinity, and potential density of modern and past water masses in the subarctic NW-Pacific realm (based on WOA data; *Locarnini et al.*, 2010). a) Water masses during modern summer (red line) and winter (blue line) in the southern Bering Sea (WOA station 34548). The blue ellipse denotes temperature and salinity conditions within the depth habitat of N. pachyderma sin., which is assumed to lie in an isopycnal layer of ~26.4-26.6 kg m^{-3} in 50-100 m water depth. b) Scenario for H1. The reconstructed average subSST$_{Mg/Ca}$ of 3-4 °C (gray bar) at all sites is projected onto the isopycnal layer of ~26.4-26.6 kg m^{-3} and indicates subsurface conditions that were saltier than today. c) Scenario for the B/A at Bering Sea sites SO201-2-85KL and -101KL (A), Bering Sea Site SO201-2-77KL and Okhotsk Sea Site LV29-114-3 (B), and NW-Pacific Site SO201-2-12KL, in comparison with the modern TS-conditions in the Kuroshio Extension area (orange line; WOA station 32070: 40°30'N, 152°30'E). Red dots mark average SST$_{Uk'37}$ temperatures and gray bars mark average subSST$_{Mg/Ca}$ temperatures at the respective sites.

The Younger Dryas to Preboreal transition

During the YD our records show minima in subSST$_{Mg/Ca}$, SST$_{Uk'37}$, and δ^{18}O$_{ivc-sw}$ with conditions that were comparable to those of H1. The YD is followed by an abrupt surface warming in the PB indicated by SST$_{UK'37}$, while the subsurface temperatures gradually decline. Only core 12KL exhibits a short excursion towards higher subsurface temperatures during the PB, accompanied by a δ^{18}O$_{ivc-sw}$ maximum. The subSST$_{Mg/Ca}$ and δ^{18}O$_{ivc-sw}$ evolution observed at sites 114-3, 12KL, and 77KL broadly matches that from further to the south in the NW-Pacific [*Sarnthein et al.*, 2004, 2006; *Gebhardt et al.*, 2008; *Sagawa and Ikehara*, 2008], which just have higher δ^{18}O$_{ivc-sw}$ values.

SST$_{Uk'37}$ indicate lowest surface temperatures during the YD. *Kienast and McKay* [2001] suggest from a core off Vancouver Island that low SST$_{Uk'37}$ during the YD were caused by the southeastward

expansion of the western Pacific Subarctic Gyre and the Bering Sea Gyre. The modelling study of *Mikolajewicz et al.* [1997] predicted that the Aleutian Low was stronger and expanded eastwards during the YD, which initiated better ventilation of thermocline waters. The well-mixed upper ocean during the YD is supported by resembling subSST$_{Mg/Ca}$ and SST$_{Uk'37}$ and is in agreement with reduced ventilation ages in the N-Pacific. Our proxy records, however, suggest regionally different developments with weak thermal stratification at sites 12KL, 77KL, and 114-3 due to reduced ΔT-values (~2 °C), and a more homogenized upper water column at sites 85KL (ΔT = 0 °C) and 101KL similar to conditions valid for H1. Subsequently during the PB, subSST$_{Mg/Ca}$ and related δ^{18}O$_{ivc-sw}$ values imply subsurface cooling and freshening (77KL, 85KL) and/or conditions comparable to the YD (114-3). Possible explanations for this observation include reduced thermal stratification and/or enhanced advection of Arctic surface waters in the course of the major opening of the Bering Strait between 12-11 ka BP [*Keigwin et al.*, 2006]. Core 12KL is an exception in this respect. The distinct and short-term subsurface warming with the onset of the PB is most probably due to the invigorated stratification of the upper water column alike during the B/A.

Holocene

Most notably for all our cores are the differently developing subSST$_{Mg/Ca}$ and SST$_{Uk'37}$ since the YD (Figure 4.5) is observed, best explained by insolation changes affecting the surface ocean, increasing seasonal contrasts, and oceanographic changes at the subsurface level that control the shape and position of the thermocline. Holocene subSST$_{Mg/Ca}$ remain either equal or stay lower than those recorded during H1 (Figure 4.5). Our subSST$_{Mg/Ca}$ well reflect modern conditions, which is consistent with other studies [*Sarnthein et al.*, 2004, 2006; *Gebhardt et al.*, 2008; *Sagawa and Ikehara*, 2008]. With respect to our salinity reconstruction, the Holocene δ^{18}O$_{ivc-sw}$ values are generally negative indicating relatively fresh conditions at all sites similar to conditions during H1, arguing for a deglacial evolution of the halocline. *Sarnthein et al.* [2004] reported a long-term decrease in subsurface salinity at Detroit Seamount, characterized by three steps of distinct salinity decline during the early to middle Holocene. From the magnitude of change, which is comparable to our results, they speculated that the modern salinity-driven stratification developed only since the Holocene. However, due to the low time-resolution of our proxy records we can not confirm the stepwise subSSS decline as observed by *Sarnthein et al.* [2004].

The low Holocene subSST$_{Mg/Ca}$ at our study sites being considerably cooler than the SST$_{Uk'37}$ in line with relatively fresh subsurface conditions indicates a strengthened temperature contrast between the surface and subsurface during summer. Dominant control of the subarctic NW-Pacific SST$_{Uk'37}$ evolution during the Holocene is attributed to Northern Hemisphere summer insolation, being additionally influenced by the opening of the Bering Strait [*Okumura et al.*, 2009; *Hu et al.*, 2010; *Max et al.*, in review]. As a consequence, stronger seasonal contrasts might have developed as the result of a prolonged summer season, enhanced sea-ice melting during summer, and stronger winter

mixing, thereby leading to the formation of the dichothermal layer. Our high ΔT-values of ~5-6 °C are then explained by higher $SST_{Uk'37}$ with respect to the deglacial situation, and by *Nps* recording gradually cooler subsurface temperatures due to the presence of the dichothermal layer. Accordingly, thermal stratification during summer was consolidated and fresher subsurface conditions were the result of a stronger summer halocline. The largest difference between $subSST_{Mg/Ca}$ and $SST_{Uk'37}$ at ~10 ka BP coincides with the early Holocene thermal maximum recorded in the western Arctic, which in Alaska and northwest Canada occurred between 11-9 ka BP [*Kaufman et al.*, 2004], further supporting this interpretation. Additionally, enhanced precipitation driven by the Westerlies, and strengthened advection of cold/fresh waters from the Alaskan Stream might have contributed to the N-Pacific cooling and freshening [*Sarnthein et al.*, 2004].

4.4.2 Scenarios for deglacial water mass changes

Our reconstructions of $subSST_{Mg/Ca}$ and $\delta^{18}O_{ivc-sw}$ depend on the calcification depth of *Nps*. Following *Kozdon et al.* [2009] we assume that today *Nps* occupies a habitat that is bound to the isopycnal layer (σ_0=26.4-26.6 kg m^{-3}) at the bottom of the summer thermocline in 50-100 m water depth. Accordingly, if the thermocline and hence the pycnocline deepens (shoals), the habitat depth of *Nps* will expand to deeper (shallower) depths as well, thereby eventually counterbalancing absolute temperature variations [*Kozdon et al.*, 2009]. Since there is no way to assess the extent of past habitat changes, we assume that the maximum habitat depth of *Nps* is at the base of the pycnocline, which today at our study sites is located at a maximum water depth of ~150 m (Figure 4.2). Based on this assumption, we use TS-diagrams to illustrate deglacial changes in water mass characteristics in the subarctic NW-Pacific (Figure 4.7). Due to both the error in $\delta^{18}O_{sw}$-reconstruction and the lack of according salinity calibrations for the Bering Sea, we refrained from converting $\delta^{18}O_{sw}$ into salinity. Instead, salinity was estimated by projecting the average $subSST_{Mg/Ca}$ estimates onto the isopycnal layer of σ_0=26.4-26.6 kg m^{-3} (Figure 4.7).

Today, the difference in temperature, salinity, and potential density in the southern Bering Sea (WOA station 34548) is depicted in Figure 4.7a and is the expression of the strong seasonality within the upper water column. At the assumed living depth of *Nps*, modern subSST are at 1-2 °C, salinity ranges from 33.0 to 33.2 psu and the seasonal contrast is small (Figure 4.2). During summer, σ_0 is mainly controlled by temperature within the upper 50 m, while the dichothermal layer is present in 50-150 m.

For the H1 cold phase we assume TS-conditions relatively similar to the modern winter situation with homogenous T, S, and σ_0 conditions down to ~150 m and the absence of the dichothermal layer (Figure 4.7b). As the reconstructed $subSST_{Mg/Ca}$ lies between 3 °C and 4 °C at all sites, implying that subsurface waters were slightly warmer and saltier than the modern winter conditions, we argue that the thermal stratification was strongly reduced. The homogenization of the upper water column must have been even more pronounced and deeper than during the modern winter situation. The most likely

cause for the less stratified water column might have been the intensified and expanded sea-ice formation during winter and the shortened summer season. The invigorated sea-ice formation might have enhanced salinity in comparison to today due to brine-rejection and light limitation might have restricted primary productivity. Indeed, during H1 alkenones were absent or below detection limit. The expanded sea-ice coverage during the extended winter season would have also reduced winter mixing, thereby preventing the formation of the dichothermal layer as a seasonal feature, which would explain the slightly higher (1-2 °C) subSST$_{Mg/Ca}$ during H1 when compared to today. The reduced thermal stratification, in consequence, could have resulted in the shallowing of the habitat of *Nps*. This notion is supported by low biogenic opal and light diatom-bound nitrogen isotope ratios ($\delta^{15}N_{db}$) in the Okhotsk Sea, Bering Sea, and the subarctic Pacific during H1 [*Brunelle et al.*, 2007, 2010] (Figure 4.8), indicative of the decrease in nitrate utilization in response to both the less-established stratification and the light-limited phytoplankton growth.

During the B/A warm phase, the oceanographic setting becomes different at the respective sites (Figure 4.7c). At Bering Sea sites 85KL and 101KL, similar mean SST$_{Uk'37}$ and subSST$_{Mg/Ca}$ of 5-6 °C point to a weak thermal stratification with higher subsurface temperature and salinity compared to today and to H1 (Figure 4.7c, A). The low gradient between SST$_{Uk'37}$ and subSST$_{Mg/Ca}$ implies that seasonal changes in thermocline depth remained small, probably a little more pronounced than during H1 as preserved alkenones suggest phytoplankton growth during the ice-free season. Nevertheless, marine productivity remained low (biogenic opal < 5 wt.%), most likely caused by a still expanded sea- ice season. The heavy $\delta^{15}N_{db}$ from nearby Bowers Ridge [*Brunelle et al.*, 2010] at a first glance implies enhanced nutrient utilization, but the data set rather reflects conditions not quite comparable to the northern part of Shirshov Ridge.

NW-Pacific Site 12KL shows much higher subSST$_{Mg/Ca}$ of ~9 °C and a further increase in subsurface salinity during the B/A (Figure 4.7c) compared to the northern Shirshov Ridge sites 85KL and 101KL. Further, the subSST$_{Mg/Ca}$ are consistently higher than the SST$_{Uk'37}$, suggesting that seasonal differences were pronounced at Site 12KL. The subSST$_{Mg/Ca}$ signal is most likely formed during late summer while the cool alkenone-derived temperatures were already recorded during early spring. The prominent seasonality in signal formation implies both an extended ice-free summer season and a strong thermal stratification during summer. Biogenic opal concentrations of up to ~12 % comparable to the Holocene values suggest enhanced marine productivity during the prolonged summer season (Figure 4.8), fostered by a better nutrient utilization or denitrification leading to heavy $\delta^{15}N_{db}$ values. The B/A subsurface temperature and salinity conditions at Site 12KL were close to conditions, which today prevail in the Kuroshio Extension area (40°30' N, 152°30' E, WOA station 32070; *Locarnini et al.*, 2010) much further to the south of the core location (Figure 4.7c). The higher subsurface salinities reconstructed for the B/A might be caused by less meltwater contribution and/or enhanced upwelling of deep waters as suggested by *Sarnthein et al.* [2004].
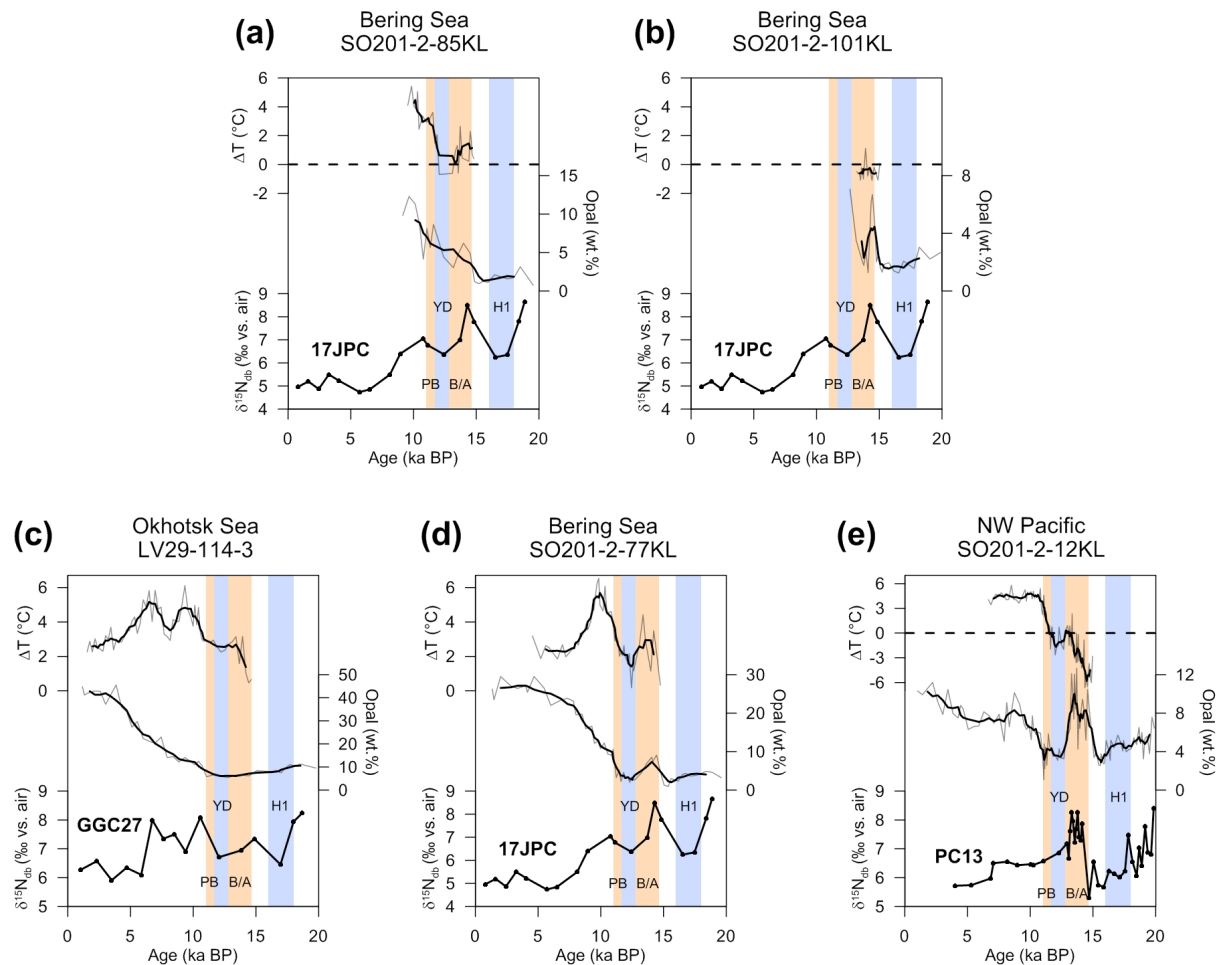
Figure 4.8: Temperature gradients (ΔT) between $SST_{Uk'37}$ and $subSST_{Mg/Ca}$, and concentrations of biogenic opal for cores from the Bering Sea (SO201-2-77KL, -85KL, -101KL), the NW-Pacific off Kamchatka (SO201-2-12KL), and the southern Okhotsk Sea (LV29-114-3). Data are smoothed by running 5-point-averages (black lines). Dashed lines indicate ΔT = 0 °C. For comparison, records of $\delta^{15}N_{db}$ from southern Okhotsk Sea core GGC27 (49°36.07' N, 150°10.78' E, 995 m), southern Bering Sea core HLY02-02-17JPC (53°55.98' N, 178°41.93' E, 2209 m), and open subarctic Pacific core PC13 (49°43.09' N, 168°18.11' E, 2393 m) are shown (data from *Brunelle et al.*, 2007, 2010). Pale orange and pale blue shadings represent the B/A and PB, and the H1 and YD, respectively.

Site 114-3 in the southern Okhotsk Sea and Site 77KL from the southernmost part of Shirshov Ridge record conditions in between these extremes (Figure 4.7c, B). We speculate that both temperature signals were generated at the same season, since contents of biogenic opal remain low (< 10 wt.%), suggesting a still shortened ice-free summer season. As a consequence, thermal stratification at these sites and hence, seasonality, must have been stronger than during H1 and more pronounced than at sites 85KL and 101KL.

According to the gradual increase in $subSST_{Mg/Ca}$ and subSSS during the B/A, we would expect a stronger seasonal contrast as well as enhanced thermal stratification of the upper water column from sites 85KL and 101KL, via sites 114-3 and 77KL, towards site 12KL. Moreover, we suggest that during the B/A increased thermal stratification was accompanied by higher subSSS, thereby resulting in a weakened (or shallowed) halocline. Since the recorded temperatures clearly exclude both, sea-ice

formation and upwelling of cold/saline subsurface water, the cause of this increase in subSSS remains elusive. This, together with the observed subSSS reduction during the Holocene, emphasizes that the halocline as a main oceanographic feature of the subarctic N-Pacific could be the result of only recent environmental change as suggested by *Sarnthein et al.* [2004].

4.4.3 What caused deglacial changes in stratification and ventilation?

Based on our findings, the deglacial to early Holocene subsurface and surface temperature and salinity evolution in the subarctic NW-Pacific appears to be related to be in-phase with the thermal evolution that is recorded in Greenland ice and in North Atlantic sediments suggesting the atmospheric and/or oceanic coupling between the North Atlantic and the North Pacific during the last deglaciation [e.g. *Max et al.*, in review]. Several modelling studies investigated the sensitivity of the PMOC in response to perturbations of the AMOC on millennial time-scales during the last deglaciation. These studies proposed an either ocean-controlled anti-phase (Atlantic-Pacific Seesaw, e.g. *Schmittner et al.*, 2003, 2007; *Saenko et al.*, 2004; *Okazaki et al.*, 2010) or an atmosphere-controlled in-phase [*Mikolajewicz et al.*, 1997; *Krebs and Timmermann*, 2007; *Okumura et al.*, 2009] evolution of sea surface temperature changes in the N-Atlantic and the N-Pacific oceans. All models predicted an enhanced PMOC at times of a weakened AMOC, whose strength during the last deglaciation was modulated by freshwater input into the Atlantic or by freshwater extraction from the Pacific.

According to model conceptions, the weakened AMOC during H1 and the YD [e.g. *McManus et al.*, 2004], which is assumed to have resulted from freshwater input into the Atlantic, leads to the southward shift of the Intertropical Convergence Zone (ITCZ) and weakened Indian and Asian summer monsoons [*Zhang and Delworth*, 2005]. Today, the salinity gradient between the Atlantic and Pacific is maintained by atmospheric moisture transport across Central America and the East Asian monsoon [*Emile-Geay et al.*, 2003], which are modulated by changes in AMOC [*Kiefer*, 2010; *Okazaki et al.*, 2010]. Consequently, a weakening of the AMOC results in a warming and salinity-increase in the N-Pacific and thus to the establishment of the PMOC [*Haug et al.*, 2005; *Chikamoto et al.*, 2012; *Menviel et al.*, 2012]. In contrast, the in-phase models [e.g. *Mikolajewicz et al.*, 1997] suggest an atmospheric forcing, which causes better ventilation of thermocline waters by atmospheric cooling. The cooling is attributed to the strengthened Aleutian Low, which increases surface heat loss and southward Ekman transport, but atmospheric bridges between the tropical N-Atlantic, eastern tropical Pacific, and N-Pacific are considered to play an important role as well [*Okumura et al.*, 2007]. Ventilation is supposed to amplify by the oceanic propagation of AMOC weakening [*Mikolajewicz et al.*, 1997]. Both, in-phase and anti-phase hypotheses, are supported by low ventilation ages in the N-Pacific during H1 and the YD.

The study of *Menviel et al.* [2012] predicts that the PMOC was established during H1 together with the removal of the subarctic N-Pacific halocline. This notion is supported by the high $\delta^{18}O_{ivc-sw}$ values recorded in NW-Pacific cores MD01-2416 [*Sarnthein et al.*, 2006; *Gebhardt et al.*, 2008] and GH02-1030 [*Sagawa and Ikehara*, 2008]. In contrast, our results for core 12KL as well as alkenone-based SST reconstructions from the subarctic N-Pacific show a significant drop in subSST$_{Mg/Ca}$ and SST$_{Uk'37}$, while $\delta^{18}O_{ivc-sw}$ values indicate fresh subsurface conditions during H1. This pattern is rather indicative of an atmospheric-controlled in-phase evolution of the N-Atlantic and the subarctic N-Pacific. High subSST$_{Mg/Ca}$ and low $\delta^{18}O_{ivc-sw}$ in the Okhotsk and Bering seas during the B/A and PB are then explained by stronger stratification of the subarctic N-Pacific due to the reduced PMOC in response to the AMOC intensification. Subsequent to the PB, the subarctic NW-Pacific is subject to enhanced thermal summer stratification, which for the Bering Sea sites is possibly related to the opening of Bering Strait resulting in stronger inflow of N-Pacific surface waters into the Bering Sea. Moreover, increased surface freshening during the Holocene results from sea-ice melting during summer, enhanced precipitation from the Westerlies and/or increased advection of cold-fresh waters from the Alaskan Stream.

With respect to the differences between our proxy records and those of cores MD01-2416 [*Sarnthein et al.*, 2004, 2006; *Gebhardt et al.*, 2008] and GH02-1030 [*Sagawa and Ikehara*, 2008], it should be noted that the former are mainly influenced by cold-fresh waters from the Alaskan Stream and EKC, whereas especially core GH02-1030 is more affected by warm and salty Kuroshio waters. Consequently, a significant increase in surface salinity during H1 was sufficient to establish a PMOC but might have been restricted to sites influenced by the Kuroshio.

4.5 Conclusions

1. We produced Mg/Ca-based records of sub sea surface temperature (subSST$_{Mg/Ca}$) and $\delta^{18}O_{ivc-sw}$ approximating subsurface salinity (subSSS) changes for the southern Okhotsk Sea, the subarctic NW-Pacific off Kamchatka, and the western Bering Sea covering the last deglaciation. Our results, which are compared with alkenone-derived sea surface temperature reconstructions (SST$_{Uk'37}$), support an atmospheric coupling and quasi-synchronous thermal evolution between the subarctic N-Pacific and the subarctic N-Atlantic, which is controlled by perturbations of the Atlantic Meridional Overturning Circulation (AMOC).

2. Our results point to synchronous changes in subSST$_{Mg/Ca}$ and subSSS in the subarctic NW-Pacific, which are different on a regional scale. During Heinrich Event 1 (H1) and the Younger Dryas (YD) our sites are characterized by the presence of cold subsurface waters, which is related to reduced upper ocean stratification due to enhanced sea-ice formation and a shortened summer season, and increased advection of waters from the Alaskan Stream and East Kamchatka Current. In contrast, warm subsurface waters prevail during the Bølling-Allerød (B/A) with increased

subsurface salinity in the NW-Pacific (Site 12KL) and Bering Sea (sites 85KL and 101KL), but fresher conditions in the southern Okhotsk Sea and Bering Sea (sites 114-3 and 77KL). This is explained by enhanced stratification of the upper water column, reduced dilution from the Alaskan Stream, and regionally different sea-ice influence. A long-term decrease in $subSST_{Mg/Ca}$ and subSSS during the Holocene argues for oceanographic changes at the subsurface level related to the opening of the Bering Strait and for an only recent establishment of modern, salinity-driven stratification since the Preboreal (PB).

3. Differences in alkenone- and Mg/Ca-based SST-reconstructions indicate deglacial oceanographic changes in the mixed layer, which are directly related to changes in Northern Hemisphere summer insolation, seasonality, and upper-ocean stratification. From our results we propose scenarios for deglacial water mass changes, which suggest that seasonality and hence thermal summer stratification, although being regionally different, was reduced during H1 and the YD, but strong during the B/A.

Acknowledgements

Supplementary Information

Deglacial development of (sub) sea surface temperature and salinity in the subarctic NW-Pacific: Implications for upper-ocean stratification

S4.1 Raw data

Figure S4.1: Raw data of benthic and planktonic $\delta^{18}O$ in comparison with planktonic foraminiferal ratios of Mg/Ca, Mn/Ca, Fe/Ca, and Al/Ca. The NGRIP record [*NGRIP members*, 2004; GICC05 timescale, *Rasmussen et al.*, 2006] is shown for comparison. Two samples were excluded due to very high Mg/Ca values and are indicated by filled red circles. Thick gray line marks the relative sea-level record of *Waelbroek et al.* [2002], which is used for ice-volume correction of planktonic $\delta^{18}O$. The B/A and PB are indicated by pale orange shadings, whereas pale blue shadings represent H1 and the YD.

S4.2 Assessment of potential contamination of foraminiferal tests

Significant linear relationships ($0.62 < R^2 < 0.85$) were found for cores 77KL, 85KL, and 101KL between foraminiferal Mn/Ca and Mg/Ca ratios indicating general covariation (Figure S4.1). Core-specific thresholds reflecting potentially contaminated samples were defined as ratios that were more than 2σ higher than the average of all measured samples per core. For Mn/Ca they ranged between

0.08-0.17 mmol mol^{-1}. Linear correlation coefficients between Fe/Ca and Mg/Ca ratios were $R^2 \leq 0.26$, except for core 77KL ($R^2 = 0.61$), which is in accordance with a strong correlation between Mn/Ca and Mg/Ca ($R^2 = 0.66$) in that core. Here, a Fe/Ca threshold of 0.85 mmol mol^{-1} was applied. Correlations between Al/Ca and Mg/Ca are insignificant ($R^2 \leq 0.18$). In general this approach shows that (i) neither Fe/Ca nor Al/Ca ratios have a significant influence on the Mg/Ca signal and that main contamination should come from Mn-bearing minerals and coatings, and (ii) that only samples from core sections older than 20 ka BP are subject to contamination. Respective samples are not relevant for our paleoceanographic discussion, which focuses on the last 20 kyr.
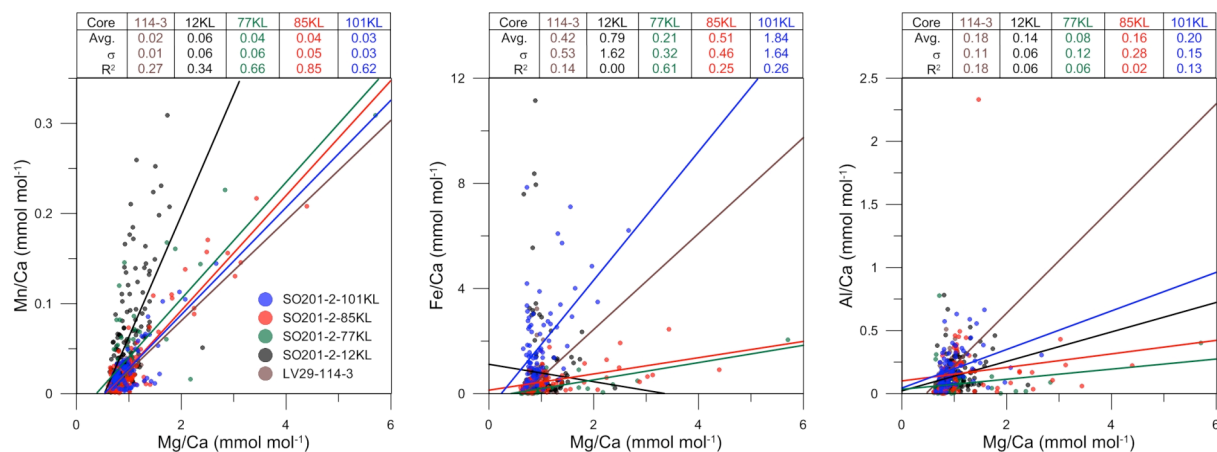
Figure S4.2: Comparison of foraminiferal Mg/Ca with foraminiferal Mn/Ca, Fe/Ca, and Al/Ca. Significant linear correlations ($R^2 > 0.6$) are found between element ratios Mg/Ca and Mn/Ca for cores 77KL, 85KL, and 101KL. Core 77KL also shows a correlation between Mg/Ca and Fe/Ca. In general, linear correlation coefficients (R^2) between Fe/Ca (Al/Ca) and Mg/Ca are low and indicate that main contamination and influence on Mg/Ca comes from Mn-bearing minerals and coatings. However, only samples older than 20 ka BP, which are not used for interpretation, seems to be affected by contamination.

In case of diagenetic overprinting by Mn-bearing minerals and coatings, the reconstructed subSST$_{Mg/Ca}$ could be too warm due to the diagenetically-induced addition of Mg. Average Mn/Ca ranged between 0.02-0.06 mmol mol^{-1}, while all core-specific thresholds for Mn/Ca were < 0.2 mmol mol^{-1}. Mn-Mg carbonates have Mg/Mn ratios of ca. 0.1 mol mol^{-1} [*Barker et al.*, 2003]. Thus, a maximum increase in Mn/Ca of 0.2 mmol mol^{-1} would lead to a Mg/Ca increase of only 0.02 mmol mol^{-1}, translating into a subSST$_{Mg/Ca}$-increase of +0.15 °C. Considering an unrealistic Mg/Mn ratio of 1 mol mol^{-1}, a correction for Mn/Ca generates therefore results that per core are on average by 0.02-0.06 mmol mol^{-1} lower in Mg/Ca (-0.2 to -0.5 °C), ultimately showing the same temporal trends. Accordingly, we rejected from correcting for Mn/Ca.

S4.3 Evaluation of correction for carbonate dissolution

Procedures to correct planktonic foraminiferal Mg/Ca for dissolution effects primarily focus on water depth-dependency [*Lea et al.*, 2000; *Dekens et al.*, 2002] and the influence of the seawater carbonate ion concentration ([CO_3^{2-}]) with respect to calcite saturation [*Regenberg et al.*, 2006]. To estimate the

dissolution effect on Mg/Ca we followed the approach of *Regenberg et al.* [2006] who proposed species-specific saturation correction routines for seven planktonic species. Therefore, for our calculations, we adopted a critical calcite saturation state for seawater ($\Delta[CO_3^{2-}]_{critical}$) of 20 µmol kg^{-1} lying within the range of 18-26 µmol kg^{-1} suggested by *Regenberg et al.* [2006].

$\Delta[CO_3^{2-}]_{critical}$ is defined as the difference between the in situ carbonate ion concentration ($[CO_3^{2-}]_{insitu}$) and the carbonate ion concentration at calcite saturation ($[CO_3^{2-}]_{sat}$), below which Mg^{2+} removal due to dissolution is assumed to start. $[CO_3^{2-}]_{sat}$ was calculated after *Jansen et al.* [2002], while $[CO_3^{2-}]_{insitu}$ was calculated using the CO2SYS Macro for MS Excel [*Pierrot et al.*, 2006] applying dissociation and equilibrium constants from *Dickson* [1990] and *Roy et al.* [2003]. Necessary input data were obtained from the World Ocean Circulation Experiment (WOCE) available at the CCHDO | CLIVAR & Carbon Hydrographic Data Office (URL: http://cchdo.ucsd.edu/). For the southern Okhotsk Sea we used WOCE line P01W (stations 7-17), while lines P13 (stations 6-15) and P14N (stations 1-15) were used for the NW-Pacific and the Bering Sea, respectively. This allowed for the calculation of $\Delta[CO_3^{2-}]$ and to determine critical water depths for the respective regions, where $\Delta[CO_3^{2-}]$ equals 20 µmol kg^{-1}. Critical water depths ranged between 120 and 200 m (Figure 4.3).

Regenberg et al. [2006] give species-specific linear correction equations for critical water depth correction (δ-correction) and for critical calcite saturation state correction (Δ-correction). To calculate Mg/Ca correction factors (ΔMg/Ca) we applied sensitivities for the respective corrections that were derived from the averages of the slopes of regression lines from all species-specific correction relationships presented in *Regenberg et al.* [2006]. For δ-correction we used an average sensitivity of 1600 m per mmol mol^{-1} Mg/Ca, and for Δ-correction we used an average sensitivity of 16 µmol kg^{-1} per mmol mol^{-1} Mg/Ca.

Depending on the core location, δ-correction resulted in a Mg/Ca gain between +0.3 and +1.3 mmol mol^{-1} (+2 °C to +10 °C applying the slope of the equation of *Kozdon et al.*, 2009), similar to the approach of *Lea et al.* [2000]. This result is intriguing as all cores show a similar middle to late Holocene (< 8 ka BP) subSST$_{Mg/Ca}$-range of 3-4 °C which is only little higher (1-2 °C) than the modern instrumental record at 50-100 m w.d.. We rather attribute this small difference to a less developed dichothermal layer during the middle to late Holocene. In contrast, the depth-corrections that were established for planktonic warm-water species *Globigerinoides ruber* and *Globigerinoides sacculifer* [*Dekens et al.*, 2002] result in constantly warmer subSST$_{Mg/Ca}$ of 2 to 3 °C. However, *Dekens et al.* [2002] modified existing Mg/Ca-T-relationships for these two species by introducing depth-dependent correction factors into the exponential part of the equations, which produces an artificial phase-shift to higher temperatures. These equations do not compare with those that are

associated with *Nps* [*Nürnberg*, 1995; *Nürnberg et al.*, 1996; *Elderfield and Ganssen*, 2000] or other cold-water species like *Globigerina bulloides* [e.g. *Mashiotta et al.*, 1999].

Δ-correction produced even higher values compensating for an unlikely loss of Mg/Ca between -1.6 and -2.1 mmol mol^{-1}. Consequently, subSST$_{Mg/Ca}$ estimates would be higher by +13 °C to +16 °C applying the temperature sensitivity given by *Kozdon et al.* [2009], which is far off the modern annual temperature range of the subarctic NW-Pacific. On the other hand, applying a correction considering a sensitivity of about 0.009 mmol mol^{-1} Mg/Ca per µmol kg^{-1} $\Delta[CO_3^{2-}]$, as found for epibenthic foraminifera *Cibicidoides wuellerstorfi* [*Elderfield et al.*, 2006; *Yu and Elderfield*, 2008], would result in ca. 0.23-0.31 mmol mol^{-1} higher Mg/Ca (ca. +2 °C) for all cores. Although this correction produces reasonable results of the combined error range from the measurement uncertainty and of the applied paleotemperature relationship itself. It is not verified for planktonic species and it does not have any influence on temporal trends.

It needs to be also mentioned that established dissolution corrections only account for modern dissolution effects and do not consider possible temporal changes in calcite preservation and their influence on Mg/Ca [e.g. *Farrell and Prell*, 1989; *Le and Shackleton*, 1992]. Our cores feature deglacial maxima of carbonate contents indicating better CaCO$_3$ preservation during the Bølling-Allrød (B/A) and Preboreal (PB), which are explained by the "CaCO$_3$ compensation" hypothesis [*Broecker and Peng*, 1987]. Hence, increased Mg/Ca during the B/A and PB could be explained by increased carbonate preservation.

Based on all considerations discussed above, we resigned from correcting the initial Mg/Ca values for potential dissolution effects although we admit that the Mg/Ca ratios are to an unknown degree affected by dissolution. Any correction would lead to increased subSST$_{Mg/Ca}$ that are either significantly different for all studied subarctic Pacific regions, or off the modern annual instrumental record, or despite being reasonable, based on procedures previously not applied to *Nps* thereby ultimately not altering temporal trends. Additional validation of our Mg/Ca-based paleotemperature reconstructions comes from a general covariation between subSST$_{Mg/Ca}$ and ice-volume corrected oxygen isotope values ($\delta^{18}O_{ivc}$) determined on the same biotic carrier. Furthermore, the range of our subSST$_{Mg/Ca}$ reconstructions is almost consistent with other deglacial Mg/Ca-derived records from the subarctic NW-Pacific using *Nps* [*Sarnthein et al.*, 2004, 2006; *Gebhardt et al.*, 2008]. However, due to the application of the temperature calibration of *Elderfield and Ganssen* [2000], these studies show a slightly higher temperature range by 1 °C to 2 °C.

S4.4 Potential diagenetic effects

In SO201-2 cores 12KL, 77KL, and 85KL, we found linear relationships between paired measurements of $\delta^{13}C$ and Mg/Ca on *Nps* ($0.34 < R^2 < 0.41$). Bering Sea cores are characterized by short intervals during 37-23 ka BP with planktonic $\delta^{13}C$-values that decrease to ca. -1.2 ‰ PDB and that appear together with both, elevated Mg/Ca-ratios, and increased Mn/Ca ratios (Figure S4.3). Mg/Ca is as high as 5.7 mmol mol^{-1} would translate into unrealistic subSST$_{Mg/Ca}$-estimates of ~41 °C. Scanning electron microscope (SEM) analyses (CamScan Serie 2 CS 44EDX, Univ. Kiel) on uncleaned tests of *Nps* with unusually high Mg/Ca (> 2 mmol mol^{-1}) from that interval show that outer and inner surfaces are covered with crystalline overgrowths of single tetrahedra-shaped crystals with a maximum size of 2-3 µm (Figure S4.4). This could indicate a potential diagenetic overprint on sediments from Shirshov Ridge older than 23 ka BP.
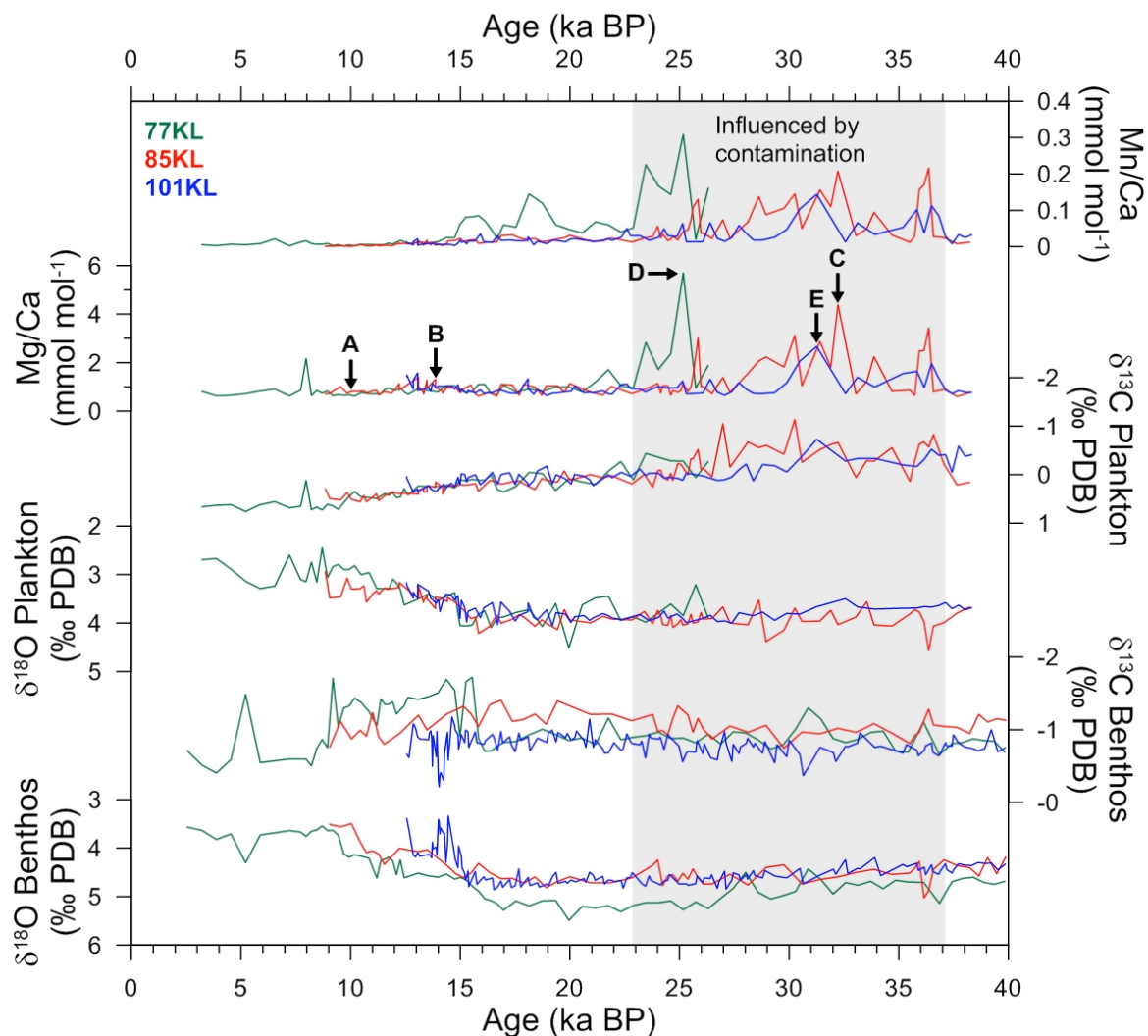
Figure S4.3: Stable carbon ($\delta^{13}C$) isotopes, stable oxygen ($\delta^{18}O$) isotopes, as well as Mg/Ca and Mn/Ca ratios of the planktonic foraminiferal species *N. pachyderma* (sin.) and of the endobenthic foraminifer *U. peregrina* for Bering Sea cores SO201-2-77KL (green lines), -85KL (red lines), and -101KL (blue lines) for the last 40 kyr. Short intervals with relatively high (> 2 mmol mol^{-1}) planktonic Mg/Ca ratios are accompanied by high Mn/Ca ratios in the time interval 37-23 ka BP (gray-shaded area). Note that, except for the excursion around 36 ka BP in core 85KL, benthic and planktonic records do not show similar oscillations in $\delta^{13}C$ and $\delta^{18}O$. Black arrows labelled with A-E mark positions of SEM images shown in Figure S4.4.
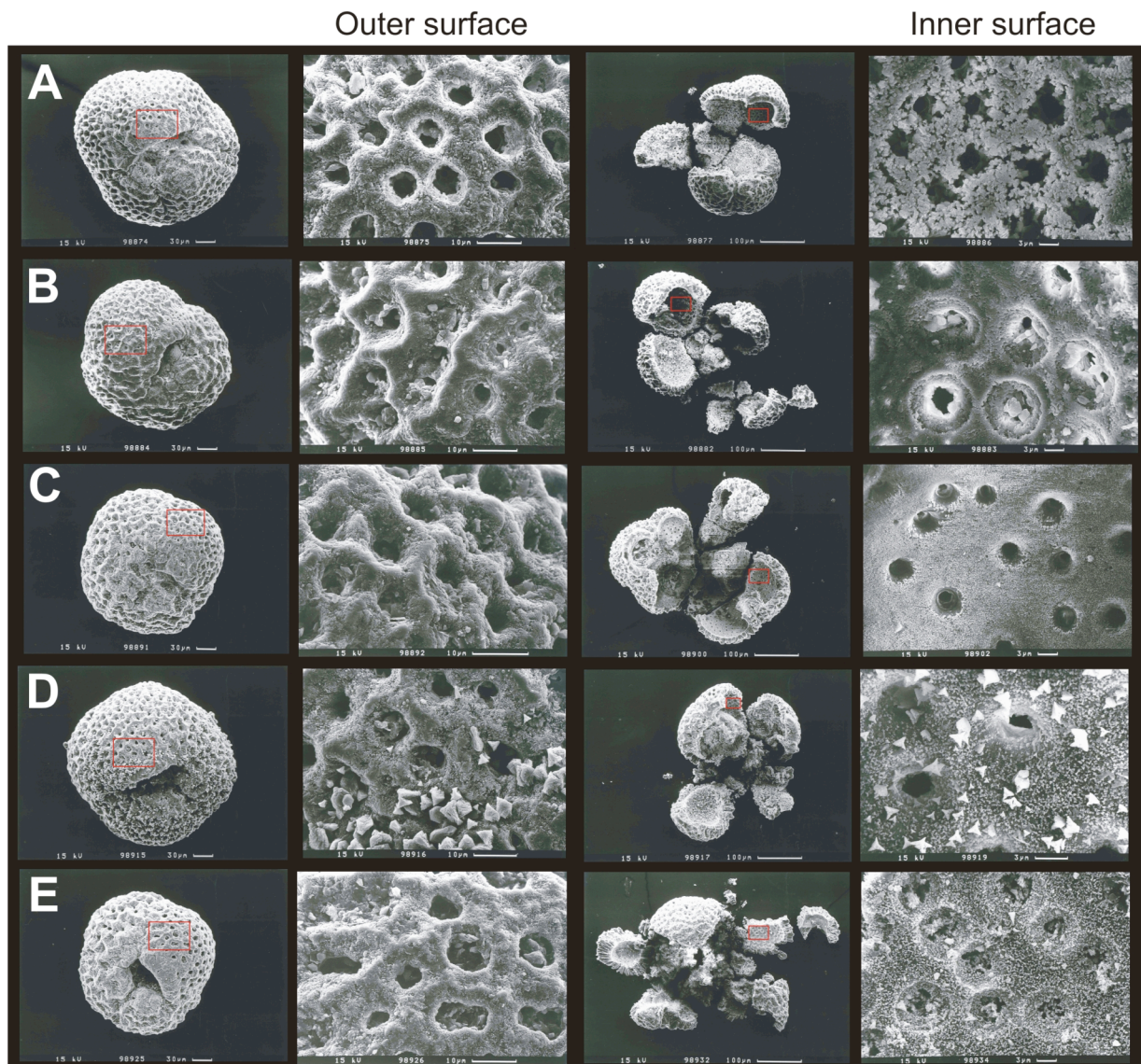
Figure S4.4: Scanning electron microscope images (CamScan Serie 2 CS 44/EDX, Univ. Kiel, Germany) of uncleaned tests of *N. pachyderma* (sin.) from Bering Sea sites. Pairs of images show an overview of opened/unopened tests and the according enlargements of the outer/inner test surfaces. The site scale is about the same for all images. Tests shown in A and B look unaltered, whereas tests in C-E show an overgrowth of tetrahedra-shaped crystals. A: SO201-2-85KL (25-26 cm, 10.0 ka BP), B: SO201-2-85KL (70-71 cm, 13.9 ka BP), C: SO201-2-85KL (245-246 cm, 32.2 ka BP), D: SO201-2-77KL (290-291 cm, 25.2 ka BP), E: SO201-2-101KL (255-256 cm, 31.3 ka BP).

However, negative δ^{13}C values related to diagenetic overgrowths of authigenic carbonate were found in Umnak Plateau sediments (southern Bering Sea), but are reported to have extreme benthic (as low as -6.8 ‰) and planktonic (as low as -13 ‰) values [*Cook*, 2006]. *Cook* [2006] speculated that due to mobilization of methane in line with the anaerobic methane oxidation, and its subsequent transport to the sediment-water interface, authigenic carbonate minerals may form due to supersaturation of pore waters with respect to carbonate. Similar coherencies are reported from Greenland Sea sediments low in CaCO$_3$, which contain benthic and planktonic foraminifera with also extremely negative δ^{13}C values (up to -6 ‰ PDB) during MIS 3 and authigenic calcite overgrowths [*Millo et al.*, 2005a, 2005b]. The authors suggested that post-depositional clathrate instability led to the supersaturation of ^{13}C-depleted

bicarbonate in pore waters from which authigenic calcite precipitated as crystalline overgrowths. Coincident large negative benthic (-5 ‰) and planktonic (-3 ‰) excursions of $\delta^{13}C$ were also observed in MIS 3 in sediments from Santa Barbara Basin (NE-Pacific), which were related to methane release in accordance with temperature changes [*Kennett et al.*, 2000].

If our foraminiferal tests actually were subject to methane-induced diagenetic overgrowth of authigenic carbonates precipitated from pore waters, tests of benthic foraminifera should be similarly affected. We therefore performed additional measurements of stable carbon and oxygen isotopes on endobenthic foraminifera *U. peregrina* (2-3 specimens, 315-355 µm size fraction). Neither *Nps* nor *U. peregrina* featured $\delta^{13}C$-variations of the magnitude described by the beforementioned studies [*Kennett et al.*, 2000; *Millo et al.*, 2005a, 2005b; *Cook*, 2006] (Figure S4.3). Both species also do not show a covariation of $\delta^{13}C$-oscillations, which argues against a methane-induced early diagenetic overprint by pore waters. We therefore consider a diagenetic influence on samples from 37-23 ka BP through calcite recrystallization possible to explain the occurrence of the tetrahedra-shaped crystals, but rather relate high Mg/Ca-ratios in *Nps* to contamination by Mn-bearing minerals or coatings.

Chapter 5: Rapid changes in North Pacific Intermediate Water Formation during the Last Glacial Termination

Lars Max[1], Lester Lembke-Jene[1], Jan-Rainer Riethdorf[2], Ralf Tiedemann[1] and Dirk Nürnberg[2]

[1]Alfred Wegener Institute for Polar and Marine Research, Am Handelshafen 12, D-27570
 Bremerhaven, Germany; E-Mail: Lars.Max@awi.de
[2]GEOMAR | Helmholtz-Zentrum für Ozeanforschung Kiel, Wischhofstr. 1-3, D-24148 Kiel, Germany

to be submitted to Nature Geoscience

Abstract

Today the formation of North Atlantic Deep Water (NADW) leads to deep convection in the North Atlantic and no deep convection occurs in the North Pacific, where only fresh intermediate water masses are formed in the Okhotsk Sea that ventilate the North Pacific. Recent studies suggest a switch to deep water formation in the subarctic North Pacific during the last glacial termination in response to a shutdown or weakening of the Atlantic Meridional Overturning Circulation (AMOC)[*Okazaki et al.*, 2010]. Here we show detailed records of past ventilation changes from the Okhotsk Sea and Bering Sea spanning the last glacial termination. Compelling evidence for intermediate water formation in these two marginal seas is given by combining marine radiocarbon ages and stable isotope ventilation records, which suggest that only the upper North Pacific (~ 1350 m) was better ventilated, whereas data from the deeper portion of the North Pacific (> 2130 m) show no evidence for deep water formation during phases of AMOC reductions.

A prime mechanism to explain the rise in atmospheric CO_2 concentrations during the last deglaciation is the removal of old and deep sequestered carbon from the North Pacific Ocean [*Galbraith et al.*, 2007; *Marchitto et al.*, 2007; *Jaccard et al.*, 2009; *Stott et al.*, 2009]. Given that the abyssal North Pacific Ocean today holds the largest quantity of dissolved inorganic carbon, it is of paramount importance to understand its exchange with the atmosphere through changes in ventilation rates in the past. At present, the subarctic North Pacific surface waters are isolated from deeper, nutrient-rich waters by a steep, year-round salinity gradient (halocline). This halocline forms a barrier for heat and gas exchange between the atmosphere and the deep ocean, as well as for the supply of nutrients into the photic zone. As the excessive evasion of nutrients into the photic zone is hampered by the halocline, the subarctic North Pacific is marked by one of the highest modern carbon export efficiencies known in the world oceans and is a net sink of atmospheric CO_2 [*Honda et al.*, 2002;

Sarmiento et al., 2004]. Today, formation of new water masses in the North Pacific is restricted to the Okhotsk Sea in the northwest Pacific (NW-Pacific), where waters are produced in coastal polynyas by brine rejection during wintertime sea-ice production [*Talley*, 1993; *Shcherbina et al.*, 2003]. These new water masses leave the Okhotsk Sea as Okhotsk Sea Intermediate Water (OSIW) (see supplementary information), mix with water in the NW-Pacific at intermediate depths and form North Pacific Intermediate Water (NPIW). The NPIW spreads eastward through the North Pacific Ocean between ca. 20° N – 40° N to the proximity of the California Current region, where it can still be recognized as positive oxygen anomaly between 300 – 800 m water depth.

It has been proposed that a better ventilated Glacial North Pacific Intermediate Water (GNPIW) formed during the Last Glacial Maximum, leading to deeper convection of the subarctic North Pacific in the upper 2000 m [*Boyle and Keigwin*, 1985; *Keigwin*, 1998; *Matsumoto et al.*, 2002]. Studies on deep-sea records (deeper than 2000 m) based on benthic carbon isotopes (δ^{13}C) and paired benthic/planktonic foraminifera ^{14}C measurements (BF-PF ages) show only minor changes in deep convection [*Keigwin*, 1987; *Lund et al.*, 2011] in the North Pacific or no ventilation changes at all in the deep Pacific Ocean [*Broecker et al.*, 2004; *Broecker et al.*, 2008]. However, studies with General Circulation Models (GCMs) point to a more rigorous ventilation of the deglacial North Pacific in response to a shutdown of the AMOC during the Heinrich 1 cold event. Accordingly, this would lead to an onset of a Pacific Meridional Overturning Circulation (PMOC), which transports heat and salt poleward and warms the subpolar North Pacific, while the North Atlantic cools (temperature seesaw)[*Bard et al.*, 2000]. An enhanced poleward transport of warm and saline waters by the PMOC would also lead to an onset of deep overturning in the subarctic North Pacific [*Okazaki et al.*, 2010], whereas a sluggish AMOC persisted during Heinrich 1 in the North Atlantic (ventilation seesaw) [*Saenko et al.*, 2004]. Strong evidence for mid-depth ventilation changes from BF-PF ages in the western subarctic North Pacific indicate significant changes in intermediate water formation during the last glacial termination [*Duplessy et al.*, 1989; *Ahagon et al.*, 2003; *Sagawa and Ikehara*, 2008]. However, if enhanced ventilation of water masses in the subarctic North Pacific was related to GNPIW, potential source regions are the Okhotsk Sea, the Bering Sea or both**.** Some evidence for deglacial changes in the ventilation history of these marginal seas stems from studies on microfossil assemblages [*Tanaka and Takahashi*, 2005] and trace-metals [*Horikawa et al.*, 2010], which point out that the Bering Sea in particular played a more active role in ventilating the North Pacific. Whether an amplified convection from the marginal seas led to changes in the ventilation of the North Pacific when the AMOC was collapsed has remained elusive in the context to understand the role of North Pacific Ocean ventilation changes during rapid climate changes.

We present new results from carbon isotope records in combination with BF-PF ages to give a first comprehensive view on past ventilation changes in the North Pacific to: (1) infer the timing and extent

of intermediate or deep water formation in the potential source regions and to: (2) assess the impact of a North Atlantic – North Pacific meridional overturning asymmetry on ventilation changes in the North Pacific during the last glacial termination. Sediment records from the Okhotsk Sea (SO178-13-6; 52° 43' N, 144° 42' E, 713 m water depth) and the western Bering Sea (SO201-2-85KL; 57° 30' N, 170° 24' E, 968 m water depth) were selected to provide new insights into the mid-depth ventilation history of the study area (Figure 5.1a). The stratigraphy is well constrained by multiple AMS-^{14}C datings (AMS-^{14}C ages, see supplementary Table S5.1 and Figure S5.1 and Figure S5.2) and detailed inter-core correlation via high-resolution X-ray fluorescence (XRF) core scanner data [*Max et al.*, in review] (see supplementary methods). $\delta^{13}C$ was measured on epibenthic foraminifera *Cibicidoides lobatulus* (see supplementary Table S5.3), proven to be a robust proxy to study changes in past ocean circulation [*Curry et al.*, 1988; *Curry and Oppo*, 2005]. These data are supplemented by a set of six BF-PF ages derived from sediment records of the NW-Pacific (see supplementary Table S5.2). In addition, we used recently published high-resolution sea surface temperature (SST) data based on alkenone paleothermometry ($U^{k'}_{37}$) from the subarctic NW-Pacific [*Max et al.*, in review] together with previously published northeast Pacific [*Barron et al.*, 2003] and North Atlantic [*Bard et al.*, 2000] SST data to study circulation changes and the AMOC/PMOC relationship to deglacial climate changes [*Okazaki et al.*, 2010].

In order to assess the timing and nature of ventilation changes in the subarctic North Pacific and its relationship to major reorganizations in the AMOC we compared our western Bering Sea intermediate-depth $\delta^{13}C$ record with published $^{231}Pa/^{230}Th$ data (proposed to reflect the strength of the AMOC) from the North Atlantic [*McManus et al.*, 2004] during the last deglaciation (Figure 5.1b). The most striking feature is that the western Bering Sea record reveals millennial-scale oscillations in $\delta^{13}C$ that indicate repeated intermediate water ventilation changes, which are strictly opposite in sign (ventilation seesaw) compared to the North Atlantic deep circulation history of the last 20 kyr (Figure 5.1b). In more detail, the western Bering Sea $\delta^{13}C$ record shows several pronounced reversals between $\delta^{13}C$ minima at 19 – 17.5 ka BP, 14.8 – 12.8 ka BP and 11.7 – 11 ka BP, and maxima in the $\delta^{13}C$ at 17 – 14.9 ka BP and 12.2 – 11.7 ka BP. The North Atlantic $^{231}Pa/^{230}Th$ record suggests that the AMOC nearly ceased and North Atlantic Deep water (NADW) formation became sluggish during Heinrich 1 (17.5 – 15 ka BP) and the Younger Dryas (12.8 – 11.8 ka BP) cold phases.

In contrast, the western Bering Sea $\delta^{13}C$ data show more rigorous ventilation of intermediate waters during the cold phases and times of reduced deep convection in the North Atlantic. Furthermore, when the North Atlantic deep overturning cell was re-established during the Bølling/Allerød (14.7 – 12.8 ka BP) and at the onset of the Holocene, active ventilation of western Bering Sea intermediate water ceased. From this we infer that the western Bering Sea was better ventilated episodically during phases of AMOC slowdown, forming a ventilation seesaw between the North Pacific and North Atlantic.
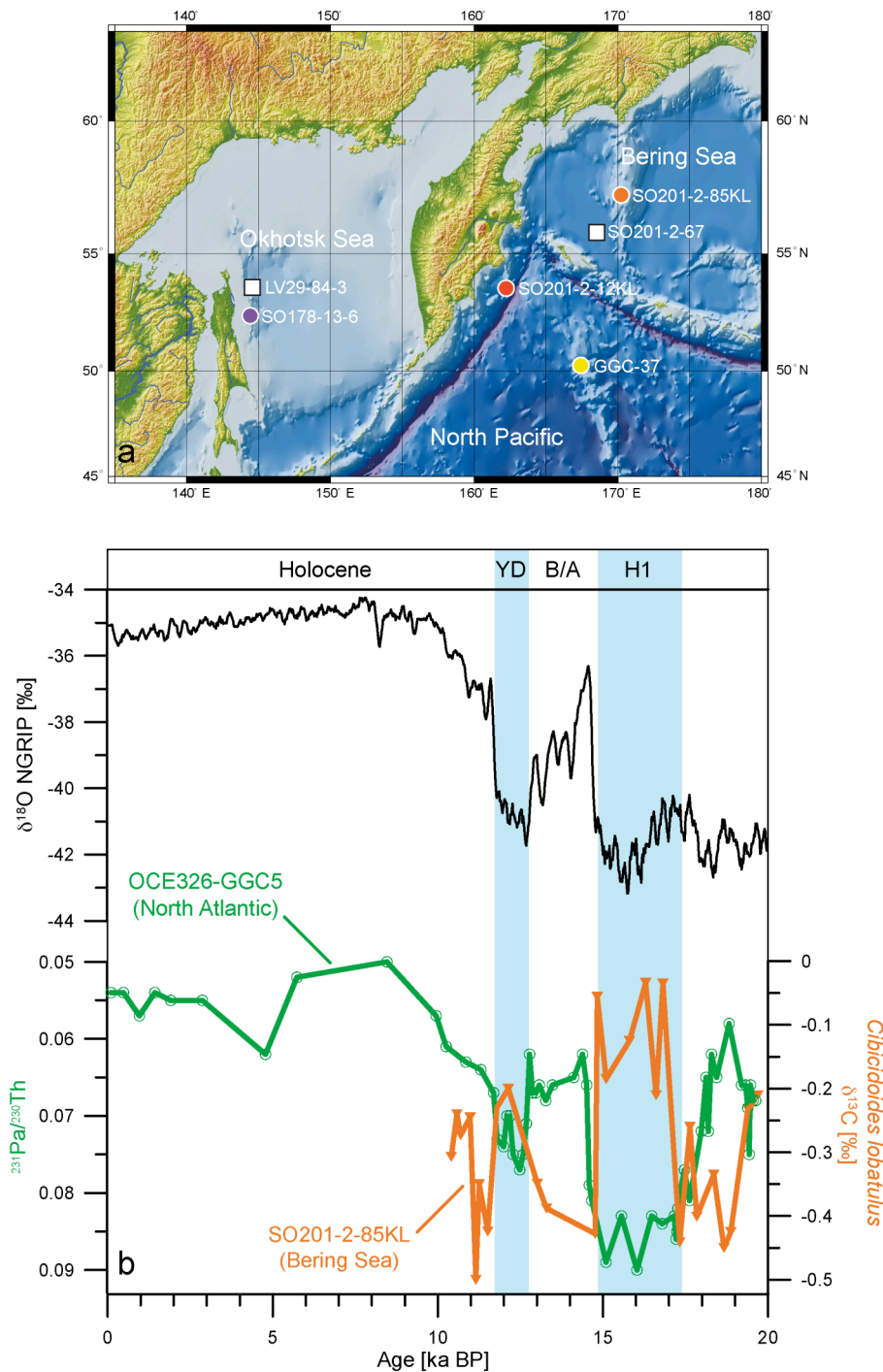
Figure 5.1: (a) Overview map of the subarctic NW-Pacific and its marginal seas with sediment core locations for SO201-2-85KL in the western Bering Sea (orange spot), SO178-13-6 in the Okhotsk Sea (purple spot), SO201-2-12KL (red spot) and GGC-37 [*Keigwin*, 1998] (yellow spot) from the NW-Pacific as well as location of water profiles of $\delta^{13}C_{DIC,}$ see supplementary Figure S5.3) indicated as white boxes. (b) NGRIP ice core record and Pa/Th ratio [*McManus et al.*, 2004] (in green) as a proxy for the AMOC strength in the North Atlantic and $\delta^{13}C$-record (in orange) of the western Bering Sea as proxy for intermediate water ventilation for the last 20 kyr.

Enhanced formation of intermediate water masses in the subarctic North Pacific becomes more apparent from the Okhotsk Sea $\delta^{13}C$ record (Figure 5.2a). Higher $\delta^{13}C$ values are associated with Heinrich 1 in the Okhotsk Sea and similar in timing to the western Bering Sea, but reveal much higher amplitudes of up to +1.0 ‰. This clearly indicates the enhanced formation of fresh, newly formed

water masses in the Okhotsk Sea during Heinrich 1 (17 – 15 ka BP), the Allerød (13.2 – 13. 5 ka BP) and Younger Dryas (11.8 – 12.2 ka BP). In particular, during Heinrich 1 the OSIW is characterized by values of up to +1.0 ‰, which are similar to modern NADW $\delta^{13}C$ signatures (+1 - 1.2 ‰) in the subarctic North Atlantic [*Curry and Oppo*, 2005]. In turn, most depleted $\delta^{13}C$ values (-0.5 to -0.8 ‰) are recorded during the early Bølling (14.7 – 14 ka BP) and the early Holocene, similar to the western Bering Sea. From this we infer a strengthened formation of NPIW in the subarctic North Pacific during phases of AMOC reductions and vice versa. Both the high magnitude of $\delta^{13}C$ values recorded in the Okhotsk Sea (-0.8 – 1.0 ‰) and the less pronounced western Bering Sea $\delta^{13}C$ values (-0.5 – 0 ‰) point to concurrent, rapid changes in ventilation of intermediate water masses in the two marginal seas during the last 20 kyr. Given the difference in $\delta^{13}C$ gradients between the two basins we conclude that the Okhotsk Sea was the major source region for young, well–ventilated intermediate water masses (NPIW) in the subarctic North Pacific during the last deglaciation.

We combined available BF-PF ages (see supplementary Table S5.2) and $\delta^{13}C$ records from the intermediate and deep NW-Pacific to assess the extent of ventilation changes during the last glacial termination (Figure 5.2, a-c). By direct comparison between intermediate and deep ventilation records ($\delta^{13}C$ signal and BF-PF ages), it becomes apparent that during Heinrich 1 the intermediate and deep water ventilation changes were opposite in sign and indicate most intensified intermediate water ventilation compared to most decreased ventilation of the deep NW-Pacific. Highest gradients in $\delta^{13}C$ and ventilation ages between intermediate and deep water during Heinrich 1 suggest the development of a shallow overturning (shallow PMOC) that leaves the North Pacific Deep Water unaffected. The ventilation asymmetry between intermediate and deep water contradicts the onset of deep water formation in the North Pacific [*Okazaki et al.*, 2010], but are in harmony with the evidence for a bathyal front at about 2000 m reported for the glacial North Pacific [*Duplessy et al.*, 1988; *Herguera*, 1992; *Keigwin*, 1998; *Matsumoto et al.*, 2002] and probably also established during Heinrich 1 of the last deglacial period. The better ventilated volumes and ages in the upper ocean during glacial conditions (< 2000 m) were related to the wind stress curl and surface buoyancy fluxes at mid- to high latitudes in the North Pacific, probably driven by enhanced meridional and zonal pressure and temperature gradients. In turn, the deeper portion of the North Pacific (> 2000 m) has been proposed to be affected by water masses formed in the Southern Ocean [*Herguera et al.*, 2010]. Similar processes could also feature the establishment of the observed ventilation asymmetry between intermediate and deep water during Heinrich 1 in the NW-Pacific but are not understood so far.

The strengthening of NPIW formation in response to AMOC reductions (ventilation seesaw) is in harmony with results of several modelling studies (GCMs), which simulate enhanced meridional overturning in the North Pacific during the last glacial termination. However, most studies suggest an establishment of a PMOC and active convection of heat and salt in the subpolar regions of the North Pacific to promote deep overturning [*Saenko et al.*, 2004; *Krebs and Timmermann*, 2007; *Schmittner*
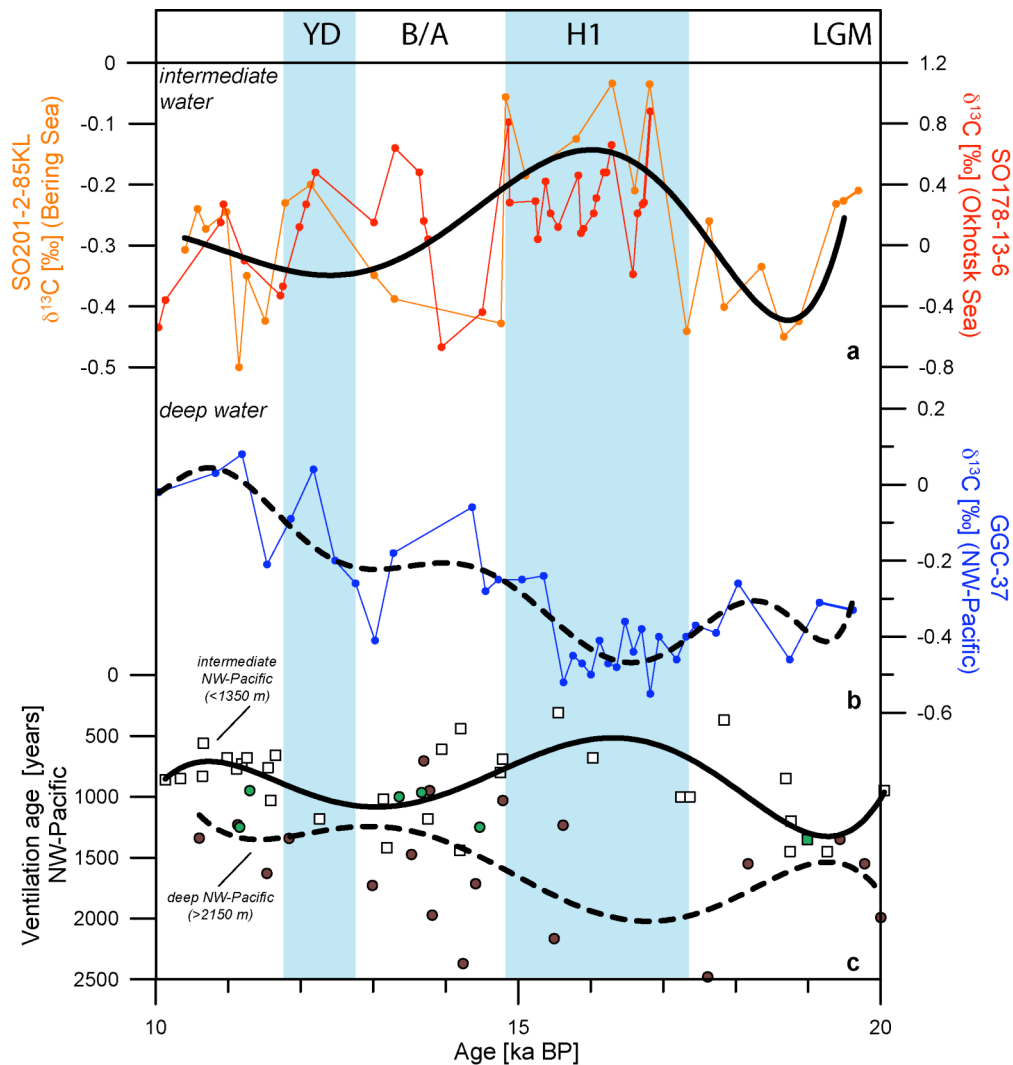
Figure 5.2: Sediment proxy records of past ventilation changes from intermediate (< 1366 m) and deep water (> 2130 m) in the NW-Pacific between 20 – 10 ka BP with (a) benthic foraminiferal δ^{13}C-records (*C. lobatulus*) from the Okhotsk Sea (red curve) and Bering Sea (orange curve) together with spline-interpolated δ^{13}C-record from the Bering Sea (thick black line) and in (b) δ^{13}C-record from sediment record GGC-37 (in blue) from the deep NW-Pacific and spline interpolation (thick stippled line) together with (c) published intermediate (open boxes) and deep water (filled brown circles) BF-PF ages [*Duplessy et al.*, 1989; *Murayama et al.*, 1992; *Keigwin*, 2002; *Ahagon et al.*, 2003; *Hoshiba et al.*, 2006; *Ikehara et al.*, 2006; *Sarnthein et al.*, 2006; *Minoshima et al.*, 2007; *Sagawa and Ikehara*, 2008] and intermediate (filled green boxes) and deep water (filled green circles) BF-PF ages from this study. Calculated splines are derived from whole set of BF-PF ages and given for intermediate (thick black line) and deep water (thick stippled line), respectively.

et al., 2007]. This scenario would lead to a more rigorous ventilation of the subarctic North Pacific accompanied with a rise in SST by up to 1.8 °C [*Okazaki et al.*, 2010] as response to a weakening of the AMOC (e.g. during Heinrich 1 or the Younger Dryas) and cooling in the North Atlantic (temperature seesaw). On the other hand, some model results proposed a cooling in the subarctic North Pacific due to a shutdown of AMOC [*Mikolajewicz et al.*, 1997; *Okumura et al.*, 2009]. There, the simulated shutdown of the Meridional Overturning Circulation in the North Atlantic triggers rapid atmospheric reorganizations in the subarctic North Pacific via an atmospheric bridge and leads to an intensification of low pressure systems (Aleutian Low), which amplifies a cooling in the subarctic North Pacific. Conversely, this mechanism would lead to a similar SST development between the

North Atlantic and the North Pacific (no temperature seesaw) and also question the mechanism of PMOC-related warming and deep overturning in the subarctic North Pacific. We used high-resolution SST data from the North Pacific [*Barron et al.*, 2003; *Max et al.*, in review] and the North Atlantic [*Bard et al.*, 2000], together with the North Greenland ice-core record (NGRIP) [*Rasmussen et al.*, 2006] to assess the proposed mechanistic links between the shutdown of the AMOC (cooling of the North Atlantic) and an onset of a PMOC (warming of the North Pacific). The comparison of SST data between the North Pacific and the North Atlantic temperature record (Figure 5.3) exhibits a similar SST development (no temperature seesaw) during the last glacial termination [*Max et al.*, in review]. The similar SST development between the North Atlantic and the North Pacific clearly shows that changes in the PMOC only have a minor influence on the NW-Pacific SST development. This calls for other mechanisms to explain enhanced intermediate or deep water formation in the North Pacific during the last glacial termination.
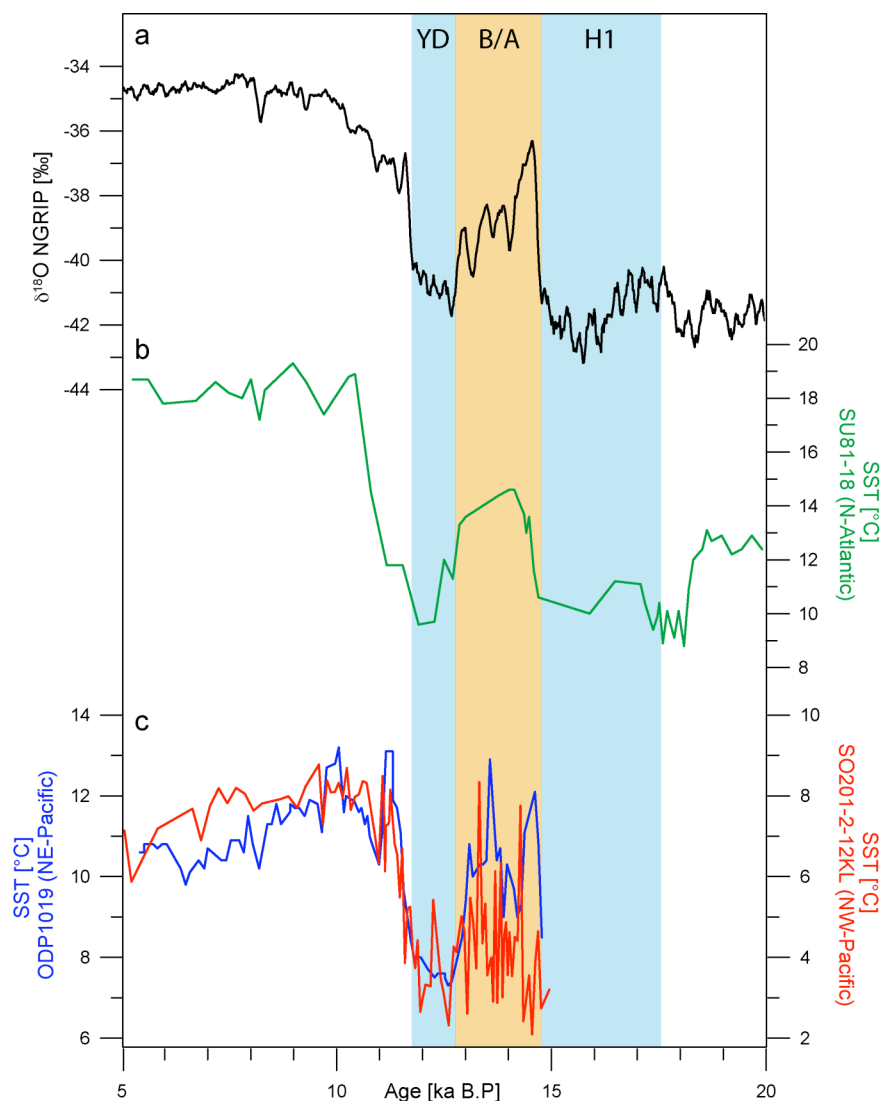
Figure 5.3: Northern Hemisphere climate fluctuations of the past 20 kyr given by (**a**) NGRIP ice core oxygen isotope record together with (**b**) alkenone-based sea surface temperature record SU81-18 from the North Atlantic (in green) [*Bard et al.*, 2000] and (**c**) alkenone-based sea surface temperature records from the NE-Pacific (in blue) [*Barron et al.*, 2003] and NW-Pacific (in red) [*Max et al.*, in review] for the last 15 kyr.

More recently, a study addressed the issue of variability in North Pacific intermediate and deep water ventilation during Heinrich events by using two coupled climate models (MIROC and LOVECLIM) with LGM background conditions [*Chikamoto et al.*, 2012]. Both model runs simulated differing strengths of the PMOC, which resulted in a cooling of the western North Pacific (no temperature seesaw) by 2.2 and 2.6 °C, respectively. The largest cooling trend appears in the western North Pacific in association with severe cooling of the overlying atmosphere in the Northern Hemisphere and intensification of the Aleutian Low [*Okumura et al.*, 2009]. Interestingly, the model-run with a weak PMOC (MIROC) results in a more pronounced cooling of the western North Pacific and also indicates a cooling in the eastern North Pacific. As a result, the mixed layer deepens near the Kamchatka region and in the western boundary currents, corresponding to strong mixing of surface and subsurface waters and shallow overturning (extending to 2000 m water depth) of the North Pacific in line with our results. On the other hand, an enhanced PMOC (LOVECLIM) would result in deeper overturning (greater than 3000 m water depth) due to a greater transport of warm and saline equatorial waters to the North Pacific (temperature seesaw) in contrast to our results.

The match between the simulated SST and ventilation changes (MIROC) and our results make a compelling case for the existence of intermediate water formation during H1 and associated onset of shallow overturning in the North Pacific. In turn, no deep water formation occurred in the subarctic North Pacific during Heinrich 1 as given by the largest intermediate to deep water BF-PF age and δ^{13}C gradients, in contrast to the simulated intensification of a PMOC and related deep overturning (LOVECLIM) [*Okazaki et al.*, 2010]. Several model studies emphasize the importance of changes in overlying atmospheric pressure regimes in the Northern Hemisphere during AMOC reductions. Accordingly, the simulated shutdown of the Meridional Overturning Circulation in the North Atlantic triggers rapid atmospheric reorganizations in the subarctic North Pacific via an atmospheric bridge and leads to an intensification of the Aleutian Low and a cooling in the North Pacific. Some studies suggest that in response to a substantial AMOC-weakening tropical Atlantic cooling induces anomalous high pressure that extends to the eastern tropical Pacific, thereby intensifying northeasterly trade winds across the central isthmus of America [*Wu et al.*, 2008]. The advection of cold and dry air from the Atlantic to the Pacific would lead to tropical precipitation anomalies in the eastern tropical North Pacific and triggers the propagation of Rossby waves, which influences the strength of the Aleutian Low [*Okumura et al.*, 2009]. Other studies emphasize the role of intensified westerly winds due to an AMOC-shutdown. This would lead to enhanced thermal advection of cold air masses to the North Pacific by prevailing westerly winds, which induce a southward shift of the oceanic frontal zones and a deepening of the wintertime Aleutian Low [*Manabe and Stouffer*, 1988; *Mikolajewicz et al.*, 1997; *Vellinga and Wood*, 2002]. A recent study also claims the sensitivity of the East Asian winter monsoon to AMOC variations by enhanced westerly winds, which are supposed to lead to an overall reduction of humidity and colder temperatures in the Northern Hemisphere [*Sun et al.*, 2012].

Altogether, our results confirm the proposed impact of rapid atmospheric teleconnections between the North Atlantic and North Pacific, which led to a cooling and shallow overturning in the western North Pacific during AMOC reductions. We conclude that intermediate water formation in the subarctic North Pacific can be explained by fast atmospheric interactions between the North Atlantic and North Pacific, which led to rapid dynamics in oceanography and circulation during the last glacial termination.

Acknowledgements

Supplementary Information

Rapid changes in North Pacific Intermediate Water formation during the Last Glacial Termination

1. Age model (AMS ^{14}C dating and X-ray fluorescence measurements)

AMS ^{14}C-ages were measured on samples of monospecific planktonic foraminifera *Neogloboquadrina pachyderma* sinistral from the 125 – 250 μm size fraction in core SO201-2-85KL. AMS ^{14}C-ages in core SO178-13-6 were measured on a mix of planktonic foraminifera (*G. bulloides* and *Neogloboquadrina pachyderma* sinistral) picked from 150 – 250 μm size fraction. The radiocarbon dating (AMS ^{14}C) has been performed by the National Ocean Science Accelerator Mass Spectrometry Facility (NOSAMS) at Woods Hole Oceanographic Institute (WHOI) and Leibniz-Laboratory for Radiometric Dating and Isotope Research at Kiel University. Radiocarbon ages have been reported according to the convention outlined by *Stuiver and Polach* [1977] and *Stuiver* [1980]. All planktonic radiocarbon ages were converted into calibrated 1-sigma calendar age ranges using the calibration tool Calib Rev 6.0 [*Stuiver and Reimer*, 1993] with the Intcal09 atmospheric calibration curve [*Reimer et al.*, 2009] and are given in Table S5.1. For reservoir age correction, reservoir ages of 900 years were applied for core SO178-13-6 and 700 years for core SO201-2-85KL, in line with reported values for the Bering and Okhotsk Sea [*Kuzmin et al.*, 2001; *Kuzmin et al.*, 2007].

Relative sedimentary elemental composition was measured using the Avaatech X-ray fluorescence (XRF) core scanner at the Alfred Wegener Institute for Polar and Marine Research except Okhotsk Sea cores LV29-114-3 and SO178-13-6, where XRF measurements were conducted at the Center for Marine Environmental Science (MARUM), Bremen. Each core segment was scanned for element analysis at 1 mA and tube voltages of 10 kV (Al, Si, S, K, Ca, Ti, Fe) and 50 kV (Ag, Cd, Sn, Te, Ba), using a sampling resolution of 1 cm and 30 s count time.

The deglacial stratigraphy is based on the set of radiocarbon measurements (Table S5.1) (AMS ^{14}C ages) and constrained with the X-ray fluorescence (XRF) core scanner data for inter-core correlation (Figure S5.1 and S5.2), described in detail by *Max et al.*, [in review]. In general, the Ca intensity records (XRF) have been used to correlate prominent similar structures between sediment records. We preferentially dated carbonate maxima (maxima in planktonic foraminifera abundance), which are indicated by maxima in Ca intensities (XRF), to avoid age artefacts due to bioturbation effects. Figure S5.1 shows the Ca intensity records and a detailed core-to-core correlation of the core sites. The Ca intensity pattern shows two intervals with high Ca intensities (carbonate maxima) between 13.390 - 11.950 ^{14}C years and 10.800 – 9.570 ^{14}C years. These pronounced carbonate maxima are well dated in the NW-Pacific realm and mark the B/A and the interval of the early Holocene [*Keigwin et al.*, 1992;

Keigwin, 1998; *Gorbarenko et al.*, 2002; *Seki et al.*, 2004; *Gorbarenko et al.*, 2005; *Cook et al.*, 2005; *Seki et al.*, 2009]. Hence, core SO178-13-6 was correlated to the established stratigraphy of Okhotsk Sea core LV129-114-3 [*Max et al.*, in review] via the Ca intensity record (XRF) and available AMS ^{14}C dates (Table S5.1 and Figure S5.2).

2. Paired benthic/planktonic radiocarbon measurements (BF-PF ages)

To infer paleo-ventilation ages in the subarctic Pacific we measured mono-specific samples of benthic foraminifera *Uvigerina peregrina* and planktonic foraminifera *Neogloboquadrina pachyderma* sinistral to assess BF-PF age differences on six samples (Table S5.2). Benthic/planktonic radiocarbon measurements from this study were compiled together with already published BF-PF ages and used to infer ventilation changes in intermediate- and deep-water of the NW-Pacific. Ventilation ages (BF-PF ages) were calculated by the difference of raw ^{14}C ages between benthic and planktonic foraminifera (Table S5.2).

3. Stable isotope measurements

Sediment samples from Core SO178-13-6 and SO201-2-85KL were freeze-dried, washed over a 63 μm screen, dried and separated in sub-fractions (63 - 150, 150 - 250, 250 - 500, > 500 μm). For stable isotope analysis, we picked the species *Cibicidoides lobatulus* (*C. lobatulus*). This species has been observed to preferentially live attached to hard substrate on or slightly above the sediment surface [*Lutze and Thiel*, 1989; *Schweizer et al.*, 2009] and studies on live specimen indicated that the species faithfully records the $\delta^{13}C_{\sum CO2}$ of overlying bottom waters. Some studies have observed a positive offset in the $\delta^{13}C$ of this species with regard to ambient bottom water for $\delta^{13}C_{DIC}$ at the time of sampling in other high latitude settings. However, this effect was shown to be likely caused by high seasonal variability of the original water $\delta^{13}C_{DIC}$ signal as indicated by time-series measurements of water column $\delta^{13}C_{DIC}$ and according calcification of *C. lobatulus* during time intervals of maximum ventilation [*Mackensen et al.*, 2000]. We thus regard *C. lobatulus* to reliably reflect the water mass $\delta^{13}C$ signal. We mostly picked between two and five specimen per sample and restricted our selection to well-preserved specimen with visible pores, clear sutures and unfilled chambers. During some intervals with low foraminifera abundance, we analyzed single specimen with sufficient size and preservation. Samples were cracked open to remove dirt particles from the inside, if necessary cleaned ultrasonically in ethanol p.a. and roasted at 200 °C for 24 h. Samples of core SO178-13-6 were measured with a Thermo Finnigan MAT 252 isotope ratio mass spectrometer coupled to an automated KIEL II CARBO preparation device at the Paleoceanography Unit's Stable Isotope Laboratory of the GEOMAR – Helmholtz Centre for Ocean Research, Kiel. Overall analytical reproducibility is ±0.04 ‰ for $\delta^{13}C$ and ±0.06 ‰ for $\delta^{18}O$. Sample measurements of core SO201-2-85KL were measured with a Thermo Finnigan MAT 253 isotope ratio mass spectrometer coupled to an automated KIEL CARBO preparation device at the Stable Isotope Laboratory of the Alfred Wegener Institute for Polar and

Marine Research, Bremerhaven. Overall analytical reproducibility is ±0.06 ‰ for $\delta^{13}C$ and ±0.08 ‰ for $\delta^{18}O$. Calibration was achieved via National Bureau of Standards NBS19 and NBS 20 material as well as through an internal laboratory standard of Solnhofen limestone. All values are reported as against the Vienna Pee Dee Belemnite Standard (expressed as ‰ vs. V-PDB) and given in Table S5.3.

4. Modern hydrography

Two stations proximal to the core sites SO201-2-85KL (for western Bering Sea SO201-2-67; 56° 04' N, 169° 14' E) and SO178-13-6 (for Okhotsk Sea station LV29-84-3, 52° 42' N, 144° 13' E) were selected to study the modern distribution of $\delta^{13}C_{DIC}$ (Figure S5.3).

For the Bering Sea samples, the water column was sampled during the expedition S0201-2 of *R/V Sonne* in 2009 [*Dullo et al.*, 2009] in eight depth intervals via a water sampling rosette device. Immediately after sub-sampling of Niskin bottles, water samples were poisoned with a saturated solution of mercury, sealed with wax and stored at 4 °C temperature until further treatment. On shore, 1 ml of water was injected through a septum into a vial with ca. 3 ml concentrated phosphoric acid flushed with pure Helium. After storage at room temperature for complete reaction the resultant CO_2 was transferred via a Finnigan Gas Bench II to a Finnigan MAT 252 gas mass spectrometer for determination of stable carbon isotope ratio at the Alfred Wegener Institute for Polar and Marine Research, Bremerhaven. Results are given in δ-notation versus V-PDB. The precision of $\delta^{13}C$ measurements based on an internal laboratory standard has been reported to be better than ±0.1 ‰.

For the Okhotsk Sea, Water samples were collected during the expedition LV29 of *R/V Akademik M.A. Lavrentyev* in 2002 [*Biebow et al.*, 2003]. Samples for carbon isotope analysis of Dissolved Inorganic Carbon (DIC) were slowly filled into 100-ml glass bottles directly after retrieval of a combined CTD water rosette sampler equipped with 12 Niskin bottles. 0.2 ml $HgCl_2$ was immediately added to each sample to stop biological activity. Bottles were closed by airtight crimp seals and stored under refrigerated, dark conditions until further treatment. Measurements of the $\delta^{13}C_{DIC}$ were carried out in the Leibniz Laboratory for Radiometric Dating and Isotope Research, Kiel using an automated Kiel DICI-II device for CO_2 extraction and a Finnigan MAT Delta E mass spectrometer for measurements (see also *Erlenkeuser et al.*, 1995; *Erlenkeuser et al.*, 1999]. Isotope results are given in the δ-notation and calibration is based on the NBS 20 carbonate isotope standard, the measurement precision of the $\delta^{13}C_{DIC}$ is ± 0.04 ‰.

The modern distribution of $\delta^{13}C_{DIC}$ show large differences between the Okhotsk Sea and Bering Sea marginal seas as indicated in Figure S5.3. In the Bering Sea, a large gradient in $\delta^{13}C_{DIC}$ is located around 100 m depth, which marks today the mixed layer depth (MLD) by mixing of surface water with underlying water masses in winter (Figure S5.3a). Beyond the MLD $\delta^{13}C_{DIC}$ values rapidly

decline to -0.6 to -0.7 ‰ and indicate the absence of fresh intermediate-water masses in the western Bering Sea today. Modern values of $\delta^{13}C_{DIC}$ are around -0.6 ‰ at the depth interval of core SO201-2-85KL.

The $\delta^{13}C_{DIC}$ profile from the Okhotsk Sea show the presence of enriched $\delta^{13}C_{DIC}$ values within the water column between 200 – 800 m (Figure S5.3b). Today, newly formed Okhotsk Sea Intermediate Water (OSIW) spreads across the Okhotsk Sea, expressed as positive $\delta^{13}C_{DIC}$ anomaly in the water profile. The modern value of Okhotsk Sea record SO178-13-6 lies at the lower boundary of OSIW with $\delta^{13}C_{DIC}$ values around -0.2 ‰.

Supplementary Tables

Table S5.1: AMS ^{14}C ages of the sediment records with calibrated calendar age ± 1σ (years) and applied reservoir age correction used in this study. AMS ^{14}C ages in italics has been derived from *Max et al.* [*in review*].

Laboratory Number	Sediment Core	Core Depth (cm)	Radiocarbon Age (years)	Calendar Age ±1σ (years)	Reservoir Age (years)
OS-85655	SO201-2-12KL	210	9390±40	9484-9527	900
KIA44680		295	10570±50	11080-11191	900
OS-87895		340	10800±65	11231-11368	900
OS-92047		508	12500±50	13340-13498	900
OS-87891		550	12900±50	13782-13918	900
OS-87902		610	13350±65	14219-14752	900
OS-92150		695	13900±55	15227-15872	900
KIA44682		820	16160±80	18491-18666	900
KIA44683		875	17090±90	19254-19457	900
transferred age	LV29-114-3	108	5850±60	5607-5730	900
OS-88042		162	8320±40	8236-8310	900
KIA30864		197	9630±50	9764-10067	900
KIA30863		232	10465±50	10808-11080	900
KIA30867		272	12290±55	13164-13308	900
KIA30865		292	13180±60	13960-14457	900
KIA30868		317	14400±80	16538-16827	900
KIA30866		352	15130±80	17117-17497	900
KIA30872*	SO178-13-6	1682.5	10560±50	10874-11183	900
KIA30869*		2072.5	13390±100	14467-14917	900
OS-85665	SO201-2-85KL	26	9950±40	10378-10507	700
KIA42231		45	10315±65	10791-10966	700
OS-85669		60	11950±45	13104-13217	700
KIA42232		70	12620±90	13665-13887	700
OS-87896		95	13850±55	15822-15803	700
OS-87890		135	17350±65	19575-19895	700
KIA42233		155	20720±160	23706-24194	700

* this study

Table S5.2: Radiocarbon measurements on paired benthic/planktonic foraminiferas in the NW-Pacific. BF-PF ages are given in years and periods are indicated by LGM, H1, B/A and Holocene, respectively.

core	water depth (m)	Calendar age (ka BP)	core depth (cm)	Planktonic 14C age (years)	±1σ (years)	Benthic 14C age (years)	±1σ (years)	BF-PF (years)	Period	Reference
North Pacific (intermediate water)										
CH84-14	978	10.34	230	10000	140	10850	140	850	Holocene	Duplessy et al.(1989)
CH84-14	978	10.64	280	10230	140	11060	150	830	Holocene	
CH84-14	978	11.19	310	10640	150	11370	130	730	Holocene	
CH84-14	978	11.55	340	10870	150	11630	180	760	Holocene	
CH84-14	978	13.14	400	12180	160	13200	150	1020	B/A	
CH84-14	978	13.76	480	12750	150	13930	220	1180	B/A	
CH84-14	978	14.21	510	13060	140	13500	200	440	B/A	
CH84-14	978	15.55	550	13830	150	14140	200	310	H1	
CH84-14	978	17.84	690	15570	210	15940	190	370	H1	
GH02-1030	1212	10.13	210	9840	40	10700	70	860	Holocene	Ikehara et al. (2006) and
GH02-1030	1212	10.66	220	10240	60	10800	70	560	Holocene	Sagawa and Ikehara (2008)
GH02-1030	1212	10.99	235	10510	60	11190	60	680	Holocene	
GH02-1030	1212	11.26	244	10690	60	11370	60	680	Holocene	
GH02-1030	1212	11.65	261	10950	60	11610	70	660	Holocene	
GH02-1030	1212	13.94	290	12900	70	13510	80	610	B/A	
GH02-1030	1212	14.19	323.5	13060	70	14500	50	1440	B/A	
GH02-1030	1212	14.78	345.5	13470	40	14160	40	690	H1	
GH02-1030	1212	17.25	435.5	15010	80	16010	90	1000	H1	
GH02-1030	1212	17.37	465.5	15140	60	16140	80	1000	H1	
GH02-1030	1212	18.69	523	16380	60	17230	100	850		
GH02-1030	1212	20.05	558	17780	70	18730	120	950	LGM	
GH02-1030	1212	21.77	630	19130	180	20590	180	1460	LGM	
MR01K03-PC4/5	1366	11.12	231-232	10600	50	11370	50	770	Holocene	Ahagon et al. (2003) and
MR01K03-PC4/5	1366	11.59	262-264	10900	55	11930	60	1030	Holocene	Hoshiba et al. (2006)
MR01K03-PC4/5	1366	12.26	291-293	11420	60	12600	50	1180	YD	
MR01K03-PC4/5	1366	13.19	311-313	12230	50	13650	100	1420	B/A	

Table S5.2 (continued)

core	water depth (m)	Calendar age (ka BP)	core depth (cm)	Planktonic ^{14}C age (years)	±1σ (years)	Benthic ^{14}C age (years)	±1σ (years)	BF-PF (years)	Period	Reference
MR01K03-PC4/5	1366	14.76	363-365	13450	85	14250	120	800	H1	Ahagon et al. (2003) and
MR01K03-PC4/5	1366	16.03	405-407	14150	55	14830	60	680	H1	Hoshiba et al. (2006)
MR01K03-PC4/5	1366	18.76	540-542	16450	110	17650	100	1200	LGM	
MR01K03-PC4/5	1366	20.64	642-644	18200	65	19650	110	1450	LGM	
Bering Sea										
SO201-2-101KL	**630**	**18.99**	**110**	**17310**	**120**	**18630**	**200**	**1350**	**LGM**	**this study**
Sea of Okhotsk										
Nesmeyanov GGC-27	995	18.75	70	16750	200	18200	95	1450		Keigwin et al. (2002)
B34-91	1227	19.26	225	17200	80	18650	110	1450	LGM	Keigwin et al. (2002)
North Pacific (deep water)										
SO201-2-12KL	**2170**	**11.30**	**340**	**10800**	**65**	**11750**	**50**	**950**	**Holocene**	**this study**
SO201-2-12KL	**2170**	**13.36**	**508**	**12500**	**50**	**13500**	**55**	**1000**	**B/A**	
SO201-2-12KL	**2170**	**13.78**	**550**	**12900**	**50**	**13850**	**50**	**950**	**B/A**	
KR02-15 PC6	2215	11.13	539.2	10610	90	11840	60	1230	Holocene	Minoshima et al. (2007)
KR02-15 PC6	2215	11.54	555.1	10860	70	12490	110	1630	Holocene	
KR02-15 PC6	2215	14.79	575.6	13470	70	14500	120	1030	H1	
KT89-18-P4	2700	10.60	185-190	9800	133	11140	207	1340	Holocene	Murayama et al. (1992)
KT89-18-P4	2700	11.84	200-204	10692	108	12034	143	1342	YD	
KT89-18-P4	2700	12.99	236-240	11622	101	13350	259	1728	YD	
KT89-18-P4	2700	13.82	268-272	12450	91	14423	254	1973	B/A	
KT89-18-P4	2700	15.62	338-342	13447	113	14681	153	1234	H1	
KT89-18-P4	2700	20.00	449-453	17275	478	19267	734	1992	LGM	
KT89-18-P4	2700	22.87	534-538	19665	303	21344	366	1689	LGM	
MD01-2416	2317	13.67	88	12690	55	13655	55	965	B/A	Sarnthein et al. (2006)
MD01-2416	2317	13.53	96	12555	60	14030	70	1475	B/A	

Table S5.2 (continued)

core	water depth (m)	Calendar age (ka BP)	core depth (cm)	Planktonic ^{14}C age (years)	±1σ (years)	Benthic ^{14}C age (years)	±1σ (years)	BF-PF (years)	Period	Reference
North Pacific (deep water)										
MD01-2416	2317	14.41	115	13205	55	14920	70	1715	B/A	Sarnthein et al. (2006)
MD01-2416	2317	14.24	136	13090	60	15460	80	2370	B/A	
MD01-2416	2317	15.50	163	13795	60	15960	100	2165	H1	
MD01-2416	2317	17.62	177	15380	70	17860	100	2480		
ODP883	2385	13.70	51	12715	50	13420	90	705	B/A	Sarnthein et al. (2006)
Bering Sea										
SO201-2-77KL	**2163**	**11.16**	**115**	**10450**	**40**	**11650**	**45**	**1250**	**Holocene**	**this study**
SO201-2-77KL	**2163**	**14.47**	**180**	**13200**	**45**	**14450**	**85**	**1250**	**B/A**	
Sea of Okhotsk										
Nesmeyanov GGC-20	1510	19.44	230	17350	100	18700	140	1350	LGM	Keigwin et al. (2002)
Nesmeyanov GGC-18	1700	18.17	214-216	16250	120	17800	140	1550	LGM	Keigwin et al. (2002)
Nesmeyanov GGC-15	1980	19.78	170	17650	80	19200	110	1550	LGM	Keigwin et al. (2002)

Table S5.3: Stable isotope measurements on epibenthic foraminifera *Cibicidoides lobatulus*.

core:	Depth (cm)	Age (ka BP)	δ¹⁸O (‰PDB)	δ¹³C (‰PDB)
SO201-2-85KL (western Bering Sea)	30	10.41	3.209	-0.307
	33	10.58	3.350	-0.240
	35	10.69	3.249	-0.273
	40	10.98	3.266	-0.245
	43	11.15	3.440	-0.500
	45	11.26	3.288	-0.350
	50	11.51	3.117	-0.424
	53	11.79	3.360	-0.230
	55	12.14	3.387	-0.200
	60	13.01	3.461	-0.349
	63	13.29	3.323	-0.388
	80	14.76	3.307	-0.428
	81	14.83	3.670	-0.056
	85	15.10	3.481	-0.185
	95	15.80	3.988	-0.125
	100	16.30	4.536	-0.034
	103	16.61	3.640	-0.210
	105	16.81	4.231	-0.035
	110	17.33	3.256	-0.441
	113	17.64	3.960	-0.260
	115	17.84	3.817	-0.401
	120	18.36	4.121	-0.335
	123	18.67	3.930	-0.450
	125	18.87	3.965	-0.425
	130	19.39	3.839	-0.232
	131	19.49	3.864	-0.227
	133	19.69	3.900	-0.210
	135	19.90	3.852	-0.518
	140	20.85	3.848	-0.570
SO178-13-6 (Okhotsk Sea)	1632.5	10.041	3.03	-0.54
	1642.5	10.137	3.06	-0.36
	1682.5	10.896	3.54	0.15
	1687.5	10.937	2.96	-0.44
	1687.5	10.937	3.34	0.27
	1722.5	11.226	3.55	-0.1
	1767.5	11.722	3.74	-0.33
	1772.5	11.753	3.45	-0.27
	1822.5	11.984	3.59	0.12
	1842.5	12.076	3.48	0.27
	1857.5	12.203	3.59	0.48
	1870.5	13.011	3.66	0.15
	1885.5	13.304	3.38	0.64
	1912.5	13.636	3.43	0.48
	1917.5	13.698	3.22	0.16
	1922.5	13.759	3.39	0.04
	1937.5	13.944	3.26	-0.67
	1972.5	14.507	4.07	-0.44
	2087.5	14.866	3.1	0.81
	2092.5	14.884	3.05	0.28

Table S5.3 (continued):

core:	Depth (cm)	Age (ka BP)	$\delta^{18}O$ (‰PDB)	$\delta^{13}C$ (‰PDB)
SO178-13-6 (Okhotsk Sea)	2157.5	15.237	3.81	0.29
	2162.5	15.272	4.04	0.04
	2177.5	15.377	4.05	0.42
	2187.5	15.447	3.82	0.21
	2202.5	15.552	3.88	0.12
	2242.5	15.833	3.9	0.46
	2247.5	15.868	3.81	0.08
	2252.5	15.903	3.86	0.11
	2272.5	16.043	3.78	0.21
	2277.5	16.078	3.88	0.31
	2292.5	16.183	3.64	0.48
	2297.5	16.218	4.12	0.48
	2307.5	16.288	3.75	0.66
	2317.5	16.583	3.11	-0.19
	2327.5	16.648	3.94	0.21
	2342.5	16.715	3.99	0.27
	2347.5	16.737	4.31	0.28
	2367.5	16.826	3.67	0.88

Supplementary Figures
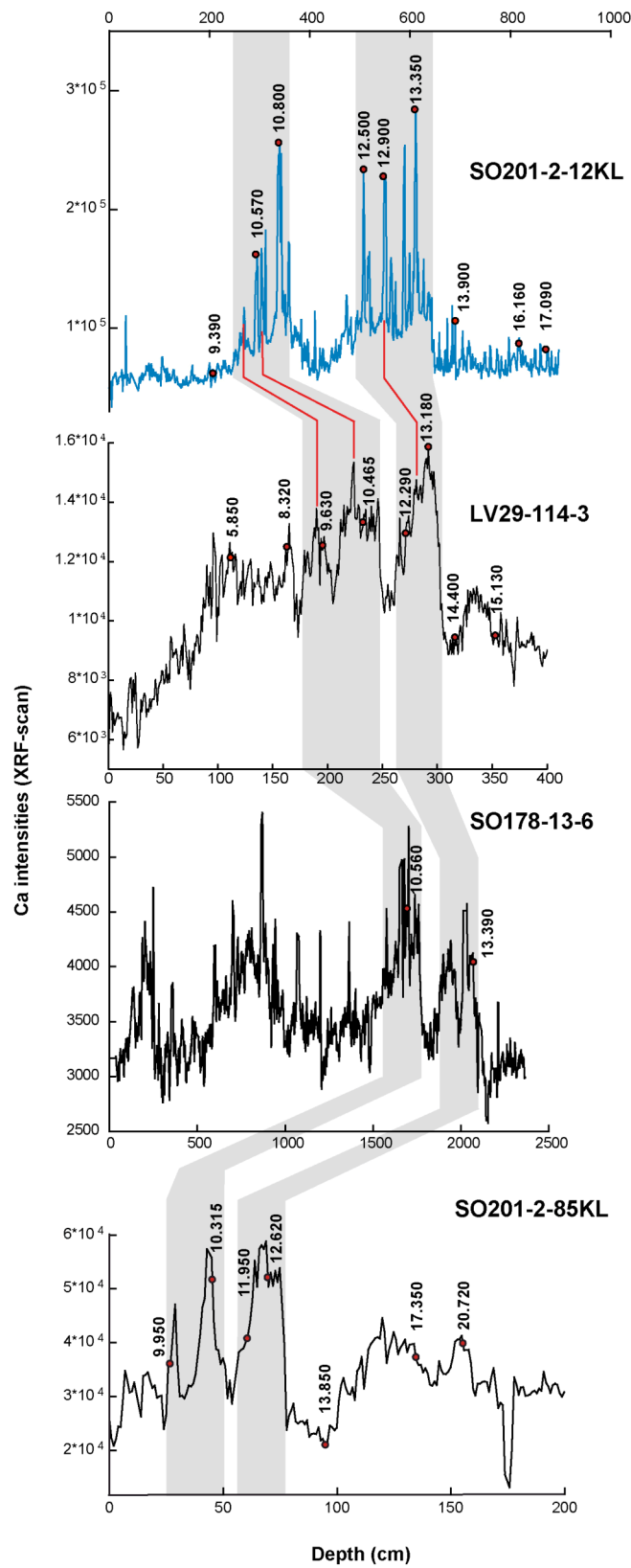
Figure S5.1: Stratigraphic framework of sediment records from the western Bering Sea (SO201-2-85KL) and Okhotsk Sea (LV29-114-3 and SO178-13-6) correlated with high-resolution record SO201-2-12KL record (blue curve) from the subarctic NW-Pacific. The stratigraphy is based on Ca intensities, derived from core logging data (XRF), together with raw AMS ^{14}C datings (red spots with vertical numbers). Grey shaded areas mark prominent carbonate maxima, red lines indicate correlation points between the sediment records.
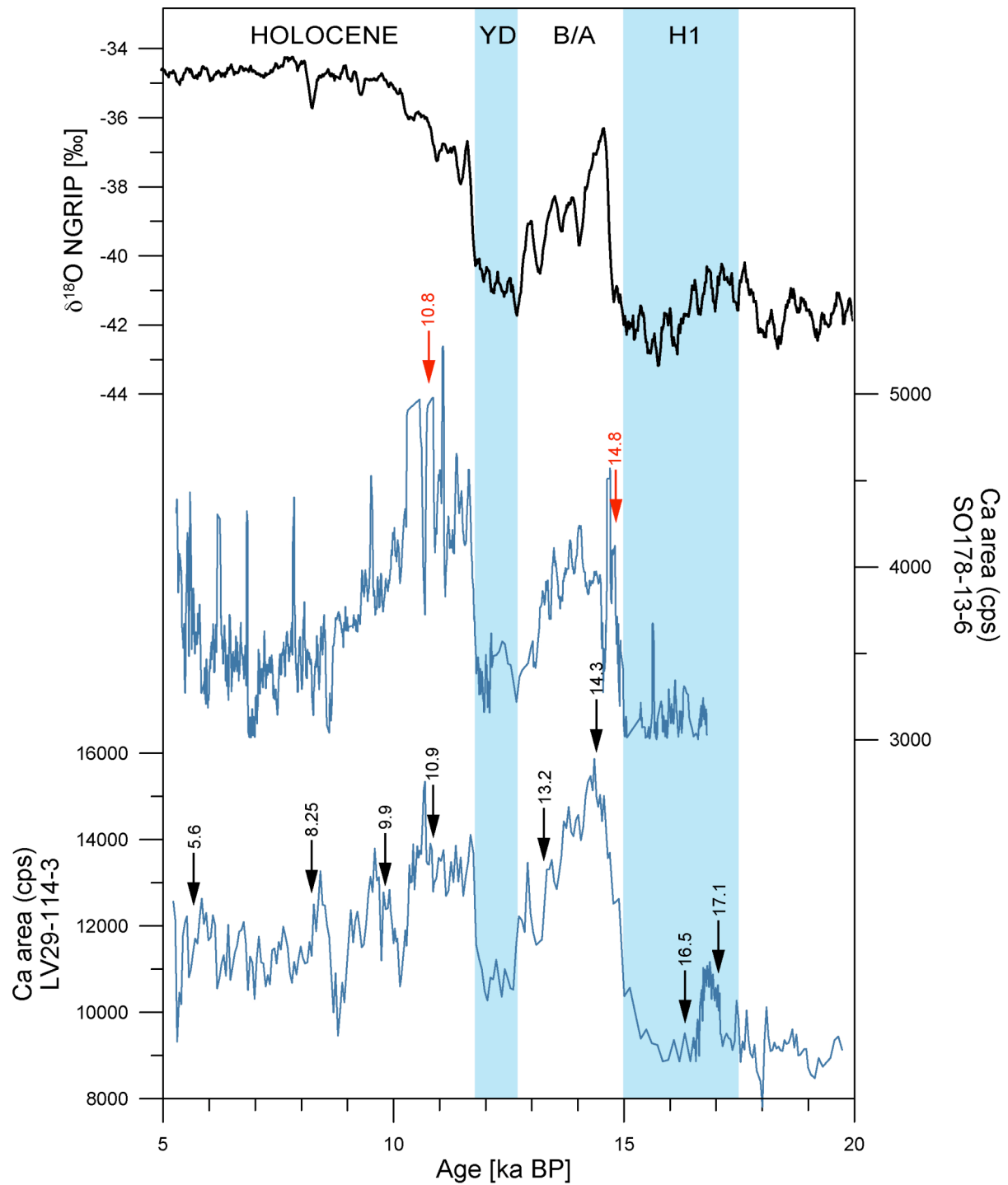
Figure S5.2: Detailed core-to-core correlation for SO178-13-6 to the established age model of LV29-114-3 via AMS ^{14}C datings and Ca intensity records (in blue), see also *Max et al.*, [in review] together with NGRIP isotope record in upper panel (in black). For this study, core SO178-13-6 was correlated via Ca intensity studies (XRF) and AMS ^{14}C datings to LV29-114-3. Black arrows with vertical numbers indicate calibrated ^{14}C ages of LV29-114-3, red arrows with vertical numbers indicate calibrated ^{14}C ages derived from SO178-13-6.
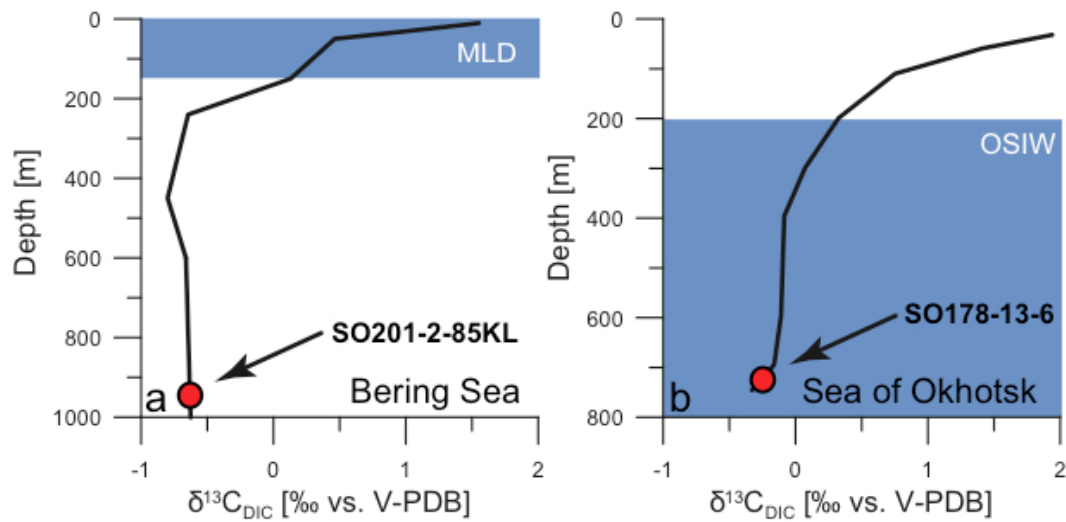
Figure S5.3: Water profiles of $\delta^{13}C_{DIC}$ for the Bering Sea (station SO201-2-67) and Okhotsk Sea (station LV29-84-3) marginal Seas given as (a) $\delta^{13}C_{DIC}$ profile of the Bering Sea together with the depth-interval of SO201-2-85KL (red spot) and (b) $\delta^{13}C_{DIC}$ profile for the Okhotsk Sea together with the depth-interval of SO178-13-6 (red spot). Blue shaded area marks the mixing depth of fresh water masses in the Bering Sea (mixed layer depth = MLD) and Okhotsk Sea (OSIW), respectively.

Chapter 6: Conclusions and further perspectives

6.1 Conclusions

In this thesis, a variety of different geochemical proxies were used to investigate the millennial-scale climate history of the subarctic NW-Pacific realm over the past 20,000 years. This includes, among others, detailed information on past changes in sea surface temperatures, sea-ice variability and intermediate water ventilation characteristics from a high-latitude region of the world ocean, supposed to be very sensitive to recurrent and rapid modifications in past global climate.

It has been shown that the deglacial SST$_{(Uk'37)}$ changes in the far northwest Pacific, the Sea of Okhotsk and western Bering Sea matched the climate variability in other parts of the North Pacific and beyond that were remarkably similar to the timing and nature of the North Atlantic/Greenland temperature variability. From this, a close linkage to deglacial variations in Atlantic Meridional Overtuning Circulation was inferred, which invoked rapid atmospheric teleconnections to allowed a quasi-synchronous SST development between the North Atlantic and the North Pacific on centennial time-scales during the last deglacial period. This is in accordance with numerous model simulations emphasized the importance of changes in overlying atmospheric pressure regimes in the Northern Hemisphere during reductions of the Meridional Overturning Cell in the North Atlantic. The cooling in the far northwest Pacific realm, as seen from the SST$_{(Uk'37)}$ reconstructions, matched the scenario of rapid atmospheric reorganizations to occur in the subarctic North Pacific during instabilities of the thermohaline circulation, thereby leading to an intensification of the Aleutian Low Pressure system and subsequent cooling in the North Pacific. Furthermore, the reconstruction of past sea-ice$_{(IP25)}$ variability for cold (Heinrich 1 and Younger Dryas) and warm (Bølling/Allerød and early Holocene) stages of the last deglaciation points to strong changes in sea-ice extent and a close coupling to SST$_{(Uk'37)}$ fluctuations in the subarctic North Pacific. Accordingly, the sea-ice advanced at least by several hundred miles during cold phases of Heinrich 1 and the Younger Dryas and, in turn, was very limited in extend during warm stages of the Bølling/Allerød and early Holocene. In particular, these results further underpinned the sensitivity of the atmosphere/cryosphere in the subarctic northwest Pacific realm to rapid climate fluctuations and further denoted the tight coupling of the North Pacific – North Atlantic climate during the last glacial termination. Apart from this, SST$_{(Uk'37)}$ reconstructions from the middle to late Holocene interval revealed complex spatial SST differences in the North Pacific realm and rather calls for local reorganizations in oceanography, changes in external forcing or a combination of both. Hence, the intra-basin SST variability in the North Pacific Ocean seems not to be related to changes in the meridional overturning in the North Atlantic during the middle to late Holocene. As no similar SST development was found during the past 7,000 years, the hypothesis of a long-term Holocene temperature seesaw between the North Atlantic and North Pacific, associated with a continuous and basin-scale warming trend to occur in the North Pacific, is rather questionable.

The reconstruction of the Mg/Ca ratio from planktonic foraminifers as proxy for sub sea surface temperature (subSST$_{(Mg/Ca)}$) in combination with SST$_{(Uk'37)}$ records for the subarctic northwest Pacific realm also showed that the structure of the upper-ocean was subject to tremendous changes during millennial-sale climate changes of the last deglaciation. Both SST$_{(Uk'37)}$ and subSST$_{(Mg/Ca)}$ reconstructions indicate deglacial oceanographic changes in the mixed layer, which were directly related to changes in upper-ocean stratification. These results suggest that seasonality and hence thermal summer stratification, although with regional differences, was reduced during cold stages of Heinrich 1 and the Younger Dryas, but intensified during the Bølling/Allerød. During cold stages of Heinrich 1 and the Younger Dryas, the upper-ocean was characterized by the presence of cold subsurface waters in the northwest Pacific realm, which were related to reduced stratification due to enhanced sea-ice formation and increased advection of water masses from the Alaskan Stream and East Kamchatka Current as major surface ocean currents. On the other hand, warmer SST$_{(Uk'37)}$ and subSST$_{(Mg/Ca)}$ during the Bølling/Allerød rather points to enhanced stratification of the upper water column related to reduced sea-ice formation and transport of water masses from the Alaskan Stream. During the onset of the Holocene, the subarctic NW-Pacific experienced a shoaling of the thermocline and the establishment of the dichothermal layer. Moreover, salinity reconstructions from planktonic foraminifers suggest a long-term decrease in surface salinity during the Holocene and further argue for an only recent establishment of the modern, salinity-driven stratification and are further explained by means of large-scale oceanographic reorganizations related to the reopening of the Bering Strait during the Preboreal.

By combination of well-established ventilation proxies, this study has been shown that the nature and timing of past intermediate water formation and ventilation switched in response to rapid climate oscillations of the last deglaciation. During the cold stage of Heinrich 1, intermediate water formation was accelerated in the marginal seas of the northwest Pacific and led to enhanced ventilation of the mid-depth North Pacific as response to reduced deep water formation in the North Atlantic. As soon as the meridional overturning cell in the North Atlantic was re-established, as during the Bølling/Allerød, the ventilation of the North Pacific rapidly ceased. From this, a flip-flop behaviour between the North Pacific and North Atlantic in ventilation rates was inferred. However, it has also been shown that only intermediate water masses are formed in the North Pacific, which resulted in enhanced shallow overturning, whereas the deeper North Pacific (deeper than 2000 m) showed no evidence for amplified ventilation and no deep water formed in the northwest Pacific during the last glacial termination.

To conclude, these results are in accordance with the proposed impact of rapid atmospheric teleconnections between the North Atlantic and North Pacific during meltwater-driven reductions of the Atlantic Meridional Overtuning Cell, which induced fast (on centennial time-scales) dynamics in climate and oceanography in the western North Pacific during the last deglaciation. Overall, the sensitivity of the subarctic North Pacific Ocean to millennial-scale climate fluctuations of the past has to be taken into account for an accurate understanding of past and future climate dynamics.

6.2 Towards MIS 5e: Rapid climate changes in the in the subarctic NW-Pacific during Termination II and beyond?

Millennial-scale climate fluctuations during the last glacial termination (Termination I) significantly affected the SST variability, the stratification of the upper-ocean and circulation of the subarctic NW-Pacific. This raises the question whether the NW-Pacific experienced similar dramatic climate fluctuations during the penultimate deglaciation (Termination II) occurred ~135.000 years ago (Figure 6.1). Information on millennial-scale climate variability during Termination II derived from high-resolution SST records is not available so far for the NW-Pacific and thus, direct comparison to millennial-scale fluctuations of the last glacial termination not feasible (Figure 6.1). On the other hand, knowledge on nature and timing of climate fluctuations during Termination II is urgently needed to understand whether the NW-Pacific experienced similar dynamics in oceanography and circulation analogue to the last glacial termination. Some evidence for rapid environmental changes during the penultimate deglaciation stems from reconstructions of past marine productivity in the NW-Pacific realm [e.g. *Nürnberg and Tiedemann*, *2004*; *Brunelle et al.*, 2010]. Accordingly, high-productivity events occurred during glacial terminations in the NW-Pacific and Sea of Okhotsk, thus hints to rapid climate variability in these regions. However, whether these environmental changes were accompanied by rapid SST variability and changes in upper-ocean stratification, as suggested for the last glacial termination, or substantially different from that needs to be evaluated by future studies.
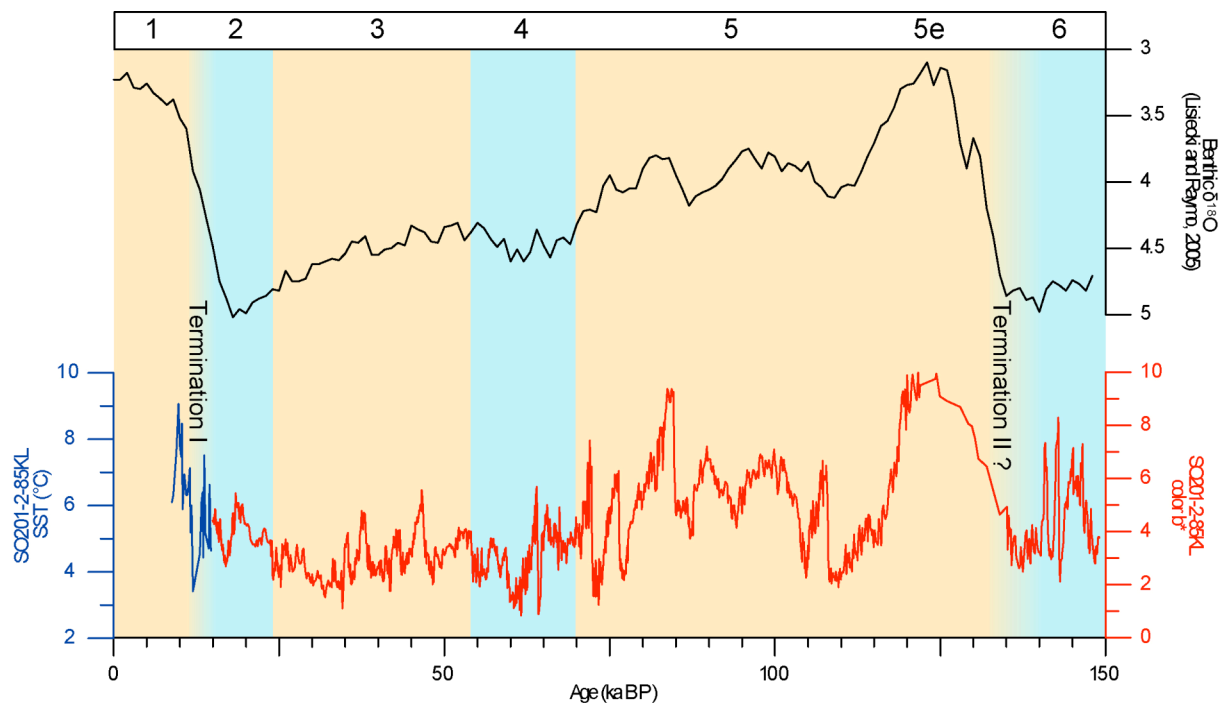
Figure 6.1: Overview of the past 150,000 years of climate history (upper curve): Global stack of benthic δ^{18}O records [*Lisiecki and Raymo*, 2005]. (lower curve) SST record SO201-2-85KL of the western Bering Sea spanning the last 15,000 years (in blue) together with color b* record (in red). Blue and yellow shaded areas mark marine isotope stages (MIS 1- 6) and are also numbered on top. The position of glacial Termination I (15,000 – 12,000 years BP) as well as Termination II (~135,000 – 130,000 years BP) is indicated.

Another focal point for future paleoceanographic studies is the climate development of the subarctic North Pacific during the last interglacial period. In particular, during the Eemian (MIS 5e, between 130.000 – 120.000 years ago) the global climate was supposed to be warmer by a few degree compared to the Holocene [*CLIMAP*, 1981]. Accordingly, the CLIMAP reconstructions of the Eemian surface ocean revealed that the North Pacific SST were up to 1 – 3 °C warmer than during the Holocene. Warmer global ocean temperatures would also have an impact on past upper-ocean stratification and the efficiency of the biological pump in the subpolar North Pacific [e.g. *Sarmiento et al.*, 2004; *Sigman et al.*, 2004]. Some studies suggest a weakening or break up of the subarctic North Pacific stratification during interglacial periods [e.g. *Jaccard et al.*, 2005]. Accordingly, this led to strong evasion of deep-sequestered carbon dioxide into the atmosphere due to less complete nutrient drawdown by biological productivity (CO_2 source). Furthermore, the subarctic North Pacific was supposed to be marked by strong density driven stratification during cold climates and deep CO_2 more effectively trapped in the abyssal ocean (CO_2 sink) [*Jaccard et al.*, 2009]. However, the mentioned scenario neglects the importance of strengthened productivity due to enhanced iron supply to the subpolar regions during glacial times. As the subarctic North Pacific region is a high-nutrient low-chlorophyll (HNLC) area today [*Tsuda*, 2003], enhanced delivery of micronutrients (e.g. via aeolian dust) could have been resulted in amplified marine productivity during glacial times.

According to the most recent climate period investigated here, the subarctic NW-Pacific region experienced rapid fluctuations in SST during the last glacial termination. The combined approach to estimate the temperature variability from alkenone-paleothermometry (surface water) and Mg/Ca-derived (subsurface water) temperature records revealed that the surface waters of the NW-Pacific region were marked by enhanced temperature gradients indicative for strong upper-ocean stratification during the Bølling/Allerød and since the onset of the Holocene. Conversely, stadial periods were marked by lower temperature gradients and are interpreted as less rigorous stratification of the upper water column in the subarctic NW-Pacific during these time-intervals. These results are apparently different to a scenario of generally better stratification during cold climate stages [*Jaccard et al.*, 2005] and less well stratified surface water masses during interglacials and leave some question marks for future paleoceanographic studies. To overcome this controversy, the combination of surface to subsurface SST records should be very useful to reconstruct glacial-interglacial changes by means of changes in upper-ocean stratification or enhanced vertical mixing of surface with subsurface water masses. Several high-resolution records from the NW-Pacific realm are now available to address this concerns through future paleoceanographic studies.

6.3 Millennial-scale NW-Pacific ventilation changes during Dansgaard-Oeschger cycles of the last 60,000 years

The NW-Pacific region was punctuated by strong millennial-scale changes in intermediate water ventilation during the last glacial termination (Figure 6.2). In particular during Heinrich 1, the intermediate water circulation was amplified as opposite to the deep water ventilation history of the North Atlantic. Whether the ventilation asymmetry between the NW-Pacific and North Atlantic also occurred during millennial-scale oscillations of the past 60,000 years is not studied, yet. A persistent link between enhanced ventilation of the North Pacific during Greenland stadials was inferred from a sediment record off Oregon in the eastern North Pacific (2700 m water depth) [*Lund and Mix*, 1998]. According to their results, millennial-scale events of improved ventilation in the eastern North Pacific occurred during cold events in Greenland, in particular, during stadials marked by meltwater events (Heinrich events). Sediment records recovered from intermediate-depth (600 - 1000 m) in the western Bering Sea also revealed millennial-scale changes in NW-Pacific intermediate water ventilation during the past 60,000 years (Figure 6.2). As shown below, times of poor ventilation remarkably correlates with several (but not all) Dansgaard-Oeschger interstadials (DOI) in the Greenland ice-core record. In turn, most enhanced ventilation seems to be coupled to stadials and are most pronounced during meltwater driven Heinrich events H1 to H4 in harmony with the results from the eastern North Pacific.
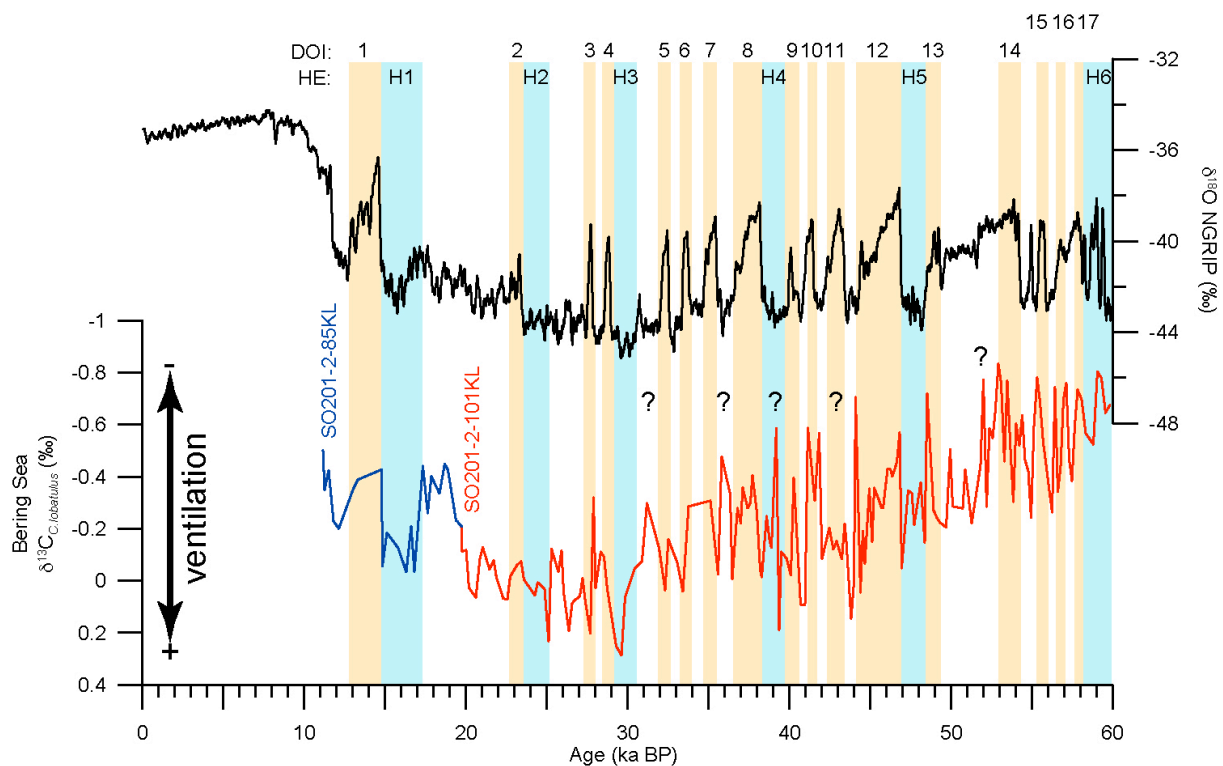
Figure 6.2: Millennial-scale climate fluctuations of the past 60.000 years. (upper curve) NGRIP ice core record with Dansgaard-Oeschger events (DOI 1 - 16) and Heinrich events (H1 – H6) [*Dansgaard et al.*, 1993; *Rasmussen et al.*, 2006]. (lower curve): $\delta^{13}C$ record from sediment core SO201-2-85KL (in blue) and SO201-2 101KL (in red) indicative of millennial-scale changes in intermediate water ventilation in the NW-Pacific.

Enhanced ventilation of the mid-depth North Pacific Ocean during cold stadials of the last 60,000 years was also inferred from several high-resolution records from the Californian margin, most famously from the Santa Barbara basin [*Behl and Kennett*, 1996]. In particular, the Santa Barbara basin is marked by laminated sediment sequences during interstadials and the Holocene, thus implying times of anoxic to suboxic conditions alternating with bioturbated, well oxygenated sediment sequences during cold stadials in the Greenland ice-core record.

Which mechanisms could drive millennial-scale ventilation changes in the NW-Pacific during Dansgaard-Oeschger cycles in the past?

A plausible mechanism to explain rapid stadial/interstadial changes in intermediate water formation in the NW-Pacific invokes mainly atmospherically driven reorganizations of the local oceanographic setting and is exemplarily shown for the Sea of Okhotsk (Figure 6.3). According to this scenario, stadial phases are marked by colder SST due to enhanced transport of cold air masses from the Arctic and leads to active sea-ice formation and high production of OSIW and as a consequence, NPIW. Conversely, during interstadial phases blocked cold air masses and an active summer monsoon could have favoured warmer SST and lowered sea surface salinities, which inhibits sea-ice formation and SOIW formation and consequently lowered the production of NPIW [*Harada et al.*, 2008].
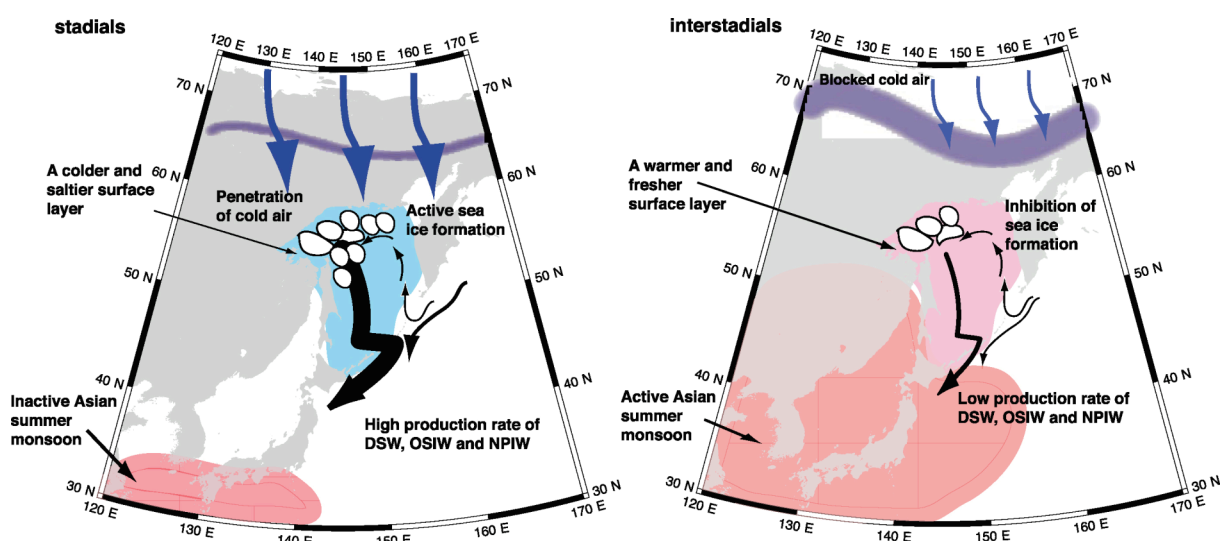
Figure 6.3: Comparison of different forcing mechanisms proposed to have an impact on NPIW formation. (left hand): environmental conditions during stadials. (right hand): environmental conditions during interstadials [modified after *Harada et al.*, 2008].

This study has been shown that increased formation of intermediate water occurred during meltwater driven events of the last glacial termination in the NW-Pacific realm and was coupled to rapid atmospheric teleconnections between the North Atlantic and North Pacific during AMOC reductions. Whether similar processes also led to enhanced NPIW formation during Dansgaard-Oeschger cycles of the past 60,000 years episodically and thus promoted better ventilation of the North Pacific needs to be evaluated by future studies.

Data Handling

All data presented in this thesis will be stored electronically and will be available online in the PANGAEA database (http://www.pangaea.de).

References

Adkins, J.F., and E. A. Boyle (1997), Changing atmospheric $\Delta^{14}C$ and the record of deep water paleo-ventilation ages, *Paleoceanography*, *12*(3), 337-344.

Ahagon, N., K. Ohkushi, M. Uchida, and T. Mishima (2003), Mid-depth circulation in the northwest Pacific during the last deglaciation: Evidence from foraminiferal radiocarbon ages, *Geophysical Research Letters*, *30*(21), doi:10.1029/2003gl018287.

Bard, E., F. Rostek, J. L. Turon, and S. Gendreau (2000), Hydrological impact of Heinrich events in the subtropical northeast Atlantic, *Science, 289*(5483), 1321-1324.

Barker, S., M. Greaves, and H. Elderfield (2003), A study of cleaning procedures used for foraminiferal Mg/Ca paleothermometry, *Geochemistry Geophysics Geosystems*, *4*(9), 8407, doi:10.1029/2003GC000559.

Barron, J. A., L. Heusser, T. Herbert, and M. Lyle (2003), High-resolution climatic evolution of coastal northern California during the past 16,000 years, *Paleoceanography*, *18*(1), doi:10.1029/2002pa000768.

Bauch, D., J. Carstens, and G. Wefer (1997), Oxygen isotope composition of living *Neogloboquadrina pachyderma* (sin.) in the Arctic Ocean, *Earth and Planetary Science Letters*, *146*, 47-58.

Bauch, D., H. Erlenkeuser, G. Winckler, G. Pavlova, and J. Thiede (2002), Carbon isotopes and habitat of polar planktic foraminifera in the Okhotsk Sea: the 'carbonate ion effect' under natural conditions, *Marine Micropaleontology, 45*(2), 83-99.

Behl, R. J., and J. P. Kennett (1996), Brief interstadial events in the Santa Barbara basin, NE Pacific, during the past 60 kyr, *Nature, 379*(6562), 243-246.

Belt, S. T., G. Masse, S. J. Rowland, M. Poulin, C. Michel, and B. LeBlanc (2007), A novel chemical fossil of palaeo sea ice: IP25, *Organic Geochemistry*, *38*(1), 16-27, doi:10.1016/J.Orggeochem.2006.09.013.

Biebow, N., R. Kulinich, and B. Baranov, eds. (2003) KOMEX II, Kurile Okhotsk Sea Marine Experiment: Cruise report RV Akademik M.A.Lavrentyev cruise 29, Leg 1 and Leg 2. *GEOMAR-Report, 110*. 190 pp., GEOMAR, Kiel. ISSN 0936-5788.

Bond, G., W. Broecker, S. Johnsen, J. Mcmanus, L. Labeyrie, J. Jouzel, and G. Bonani (1993), Correlations between Climate Records from North-Atlantic Sediments and Greenland Ice, *Nature, 365*(6442), 143-147.

Boyle, E.A. (1983), Manganese carbonate overgrowths on foraminifera tests, *Geochimica et Cosmochimica Acta*, *47*, 1815-1819.

Boyle, E. A., and L. D. Keigwin (1985), Comparison of Atlantic and Pacific Paleochemical Records for the Last 215,000 Years - Changes in Deep Ocean Circulation and Chemical Inventories, *Earth and Planetary Science Letters*, *76*(1-2), 135-150.

Brassell, S. C., G. Eglinton, I. T. Marlowe, U. Pflaumann, and M. Sarnthein (1986), Molecular Stratigraphy - a New Tool for Climatic Assessment, *Nature*, *320*(6058), 129-133.

Broecker, W.S., and T. -H. Peng (1987), The role of $CaCO_3$ compensation in the glacial to interglacial atmospheric CO_2 change, *Global Biogeochemical Cycles*, *1*(1), 15-29.

Broecker, W., S. Barker, E. Clark, I. Hajdas, G. Bonani, and L. Stott (2004), Ventilation of the glacial deep Pacific Ocean, *Science*, *306*(5699), 1169-1172.

Broecker, W., E. Clark, and S. Barker (2008), Near constancy of the Pacific Ocean surface to mid-depth radiocarbon-age difference over the last 20 kyr, *Earth and Planetary Science Letters*, *274*(3-4), 322-326, doi:10.1016/J.Epsl.2008.07.035.

Brunelle, B. G., D. M. Sigman, M. S. Cook, L. D. Keigwin, G. H. Haug, B. Plessen, G. Schettler, and S. L. Jaccard (2007), Evidence from diatom-bound nitrogen isotopes for subarctic Pacific stratification during the last ice age and a link to North Pacific denitrification changes, *Paleoceanography*, *22*(1), doi:10.1029/2005pa001205.

Brunelle, B. G., D. M. Sigman, S. L. Jaccard, L. D. Keigwin, B. Plessen, G. Schettler, M. S. Cook, and G. H. Haug (2010), Glacial/interglacial changes in nutrient supply and stratification in the western subarctic North Pacific since the penultimate glacial maximum, *Quaternary Science Reviews*, *29*(19-20), 2579-2590, doi:10.1016/j.quascirev.2010.03.010.

Caissie, B. E., J. Brigham-Grette, K. T. Lawrence, T. D. Herbert, and M. S. Cook (2010), Last Glacial Maximum to Holocene sea surface conditions at Umnak Plateau, Bering Sea, as inferred from diatom, alkenone, and stable isotope records, *Paleoceanography*, *25*, doi:10.1029/2008pa001671.

Calvo, E., J. O. Grimalt, and E. Jansen (2002), High resolution $U^{k'}_{37}$ sea surface temperature reconstruction in the Norwegian Sea during the Holocene, *Quaternary Science Reviews*, *21*(12-13), 1385-1394.

Charles, C. D., and R. G. Fairbanks (1992), Evidence from Southern-Ocean Sediments for the Effect of North-Atlantic Deep-Water Flux on Climate, *Nature*, *355*(6359), 416-419.

Chikamoto, M. O., L. Menviel, A. Abe-Ouchi, R. Ohgaito, A. Timmermann, Y. Okazaki, N. Harada, A. Oka, and A. Mouchet (2012), Variability in North Pacific intermediate and deep water ventilation during Heinrich events in two coupled climate models, *Deep-Sea Research Part II-Topical Studies in Oceanography*, (61-64), 114-126.

CLIMAP Project Members, Seasonal reconstructions of the Earth's surface at the Last Glacial Maximum, *Geol. Soc. Am. Map Chart Ser.*, *MC-36*, 1 – 18, Geol. Soc. Am., Boulder, Colo., 1981.

Cook, M. S., L. D. Keigwin, and C. A. Sancetta (2005), The deglacial history of surface and intermediate water of the Bering Sea, *Deep-Sea Res. Part II-Topical. Studies in Oceanography*, *52*(16-18), 2163-2173, doi:10.1016/j.dsr2.2005.07.004.

Cook, M. S. (2006), The paleoceanography of the Bering Sea during the last glacial cycle. *PhD Thesis*, Massachusetts Institute of Technology, Cambridge, and Woods Hole Oceanographic Institution, Woods Hole, USA, 126 pp.

Curry, W. B., J. C. Duplessy, L. D. Labeyrie, and N. J. Shackleton (1988), Changes in the distribution of delta C-13 of deep water TCO2 between the last glaciation and the Holocene, *Paleoceanography*, *3*(3), 317-341.

Curry, W. B., and D. W. Oppo (2005), Glacial water mass geometry and the distribution of delta C-13 of Sigma CO2 in the western Atlantic Ocean, *Paleoceanography*, *20*(1), doi:10.1029/2004pa001021.

Dansgaard, W., S. J. Johnsen, H. B. Clausen, D. Dahljensen, N. S. Gundestrup, C. U. Hammer, C. S. Hvidberg, J. P. Steffensen, A. E. Sveinbjornsdottir, J. Jouzel, and G. Bond (1993), Evidence for General Instability of Past Climate from a 250-Kyr Ice-Core Record, *Nature*, *364*(6434), 218-220.

Debret, M., M. Desmet, W. Balsam, Y. Copard, P. Francus, and C. Laj (2006), Spectrophotometer analysis of Holocene sediments from an anoxic fjord: Saanich Inlet, British Columbia, Canada, *Marine Geology*, *229*(1-2), 15-28, doi:10.1016/J.Margeo.2006.01.005.

Dekens, P. S., D. W. Lea, D. K. Pak, and H. J. Spero (2002), Core top calibration of Mg/Ca in tropical foraminifera: Refining paleotemperature estimation, *Geochemistry Geophysics Geosystems*, *3*(4), doi:10.1029/2001GC000200.

Demaster, D. J. (1981), The Supply and Accumulation of Silica in the Marine-Environment, *Geochimica Et Cosmochimica Acta*, *45*(10), 1715-1732.

Dickson, A.G. (1990), Thermodynamics of the dissociation of boric acid in synthetic seawater from 273.15 to 318.15 K, *Deep Sea Research Part A, Oceanographic Research Papers*, *37*(5), 755-766.

Dullo, W.-C., B. Baranov, and C. van den Bogaard (Eds.), 2009. FS Sonne Fahrtbericht / Cruise Report SO201-2 KALMAR, Busan/Korea-Tomakomai/Japan, 30.08.-08.10.2009. *IFM-GEOMAR Report 35*, 233 pp.

Duplessy, J. C., N. J. Shackleton, R. G. Fairbanks, L. Labeyrie, D. Oppo, and N. Kallel (1988), Deepwater source variations during the last climatic cycle and their impact on the global deepwater circulation, *Paleoceanography*, *3*(3), 343-360.

Duplessy, J. C., M. Arnold, E. Bard, A. Juilletleclerc, N. Kallel, and L. Labeyrie (1989), Ams C-14 Study of Transient Events and of the Ventilation Rate of the Pacific Intermediate Water during the Last Deglaciation, *Radiocarbon*, *31*(3), 493-502.

Elderfield, H., and G. Ganssen (2000), Past temperature and $\delta^{18}O$ of surface ocean waters inferred from foraminiferal Mg/Ca ratios, *Nature*, *405*, 442-445

Elderfield, H., M. Vautravers, and M. Cooper (2002), The relationship between shell size and Mg/Ca, Sr/Ca, $\delta^{18}O$, and $\delta^{13}C$ of species of planktonic foraminifera, *Geochemistry Geophysics Geosystems*, *3* (8), doi:10.1029/2001GC000194.

Elderfield, H., J. Yu, P. Anand, T. Kiefer, and B. Nyland (2006), Calibrations for benthic foraminiferal Mg/Ca paleothermometry and the carbonate ion hypothesis, *Earth and Planetary Science Letters*, *250*, 633-649.

Elias, S. A., S. K. Short, C. H. Nelson, and H. H. Birks (1996), Life and times of the Bering land bridge, *Nature*, *382*(6586), 60-63.

Elias, S. A., S. K. Short, and H. H. Birks (1997), Late Wisconsin environments of the Bering Land Bridge, *Palaeogeography, Palaeoclimatology Palaeoecology*, *136*(1-4), 293-308.

Emeis, K. C., and A. G. Dawson (2003), Holocene palaeoclimate records over Europe and the North Atlantic, *Holocene*, *13*(3), 305-309, doi:10.1191/0959683603hl622ed.

Emile-Geay, J., M. A. Cane, N. Naik, R. Seager, A. C. Clement, and A. van Geen (2003), Warren revisited: Atmospheric freshwater fluxes and "Why is no deep water formed in the North Pacific", *Journal of Geophysical Research*, *108*(C6), 3178, doi:10.1029/2001JC001058.

Erlenkeuser, H., R.F. Spielhagen, and E. Taldenkova (1999), Stable isotopes in modern water and bivalve samples from the Kara Sea. In: J. Matthiessen, O.V. Stepanets, R. Stein, D.K. Fütterer, and E.M. Galimov (Eds.), The Kara Sea Expedition of RV Akademik Boris Petrov 1997: First Results of a Joint Russian-German Pilot Study. *Berichte zur Polarforschung/Reports on Polar Research 300*, 80-90.

Erlenkeuser, H., and the TRANSDRIFT II Shipboard Scientific Party (1995), Stable carbon isotope ratios in the waters of the Laptev Sea/Sept. 94. In: H. Kassens, D. Piepenburg, J. Thiede, L. Timokhov, H.-W. Hubberten, and S. M. Priamikov (Eds.) "Russian-German Cooperation: Laptev Sea System", *Berichte zur Polarforschung/Reports on Polar Research 176*, 170-177.

Fahl, K., and R. Stein (in review), Modern seasonal variability and deglacial/Holocene change of central Arctic Ocean sea-ice cover: New insights from biomarker proxy records, *Earth and Planetary Science Letters*.

Farrell, J. W., and W. L. Prell (1989), Climatic change and $CaCO_3$ preservation: An 800,000 year bathymetric reconstruction from the central equatorial Pacific Ocean, *Paleoceanography*, *4*(4), 447-466.

Fleming, K., P. Johnston, D. Zwartz, Y. Yokoyama, K. Lambeck, and J. Chappell (1998), Refining the eustatic sea-level curve since the Last Glacial Maximum using far- and intermediate-field sites, *Earth and Planetary Science Letters, 163*(1-4), 327-342.

Galbraith, E. D., S. L. Jaccard, T. F. Pedersen, D. M. Sigman, G. H. Haug, M. Cook, J. R. Southon, and R. Francois (2007), Carbon dioxide release from the North Pacific abyss during the last deglaciation, *Nature*, *449*(7164), 890-899, doi:10.1038/Nature06227.

Gebhardt, H., M. Sarnthein, P. M. Grootes, T. Kiefer, H. Kuehn, F. Schmieder, and U. Rohl (2008), Paleonutrient and productivity records from the subarctic North Pacific for Pleistocene glacial terminations I to V, *Paleoceanography*, *23*(4), doi:10.1029/2007pa001513.

Gorbarenko, S. A., T. A. Khusid, I. A. Basov, T. Oba, J. R. Southon, and I. Koizumi (2002), Glacial Holocene environment of the southeastern Okhotsk Sea: evidence from geochemical and palaeontological data, *Palaeogeography, Paleoclimatology Palaeoecology*, *177*(3-4), 237-263.

Gorbarenko, S.A., J. R. Southon, L. D. Keigwin, M. V. Cherepanova, and I. G. Gvozdeva, (2004), Late Pleistocene—Holocene oceanographic variability in the Okhotsk Sea: Geochemical, lithological and paleontological evidence, *Palaeogeography Palaeoclimatology Palaeoecology*, *209*, 281-301.

Gorbarenko, S. A., I. A. Basov, M. P. Chekhovskaya, J. Southon, T. A. Khusid, and A. Artemova (2005), Orbital and millennium scale environmental changes in the southern Bering Sea during the last glacial-Holocene: Geochemical and paleontological evidence, *Deep-Sea Research Part II-Topical Studies in Oceanography*, *52*(16-18), 2174-2185, doi:10.1016/J.Dsr2.2005.08.005.

Greaves, M., N. Caillon, H. Rebaubier, G. Bartoli, S. Bohaty, I. Cacho, L. Clarke, M. Cooper, C. Daunt, M. Delaney, P. deMenocal, A. Dutton, S. Eggins, H. Elderfield, D. Garbe-Schoenberg, E. Goddard, D. Green, J. Groeneveld, D. Hastings, E. Hathorne, K. Kimoto, G. Klinkhammer, L. Labeyrie, D. W. Lea, T. Marchitto, M. A. Martinez-Boti, P. G. Mortyn, Y. Ni, D. Nuernberg, G. Paradis, L. Pena, T. Quinn, Y. Rosenthal, A. Russell, T. Sagawa, S. Sosdian, L. Stott, K. Tachikawa, E. Tappa, R. Thunell, and P. A. Wilson (2008), Interlaboratory comparison study of calibration standards for foraminiferal Mg/Ca thermometry, *Geochemistry Geophysics Geosystems*, *9*(8), Q08010, doi:10.1029/2008GC001974.

Groeneveld, J., D. Nürnberg, R. Tiedemann, G.-J. Reichart, S. Steph, L. Reuning, D. Crudeli, and P. Mason (2008), Foraminiferal Mg/Ca increase in the Caribbean during the Pliocene: Western Atlantic Warm Pool formation, salinity influence, or diagenetic overprint?, *Geochemistry Geophysics Geosystems*, *9*(1), Q01P23, doi:10.1029/2006GC001564.

Grootes, P. M., M. Stuiver, J. W. C. White, S. Johnsen, and J. Jouzel (1993), Comparison of Oxygen-Isotope Records from the Gisp2 and Grip Greenland Ice Cores, *Nature*, *366*(6455), 552-554.

Harada, N., K. H. Shin, A. Murata, M. Uchida, and T. Nakatani (2003), Characteristics of alkenones synthesized by a bloom of Emiliania huxleyi in the Bering Sea, *Geochimica Et Cosmochimica Acta*, *67*(8), 1507-1519, doi:10.1016/S0016-7037(02)01318-2.

Harada, N., M. Sato, A. Shiraishi, and M. C. Honda (2006a), Characteristics of alkenone distributions in suspended and sinking particles in the northwestern North Pacific, *Geochimica Et Cosmochimica Acta*, *70*(8), 2045-2062, doi:10.1016/j.gca.2006.01.024.

Harada, N., N. Ahagon, T. Sakamoto, M. Uchida, M. Ikehara, and Y. Shibata (2006b), Rapid fluctuation of alkenone temperature in the southwestern Okhotsk Sea during the past 120 ky, *Global and Planetary Change*, *53*(1-2), 29-46, doi:10.1016/J.Gloplacha.2006.01.010.

Harada, N., M. Sato, and T. Sakamoto (2008), Freshwater impacts recorded in tetraunsaturated alkenones and alkenone sea surface temperatures from the Okhotsk Sea across millennial-scale cycles, *Paleoceanography*, *23*(3), doi:10.1029/2006pa001410.

Harada, N., M. Sato, O. Seki, A. Timmermann, H. Moossen, J. Bendle, Y. Nakamura, K. Kimoto, Y. Okazaki, K. Nagashima, S. A. Gorbarenko, A. Ijiiri, T. Nakatsuka, L. Menviel, M. O. Chikamoto, A. Abe-Ouchi, and S. Schouten (2012), Sea Surface temperature changes in the Okhotsk Sea and adjacent North Pacific during the last glacial maximum and deglaciation, *Deep-Sea Research Part II-Topical Studies in Oceanography*, (61- 64), 93-105.

Haug, G. H., D. M. Sigman, R. Tiedemann, T. F. Pedersen, and M. Sarnthein (1999), Onset of permanent stratification in the subarctic Pacific Ocean, *Nature*, *401*(6755), 779-782,

Haug, G.H., A. Ganopolski, D. M. Sigman, A. Rosell-Mele, G. E. A. Swann, R. Tiedemann, S. L. Jaccard, J. Bollmann, M. A. Maslin, M. J. Leng, and G. Eglinton (2005), North Pacific seasonality and the glaciation of North America 2.7 million years ago, *Nature*, *433*, 821-825.

Healy-Williams, N. (1992), Stable isotope differences among morphotypes of *Neogloboquadrina pachyderma* (Ehrenberg): implications for high-latitude palaeoceanographic studies, *Terra Nova*, *4*, 693-700.

Hendy, I. L., J. P. Kennett, E. B. Roark, and B. L. Ingram (2002), Apparent synchroneity of submillennial scale climate events between Greenland and Santa Barbara Basin, California from 30-10 ka, *Quaternary Science Reviews*, *21*(10), 1167-1184.

Herguera, J. C. (1992), Evidence for a bathyal front at 2000-m depth in the glacial Pacific, based on a depth transect on Ontong Java Plateau, *Paleoceanography*, *7*(3), 273-288.

Herguera, J. C., T. Herbert, M. Kashgarian, and C. Charles (2010), Intermediate and deep water mass distribution in the Pacific during the Last Glacial Maximum inferred from oxygen and carbon stable isotopes, *Quaternary Science Reviews*, *29*(9-10), 1228-1245, doi:10.1016/J.Quascirev.2010.02.009.

Honda, M. C., K. Imai, Y. Nojiri, F. Hoshi, T. Sugawara, and M. Kusakabe (2002), The biological pump in the northwestern North Pacific based on fluxes and major components of particulate matter obtained by sediment-trap experiments (1997-2000), *Deep-Sea Research Part II-Topical Studies in Oceanography*, *49*(24-25), 5595-5625.

Horikawa, K., Y. Asahara, K. Yamamoto, and Y. Okazaki (2010), Intermediate water formation in the Bering Sea during glacial periods: Evidence from neodymium isotope ratios, *Geology*, *38*(5), 435-438, doi:10.1130/G30225.1.

Hoshiba, M., N. Ahagon, K. Ohkushi, M. Uchida, I. Motoyama, and A. Nishimura (2006), Foraminiferal oxygen and carbon isotopes during the last 34 kyr off northern Japan, northwestern Pacific, *Marine Micropaleontology*, *61*(4), 196-208. doi:10.1016/J.Marmicro.2006.07.001.

Hu, A. X., G. A. Meehl, B. L. Otto-Bliesner, C. Waelbroeck, W. Q. Han, M. F. Loutre, K. Lambeck, J. X. Mitrovica, and N. Rosenbloom (2010), Influence of Bering Strait flow and North Atlantic circulation on glacial sea-level changes, *Nature Geoscience*, *3*(2), 118-121, doi:10.1038/Ngeo729.

Huang, R. X., M. A. Cane, N. Naik, and P. Goodman (2000), Global adjustment of the thermocline in response to deepwater formation, *Geophysical Research Letters*, *27*(6), 759-762.

Hut, G. (1987), Consultants group meeting on stable isotope reference samples for geochemical and hydrological investigations, *Report to the Director General, International Atomic Energy Agency*, Vienna, 42 pp.

Ikehara, K., K. Ohkushi, A. Shibahara, and M. Hoshiba (2006), Change of bottom water conditions at intermediate depths of the Oyashio region, NW Pacific over the past 20,000 yrs, *Global and Planetary Change*, *53*(1-2), 78-91, doi:10.1016/J.Gloplacha.2006.01.011.

Jaccard, S. L., G. H. Haug, D. M. Sigman, T. F. Pedersen, H. R. Thierstein, and U. Rohl (2005), Glacial/interglacial changes in subarctic North Pacific stratification, *Science*, *308*(5724), 1003-1006, doi:10.1126/Science.1108696.

Jaccard, S. L., E. D. Galbraith, D. M. Sigman, G. H. Haug, R. Francois, T. F. Pedersen, P. Dulski, and H. R. Thierstein (2009), Subarctic Pacific evidence for a glacial deepening of the oceanic respired carbon pool, *Earth and Planetary Science Letters*, *277*(1-2), 156-165, doi:10.1016/J.Epsl.2008.10.017.

Jansen, H., R. E. Zeebe, and D. A. Wolf-Gladrow, (2002), Modeling the dissolution of settling $CaCO_3$ in the ocean, *Global Biogeochemical Cycles* , *16*(2), 1027, doi:10.1029/2000GB001279.

Katsuki, K., and K. Takahashi (2005), Diatoms as paleoenvironmental proxies for seasonal productivity, sea-ice and surface circulation in the Bering Sea during the late Quaternary, *Deep-Sea Res. Part II-Topical Studies in Oceanography*, *52*(16-18), 2110-2130, doi:10.1016/J.Dsr2.2005.07.001.

Katsuki, K., B. K. Khim, T. Itaki, N. Harada, H. Sakai, T. Ikeda, K. Takahashi, Y. Okazaki, and H. Asahi (2009), Land-sea linkage of Holocene paleoclimate on the Southern Bering Continental Shelf, *Holocene*, *19*(5), 747-756. doi:10.1177/0959683609105298.

Kaufman, D.S., T. A. Ager, N. J. Anderson, P. M. Anderson, J. T. Andrews, P. J. Bartlein, L. B. Brubaker, L. L. Coats, L. C. Cwynar, M. L. Duvall, A. S. Dyke, M. E. Edwards, W. R. Eisner, K. Gajewski, A. Geirsdóttir, F. S. Hu, A. E. Jennings, M. R. Kaplan, M. W. Kerwin, A. V. Lozhkin, G. M. MacDonald, G. H. Miller, C. J. Mock, W. W. Oswald, B. L. Otto-Bliesner, D. F. Porinchu, K. Rühland, J. P. Smol, E. J. Steig, and B. B. Wolfe (2004), Holocene thermal maximum in the western Arctic (0-180°W), *Quaternary Science Reviews*, *23*, 529-560.

Keigwin, L. D. (1987), North Pacific Deep-Water Formation during the Latest Glaciation, *Nature*, *330*(6146), 362-364.

Keigwin, L. D., G. A. Jones, and P. N. Froelich (1992), A 15,000 Year Paleoenvironmental Record from Meiji Seamount, Far Northwestern Pacific, *Earth and Planetary Science Letters*, *111*(2-4), 425-440.

Keigwin, L. D. (1998), Glacial-age hydrography of the far northwest Pacific Ocean, *Paleoceanography*, *13*(4), 323-339.

Keigwin, L. D. (2002), Late Pleistocene-Holocene paleoceanography and ventilation of the Gulf of California, *Journal of Oceanography*, *58*(2), 421-432.

Keigwin, L.D., J. P. Donnelly, M. S. Cook, N. W. Driscoll, and J. Brigham-Grette (2006), Rapid sea-level rise and Holocene climate in the Chukchi Sea, *Geology*, *34*(10), 861-864, doi:10.1130/G22712.1.

Kennett, J. P., K. G. Cannariato, I. L. Hendy, and R.J. Behl (2000), Carbon isotopic evidence for methane hydrate instability during Quaternary interstadials, *Science*, *288*, 128-133.

Kiefer, T., M. Sarnthein, H. Erlenkeuser, P. M. Grootes, and A. P. Roberts (2001), North Pacific response to millennial-scale changes in ocean circulation over the last 60 kyr, *Paleoceanography*, *16*(2), 179-189.

Kiefer, T., and M. Kienast (2005), Patterns of deglacial warming in the Pacific Ocean: a review with emphasis on the time interval of Heinrich event 1, *Quaternary Science Reviews*, *24*(7-9), 1063-1081.

Kiefer, T. (2010), When still waters ran deep, *Science*, *329*, 290-291.

Kienast, S. S., and J. L. McKay (2001), Sea surface temperatures in the subarctic Northeast Pacific reflect millennial-scale climate oscillations during the last 16 kyrs, *Geophysical Research Letters*, *28*(8), 1563-1566.

Kim, J. H., N. Rimbu, S. J. Lorenz, G. Lohmann, S. I. Nam, S. Schouten, C. Ruhlemann, and R. R. Schneider (2004), North Pacific and North Atlantic sea-surface temperature variability during the Holocene, *Quaternary Science Rev*iews, *23*(20-22), 2141-2154.

Kohfeld, K.E., R. G. Fairbanks, S. L. Smith, and I. D. Walsh (1996), *Neogloboquadrina pachyderma* (sinistral coiling) as paleoceanographic tracers in polar oceans: Evidence from Northeast Water Polynya plankton tows, sediment traps, and surface sediments, *Paleoceanography*, *11*(6), 679-699.

Kotilainen, A. T., and N. J. Shackleton (1995), Rapid Climate Variability in the North Pacific-Ocean during the Past 95,000 Years, *Nature*, *377*(6547), 323-326.

Kowalik, Z., J. L. Luick, and T. C. Royer (1994), On the dynamics of the Alaska Coastal Current, *Continental Shelf Research*, *14*(7/8), 831-845.

Kozdon, R., A. Eisenhauer, M. Weinelt, M. Y. Meland, and D. Nürnberg (2009), *Geochemistry Geophysics Geosystems*, *10*(3), Q03005, doi:10.1029/2008GC002169.

Krebs, U., and A. Timmermann (2007), Tropical air-sea interactions accelerate the recovery of the Atlantic Meridional Overturning Circulation after a major shutdown, *Journal of Climate*, *20*(19), 4940-4956, doi:10.1175/Jcli4296.1.

Kroopnick, P. M. (1985), The Distribution of C-13 of Sigma-CO2 in the World Oceans, *Deep-Sea Research Part a-Oceanographic Research Papers*, *32*(1), 57-84.

Kuroyanagi, A., and H. Kawahata (2004), Vertical distribution of living planktonic foraminifera in the seas around Japan, *Marine Micropaleontology*, *53*, 173-196.

Kuzmin, Y. V., G. S. Burr, and A. J. T. Jull (2001), Radiocarbon reservoir correction ages in the Peter the Great Gulf, Sea of Japan, and eastern coast of the Kunashir, southern Kuriles (northwestern Pacific), *Radiocarbon*, *43*(2A), 477-481.

Kuzmin, Y. V., G. S. Burr, S. V. Gorbunov, V. A. Rakov, and N. G. Razjigaeva (2007), A Tale of Two Seas: Reservoir Age Correction Values (R, Delta R) for the Sakhalin Island (Sea of Japan and Okhotsk Sea), *Nuclear Instruments & Methods in Physics Research Section B-Beam Interactions with Materials and Atoms*, *259*(1), 460–462. doi:10.1016/j.nimb.2007.01.308.

Laskar, J., P. Robutel, F. Joutel, M. Gastineau, A. C. M. Correia, and B. Levrard (2004), A long-term numerical solution for the insolation quantities of the Earth, *Astronomy and Astrophysics, 428(1*), 261-285, doi:10.1051/0004-6361:20041335.

Le, J., and N. J. Shackleton (1992), Carbonate dissolution fluctuations in the western equatorial Pacific during the late Quaternary, *Paleoceanography*, 7(1), 21-42.

Lea, D.W., D. K. Pak, and H. J. Spero (2000), Climate impact of Late Quaternary equatorial Pacific sea surface temperature variations, *Science*, *289*, 1719-1724.

Leduc, G., R. Schneider, J.-H. Kim, and G. Lohmann (2010), Holocene and Eemian sea surface temperature trends as revealed by alkenone and Mg/Ca paleothermometry, *Quaternary Science Reviews*, *29*, 989-1004.

Lisiecki, L. E., and M. E. Raymo (2005), A Pliocene-Pleistocene stack of 57 globally distributed benthic delta O-18 records (vol 20, art no PA1003, 2005), *Paleoceanography*, *20*(2), doi:10.1029/2005pa001164.

Locarnini, R.A., A. V. Mishonov, J. I. Antonov, T. P. Boyer, and H. E. Garcia (2010), World Ocean Atlas 2009, Volume 1: Temperature, *In* Levitus, S. (Ed.), *NOAA Atlas NESDIS 68, U.S. Government Printing Office*, Washington, D.C., 184 pp.

Lund, D. C., and A. C. Mix (1998), Millennial-scale deep water oscillations: Reflections of the North Atlantic in the deep Pacific from 10 to 60 ka, *Paleoceanography*, *13*(1), 10-19.

Lund, D. C., A. C. Mix, and J. Southon (2011), Increased ventilation age of the deep northeast Pacific Ocean during the last deglaciation, *Nature Geoscience*, *4*(11), 771-774, doi:10.1038/Ngeo1272.

Lutze, G. F., and H. Tiel (1989), Epibenthic foraminifera from elevated microhabitats: Cibicidoides wuellerstorfi and Planulina ariminensis, *Journal of Foraminiferal Research*, *19*, 153–158.

Mackensen, A., H. W. Hubberten, T. Bickert, G. Fischer, and D. K. Futterer (1993), The Delta-C-13 in Benthic Foraminiferal Tests of Fontbotia-Wuellerstorfi (Schwager) Relative to the Delta-C-13 of Dissolved Inorganic Carbon in Southern-Ocean Deep-Water - Implications for Glacial Ocean Circulation Models, *Paleoceanography*, *8*(5), 587-610.

Mackensen, A., S. Schumacher, J. Radke, and D.N. Schmidt (2000), Microhabitat Preferences and Stable Carbon Isotopes of Endobenthic Foraminifera: Clue to Quantitative Reconstruction of Oceanic New Production, *Marine Micropaleontology*, *40*(3), 233–258.

Manabe, S., and R. J. Stouffer (1988), Two stable equilibria of a coupled ocean-atmosphere model, *Journal of Climate*, *1*, 841-866.

Mantua, N. J., S. R. Hare, Y. Zhang, J. M. Wallace, and R. C. Francis (1997), A Pacific interdecadal climate oscillation with impacts on salmon production, *Bulletin of the American Meteorological Society*, *78*(6), 1069-1079.

Marchal, O., I. Cacho, T. F. Stocker, J. O. Grimalt, E. Calvo, B. Martrat, N. Shackleton, M. Vautravers, E. Cortijo, S. van Kreveld, C. Andersson, N. Koc, M. Chapman, L. Sbaffi, J. C. Duplessy, M. Sarnthein, J. L. Turon, J. Duprat, and E. Jansen (2002), Apparent long-term cooling of the sea surface in the northeast Atlantic and Mediterranean during the Holocene, *Quaternary Science Reviews*, *21*(4-6), 455-483.

Marchitto, T. M., S. J. Lehman, J. D. Ortiz, J. Fluckiger, and A. van Geen (2007), Marine radiocarbon evidence for the mechanism of deglacial atmospheric CO(2) rise, *Science*, *316*(5830), 1456-1459, doi:10.1126/Science.1138679.

Mashiotta, T.A., D. W. Lea, and H. J. Spero (1999), Glacial—interglacial changes in Subantarctic sea surface temperature and d^{18}O-water using foraminiferal Mg, *Earth and Planetary Science Letters*, *170*, 417-432.

Matsumoto, K., T. Oba, J. Lynch-Stieglitz, and H. Yamamoto (2002), Interior hydrography and circulation of the glacial Pacific Ocean, *Quaternary Science Reviews*, *21*(14-15), 1693-1704.

Max, L., J. R. Riethdorf, R. Tiedemann, M. Smirnova, L. Lembke-Jene, K. Fahl, D. Nürnberg, A. Matul, and G. Mollenhauer (in review), Sea surface temperature variability and sea-ice extent in the subarctic Northwest Pacific during the past 15.000 years, *Paleoceanography*.

McManus, J. F., R. Francois, J. M. Gherardi, L. D. Keigwin, and S. Brown-Leger (2004), Collapse and rapid resumption of Atlantic meridional circulation linked to deglacial climate changes, *Nature*, *428*(6985), 834-837, doi:10.1038/Nature02494.

McNeely, R., A. S. Dyke, and J. R. Southon (2006), Canadian marine reservoir ages, preliminary data assessment, *Geological Survey Canada*, 3 pp.

Meheust, M., R. Stein, and K. Fahl (2012), Deglacial-Holocene variability of sea ice and surface water temperature in the Bering Sea: Reconstruction based on IP25 and alkenone data, in *Geophysical Research Abstracts*, EGU General Assembly, Vienna 22-27 April, Abstract EGU2012-3319-3.

Menviel, L., A. Timmermann, O. Elison Timm, A. Mouchet, A. Abe-Ouchi, M. O. Chikamoto, N. Harada, R. Ohgaito, and Y. Okazaki (2012), Removing the North Pacific halocline: Effects on global climate, ocean circulation and the carbon cycle, *Deep-Sea Research Part II-Topical Studies in Oceanography*, 61-64, 106-113.

Mikolajewicz, U., T. J. Crowley, A. Schiller, and R. Voss (1997), Modelling teleconnections between the North Atlantic and North Pacific during the Younger Dryas, *Nature*, *387*(6631), 384-387.

Millo, C., M. Sarnthein, H. Erlenkeuser, and T. Frederichs (2005a), Methane-driven late Pleistocene $d^{13}C$ minima and overflow reversals in the southwestern Greenland Sea, *Geology*, *33*(11), 873-876.

Millo, C., M. Sarnthein, H. Erlenkeuser, P. M. Grootes, and N. Andersen (2005b), Methane-induced early diagenesis of foraminiferal tests in the southwestern Greenland Sea, *Marine Micropaleontology*, *58*, 1-12.

Minoshima, K., H. Kawahata, T. Irino, K. Ikehara, K. Aoki, M. Uchida, M. Yoneda, and Y. Shibata (2007), Deep water ventilation in the northwestern North Pacific during the last deglaciation and the early Holocene (15-5 cal. kyr BP) based on AMS C-14 dating, *Nuclear Instruments & Methods in Physics Research Section B-Beam Interactions with Materials and Atoms*, *259*(1), 448-452, doi:10.1016/J.Nimb.2007.01.225.

Minoshima, K., H. Kawahata, and K. Ikehara (2007), Changes in biological production in the mixed water region (MWR) of the northwestern North Pacific during the last 27 kyr, *Palaeogeography Palaeoclimatology Palaeoecology*, *254*(3-4), 430-447, doi:10.1016/J.Palaeo.2007.06.022.

Miura, T., T. Suga, and K. Hanawa (2002), Winter mixed layer and formation of dichothermal water in the Bering Sea, *Journal of Oceanography*, *58*, 815-823.

Mix, A. C., N. G. Pisias, R. Zahn, W. Rugh, C. Lopez, and K. Nelson (1991), Carbon 13 in Pacific deep and intermediate waters, 0-370 ka: Implications for ocean circulation and Pleistocene CO2, *Paleoceanography*, *6*(2), 205-226.

Mix, A. C., D. C. Lund, N. G. Pisias, P. Bodèn, L. Bornmalm, M. Lyle, and J. Pike (1999), Rapid Climate Oscillations in the Northeast Pacific During the Last Deglaciation Reflect Northern and Southern Hemisphere Sources, *Geophysical Monograph*, *112*, 21.

Mohiuddin, M.M., A. Nishimura, and Y. Tanaka (2005), Seasonal succession, vertical distribution, and dissolution of planktonic foraminifera along the Subarctic Front: Implications for paleoceanographic reconstruction in the northwestern Pacific, *Marine Micropaleontology*, *55*, 129-156.

Müller, P. J., and R. Schneider (1993), An Automated Leaching Method for the Determination of Opal in Sediments and Particulate Matter, *Deep-Sea Research Part I*, *40*(3), 425-444.

Müller, P. J., G. Kirst, G. Ruhland, I. von Storch, and A. Rosell-Mele (1998), Calibration of the alkenone paleotemperature index $U^{k'}_{37}$ based on core-tops from the eastern South Atlantic and the global ocean (60 degrees N-60 degrees S), *Geochimica Et Cosmochimica Acta*, *62*(10), 1757-1772.

Müller, J., G. Masse, R. Stein, and S. T. Belt (2009), Variability of sea-ice conditions in the Fram Strait over the past 30,000 years, *Nature Geoscience*, *2*(11), 772-776, doi:10.1038/Ngeo665.

Müller, J., A. Wagner, K. Fahl, R. Stein, M. Prange, and G. Lohmann (2011), Towards quantitative sea ice reconstructions in the northern North Atlantic: A combined biomarker and numerical modelling approach, *Earth and Planetary Science Letters*, *306*(3-4), 137-148. doi:10.1016/J.Epsl.2011.04.011.

Mulitza, S., D. Boltovskoy, B. Donner, H. Meggers, A. Paul, and G. Wefer (2003), Temperature: $\delta^{18}O$ relationships of planktonic foraminifera collected from surface waters, *Palaeogeography, Palaeoclimatology, Palaeoecology*, *202*, 143-152.

Murayama, M., A. Taira, H. Iwakura, E. Matsumoto, and T. Nakamura (1992), Northwest Pacific deep water ventilation rate during the past 35,000 years with the AMS 14C foraminifera ages, *Summaries of Researchers Using AMS at Nagoya University* (Nagoya University Center for Chronological Research), Nagoya, Japan (in Japanese with english abstract), *3*, 114-121.

Niebauer, H. J. (1988), Effect of El Nino Southern Oscillation and North Pacific Weather Patterns on Interannual Variability in the Subarctic Bering Sea, *Journal of Geophysical Research-Oceans*, *93*(C5), 5051-5068.

Niebauer, H. J. (1998), Variability in Bering Sea ice cover as affected by a regime shift in the North Pacific in the period 1947-1996, *Journal of Geophysical Research-Oceans*, *103*(C12), 27717-27737.

Niebauer, H.J., N. A. Bond, L. P. Yakunin, and V. V. Plotnikov (1999), An update on the climatology and sea ice of the Bering Sea. In: Loughlin, T.R., and K. Ohtani (Eds.), Dynamics of the Bering Sea, *University of Alaska Sea Grant*, pp. 29-59.

North Greenland Ice Core Project members (2004), High-resolution record of northern hemisphere climate extending into the last interglacial period. *Nature*, *431*, 147-151.

Nürnberg, D. (1995), Magnesium in tests of *Neogloboquadrina pachyderma* sinistral from high northern and southern latitudes, *Journal of Foraminiferal Research*, *25*(4), 350-368.

Nürnberg, D., J. Bijma, and C. Hemleben (1996), Assessing the reliability of magnesium in foraminiferal calcite as a proxy for water mass temperatures, *Geochimica et Cosmochimica Acta*, *60*(5), 803-814.

Nürnberg, D., and R. Tiedemann (2004), Environmental change in the Sea of Okhotsk during the last 1.1 million years, *Paleoceanography*, *19*(4), 1-23, doi:10.1029/2004pa001023.

Ohkouchi, N., H. Kawahata, M. Murayama, M. Okada, T. Nakamura, and A. Taira (1994), Was Deep-Water Formed in the North Pacific during the Late Quaternary - Cadmium Evidence from the Northwest Pacific, *Earth and Planetary Science Letters*, *124*(1-4), 185-194.

O'Neil, J.R., R. N. Clayton, and T. K. Mayeda (1969), Oxygen isotope fractionation in divalent metal carbonates, *Journal of Chemical Physics*, *51*(12), 5547-5558.

Ohkushi, K., M. Uchida, N. Ahagon, T. Mishima, and T. Kanematsu (2004), Glacial intermediate water ventilation in the northwestern Pacific based on AMS radiocarbon dating, *Nuclear Instruments and Methods in Physics Research B*, 223-224, 460-465.

Ohtani, K., Y. Akiba, and A. Y. Takenouti (1972), Formation of western subarctic water in the Bering Sea In: *Biological oceanography of the northern North Pacific Ocean, Idemitsu Shoten Publ. Co*, edited by A. Y. Takenouti, pp. 32-44.

Okazaki, Y., K. Takahashi, K. Katsuki, A. Ono, J. Hori, T. Sakamoto, M. Uchida, Y. Shibata, M. Ikehara, and K. Aoki (2005), Late Quaternary paleoceanographic changes in the southwestern Okhotsk Sea: Evidence from geochemical, radiolarian, and diatom records, *Deep-Sea Research PartII-Topical Studies Oceanography*, *52*(16-18), 2332-2350, doi:10.1016/j.dsr2.2005.07.007.

Okazaki, Y., A. Timmermann, L. Menviel, N. Harada, A. Abe-Ouchi, M. O. Chikamoto, A. Mouchet, and H. Asahi (2010), Deepwater Formation in the North Pacific During the Last Glacial Termination, *Science*, *329*(5988), 200-204, doi:10.1126/Science.1190612.

Okumura, Y. M., C. Deser, A. Hu, A. Timmermann, and S. P. Xie (2009), North Pacific Climate Response to Freshwater Forcing in the Subarctic North Atlantic: Oceanic and Atmospheric Pathways, *Journal of Climate*, *22*(6), 1424-1445, doi:10.1175/2008jcli2511.1.

Overland, J. E., N. A. Bond, and J. M. Adams (2002), The relation of surface forcing of the Bering Sea to large-scale climate patterns, *Deep-Sea Research Part II-Topical Studies in Oceanograohy*, *49*(26), 5855-5868.

Pierrot, D., E. Lewis, and D. W. R. Wallace (2006), MS Excel program developed for CO2 system calculations. ORNL/CDIAC-105a. *Carbon Dioxide Information Analysis Center, Oak Ridge National Laboratory, U.S. Department of Energy*, Oak Ridge, Tennessee, doi:10.3334/CDIAC/otg.CO2SYS_XLS_CDIAC105a.

Pisias, N. G., A. C. Mix, and L. Heusser (2001), Millennial scale climate variability of the northeast Pacific Ocean and northwest North America based on radiolaria and pollen, *Quaternary Science Reviews*, *20*(14), 1561-1576.

Prahl, F. G., and S. G. Wakeham (1987), Calibration of Unsaturation Patterns in Long-Chain Ketone Compositions for Paleotemperature Assessment, *Nature*, *330*(6146), 367-369.

Prahl, F.G., L. Muehlhausen, and D. L. Zahnle (1998), Further evaluation of long-chain alkenones as indicators of paleoceanographic conditions, *Geochimica et Cosmochimica Acta*, *52*, 2303-2310.

Rahmstorf, S. (1995), Bifurcations of the Atlantic Thermohaline Circulation in Response to Changes in the Hydrological Cycle, *Nature*, *378*(6553), 145-149.

Rasmussen, S. O., K. K. Andersen, A. M. Svensson, J. P. Steffensen, B. M. Vinther, H. B. Clausen, M. L. Siggaard-Andersen, S. J. Johnsen, L. B. Larsen, D. Dahl-Jensen, M. Bigler, R. Rothlisberger, H. Fischer, K. Goto-Azuma, M. E. Hansson, and U. Ruth (2006), A new Greenland ice core chronology for the last glacial termination, *Journal of Geophysical Research-Atmospheres*, *111*(D6), doi:10.1029/2005jd006079.

Reimer, P. J., M. G. L. Baillie, E. Bard, A. Bayliss, J. W. Beck, P. G. Blackwell, C. B. Ramsey, C. E. Buck, G. S. Burr, R. L. Edwards, M. Friedrich, P. M. Grootes, T. P. Guilderson, I. Hajdas, T. J. Heaton, A. G. Hogg, K. A. Hughen, K. F. Kaiser, B. Kromer, F. G. McCormac, S. W. Manning, R. W. Reimer, D. A. Richards, J. R. Southon, S. Talamo, C. S. M. Turney, J. van der Plicht, and C. E. Weyhenmeye (2009), Intcal09 and Marine09 Radiocarbon Age Calibration Curves, 0-50,000 Years Cal Bp, *Radiocarbon*, *51*(4), 1111-1150.

Regenberg, M., D. Nürnberg, S. Steph, J. Groeneveld, D. Garbe-Schönberg, R. Tiedemann, and W.-C. Dullo (2006), Assessing the effect of dissolution on planktonic foraminiferal Mg/Ca ratios: Evidence from Caribbean core tops, *Geochemistry Geophysics Geosystems*, *7*(7), Q07P15, doi:10.1029/2005GC001019.

Richter, T., S. van der Gaast, B. Koster, A. Vaars, R. Gieles, H. de Stigter, H. De Haas, and T. van Weering (2006), The Avaatech XRF core scanner: technical description and applications to NE Atlantic sediments, *Geological Society Special Publication*, *267*, 39-50.

Rosenthal, Y., G. P. Lohmann, K. C. Lohmann, and R. M. Sherrell (2000), Incorporation and preservation of Mg in *Globigerinoides sacculifer*: Implications for reconstructing the temperature and $^{18}O/^{16}O$ of seawater, *Paleoceanography*, *15*(1), 135-145.

Rosenthal, Y., S. Perron-Cashman, C. H. Lear, E. Bard, S. Barker, K. Billups, M. Bryan, M. L. Delaney, P. B. deMenocal, G. S. Dwyer, H. Elderfield, C. R. German, M. Greaves, D. W. Lea, T. M. Marchitto Jr., D. K. Pak, G. L. Paradis, A. D. Russell, R. R. Schneider, K. Scheiderich, L. Stott, K. Tachikawa, E. Tappa, R. Thunell, M. Wara, S. Weldeab, and P. A. Wilson (2004), Interlaboratory comparison study of Mg/Ca and Sr/Ca measurements in planktonic foraminifera for paleoceanographic research, *Geochemistry Geophysics Geosystems*, *5*(4), Q04D09, doi:10.1029/2003GC000650.

Roy, R.N., L. N. Roy, K. M. Vogel, C. Porter-Moore, T. Pearson, C. E. Good, F. J. Millero, and D. M. Campbell (1993), The dissociation constants of carbonic acid in seawater at salinities 5 to 45 and temperatures 0 to 45 C, *Marine Physical Chemistry*, *44*(2-4), 249-267.

Saenko, O. A., A. Schmittner, and A. J. Weaver (2004), The Atlantic-Pacific seesaw, *Journal of Climate*, *17*(11), 2033-2038.

Sagawa, T., and K. Ikehara (2008), Intermediate water ventilation change in the subarctic northwest Pacific during the last deglaciation, *Geophysical Research Letters*, *35*(24), doi:10.1029/2008gl035133.

Sakamoto, T., M. Ikehara, M. Uchida, K. Aoki, Y. Shibata, T. Kanamatsu, N. Harada, K. Iijima, K. Katsuki, H. Asahi, K. Takahashi, H. Sakai, and H. Kawahata (2006), Millennial-scale variations of sea-ice expansion in the southwestern part of the Okhotsk Sea during the past 120 kyr: Age model and ice-rafted debris in IMAGES Core MD01-2412, *Global and Planetary Change*, *53*(1-2), 58-77, doi:10.1016/J.Gloplacha.2006.01.012.

Sancetta, C. (1983), Effect of Pleistocene Glaciation Upon Oceanographic Characteristics of the North Pacific-Ocean and Bering Sea, *Deep-Sea Research Part a-Oceanographic Research Papers*, *30*(8), 851-869.

Sancetta, C., and S. W. Robinson (1983), Diatom Evidence on Wisconsin and Holocene Events in the Bering Sea, *Quaternary Research*, *20*(2), 232-245.

Sancetta, C. (1992), Primary Production in the Glacial North-Atlantic and North Pacific Oceans, *Nature*, *360*(6401), 249-251.

Sarmiento, J. L., N. Gruber, M. A. Brzezinski, and J. P. Dunne (2004), High-latitude controls of thermocline nutrients and low latitude biological productivity, *Nature*, *427*(6969), 56-60, doi:10.1038/Nature02127.

Sarnthein, M., H. Gebhardt, T. Kiefer, M. Kucera, M. Cook, and H. Erlenkeuser (2004), Mid Holocene origin of the sea-surface salinity low in the subarctic North Pacific, *Quaternary Science Reviews*, *23*(20-22), 2089-2099.

Sarnthein, M., T. Kiefer, P. M. Grootes, H. Elderfield, and H. Erlenkeuser (2006), Warmings in the far northwestern Pacific promoted pre-Clovis immigration to America during Heinrich event 1, *Geology*, *34*(3), 141-144, doi:10.1130/G22200.1.

Sarnthein, M., P. M. Grootes, J. P. Kennett, and M.-J. Nadeau (2007), 14C Reservoir ages show deglacial changes in ocean currents and carbon cycle, *Past and Future Changes of the Oceanic Meridional Overturning Circulation: Mechanism and Impacts, AGU Monogr. Ser.*, *173*, 175-196.

Sawada, K., and N. Handa (1998), Variability of the path of the Kuroshio ocean current over the past 25,000 years, *Nature*, *392*, 592-595.

Schlitzer, R. (2011). Ocean Data View (ODV): Bremerhaven, Germany, available online from: http://odv.awi.de/

Schmidt, M.W., H. J. Spero, and D. W. Lea (2004), Links between salinity variation in the Caribbean and North Atlantic thermohaline circulation, *Nature*, *428*, 160-163.

Schmittner, A., O. A. Saenko, and A. J. Weaver (2003), Coupling of the hemispheres in observations and simulations of glacial climate change, *Quaternary Science Reviews*, *22*, 659-671.

Schmittner, A., E. D. Galbraith, S. W. Hostetler, T. F. Pedersen, and R. Zhang (2007), Large fluctuations of dissolved oxygen in the Indian and Pacific oceans during Dansgaard- Oeschger oscillations caused by variations of North Atlantic Deep Water subduction, *Paleoceanography, 22(3)*, doi:10.1029/2006pa001384.

Schweizer, M., J. Pawlowski, T. Kouwenhoven, and B. van der Zwaan (2009), Molecular Phylogeny of Common Cibicidids and Related Rotaliida (Foraminifera) Based on Small Subunit Rdna Sequences, *Journal of Foraminiferal Research*, *39*(4), 300-315.

Seki, O., R. Ishiwatari, and K. Matsumoto (2002), Millennial climate oscillations in NE Pacific surface waters, *Geophysical Research Letters*, *29*(23), doi:10.1029/2002gl015200.

Seki, O., K. Kawamura, M. Ikehara, T. Nakatsuka, and T. Oba (2004a), Variation of alkenone sea surface temperature in the Sea of Okhotsk over the last 85 kyrs, *Organic Geochemistry*, *35*(3), 347-354, doi:10.1016/J.Orggeochem.2003.10.011.

Seki, O., M. Ikehara, K. Kawamura, T. Nakatsuka, K. Ohnishi, M. Wakatsuchi, H. Narita, and T. Sakamoto (2004b), Reconstruction of paleoproductivity in the Sea of Okhotsk over the last 30 kyr, *Paleoceanography*, *19*(1), doi:10.1029/2002pa000808.

Seki, O., T. Nakatsuka, K. Kawamura, S. I. Saitoh, and M. Wakatsuchi (2007), Time-series sediment trap record of alkenones from the western Sea of Okhotsk, *Marine Chemistry, 104*(3-4), 253-265, doi:10.1016/J.Marchem.2006.12.002.

Seki, O., T. Sakamoto, S. Sakai, S. Schouten, E. C. Hopmans, J. S. Sinninghe Damste, and R. D. Pancost (2009), Large changes in seasonal sea ice distribution and productivity in the Sea of Okhotsk during the deglaciations, *Geochemistry, Geophysics, Geosystems*, *10*(10), doi:10.1029/2009GC002613.

Shackleton, N.J. (1974), Attainment of isotopic equilibrium between ocean water and the benthonic foraminifera genus *Uvigerina*: Isotopic changes in the ocean during the last glacial, *Colloques Internationaux du C.N.R.S. 219 – Les Méthodes Quantitatives D'étude des Variations du Climat au Cours du Pléistocène*, 203-209.

Shcherbina, A. Y., L. D. Talley, and D. L. Rudnick (2003), Direct observations of North Pacific ventilation: Brine rejection in the Okhotsk Sea, *Science*, *302*(5652), 1952-1955.

Sigman, D.M., and E. A. Boyle (2000), Glacial/interglacial variations in atmospheric carbon dioxide, *Nature*, *407*, 859-869.

Sigman, D.M., and G. H. Haug (2003), The biological pump in the past. In: Elderfield, H. (Ed.), *Treatise on Geochemistry*, Vol. 6: The Oceans and Marine Geochemistry, Elsevier-Pergamon, pp. 491-528.

Sigman, D. M., S. L. Jaccard, and G. H. Haug (2004), Polar ocean stratification in a cold climate, *Nature*, *428*(6978), 59-63.

Sigman, D.M., M. P. Hain, and G. H. Haug (2010), The polar ocean and glacial cycles in atmospheric CO_2 concentration, *Nature*, *466*, 47-55.

Sikes, E. L., J. K. Volkman, L. G. Robertson, and J. J. Pichon (1997), Alkenones and alkenes in surface waters and sediments of the Southern Ocean: Implications for paleotemperature estimation in polar regions, *Geochimica Et Cosmochimica Acta*, *61*(7), 1495-1505.

Simstich, J., M. Sarnthein, and H. Erlenkeuser (2003), Paired $\delta^{18}O$ signals of *Neogloboquadrina pachyderma* (s) and *Turborotalia quinqueloba* show thermal stratification structure in Nordic Seas, *Marine Micropaleontology*, *48*, 107-125.

Southon, J. R., D. E. Nelson, and J. S. Vogel (1990), A record of past ocean-atmosphere radiocarbon differences from the Northeast Pacific, *Paleoceanography*, *5*(2), 10.

Stabeno, P. J., J. D. Schumacher, and K. Ohtani (1999), The Physical Oceanography of the Bering Sea, in *Dynamics of the Bering Sea*, edited by T. R. Loughlin and K. Ohtani, pp. 1-28, University of Alaska Grant, Fairbanks.

Stott, L. D., M. Neumann, and D. Hammond (2000), Intermediate water ventilation on the northeastern Pacific margin during the late Pleistocene inferred from benthic foraminiferal delta C-13, *Paleoceanography*, *15*(2), 161-169.

Stott, L., J. Southon, A. Timmermann, and A. Koutavas (2009), Radiocarbon age anomaly at intermediate water depth in the Pacific Ocean during the last deglaciation, *Paleoceanography*, *24*, Artn Pa2223, doi:10.1029/2008pa001690.

Stuiver, M., and H. A. Polach (1977), Reporting of C-14 Data - Discussion, *Radiocarbon*, *19*(3), 355-363.

Stuiver, M. (1980), Workshop on C-14 Data Reporting, *Radiocarbon*, *22*(3), 964-966.

Stuiver, M., and P. J. Reimer (1993), Extended C-14 Data-Base and Revised Calib 3.0 C-14 Age Calibration Program, *Radiocarbon*, *35*(1), 215-230.

Sun, Y. B., S. C. Clemens, C. Morrill, X. P. Lin, X. L. Wang, and Z. S. An (2012), Influence of Atlantic meridional overturning circulation on the East Asian winter monsoon, *Nature Geoscience*, *5*(1), 46-49, doi:10.1038/Ngeo1326.

Talley, L. D. (1993), Distribution and Formation of North Pacific Intermediate Water, *Journal of Physical Oceanography*, *23*(3), 517-537.

Talley, L. D. (2008), Freshwater transport estimates and the global overturning circulation: Shallow, deep and throughflow components, *Progress in Oceanography*, *78*(4), 257-303, doi:10.1016/J.Pocean.2008.05.001.

Takahashi, K., N. Fujitani, and M. Yanada (2002), Long term monitoring of particle fluxes in the Bering Sea and the central subarctic Pacific Ocean, 1990-2000, *Progress in Oceanography*, *55*, 95-112.

Tanaka, S., and K. Takahashi (2005), Late Quaternary paleoceanographic changes in the Bering Sea and the western subarctic Pacific based on radiolarian assemblages, *Deep-Sea Research Part II-Topical Studies in Oceanography*, *52*(16-18), 2131-2149, doi:10.1016/J.Dsr2.2005.07.002.

Ternois, Y., K. Kawamura, N. Ohkouchi, and L. Keigwin (2000), Alkenone sea surface temperature in the Okhotsk Sea for the last 15 kyr, *Geochemical Journal*, *34*(4), 283-293.

Timmermann, A., L. Menviel, Y. Okumura, A. Schilla, U. Merkel, O. Timm, A. X. Hu, B. Otto-Bliesner, and M. Schulz (2010), Towards a quantitative understanding of millennial-scale Antarctic warming events, *Quaternary Science Reviews*, *29*(1-2), 74-85, doi:10.1016/J.Quascirev.2009.06.021.

Tomczak, M., and J. S. Godfrey (1994), Regional Oceanography: An Introduction, *Pergamon*, 422 pp.

Tsuda A., S. Takeda, H. Saito, J. Nishioka, Y. Nojiri, I. Kudo, H. Kiyosawa, A. Shiomoto, K. Imai, T. Ono, A. Shimamoto, D. Tsumune, T. Yoshimura, T. Aono, A. Hinuma, M. Kinugasa, K. Suzuki, Y. Sohrin, Y. Noiri, H. Tani, Y. Deguchi, N. Tsurushima, H. Ogawa, K. Fukami, K. Kuma, and T. Saino (2003), A mesoscale iron enrichment in the western subarctic Pacific induces a large centric diatom bloom. *Science, 300*, 958-961, doi:10.1126/science.1082000.

Van Scoy, K. A., D. B. Olson, and R. A. Fine (1991), Ventilation of North Pacific Intermediate Waters - the Role of the Alaskan Gyre, *Journal of Geophysical Research-Oceans*, *96*(C9), 16801-16810.

Vellinga, M., and R. A. Wood (2002), Global climatic impacts of a collapse of the Atlantic thermohaline circulation, *Climatic Change*, *54*(3), 251-267.

Volkman, J. K., G. Eglinton, E. D. S. Corner, and T. E. V. Forsberg (1980), Long-chain alkenes and alkenones in the marine coccolithophorid Emiliania huxleyi, *Phytochemistry*, *19*(12), 2619-2622, doi:10.1016/S0031-9422(00)83930-8.

Waelbroek, C., L. Labeyrie, E. Michel, J. C. Duplessy, J. F. McMannus, K. Lambeck, E. Balbon, and M. Labracherie (2002), Sea-level and deep water temperature changes derived from benthic foraminifera isotopic records, *Quaternary Science Reviews*, *21*, 295-305.

Warren, B. A. (1983), Why Is No Deep-Water Formed in the North Pacific, *Journal of Marine Research*, *41*(2), 327-347.

Weingartner, T.J., S. L. Danielson, and T. C. Royer (2005), Freshwater variability and predictability in the Alaska Coastal Current, *Deep-Sea Research II*, *52*, 169-191.

Wu, L. X., C. Li, C. X. Yang, and S. P. Xie (2008), Global teleconnections in response to a shutdown of the Atlantic meridional overturning circulation, *Journal of Climate*, *21*(12), 3002-3019, doi:10.1175/2007jcli1858.1.

Yamamoto, M., N. Tanaka, and S. Tsunogai (2001), Okhotsk Sea intermediate water formation deduced from oxygen isotope systematics, *Journal of Geophysical Research*, *106*(C12), 31075-31084.

Yasuda, I. (1997), The origin of the North Pacific Intermediate Water, *Journal of Geophysical Research*, *102*(C1), 893-909.

Yin, J. J., and R. J. Stouffer (2007), Comparison of the stability of the Atlantic thermohaline circulation in two coupled atmosphere-ocean general circulation models, *Journal of Climate*, *20*(17), 4293-4315, doi:10.1175/Jcli4256.1.

Yokoyama, Y., K. Lambeck, P. De Deckker, P. Johnston, and L. K. Fifield (2000), Timing of the Last Glacial Maximum from observed sea-level minima, *Nature*, *406*, 713-716.

Yoneda, M., H. Uno, Y. Shibata, R. Suzuki, Y. Kumamoto, K. Yoshida, T. Sasaki, A. Suzuki, and H. Kawahata (2007), Radiocarbon marine reservoir ages in the western Pacific estimated by pre-bomb molluscan shells, *Nuclear Instruments & Methods in Physics Research Section B-Beam Interactions with Materials and Atoms*, *259*(1), 432-437, doi:10.1016/J.Nimb.2007.01.184.

You, Y. (2003), Implications of cabbeling on the formation and transformation mechanism of North Pacific Intermediate Water, *Journal of Geophysical Research*, *108*(C5), 3134, doi:10.1029/2001JC001285.

Yu, J., and H. Elderfield (2008), Mg/Ca in the benthic foraminifera *Cibicidoides wuellerstorfi* and *Cibicidoides mundulus*: Temperature versus carbonate ion saturation, *Earth and Planetary Science Letters*, *276*, 129-139.

Zahn, R., and M. Sarnthein (1986), Benthic foraminiferal Delta-C-13 and accumulation rates of organic carbon: Uvigerina peregrina group and C. wuellerstorfi, *Paleoceanography*, *1*, 27-42.

Zhang, R., and T. L. Delworth (2005), Simulated tropical response to a substantial weakening of the Atlantic thermohaline circulation, *Journal of Climate*, *18*(12), 1853-1860.

Zhang, J. L., R. Woodgate, and R. Moritz (2010), Sea Ice Response to Atmospheric and Oceanic Forcing in the Bering Sea, *Journal of Physical Oceanography*, *40*(8), 1729-1747, doi:10.1175/2010jpo4323.1.

Appendix 1:

Millennial-scale variability of marine productivity and terrigenous matter supply in the western Bering Sea during the last glacial-interglacial cycle

Jan-Rainer Riethdorf[1], Dirk Nürnberg[1], Lars Max[2], Ralf Tiedemann[2], Sergey Gorbarenko[3], Mikhail Malakhov[4]

[1]GEOMAR | Helmholtz-Zentrum für Ozeanforschung Kiel, Wischhofstr. 1-3, D-24148 Kiel, Germany; E-Mail: jriethdorf@geomar.de
[2]Alfred Wegener Institute for Polar and Marine Research, Am Handelshafen 12, D-27570 Bremerhaven, Germany
[3]Pacific Oceanological Institute, Far Eastern Branch, Russian Academy of Sciences, Baltiskaya St. 43, 690041 Vladivostok, Russia
[4]North Eastern Interdisciplinary Science Research Institute, Far Eastern Branch, Russian Academy of Sciences, Portovaya St. 16, 685000 Magadan, Russia

Abstract

Piston cores, recovered from intermediate water levels in the western Bering Sea, were used to reconstruct millennial-scale changes in marine productivity and terrigenous matter supply over the past ca. 180,000 years. Age models rely on a combination of benthic oxygen isotope stratigraphy, magnetostratigraphy, radiocarbon dating, and intercore correlations via high-resolution core logging data (color b*, XRF scans), which provide a pattern of variability that strongly corresponds to Dansgaard-Oeschger climate variability registered in the NGRIP ice core record. Reconstructions are based on a geochemical multi-proxy approach indicating closely interacting processes that control biological productivity and terrigenous matter supply comparable to the situation in the Okhotsk Sea. During the last glaciation, increased amounts of siliciclastics and contents of lithogenous elements (Al, Fe, Ti), but reduced contents of TOC, $CaCO_3$, biogenic opal, and biogenic Ba point towards higher terrigenous input and prohibited primary production. Minor increases in marine productivity occur during warm stages of MIS5, but maxima are observed during interglacials and the last glacial termination. Anticorrelated proxy behaviour, fairly constant Al/Ti and Fe/Al ratios, and high [C/N] ratios suggest that seasonal sea-ice formation is the dominant transport mechanism for terrigenous material. Accordingly, sea-ice dynamics are thought to be strongly related to changes in surface productivity, terrigenous fluxes, and upper ocean stratification at our study sites. From our results we propose scenarios for environmental change in the Bering Sea during the last glacial-interglacial cycle. Abrupt environmental changes recorded during the last glacial period supposedly apply to the deglacial situation and are potentially connected to North Atlantic Dansgaard-Oeschger events, supporting an atmospheric coupling mechanism of Northern Hemisphere climates.

Appendix 2:

Paleoceanographic conditions in the western Bering Sea during the late Quaternary

E.A. Ovsepyan[1], E.V. Ivanova[1], L. Max[2], J.-R. Riethdorf[3], D. Nürnberg[3], R. Tiedemann[2]

1 - P. P. Shirshov Institute of Oceanology Russian Academy of Sciences, Nakhimovsky Prospekt 36, 117997, Moscow, Russia
2 - Alfred Wegener Institute for Polar and Marine Research, Am Handelshafen 12, D-27570 Bremerhaven, Germany
3 – GEOMAR | Helmholtz-Zentrum für Ozeanforschung Kiel, Wischhofstr. 1-3, D-24148 Kiel, Germany

Abstract

Benthic and planktic foraminiferal assemblages and distribution of coarse sediment fractions are studied from the upper 4.5 m of the core SO201-2-85KL retrieved from the Shirshov Ridge. This part of the core covers 7.5 - 50 kyr. Low sea-surface biological productivity, ice rafting and oxygenated bottom-water are suggested for MIS 3-2. A productivity spike caused by reorganization of the Bering Sea circulation in the early deglaciation is inferred from a maximum of planktic foraminiferal abundance and was not previously known in the region. The late part of Bølling/Allerød interstadial and the Early Holocene are characterized by a two-step increase in productivity and strong oxygen-depleted conditions in bottom and pore waters. Slight decrease in productivity and intensification of bottom-water ventilation characterize the Younger Dryas in this region.

Name: Lars Max Datum: 18.05.2012

Anschrift: Dobbenweg 12, 28203, Bremen

Erklärung

Hiermit versichere ich, dass ich

1. die Arbeit ohne unerlaubte fremde Hilfe angefertigt habe,

2. keine anderen als die von mir angegebenen Quellen und Hilfsmittel benutzt habe und

3. die den benutzten Werken wörtlich oder inhaltlich entnommenen Stellen als solche kenntlich gemacht habe.

_____, den ....

(Unterschrift)